JAERI 1322

JAERI 1322

Seismic Study on High Temperature Gas-Cooled Reactor Core

April 1991

日 本 原 子 力 研 究 所

Japan Atomic Energy Research Institute

JAERI レポートは，日本原子力研究所が研究成果編集委員会の審査を経て不定期に公刊している研究報告書です。

入手の問合わせは，日本原子力研究所技術情報部情報資料課（〒319-11茨城県那珂郡東海村）あて，お申しこしください。なお，このほかに財団法人原子力弘済会資料センター（〒319-11 茨城県那珂郡東海村日本原子力研究所内）で複写による実費頒布をおこなっております。

JAERI reports are reviewed by the Board of Editors and issued irregularly.

Inquiries about availability of the reports should be addressed to Information Division Department of Technical Information, Japan Atomic Energy Research Institute, Tokai-mura, Naka-gun, Ibaraki-ken 319-11, Japan.

編集兼発行　日本原子力研究所
印　　刷　いばらき印刷㈱

Seismic Study on High Temperature Gas-Cooled Reactor Core

Takeshi IKUSHIMA

Department of Fuel Safety Research
Tokai Research Establishment
Japan Atomic Energy Research Institute
Tokai-mura, Naka-gun, Ibaraki-ken

(Received July 19, 1990)

Abstract

The resistance against earthquakes of a high temperature gas-cooled reactor (HTGR) core with block-type fuel is not yet fully ascertained. Seismic studies must be made if such a reactor plant is to be installed in the areas with frequent earthquakes.

The experimental and analytical studies for the seismic response of the HTGR core were carried out. First, the fundamental behavior, such as the softening characteristic of a single stacked column (which is piled up with blocks) and the hardening characteristic with the block impact were clarified from the seismic experiments. Second, the displacement and the impact characteristics of the two-dimensional vertical core and the two-dimensional horizontal core were studied from the seismic experiments. Finally, analytical methods and computer programs for the seismic response of HTGR cores were developed.

Keywords : Seismic Test, Seismic Response, Vibration Test, HTGR Core, Block Type Fuel, Aseismic Design, Impact Response, Seismic Analysis, Nonlinear Vibration, Hardening Characteristic, Two-dimensional Vertical Model, Two-dimensional Horizontal Model

高温ガス冷却炉炉心の耐震研究

日本原子力研究所燃料安全工学部

幾島　毅

(1990年7月19日受理)

要　　旨

ブロック型燃料から構成された高温ガス冷却炉が地震の起りうる地域に建設される場合には，炉心の耐震性を明らかにするための研究が必要とされる。

本論文は高温ガス冷却炉炉心の耐震性に関する基礎的な実験と解析に関するものであり，内容は次のとおりである。最初に，黒鉛ブロックを積み上げたカラムの基本的な振動特性であるソフトスプリング特性および衝突時のハードスプリング特性について実験によって明らかにした。次に，2次元垂直炉心および2次元水平炉心による耐震実験を行い，変位特性および衝突特性を明らかにした。そして，これらの実験結果をもとに高温ガス冷却炉炉心の地震応答解析法と計算プログラムを開発した。

CONTENTS

目　　次

List of Tables

List of Figures

List of Photographs

Executive Summary

The experimental and analytical studies of seismic response for the block type HTGR core designs were studiled. First, fundamental dynamic behavior of graphite blocks, such as impact response as well as the soft spring characteristics of a single stacked column, was clarified. Second, dynamic behavior of two -dimensional vertical and horizotal cores was investigated for development of analytical methods. Finally, analytical methods of seismic response for the block type HTGR core designs were developed.

In Chapter 1, preceeding works concerning the HTGR core seismic researches were surveyed and evaluated from stand points of the HTGR core designs.

In Chapter 2, basic theory of models can be derived from dimensional analysis, that is the Buckingham π theorem, to obtain scale factors for seismic test models. Furthermore collision tests between two graphite blocks have been performed to make clear the coefficient of restitution and the contact duration time in an impact.

In Chapter 3, dyamic characteristics of a single stacked column were examined. The column has a nonlinear resonance and exhibits a hysterisis response with jump points. These are the column softening characteristics due to column rocking, interface friction between blocks and loose dowel connections.

In Chapter 4, a seismic analysis method for the block column has been developed. The numerical results were compared with the experimental results for both the free and forced excitation of the single stacked column. Good agreement was obtained between analytical and experimental results.

In Chapter 5, dynamic characteristics, such as softening of the single stacked column were examined. The softening characteristics are caused by the column rocking, the block upper and lower face frictions and loose dowel connections. Whirling phenomenon of the column occurs under certain excitation conditions. The column vibrates at subharmonic frequency under the centain excitation conditions.

In Chapter 6, a simplified analysis model for a HTGR core seismic response is conceived. In the simplified model, one degree-of-freedom mass with nonlinear column characteristics is used instead of the single stacked column. Validity of the simplified model was shown. The computer cost of time history analysis of the HTGR core by the simplified model is significantly lower than by the detaild model.

In Chapter 7, an experimental study has been carried out with a two-dimensional core model which is a vertical slice along the axis of the HTGR core. At the low excitation frequency, the core oscillates as a tightly lumped mass between the side reflector boundaries. The core lumping increases with increasing exitation frequency. At still higher frequency, the core lumping rapidly decreases and subharmonic vibration occurs. The soft spring support with hard stopping by the reflector side support structure causes large column displacements, thus affecting the insertion of control rods. The soft spring support slightly reduces the impact reaction forces but increases dowel forces. The resonant frequency decreases with a decrease of support stiffness.

In Chapter 8, a seismic analysis method for the block column of the HTGR core has been developed. The analytical results were compared with experimental data for horizontal forced vibration of a series of many interacting stacked columns. Good agreement was obtained between analytical the experimental. Using this method, forces in dowel pins and around the holes can be calculated. The dowel pin forces of the analysis were compared with experimental data. The analytical values were in good agreement with the exprimental ones.

In Chapter 9, experimental results of a two-dimensional horizontal sliced model of the HTGR core were presented. The maximum impact forces occur during the flat-to-flat impact between hexagonal fuel blocks. There is a most favorable stiffness of the side support which reduces the impact reaction forces.

In Chapter 10, a seismic analysis method has been derived for the horizontal two-dimensional core

consisting of the block type fuel HTGR. For the purpose of comparison between the analytical and experimental values, calculations were made. The results of displacements and impact reaction forces due to input acceleration are in good agreement, showing validity of this analysis method.

In Chapter 11, a comparison of response characteristics of two-dimensional cores has been carried out in order to obtain seismic response characteristics of a real HTGR core. From the results of the seismic experiment with the scale model, it is verified the real core response can be predicted with the two following methods. These are the application of similarity laws to the experimental results and the use of the computer programs which are verified, on the basis of the model experiments. The response values of the real HTGR core could be estimated from the experimental and analytical results of the two-dimensional vertical and horizontal core models.

In Chapter 12, author presented aseismic design considerations of the block type fuel HTGR core on the basis of previous results.

1. Introduction

With the oil crisis in the autumn of 1973 as a turning point, the energy problem became intensified to a worldwide level. Voices were thus raised stating the necessity for development of new sources of energy, such as atomic energy.

High temperature gas-cooled reactors (HTGR) are expected to achieve high thermal efficiency and to reduce heat and radiation pollution as compared with the convetional reactors and also have a possiblility of diversification of energy sources in production system of nuclear thermal energy. Furthermore, the reactors make possible plural energy use in combining enrgy systems.

In the field of HTGRs, two major aspects are being investigated in Japan: research and development of an experimental high temperature gas-cooled reactor as a process heat source for use in fields such as steel making and chemical industry, has been promoted by Japan Atomic Energy Research Institute (JAERI) since 1969 with close cooperation of other domestic organizations; and study on the introducton of a power generating HTGR with high thermal efficiency by an electric power company.

However, the reactor core is capable of high temperature (abour 800 to 1000℃) and is composed of many graphite blocks, so that seismic safety will become one of the most important points in construction of the HTGR in Japan which is known as an earthquake country.

In the electric power generating HTGR designed by General Atomic Co., and the experimental HTGR being designed by JAERI, the reactor cores consist of hexagonal graphite blocks as shown is Fig. 1.1 and 1.2. These graphite blocks are stacked in several hundred columns. The reactor core is enclosed

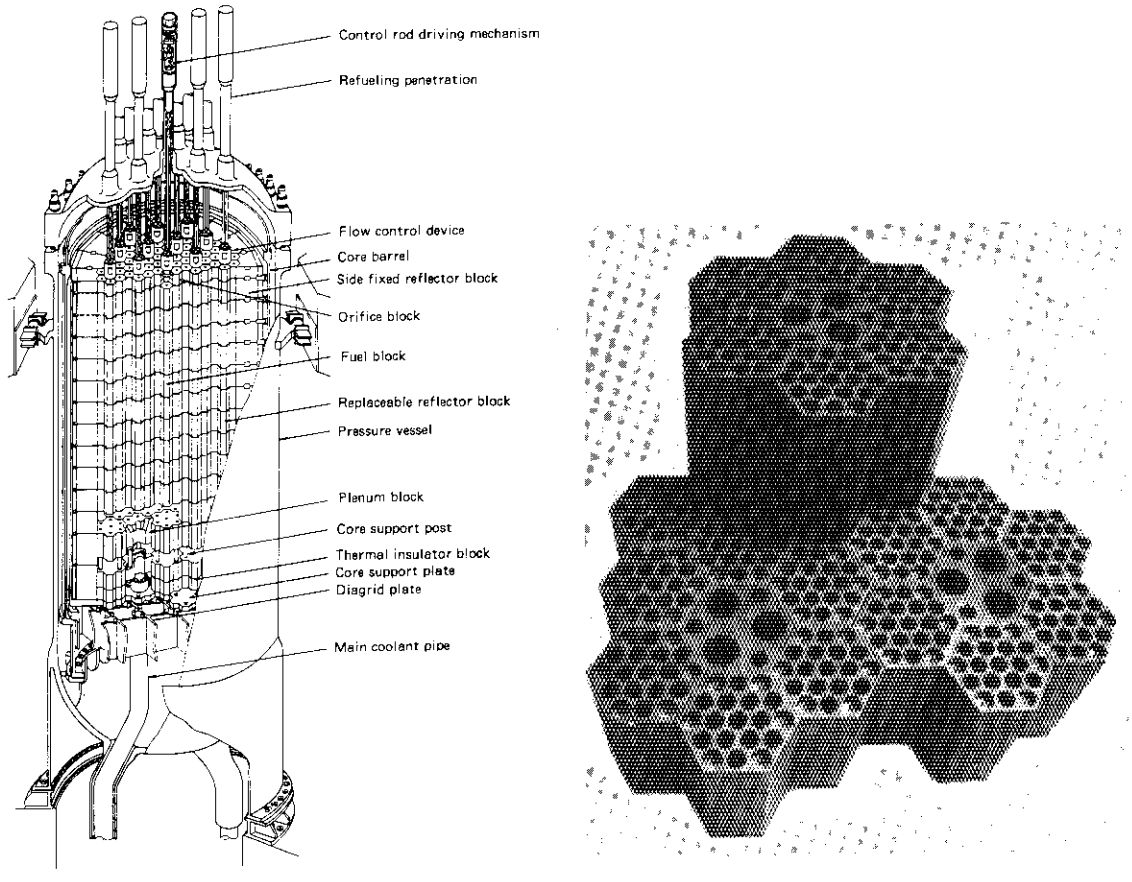

(a) Vertical view (b) Fuel blocks

Fig. 1.1 Vertical view of an experimental HTGR

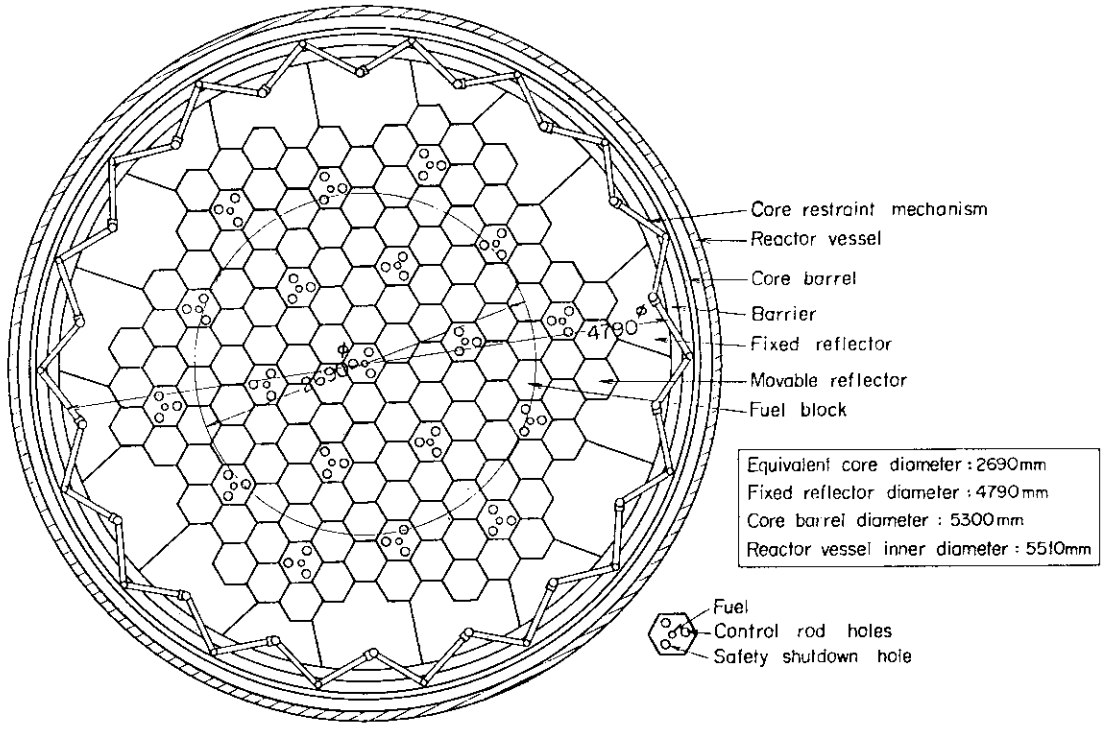

Fig. 1.2 Core horizontal view

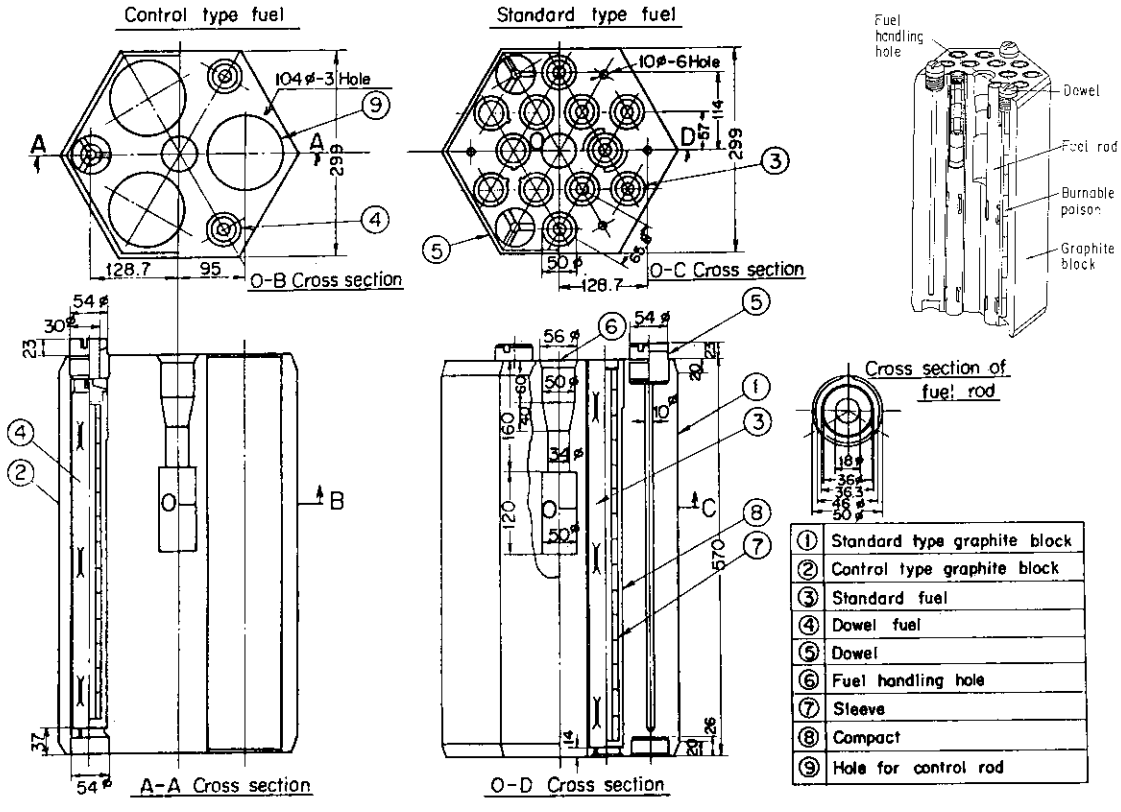

Fig. 1.3 Graphite fuel block

in a core barrel and the column is restrained horizontally at the top with a keyed orifice block of a heatresisting alloy. The column bottoms are restrained with dowel pins on the core support blocks as shown in Fig. 1.3. On the periphery, a fixed reflector is restrained by the core barrel. Blocks in the core are aligned in the columns by dowel pins. Each column is separated from adjacent columns by small gaps. The gaps are is initially several millimeters. After residence in the core, however, the block diameter is reduced in size due to fast neutron irradiation, so that the gaps increase to make as 4～6 mm.

These large gaps together with the large number of columns may result in large cumulative gaps during a seismic excitation. The cumulative gaps across the core diameter are significant since it may affect the ability to insert the control and shutdown material into the core. Moreover, because of these gaps, columns may repeatedly impact against each other during a seismic excitation.

To meet this requirement, the following information is necessary from analyses and/or experiments:

(1) deflections and disarrays which could cause disengagement of dowels and affect control rod insertion,

(2) impact forces of blocks, and

(3) shear forces on the dowels.

For this purpose Neylon, Olsn et al. in research groups of General Atomic made extensive studies from the elucidation of block impact phenomena to column vibration and three-dimensional core vibration tests including their analyses for developing power generating HTGRs[1]～[26]. Muto et al. made block impact tests, two-dimensional vertical core and two-dimensional horizontal core vibration tests and developed seismic simulation computer programs for introducting HTGRs to Japan[27]～[30]. Bezler, Curreri et al. in research groups of Brookheaven National Laboratory made one-dimensional and two-dimen-siomal vertical core vibration tests and developed seismic simulation computer programs for safety analysis of the HTGR core under seismic disturbanse[31]～[41]. Dove and Bennett et al. in a research group of Los Alamos National Laboratory made one-dimensional and two-dimensional vertical core vibration tests and developed a seismic simulation computer program for the study of scaling laws concerned with safety analysis of the HTGR core under seismic disturbance[42]～[45]. Ishizuka et.al. in a research group in Fuji Electric Co. made block impact tests, single column and two-dimensional horizontal core vibration tests and developed seismic simulation computer programs for developing the HTGR[46]～[49]. Some other research groups made HTGR core seismic studies[50]～[57] and these studies are summarized in Table 1.1 and 1.2.

There are many seismic studies of the HTGR core as mentioned above. However, the tools i.e. computer programs for the seismic design of the Experimental HTGR and the experimental data for the validation of the programs are very insufficient. And the extensive studies for the design have been requested.

The author has carried out extensive studies for the elucidation of stacked columns vibration characteristics of two-dimensional vertical core and two-dimensional horizontal core vibration tests and

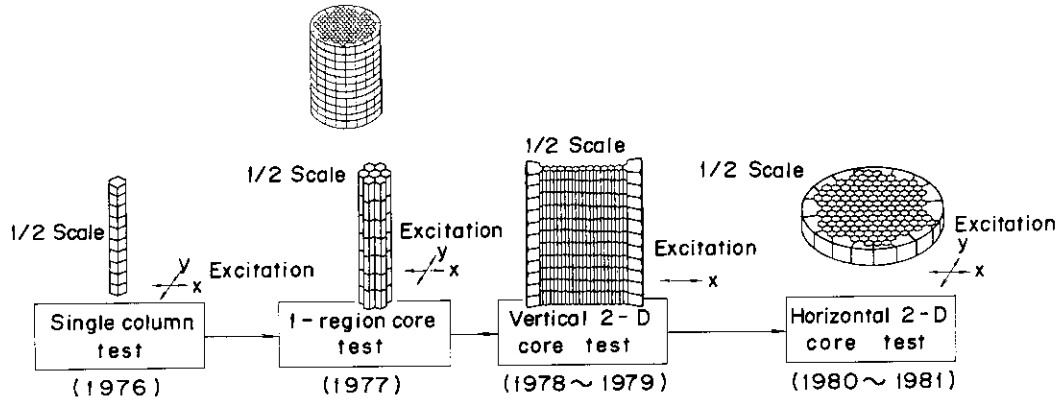

Fig. 1.4 Core seismic test program

developed seismic simulation methods and computer programs as shown in Fig. 1.4.

Largest possible test blocks within the limitation of the usable shaking tables, scaled to 1/2 by dimension and to 1/4 by weight of the real fuel block design, have been used in order to obtain the data with sufficient accuracy,.

The remainder of this report is arranged as follows.

In chapter 1, the seismic study of block-type fuel HTGR cores so far tried are surveyed, and the seismic research of HTGR core is considered.

In chapter 2, similarity laws are introduced for vibration experiments. The collision characteristics are also examined by collision tests for seismic analysis. The characteristics are the coefficient of restitution and contact duration.

In chapter 3, the fundamental column characteristics of softening and hardening behavior are described.

In chapter 4, an analytical method for predicting the behavior of a block type HTGR core under seismic excitation is discussed.

In chapter 5, the vibration characteristics of a column in three-dimensional space and impact response characteristics of graphite blocks are discussed. The whirling phenomenon, subharmonic vibration, and effects of pressure difference between upper and lower core are also discussed.

In chapter 6, a simplified modeling of the seismic response of HTGR core consisting of graphite blocks is described.

In chapter 7, a seismic experiment on a one-half scale two-dimensional vertical model is presented. The vibration and impact characteristics suck as effects of side support stiffness, effects of gas pressure simulating spring and also shown the dowel force frequency response are presented.

In chapter 8, an analytical method for multi-column interaction under seismic excitation is presented. The analytical results are compared with experimental ones. It can be shown that the analytical method is useful to predict the behavior of the HTGR core to seismic input.

In Chapter 9, a sismic experiment on a one-half scale two-dimensional horizontal core is presented. Vibration and impact characteristics such as effects of side reaction force response are presented.

In Chapter 10, an analytical method for a two-dimensional horizontal core model under seismic excitation is presented. The analytical results are compared with experimental ones. It can be shown that analytical method is useful to predict the behavior of the HTGR core to seismic input.

In Chapter 11, the comparative studies of the two models experiments and analyses, which are the two-dimensional vertical core model and two-dimensional horizontal core model, are presented to estimate a real core response under seismic excitation.

In Chapter 12, the results are summarized and an aseismic design consideration for the HTGR core structure is given.

Table 1.1 Experimental studies on HTGR core seismic

Items	Objectives	Obtains	Researchers	References
1.1 Collision Dynamics Test				
◦Collision dynamics test (1/5, 1/2, 1/1 scale, 2 – 5 elements)	◦Study collision behavior ◦Verify scaling law	◦Coefficient of restitution ◦Contact time ◦Correlation with analytical collision model	Rodkin	GA-A 14728 (1978).
◦Collision dynamics test (1/5, 1/2, 1/1 scale, 2 elements	◦Study collision behavior	◦Coefficient of restitution ◦Contact time	Ikushima	JAERI-M 7727 (1978).
◦Collision dynamics test (1/5 scale, 2 elements)	◦Study collision behavior ◦Verify scaling low	◦Coefficient of restitution ◦Contact time	Ishizuka	SMiRT-4, K 7/9(1977). J. FAPIG, 79 [11] (1975).
◦Collision dynamics test (1/5, 1/1 scale, 2 elements	◦Study collision behavior ◦Verify scaling law	◦Coefficient of restitution ◦Search 1/5 scale model block geometry ◦Relationship between impact mode and coefficient of restitution	Muto et al.	SMiRT-3, K 8/8 (1975).
1.2 Basic Rocking Test				
◦Basic rocking test (1/5, 1/1 scale, 2 – 4 elements	◦Study block rocking behavior	◦Correlation with analytical collision and rocking models.	Nau and Olsen	GA-A 14087 (1978).
1.3 1D Horizontal Core Test (horizontal strip diametrically across the core)				
◦1D horizontal core test (1/5 scale, 27 elements	◦Study dynamic properties	◦Effect of lateral support stiffness ◦Lumping ◦Lateral support loads ◦Correlation with analytical collision model	Muto	SMiRT-3, K 8/8 (1975).
◦1D horizontal core test (1/5 scale, 3 ~ 7 elements	◦Study dynamic properties	◦Effect of lateral support stiffness ◦Lateral support loads ◦Correlation with computer program	Ishizuka	SMiRT-4, K 7/9 (1977). J. FAPIG, 79 [11] (1975).
◦1D horizontal core test (6 elements)	◦Scaling laws	◦Scaling laws (length, time, force, material)	Dove and Bennett	LA-5821-MS (1975) LA-NUREG-6377-MS (1976) LA-UR-77-2010 (1977)
◦1D horizontal core test (1/5 scale, 9 elements	◦To correlate computer program		Zako	Proceeding of JSME, 780-14, (1978).
1.4 Single Column Test				
◦Single column test (1/5 scale, 10 elements	◦Study core column dynamic properties ◦Study simultaneous horizontal and vertical excitation	◦Rocking angles ◦Block forces ◦Dowel forces ◦Support loads ◦Correlation with computer program	Fischer	GA-A 14664 (1979).
◦Single column test (1/2 scale, 13 elements	◦Study core column dynamic properties	◦Column softening and hardening characteristics ◦Resonance frequency and mode shape ◦Support loads ◦Effect of gap between column and boundary ◦Correlation with computer program	Ikushima	JAERI-M 7727 (1978). J. At. Energy Soc. Japan, 22-1 (1980). Nucl. Sci. Tech. 16-[8], (1979).
◦Single column (1/5 scale, 11 elements	◦Study core column dynamic properties	◦Column softening characteristics ◦Effect of gap between column and boundary ◦Correlation with computer program	Ishizuka	SMiRT-4, K 8/8 (1977). J. FAPIG, 79 [11] (1978).

Table 1.1 (Continued)

Items	Objectives	Obtains	Researchers	References
∘Single column (1/5 scale, 9 elements)	∘Study core column dynamic properties	∘Column softening characteristics ∘Effect of top gap ∘Effect of top block weight ∘Correlation with computer program	Zako	Proceeding of JSME, 780-6, (1978) and 790-5, (1979).
1.5 One Region Core Model Test (7 column)				
∘One-region core model test (1/2 scale, 13 elements/column)	∘Study column dynamic characteristics ∘Effect of excitation direction ∘Effect of gas pressure difference	∘Whirling phenomenon ∘Column softening and hardening characteristics ∘Column damping ∘Column statistic stiffness ∘Correlation with computer program	Ikushima	Nucl. Sci. Tech. 17 [9] (1980). J. MHI Tech. Report, 16-[5], (1979). Trans. JSME 47-415(C), (1981).
1.6 2D Vertical Slice Core Model Test (series of colum diametrically across the core)				
∘2D vertical core model test 1/5 scale, 25 (columns with lateral columns	∘Study core dynamic characteristics ∘Effect of lateral support stiffness	∘Lateral support loads ∘Vibration mode ∘Lumping ∘Correlation with computer program	Muto	SMiRT-4, K 7/8 J. At. Energy Soc. Japan, 19 [12], (1977).
∘2D vertical core model test 1/2 scale, 12 (columns with lateral columns	∘Study core dynamic characteristics ∘Effect of lateral support stiffness ∘Effect of top gap width	∘Vibration mode ∘Lateral support loads ∘Dowel pin and socket forces ∘Correlation with computer program	Ikushima	J. Nucl. Sci. Tech. 18[7], (1981). JAERI 1282 (1983).
∘2D vertical core model test (1/5 scale, 7 columns with lateral columns)	∘Study core dynamic characteristics ∘Study simultaneous horizontal and vertical exciation	∘Vibration mode ∘Correlation with computer program	Bezler	Proceeding of 2nd Japan-US HTGR Safety Meeting (1977).
∘2D vertical core model test (1/5 scale, 3 columns with lateral columns)	∘Study core dynamic characteristics ∘Effect of lateral support stiffness	∘Vibration mode ∘Correlation with computer program	Zako	Proceeding of JSME, 800-3 (1980), and 800-12 (1980).
1.7 2D Horizontal Core Mode Test				
∘2D horizontal core model test (1/5 scale, 73, elements	∘Study core dynamic characteristics ∘Effect of excitation axis ∘Study simultaneous two-axis excitation	∘In-core velocities and forces ∘Boundary displacements, velocities and forces ∘Correlation with computer program	Petersen Waldman	CA-A 14087 (1978). GA-A 14548 (1978).
∘2D horizontal core model test (1/5 scale, 577 elements	∘Study core dynamic characteristics	∘Boundary force distribution ∘Correlation with computer program	Muto	SMiRT-5, K 12/2, (1979).
∘2D horizontal core model test (1/5 scale, 61 elements	∘Study core dynamic characteristics	∘In-core displacements and velocities	Ishizuka	SMiRT-4, K 7/9, (1977). J. PAPIG, 79 [11], (1975).
∘2D horizontal core model test (1/2 scale, 139 elements	∘Study core dynamic characteristics ∘Effect of excitation axis ∘Study simultaneous two-axis excitation ∘Effect of lateral support stiffness	∘In-core displacements and forces ∘Boundary displacements and forces ∘Correlation with computer program	Ikushima	Trans. JSME, 51-464(C), (1985). Bulltin JSME, 28-246(C), (1985). JAERI M 88-085 (1988).
1.8 3D Core Model Test				
∘3D core model test (uniaxial, 1/5 scale, full array	∘Study core dynamic characteristics ∘Effect of excitation axis ∘Effect of lateral support stiffness ∘Effect of seismic wave properties	∘In-core velocities and forces ∘Boundary displacements and velocities ∘Support force ∘Correlation with computer programs	Olsen	GA-A 14546 (1978). CA-A 14812 (1979). SMiRT-4, K 7/7 (1977). (1977).

Table 1.1 (Continued)

Items	Objectives	Obtains	Researchers	References
◦3D core model test (uniaxial, 1/4 scale, 83 columns)	◦Study core dynamic characteristics	◦Vibration characteristics ◦Boundary forces ◦Correlation with computer programs	Buland	CEA-CONF 3226 (1975). SMiRT-3, K 8/9 (1975).
◦3D core model test	◦Study core dynamic characteristics	◦Vibration characteristics	Curreri	SMiRT-5, K 12/1 (1979).
1.9 Dowel Force Test				
◦Dowel force test (1/5 scale, full array)	◦Magnitude and direction of dowel and socket forces	◦Dowel force ◦In-core forces ◦Edge and corner load ◦Correlation with computer programs	Rakowski Chiang	GA-A 14088 (1979). GA-A 13861 (1976).
1.10 Block Impact Test				
◦Block impact test	◦Study fatigue strength ◦Contact ◦Contact phenomena	◦Block fatigue strength ◦Wave propergation ◦Contact time ◦Rebound velocity ◦Correlation with analytical method	Olsen Tzung	GA-A 13920 (1980). SMiRT-4, K 1/5 (1977). GA-A 14359 (1977).

Table 1.2 Computer programs and analytical studies on HTGR core seismic

Items	Models	Calculates	Researchers	References
2.1 1D Horizontal Model (horizontal strip diametrically across the core)				
◦CRUNCH-1D	◦Spring dashpot model ◦Impact-momentum model ◦Effective core column restraints and core support floor are included.	◦In-core horizontal (flat-to-flat) impact forces ◦Lateral support force	Rickard	GA-A 14120 (1977).
◦PRELUDE	◦Spring dashpot model ◦Effective core column restraints and core support floor are included.	◦Horizontal impact forces ◦Lateral support forces ◦Effect of gap	Ikushima	JAERI-M 5560 (1974). SMiRT-3, K 8/7 (1975).
◦COLLAN-1	◦Impact-momentum model	◦Lateral support forces ◦Core lumping	Muto	SMiRT-3, K 8/8 (1975).
◦VIBRA	◦Spring dashpot model ◦Impact-momentum model ◦Effects of core column restraints and core support floor are included.	◦Horizontal impact forces ◦Lateral support forces	Ishizuka	SMiRT-4, K 7/9 (1977). J. Fuji Giho 48 [8], (1975).
◦OSCIL	◦Spring dashpot model ◦Effects of core column restraints and core support floor are included.	◦Horizontal impact forces ◦Lateral support forces ◦Subbarmonic resonance	Bezler Curreri Reich	BNL-21023 (1976). SMiRT-4, K 7/2(1977). SMiRT-4, K 7/4(1977). SMiRT-4, K 7/3(1977). SMiRT-4, K 8/9(1977).
◦FYSMOD	◦Spring dashpot model ◦Effects of core column restraints and core support floor are included.	◦Horizontal impact forces ◦Lateral support forces	Merson and Bennett	LA-NUREG-6473-MS (1976).
2.2 Single Column (2D vertical model)				
◦COCO	◦Entire core column, core support block and post ◦Spring dashpot model ◦Three-degree-of-freedom (horizontal and vertical displacements and rotation)	◦Response to simultaneous horizontal and vertical inputs ◦Block impact forces ◦Boundary impact forces ◦Dowel forces	Lee Rickard	Nucl. Eng. Design 32, (1975). SMiRT-3, K 8/5 (1975). GA-A 14600 (1978).

Table 1.2 (Continued)

Items	Models	Calculates	Researchers	References
◦SONATINA-1	◦Core column and lateral blocks are included. ◦Spring dashpot model ◦Three-degree-of-freedom (horizontal and vertical displacements and rotation)	◦Response to simultaneous horizontal and vertical inputs ◦Block impact forces ◦Boundary impact forces ◦Dowel forces	Ikushima	Nucl. Eng. Design, 55 (1979). JAERI-M 9165 (1980).
◦COLUMN-3	◦Core column and lateral blocks are included. ◦Spring deshpot model ◦Three-degree-of-freedom (horizontal and vertical displacements and rotation)	◦Response to horizontal input ◦Block impact forces ◦Boundary impact forces ◦Dowel forces	Ishizuka and Hayakawa	SMiRT-4, K 7/9 (1977). J. FAPIG, 91 [3], (1979).
◦IHI-code	◦Same as above	◦Same as above	Zako	Proceeding of JSME, 800-12, (1980).
◦MHI-code	◦Same as above	◦Same as above	Honma	J. MHI Tech. Report, 16 [5], (1979).
2.3 Single Column (3D model)				
◦COLLAN-3	◦Impact-momentum model ◦Five-degree-of-freedom	◦Response to simultaneous two horizontal and one vertical inputs ◦Three-dimensional block movement	Muto and Takase	Proceeding of JSME, 800-9, (1980). Proceeding of 2nd Japan-US HTGR Safety Meeting (1977).
2.4 2D Vertical Slice Core Model (series of columns diametrically across the core)				
◦MCOCO	◦Including core support block and posts. ◦Spring dashpot model	◦Response to simultaneous horizontal and vertical inputs ◦In-core impact forces ◦Dowel forces ◦Core support block forces ◦Horizontal and vertical support forces	Tompson Shatoff Lee	GA-A 14764 (1978). GA-A 15370 (1979). SMiRT-3, K 8/5 (1975).
◦SONATINA-2V	◦Core column and lateral blocks are included. ◦Spring dashpot model	◦Response to simultaneous horizontal and vertical inputs ◦In-core impact forces ◦Dowel forces ◦Lateral support forces	Ikushima	Trans. JSME, 48-426(C), (1982). Bulletin JSME, 25-208, (1982). JAERI 1279 (1982).
◦COLLAN-2V	◦Core column and lateral blocks are included. ◦Impact momentum model	◦Response to simultaneous horizontal and vertical inputs ◦Lateral support forces	Muto	SMiRT-4, K 7/8 (1977).
◦COLPLANE	◦Core column and lateral blocks are included ◦Spring dashpot model	◦Response to simultaneous horizontal and vertical inputs ◦In-core impact forces ◦Dowel forces ◦Lateral support forces	Ishizuka	J. FAPIG, 79 [11], (1975). J. FAPIG, 91 [3], (1979).
◦IHI-code	◦Same as above	◦Same as above	Zako	Proceeding of JSME, 800-12 (1980).
◦OSCVERT	◦Spring dashpot model	◦In-core impact forces ◦Dowel forces	Lasker	SMiRT-4, K 7/1 (1977).
2.5 2D Horizontal One Layer Core Model				
◦CRUNCH-2D	◦Spring dashpot model ◦Effects of core column restraints and core support floor are included.	◦Response to simultaneous two axis horizontal inputs ◦In-core horizontal (flat-to-flat) impact forces ◦Radial and tangential spring pack support forces	Tow	GA-A 14765 (1978).

Table 1.2 (Continued)

Items	Models	Calculates	Researchers	References
◦SONATINA-2H	◦Spring dashpot model ◦Effects of core column restraints and core support floor are included.	◦Response to simultaneous two axis horizontal inputs ◦In-core horizontal impact forces ◦Lateral support forces	Ikushima	J. Nucl. Sci. Tech. (to be published). JAERI M 89- (to be published).
◦COLLAN-2H	◦Impact momentum model	◦Response simultaneous two axis horizontal inputs ◦Lateral support forces	Muto	SMiRT-5, K 12/2 (1979).
◦PUCK	◦Spring dashpot model	◦In-core horizontal impact forces ◦In-core displacements	Ishizuka	SMiRT-4, K 7/9 (1977). J. FAPIG, 79 [11], (1975).
2.6 Control Rod Analysis				
◦COCOROD	◦Dynamic interaction between a control rod and a core column ◦Rod insertion ◦Spring dashpot model	◦Response to simultaneous horizontal and vertican inputs ◦Control rod impact loads ◦Control rod shock absorber loads	Lee	GA-A 14351 (1977). SMiRT-4, K 7/6 (1977).

Nomenclature of Chapter 4 and Chapter 8

a : block rocking spring half width
b : block geometric half width
C : damping coefficient
C^B : damping coefficient associated with ε
C^C : damping coefficient of displacement detector
C^D : damping coefficient associated with β
C^M : damping coefficient of reflector restraint structure
C^V : damping coefficient associated with γ
d : distance of dowel from block center line
F^{BL} : horizontal impact force acting at bottom of left side
F^{BR} : horizontal impact force acting at bottom of right side
F^{DL} : dowel force acting at left dowel
F^{DR} : dowel force acting at right dowel
F^F : friction force acting at horizontal interface between blocks
F^M : reflector restraint force
F^{ML} : horizontal impact force acting at upper-middle of left side
F^{MR} : horizontal impact force acting at upper-middle of right side
F^{NL} : horizontal impact force acting at lower-middle of left side
F^{NR} : horizontal impact force acting at lower-middle of right side
F^{OP} : restraint force between top orifice blocks
F^{RF} : friction force acting at horizontal interface between reflectors
F^P : vertical gas pressure force acting at block center
F^{TL} : horizontal impact force at top of left side
F^{TR} : horizontal impact force at top of right side
F^{VL} : vertical impact force acting at left corner
F^{VR} : vertical impact force acting at right corner
$f(v)$: prescribed function for friction characteristics
g : gravity constant
h : block half height
I : block mass moment of inertia
K^B : spring constant associated with ε
K^D : spring constant associated with β
K^M : spring constant of reflector restraint structure
K^V : spring constant associated with γ
m : mass of block
m_s : mass of core support plate
n : total number of blocks in column
u : horizontal block displacement at center gravity
u_O : boundary displacement
u_S : core suppor plate displacement
v : velocity
w : vertical block displacement at center gravity
w_O : boundary vertical displacement

w^L : vertical force due to block weight and pressure difference acting at lower part of block
w^U : vertical force due to block welght and pressure difference acting at upper part of block
β : dowel spring deformation
γ : spring deformation of a spring-dashpot unit at interface between blocks (vertical direction)
δ : initial gap between blocks
δ_L : gap on left side of dowel
δ_R : gap on right side of dowel
ε : spring deformation of a spring-dashpot unit at interface between blocks (horizontal direction)
θ : block rotation angle
μ_k : coefficient of dynamic friction
μ_s : coefficient of static friction
ω : relative velocity between dowel pin and hole
$\dot{(\ )}$,$\ddot{(\ )}$: dots denotes time derivatives of ( )

Nomenclature of Chapter 10

C : damping coefficient
C_n^{CX} : x-component of restoring damping coefficient of n-th fuel block
C_n^{CY} : y-component of restoring damping coefficient of n-th fuel block
C_n^{GX} : x-component of support damping coefficient of n-th side reflector block
C_n^{GY} : y-component of support damping coefficient of n-th side reflector block
C_n^R : damping coefficient associated with velocity of n-th block
F : force
F_{bi}^{CX} : x-component of reaction force acting on core support block by fuel block and side reflector block
F_{bi}^{CY} : y-component of reaction force acting on core support block by fuel block and side reflector block
F_n^{CX} : x-component of restoring force of n-th side reflector block
F_n^{CY} : y-component of restoring force of n-th side reflector block
F_n^D : damping force
F_b^{GX} : x-component of reaction force acting on core support block by restraint structure
F_b^{GY} : y-component of reaction force acting on core support block by restraint structure
F_n^{GX} : x-component of support force of n-th side reflector block
F_n^{GY} : y-component of support force of n-th side reflector block
F_{ni}^{KX} : x-component of key reaction force of n-th side reflector block
F_{ni}^{KY} : y-component of key reaction force of n-th side reflector block
F_{nij}^{RX} : x-component of impact force caused by surface ⓘ of corner ⓘ of n-th block
F_{nij}^{RY} : y-component of impact force caused by surface ⓘ of corner ⓘ of n-th block
F_n^s : impact spring force
F_{ni}^{SX} : x-component of impact force caused by impact between i-th block and i-th surface of n-th block
F_{ni}^{SY} : y-component of impact force caused by impact between i-th block and i-th surface of n-th block
I_n : mass moment of intertia of n-th block
K : spring constant

K_n^{CX} : x-component of restoring spring constant of n-th fuel block
K_n^{CY} : y-component of restoring spring constant of n-th fuel block
K_n^{GX} : x-component of support spring constant of n-th side reflector block
K_n^{GY} : y-component of support spring constant of n-th side reflector block
K_n^R : spring constant associated with δ_{ni}
M : moment
M_n^C : moment generated by forces F_n^{CX} and F_n^{CY}
M_{ni}^G : moment generated by forces F_{ni}^{GX} and F_{ni}^{GY}
M_{ni}^K : moment generated by forces F_{ni}^{KX} and F_{ni}^{KY}
M_{nij}^R : moment generated by forces F_{nij}^{RX} and F_{nij}^{RY}
M_{ni}^S : moment generated by forces F_{ni}^{SX} and F_{ni}^{SY}
m_b : mass of core support block
m_n : mass of n-th block
NCR : number of possible impact corners of n-th side reflector block
NH : mumber of fuel blocks around n-th side reflector block
NR : number of side reflector blocks around n-th side reflector block
v : relative velocity between impacting blocks
(v_{kix}, v_{kiy}) : x-and y-component of velocity of i-th block
(v_{knx}, v_{kny}) : x-and y-component of velocity of n-th block
x : x coordinate or x-direction displacement
x_b : x-direction displacement of core support block
x_i : x-direction displacement of i-th block
x_n : x-direction displacement of n-th block
x_{oi} : initial x coordinate of i-th block
x_{on} : initial x coordinate of n-th block
x_{pn} : x coordinate of point P of n-th block
x_{ipi} : x coordinate of point P of i-th block (coordinate origin is at i-th block's center of gravity)
x_{ipn} : x coordinate of point P of i-th block (coordinate origin is at n-th block's center of gravity)
x_{kii} : x coordinate of corner of i-th reflector block keyway (coordinate origin is at n-th reflector block's center of gravity)
x_{kin} : x coordinate of corner of i-th reflector block keyway (coordinate origin is at n-th reflector block's center of gravity)
x_{knn} : x coordinate of corner of n-th reflector block keyway (coordinate origin is at n-th reflector block's center of gravity)
x_{npn} : x coordinate of point P of n-th block (coordinate origin is at n-th block's center of gravity)
x_{pno} : x coordinate of point P of n-th block (coordinate origin is at n-th block's center of gravity)
$\dot{x}$: x-component of velocity
$\ddot{x}$: x-component of acceleration
$\ddot{x}_o$: x-component of input acceleration
y : y coordinate or y-direction displacement
y_b : y-direction displacement of core support block
y_i : y-direction displacement of i-th block
y_n : y-direction displacement of n-th block
y_{oi} : initial y coordinate of i-th block
y_{on} : initial y coordinate of n-th block
y_{pn} : y coordinate of point P of n-th block
y_{ipi} : y coordinate of point P of i-th block (coordinate origin is at i-th block's center of gravity)
y_{ipn} : y coordinate of point P of i-th block (coordinate origin is at n-th block's center of gravity)

y_{kii} : y coordinate of corner of i-th reflector block keyway (coordinate origin is at i-th reflector block's center of gravity)

y_{kin} : y coordinate of corner of i-th reflector block keyway (coordinate origin is at n-th reflector block's center of gravity)

y_{knn} : y coordinate of corner of n-th reflector block keyway (coordinate origin is at n-th reflector block's center of gravity)

y_{npn} : y coordinate of point P of n-th block (coordinate origin is at n-th block's center of gravity)

y_{pno} : y coordinate of point P of n-th block (coordinate origin is at n-th block's center of gravity)

$\dot{y}$: y-component of velocity

$\ddot{y}$: y-component of acceleration

$\ddot{y}_o$: y-component of input acceleration

δ : gap width between blocks

δ_g : gap width between key and keyway

δ_{gx} : x-direction gap width between key and keyway

δ_{gy} : y-direction gap width between key and keyway

δ_{nl} : spring deformation of spring dashpot unit acting between blocks

θ_n : rotation of n-th block

$\dot{\theta}_n$: angular velocity of n-th block

$\ddot{\theta}_n$: angular acceleration of n-th block

μ : friction factor

2. Similarity Laws and Collision Test

2.1 Similarity laws

The basic theory models can be derived from dimensional analysis known as the Buckingham π theorem. Physical variables can be arranged in dimensionless groups so that the equation of describing system is

$$\phi(\pi_1,\pi_2,\ldots)=0\,. \tag{2.1}$$

Since these π terms are independent, solving this equation for the π factor which contains the variable of primary importance in the particular problem yields

$$\pi_1=\theta(\pi_2,\pi_3,\ldots)\,. \tag{2.2}$$

Since Eq. (2.2) is a general relationship, it will apply to both prototype and model

$$\pi_{1p}=\theta(\pi_{2p},\pi_{3p},\ldots)\,, \tag{2.3a}$$
$$\pi_{1m}=\theta(\pi_{2m},\pi_{3m},\ldots)\,, \tag{2.3b}$$

where suffixes p and m mean prototype and model respectively. If the model is designed and tested so that

$$\left.\begin{aligned}&\pi_{2m}=\pi_{2p}\,,\\&\pi_{3m}=\pi_{3p}\,,\\&\quad\vdots\end{aligned}\right\} \tag{2.4}$$

then the functions are equal

$$\theta(\pi_{2p},\pi_{3p},\ldots)=\theta(\pi_{2m},\pi_{3m},\ldots)\,. \tag{2.5}$$

Thus

$$\pi_{1p}=\pi_{1m}\,. \tag{2.6}$$

Equations (2.4) are called the design conditions which specify the design and method of testing of the model. Equation (2.6) is called the prediction equation and prototype behavior can be determined in terms of the model behavior.

Applying similitude to the HTGR core behavior, the quantities involved in mechanics have form of those given in Table 2.1. Since there are in fourteen terms and they can all be expressed dimensionally in terms of three basic dimensions of Length, L; Mass, M; Time, T; eleven dimensionless groups will be required from the Buckingham π theorem.

$$\pi_1=\theta(\pi_2,\pi_3,\pi_4,\ldots,\pi_{11})\,. \tag{2.7}$$

This dimensionless term must have the form

$$\begin{aligned}&\ell^{\ell}\cdot\delta^{\delta}\cdot A^{A}\rho^{\rho}\cdot E^{E}\cdot F^{F}\cdot I^{I}\cdot t^{t}\cdot v^{v}\cdot\alpha^{\alpha}\cdot K^{K}\cdot C^{C}\cdot\sigma^{\sigma}\cdot e^{e}\\&\quad=[L]^{\ell}[L]^{\delta}[L^2]^{A}[L^{-3}M]^{\rho}[L^{-1}MT^{-2}]^{E}[LMT^{-2}]^{F}[L^4]^{I}[T]^{t}[LT^{-1}]^{v}[LT^{-2}]^{\alpha}\,,\\&*\,[MT^{-2}]^{K}[MT^{-1}]^{C}[L^{-1}MT^{-2}]^{\sigma}\\&\quad=[L^{\ell+\delta+2A-3\rho-E-F+4I+v-\alpha-\sigma}\cdot M^{\rho+E+F-K+C+\sigma}\cdot T^{-2E-2F+t-v-2\alpha-2K-C-2\sigma}]\,.\end{aligned} \tag{2.8}$$

Table 2.1 Dimension of mechanical quantities

Quantity	Variable	Dimensional form (Absolute system)		
Length	ℓ	L		
Displacement	δ	L		
Area	A	L^2		
Density	ρ	L^{-3}	M	
Young' s modulus	E	L^{-1}	M	T^{-2}
Force	F	L	M	T^{-2}
Moment of inertia	I	L^4		
Time	t			T
Velocity	v	L		T^{-1}
Acceleration	α	L		T^{-2}
Spring constant	K		M	T^{-2}
Damping coefficient	C		M	T^{-1}
Stress	σ	L^{-1}	M	T^{-2}
Cofficient of restitution	e	Dimensionless		

L : lenth
M : mass
T : time

For this term to be dimensionless, the following conditions must be satisfied

$$\left.\begin{aligned} &\ell+\delta+2A-3\rho-E+F+4I+v+\alpha-\sigma=0\,, \\ &\rho+E+F+K+C+\sigma=0\,, \\ &-2E-2F+t-v-2\alpha-2K-C-2\sigma=0\,. \end{aligned}\right\} \tag{2.9}$$

Now, dimensionless π factors, $\pi_1 \sim \pi_{11}$ are derived from solving Eq. (2.9).
Rearrage Eq. (2.9)

$$\left.\begin{aligned} &\ell-E-3\rho=-\delta-2A-F-4I-v-\alpha+\sigma\,, \\ &E+\rho=-F-K-C-\sigma\,, \\ &-2E=2F-t-v+2\alpha+2K+C+2\sigma\,. \end{aligned}\right\} \tag{2.10}$$

Assuming δ is untity and other terms are zero on the right side of Eq. (2.10), we obtain

$$\ell=-1,\ E=0,\ \rho=0,$$

the π_1 term becomes

$$\pi_1=\frac{\delta}{\ell}\,.$$

Similarly, the $\pi_2 \sim \pi_{11}$ terms become

$$\pi_2=\frac{v^2\rho}{E}\,,$$

$$\pi_3=\frac{\alpha\ell\rho}{E}\,,$$

$$\pi_4=\frac{\sigma}{E}\,,$$

$$\pi_5=\frac{C^2}{\ell^4 E\rho}\,,$$

$$\pi_6=\frac{A}{\ell^2}\,, \tag{2.11}$$

$$\pi_7=\frac{I}{\ell^4},$$

$$\pi_8=\frac{F}{E\ell^2},$$

$$\pi_9=\frac{t^2E}{\ell^2\rho},$$

$$\pi_{10}=\frac{K}{\ell E},$$

$$\pi_{11}=e.$$

The original variables can be grouped in any way desired so that the π terms are dimensionless and independent.

We obtain similarity laws from eqs. (2.4), (2.6) and (2.11) (see Table 2.2).

$$\left.\begin{aligned}
&\frac{\delta_m}{\ell_m}=\frac{\delta_p}{\ell_p} \text{ or } \frac{\delta_p}{\delta_m}=\frac{\ell_p}{\ell_m}=\lambda && \text{; length scale}\\
&\frac{v_m^2\rho_m}{E_m}=\frac{v_p^2\rho_p}{E_p} \text{ or } \frac{v_p}{v_m}=\sqrt{\frac{E_p}{E_m}\cdot\frac{\rho_m}{\rho_p}} && \text{; velocity scale}\\
&\frac{\alpha_m\ell_m\rho_m}{E_m}=\frac{\alpha_p\ell_p\rho_p}{E_p} \text{ or } \frac{\alpha_p}{\alpha_m}=\frac{1}{\lambda}\cdot\frac{E_p}{E_m}\cdot\frac{\rho_m}{\rho_p} && \text{; acceleration scale}
\end{aligned}\right\} \quad (2.12)$$

$$\left.\begin{aligned}
&\frac{\sigma_m}{E_m}=\frac{\sigma_p}{E_p} \text{ or } \frac{\sigma_p}{\sigma_m}=\frac{E_p}{E_m} && \text{; stress scale}\\
&\frac{C_m^2}{\ell_m^4E_m\rho_m}=\frac{C_p^2}{\ell_p^4E_p\sigma_p} \text{ or } \frac{C_p}{C_m}=\lambda^2\sqrt{\frac{E_p}{E_m}\cdot\frac{\rho_p}{\rho_m}} && \text{; damping scale}\\
&\frac{A_m}{\ell_m^2}=\frac{A_p}{\ell_p^2} \text{ or } \frac{A_p}{A_m}=\lambda^2 && \text{; area scale}\\
&\frac{I_m}{\ell_m^4}=\frac{I_p}{\ell_p^4} \text{ or } \frac{I_p}{I_m}=\lambda^4 && \text{; moment of inertia scale}\\
&\frac{F_m}{E_m\ell_m^2}=\frac{F_p}{E_p\ell_p^2} \text{ or } \frac{F_p}{F_m}=\lambda^2\frac{E_p}{E_m} && \text{; force scale}\\
&\frac{t_m^2E_m}{\ell_m^2\rho_m}=\frac{t_p^2E_p}{\ell_p^2\rho_p} \text{ or } \frac{t_p}{t_m}=\lambda\sqrt{\frac{E_m}{E_p}\cdot\frac{\rho_m}{\rho_p}} && \text{; time scale}\\
&\frac{K_m}{\ell_mE_m}=\frac{K_p}{\ell_pE_p} \text{ or } \frac{K_p}{K_m}=\lambda\frac{E_p}{E_m} && \text{; stiffness scale}\\
&\frac{e_p}{e_m}=1 && \text{; restitution scale}
\end{aligned}\right\} \quad (2.13)$$

From the results of a seismic experiment with a scale model, response values in the real core can be predicted in the two ways as shown in Fig. 2.1. One is application of similarity laws to the experimental results, while another is the use of a computer program, which is verified on the basis of the model experiment. Similarity laws are necessary in the former case.

2.2 Collision test

For the seismic simulation analysis of column behavior including impacts, it is necessary to make clear the coefficient of restitution and contact duration in an impact. Collision tests between two hexagonal blocks have been performed. The test objectives were as follows:

(1) determine relationshhp of the coefficient of restitution to block impact velocity, and

(2) provide data in terms of the contact duration as function of block impact velocity.

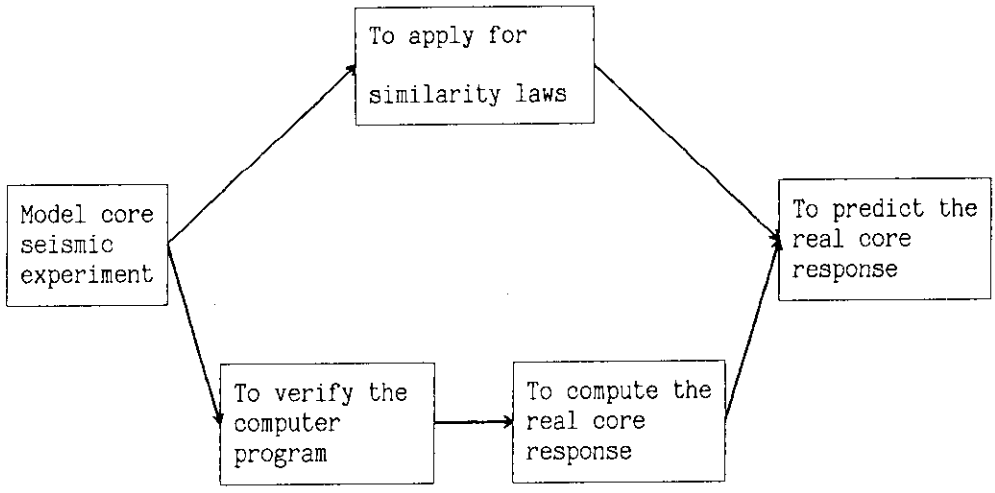

Fig. 2.1 Flow sheet for prediction method of real core response from model core seismic experiment

The objectives were achieved through pendulum collision tests. All collisions were flat-on collisions. The pendulum tests consisted of the impact of one block moving toward another stationary block. The velocites just prior to impact ranged from 10 to 200 cm/s. These are expected values of the fuel block impact velocity for HTGR core seismic design condition.

The pendulum test rig is shown in Fig. 2.2. Since the support of the graphite block was made of wire, its weight and rotary inertia were small compared with that of the graphite blocks. Bearings were used at the pivot points. Friction loss was negligible.

The eddy current displacement detector was used. This signal was used to get impact and rebound velocities of blocks. The coefficient of resitution is calculated from the ratio of post and pre-impact velocities.

$$e=\frac{\dot{x}_{i1}-\dot{x}_{j1}}{\dot{x}_{i0}-\dot{x}_{j0}} \tag{2.14}$$

e : the coefficient of restitution

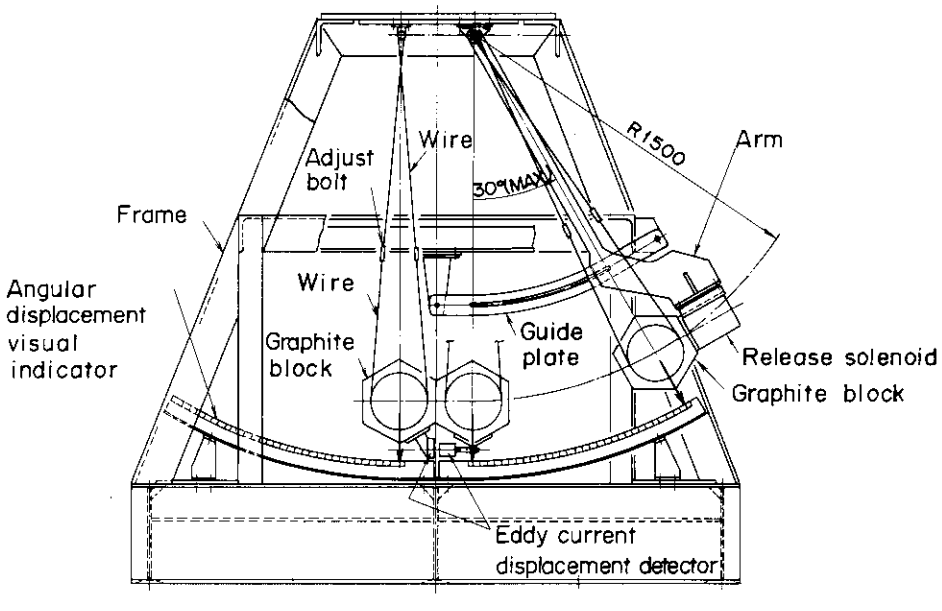

Fig. 2.2 Graphite block pendulum collision test rig

$\dot{x}_{i0}$: mass i velocity before impact
$\dot{x}_{j0}$: mass j velocity before impact
$\dot{x}_{i1}$: mass i velocity after impact
$\dot{x}_{j1}$: mass j velocity after impact

The coefficient of restitutions as function of impact velocity for the two blocks collision tests are shown in Fig. 2.3. In the figure, data for both cases of graphite blocks and attached mass (lead cylinder) blocks are shown. With the linear least square line characterizing the data points, with the exception of a few points moderately scattered, the coefficient of restitution slightly decreases with impact velocity. The values of the coefficient of restitution for the attached mass block are lower than for the graphite block alone. The reason is that damping between for graphite block and lead cylinder could have contributed to an energy loss. This loss was incorporated into the estimate of the coefficient of restitution.

The contact duration was measured from wave form of impact accelration of the pendulum collision test. The contact time as function of impact velocity are shown in Fig. 2.4. In the figure, data for both

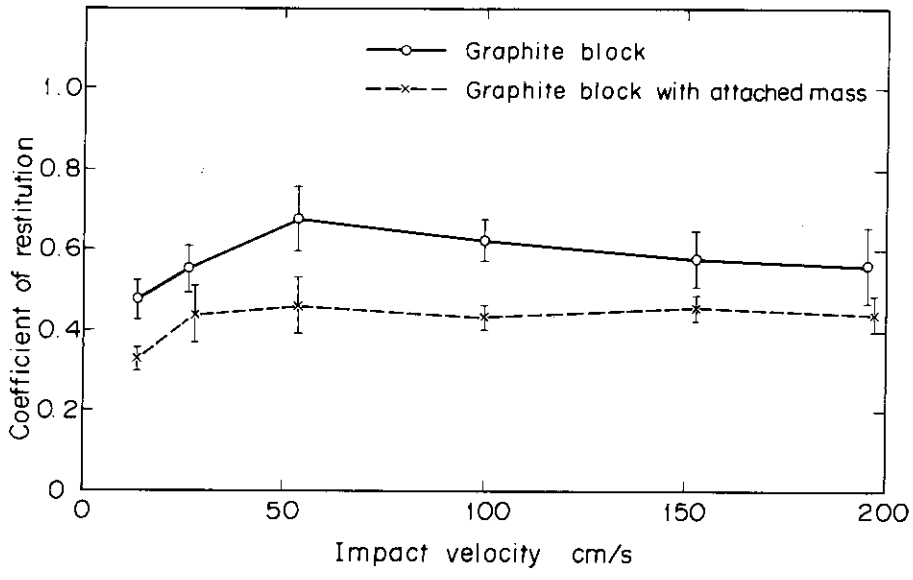

Fig. 2.3 Coefficient of restitution vs. impact velocity for one-half scale hexagonal block.

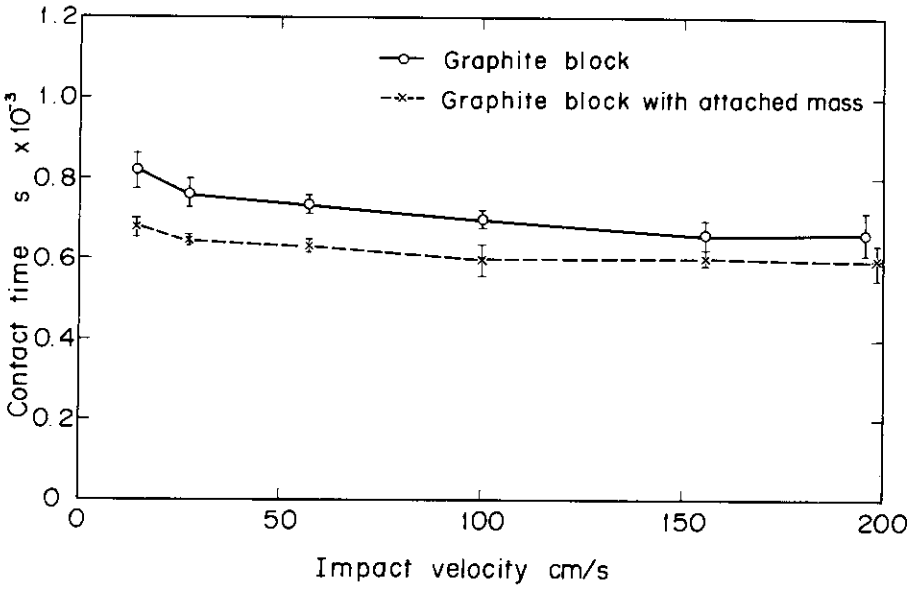

Fig. 2.4 Contact time vs. impact velocity for one-half scale hexagonal block.

Table 2.2 Scaling factor of the model

Physical quantity	Dimension		Scaling laws	Scaling factor under $\frac{E_p}{E_m}=1, \frac{\rho_p}{\rho_m}=\frac{1}{2}, \lambda=2$
Length	ℓ	(m)	$\ell_p=\lambda\ell_m$	$\ell_p=2\ell_m$
Displacement	x	(m)	$x=\lambda x_m$	$x_p=2x_m$
Velocity	v	(m/s)	$v_p=\sqrt{\frac{E_p}{E_m}\cdot\frac{\rho_m}{\rho_p}}\,v_m$	$v_p=\sqrt{2}v_m$
Acceleration	α	(m/s^2)	$\alpha_p=\frac{1}{\lambda}\cdot\frac{E_p}{E_m}\cdot\frac{\rho_m}{\rho_p}\alpha_m$	$\alpha_p=\alpha_m$
Stress	σ	(kN/m^2)	$\sigma_p=\frac{E_p}{E_m}\sigma_m$	$\sigma_p=\sigma_m$
Damping	C	(kN • s/m)	$C_p=\lambda^2\sqrt{\frac{E_p}{E_m}\cdot\frac{\rho_p}{\rho_m}}\,C_m$	$C_p=2\sqrt{2}C_m$
Force	F	(kN)	$F_p=\lambda^2\frac{E_p}{E_m}F_m$	$F_p=4F_m$
Time	t	(s)	$t_p=\sqrt{\frac{E_m}{E_p}\cdot\frac{\rho_m}{\rho_p}}\,t_m$	$t_p=\sqrt{2}t_m$
Stiffness	K	(kN/m)	$K_p=\lambda\frac{E_p}{E_m}K_m$	$K_p=2K_m$
Coefficient of restitution	e	(−)	$e_p=e_m$	$e_p=e_m$
Freqxency	f	(1/s)	$f_p=\frac{1}{\lambda}\sqrt{\frac{E_p}{E_m}\cdot\frac{\rho_m}{\rho_p}}\,f_m$	$f_p=\frac{1}{\sqrt{2}}f_m$
Mass	m	(kg)	$m_p=\lambda^3\frac{\rho_p}{\rho_m}m_m$	$m_p=4m_m$

suffix m : model
p : prototype
λ : scale factor

cases of graphite blocks and attached mass blocks are shown. Both test data shows a decreasing trend with increasing values of impact velocity. The values of the contact duration for the attached mass block are lower than for the graphit block alone. The reason is that stiffness of the attached mass block is higher than that of the graphite block.

2.3 Concluding remarks

(1) The similarity laws in which the acceleration of gravity on rocking vibration is indentical were derived.

(2) The coefficient of restitution is about 0.6 and the contact duration is about 0.7 milli-seconds. Both values slightly decrease with impact velocities.

3. Two-dimensional Column Response Characteristics

3.1 Introduction

Nonlinear vibration behavior due to block rocking and impact is a important aspect of the block-type fuel HTGR core. To reveal the effects of block rocking and impact on the column vibration characteristics, vibration tests have been performed with a single stacked column which is a fundamental element of the HTGR core structure.

The test objectives were as follows :

(1) to examine column dynamic behavior and impact response characteristics,

(2) to develop mathematical models and computer programs on the basis of test results obtained, and

(3) to provide preliminary design data for HTGR core structures by using the model scaling laws.

3.2 Experimental apparatus and method

3.2.1 Experimental apparatus

As shown in Photo. 3.1, a single stacked column was used. The column consisted of twelve hexagonal graphite blocks and one steel block all of the same shape, totalling thirteen layered blocks. The column was set to a support frame and stood by itself slightly apart from two side impact plates. The width of the gaps between the column and the side impact plates were changed by means of support bolts of the impact plates. In this way, dependences of motion of the column and their impact characteristics, on the gap

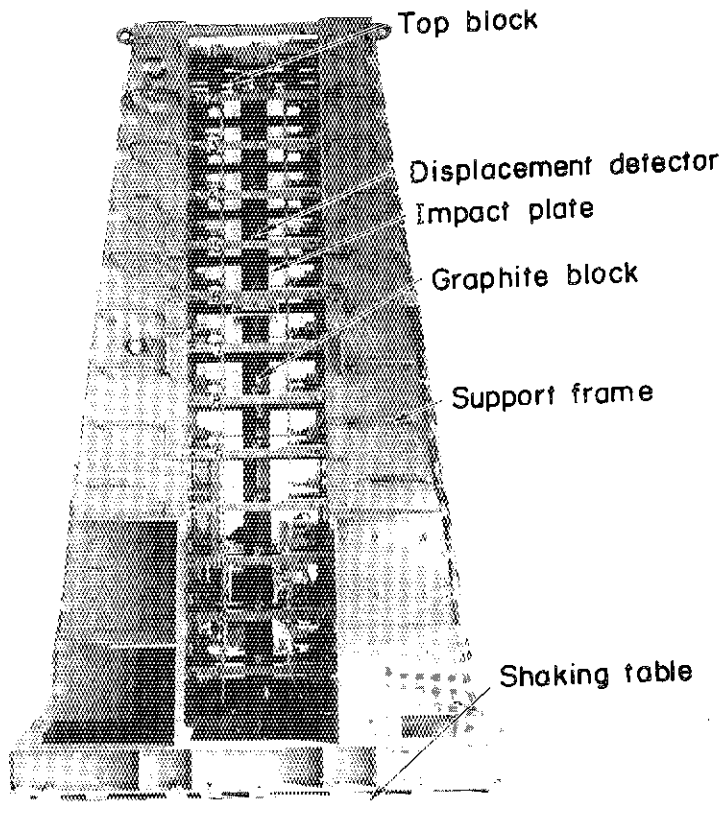

Photo. 3.1 External appearance of one stacked column model

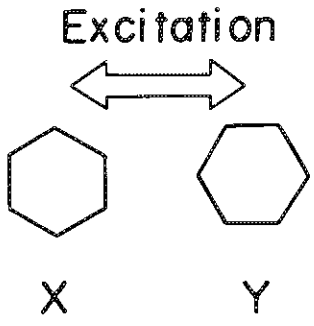

Fig. 3.1 Block direction against excitation

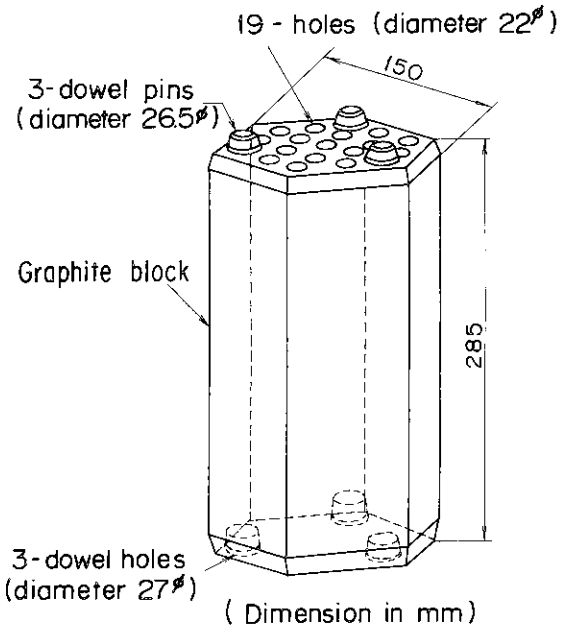

Fig. 3.2 Graphite fuel block

width, were examined. As indicated in Fig. 3.1, excitations (shaking) of the column were in two alternative directions, at right angles to each other. The vibration characteristics of the column, depending on excitation direction, were thus examined. Two different impact plates were provided for the above purpose, i. e. flat type and V-shaped groove type. The support frame was a steel box type, having sufficient rigidity (primary natural frequency 18 Hz) . The frame within the column was fixed on a shaking table.

The graphite fuel blocks, as shown in Fig. 3.2, were hexagonal prisms, 150mm in width between sides and 285 mm in length. Material was a nuclear-grade graphite. In each block, there were three dowels on the top and three dowel holes on the bottom, for longitudinal connection of respective blocks. Therefore, in the column, horizontal displacement between layered block is restrained, but block rocking in vertical plane is permitted. This arrangement is also similar in a bottm block. The graphite blocks were dimension scaled by 1/2 and weight scaled by 1/8 of the real fuel blocks of the experimental HTGR.

Measurements were made of displacements between the blocks and the support frame, and horizontal and vertical impact accelerations between blocks. The displacement detectors used were differential

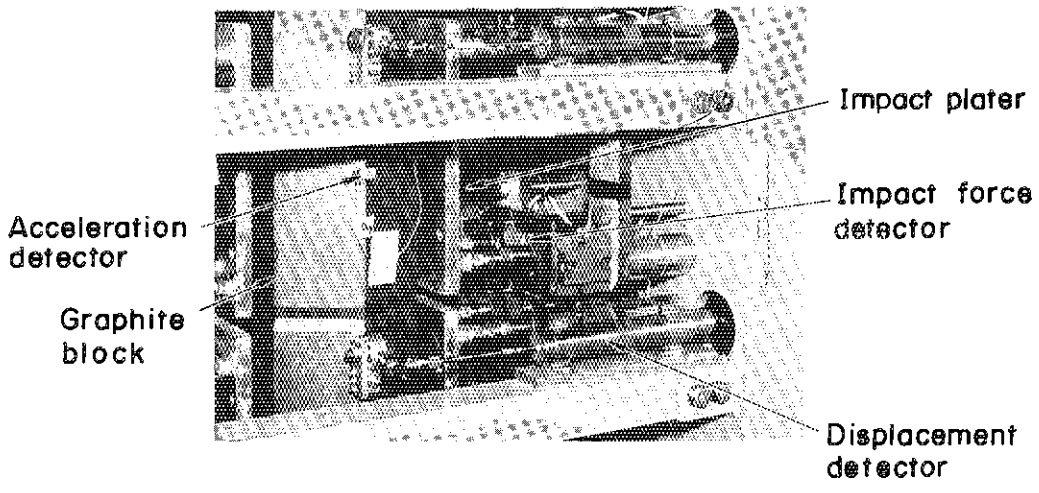

Photo. 3.2 Instrumentation

transformer and sliding resistance types. To measure the impact reaction forces, strain gauges were set on the support bolts of the impact plate. The impact accelerometer used was piezoelectric type. In order to record the excitation condions. strain gauge type accelerometers were set on the support frame and the shaking table. A detailed view of the instruments is shown in Photo. 3.2

3.2.2 Experimental method

Uni-axial horizontal excitation tests were made on the single stacked column on the shaking table. Excitation conditions were ranging in frequency from 0.8 to 15Hz, acceleration from 100 to 900 Gal, constant excitation amplitude from 1.5 to 25 mm, gaps between column and impact plates 5, 15, 25, and 100 mm except the top block, and two alternative excitation directions. Sinusoidal waves, response waves from earthquakes such as the El Centrol 1940 NS, Taft 1950 EW and Ibaragi (Japan) 1964 EW and beat waves were used to vibrate the shaking table horizontally. According to the similarity laws, the time scale was reduced by $1/\sqrt{2}$.

The effects of varying gap width, excitation frequency and acceleration, and excitation direction were then examined on column motion and impact characteristics.

3.3 Results and discussions

3.3.1 Vibration characteristics

(1) Displacement characteristics

The column displacement characteristics are shown in Fig. 3.3 at constant excitation amplitudes. With an increase of the excitation amplitude, the frequency for rapid rise of displacements, i. e. the jump -up frequency shifts to a lower frequency. These are the nonlinear spring characteristics due to block rocking and frictional force, i. e. tke column soft spring characteristics.

(2) Comparison between frequency sweep-up and sweep-down

Figure 3.4 shows the displacement characteristics for increasing i. e. sweep-up and decreasing i. e. sweep-down of excitation frequency at a constant input acceleration. The jump-up frequency for rapid rise of displacement is higher in sweep-up than in sweep-down. As shown in Fig. 3.4, there is a hysteresis with a leap at low input frequency due to the column softening characteristics.

(3) Effect of excitation direction

The displacement is slightly higer for a Y than for an X excitation directions.

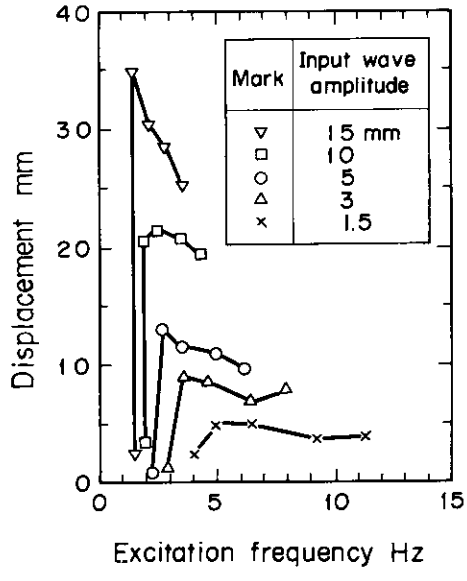

Fig. 3.3 Displacement characteristics

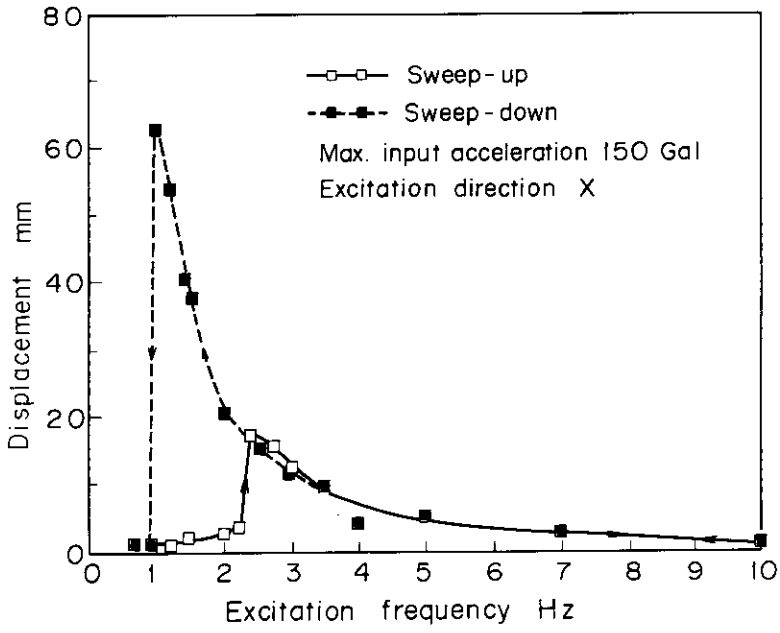

Fig. 3.4 Comparison between sweep-up and sweep-down response on displacement

Table 3.1 Column damping factor

Excitation direction	Top block gap(mm)	Damping factor (percent of critical damping)		
		Max. displacement of step wave input (mm)		
		15	30	60
X	0	30	27	34
X	10	—	—	36
Y	0	29	29	37

(4) Effect of top gap width

The jump-up frequency of the column displacements shifts to a lower frequency with a large gap of the top block compared with having a small gap. An increase in the top gap pushes the maximum displacement point of the column upward and causes subharmonic vibration.

(5) Damping factor of column

Step waves were used to estimate the damping factor of the column. Table 3.1 shows the damping factor of the column. It is seen that the damping factor increases with increasing displacement.

3.3.2 Impact characteristics

(1) Effect of input acceleration level

In Fig. 3.5 the impact forces as function of input acceleration levels are shown. It is seen that increasing the input acceleration level causes the resonant frequency to shift to an higher frequency, the impcat forces to increase, and the frequency for rapid drop of the impact forces i. e. the jump-down frequency to increase. These are the nonlinear spring characteristics due to column impacts, i. e. tke hardening characteristics.

(2) Effect of gap width

Figure 3.6 shows relationship between excitation frequency and impact velocity, and relationship

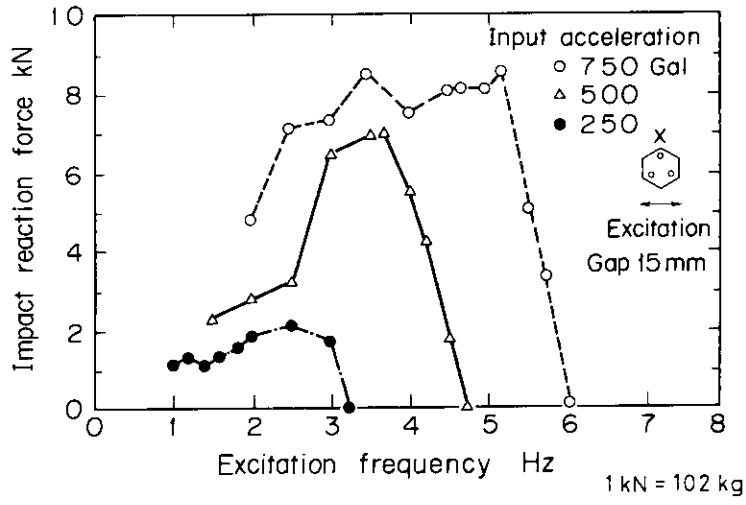

Fig. 3.5 Effect of input wave frequency and acceleration level on impact responce

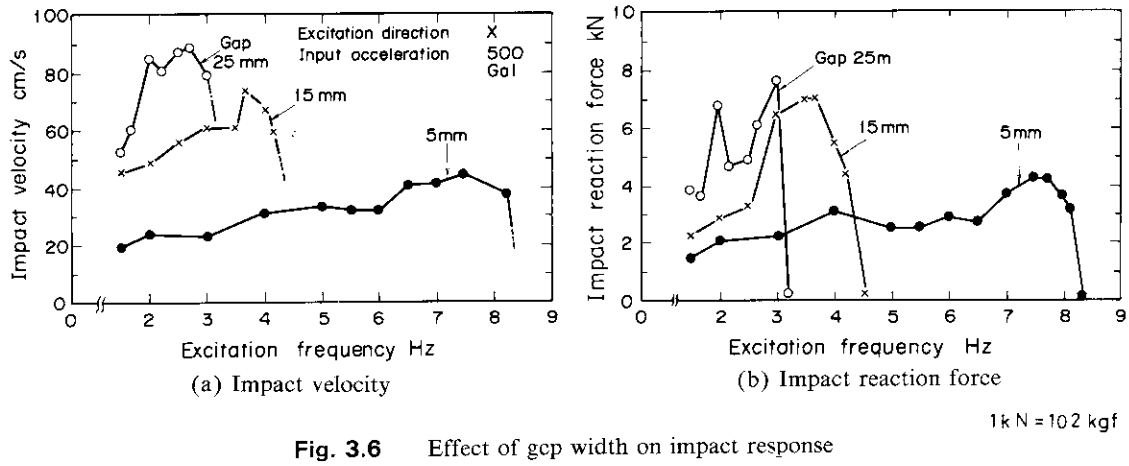

Fig. 3.6 Effect of gcp width on impact response

between excitation frequency and impact force both with gap width parameter varying. It is seen that impact velocity and impact force (also acceleration) have the same trend as excitation frequency is varied.

An increase of the gap width causes both the jump-up and jump-down frequencies of the impact forces to shift to lower frequencies. The range of impact frequency gets smaller with increacsing gap width. The impact forces increase with increasing gap width. This is because the velocity of the block prior to an impact increases with gap width. This situation may be explained in detail as follows.

The impact velocity depends on relative velocity of the boundary and block. This then varies with phase at the time of an impact between the boundary and block. The phase is defined as θ in Fig. 3.7 (a) . The displacement between the boundary and block during a half cycle of the sinusoidal wave in absolute coordinates is shown in the figure. As may be seen in this figure under a constant excitation foequency, with an increase in the gap width, the phase, θ, at the time of an impact increases. The impact velocity also increases, as seen in Fig. 3.7 (b) .

In excitation under constant input acceleration, excitation amplitude and excitation velocity are inversely proportional to square of excitation frequency and excitation frequency, respectively. Hence, with an increase in excitation frequency, response displacement and velocity of the block decrease. Therefore, beyond a certain level of excitation frequency, the response displacement of the block is smaller than the gap width, so that impact no longer occurs. With an increase in the gap width, the limiting frequency causing an impact thus decreases. At low excitation frequency, since the gap width is small relative to displacement amplitude of the boundary (equal to the excitation displacement) , the phase at

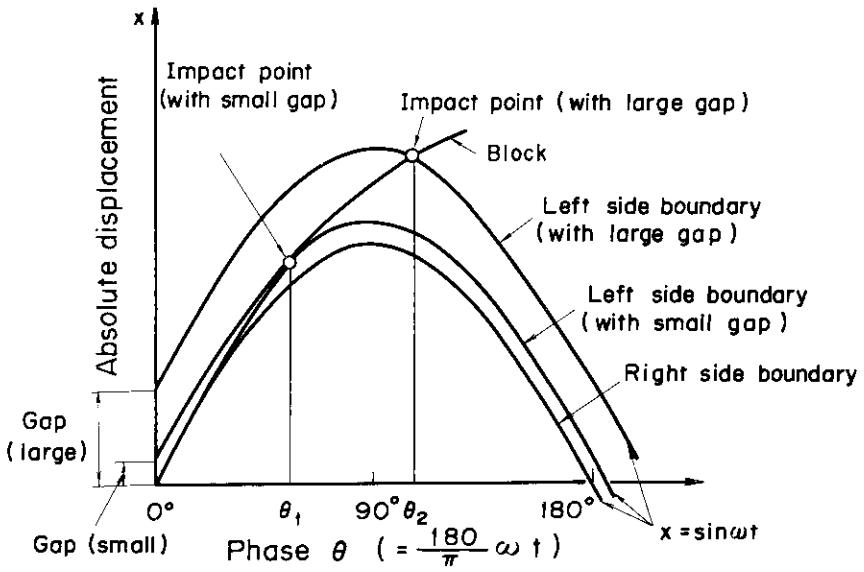

(a) Absolute displacement

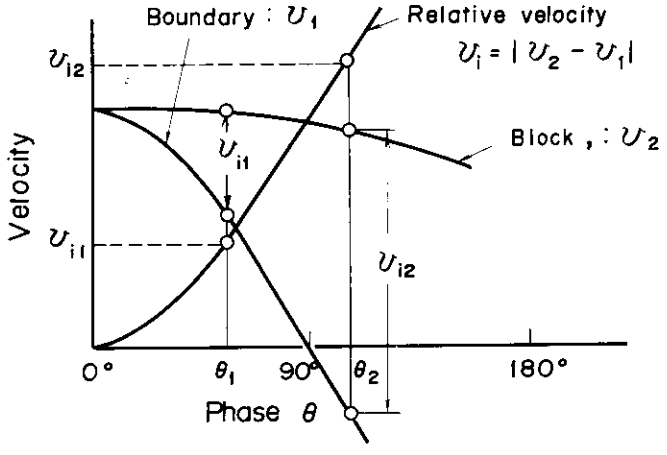

(b) Velocity

Fig. 3.7 Motion of Block and boundary

the time of an impact is small. With an increase in excitation frequency, the displacement amplitude of the boundary decreases. Since this is equivalent to a relative increase in the gap width, an increase of phase at the time of an impact results. Impact velocity, therefore, increases with increasing excitation frequency, and becomes a maximum in the vicinity of the limiting excitation frequency. Impact force, in relation to impact velocity, shows a similar tendency.

(3) Differences with column excitation direction

At input accelerations over 500 Gal, the impact velocities, impact forces and impact accelerations are smaller for the Y-direction excitation than for the X-eirection eucitation. this is possibly because for the Y-direction excitation the whirling is large compared with the case of the X-direction excitation. Therefore impacts of the blocks occur by sliding along one side of V-shaped groove plates. The impact values are thus reduced by an amount of momentum consumed in sliding friction. At input accelerations of 500 Gal and above, however, no significant differences are observed.

(4) Statistical distribution of maximum impact force

In the experimental results described thus far, scattering of impact forces occur even in the case of sinusoidal wave exitations considered as steady vibrations. In order to examine the extent of scattering, maximum force, mean force, standard deviation and coefficient of variation were obtained. In Table 3.2

Table 3.2 Histograms of impact reaction force

Excitation frequency Hz			2.5	3.5	5.0
Block No.			No.9		
Impact reaction force	max. value	kN	8.06	9.25	8.89
	mean value	kN	6.67	5.78	4.84
	standard deviation	kN	1.35	1.64	1.45
	variation factor	%	20	28	30
Histograms			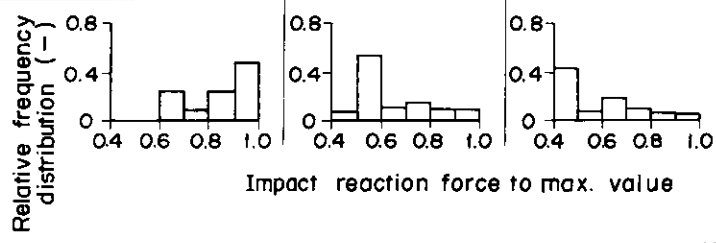		

Note (1) Max. input acceleration 750 Gal 1kN=102kgf
(2) Gap width 15mm

a statistical distribution of the impact forces for an input accleration 750 Gal, X-direction excitation, gap width between column and impact plates of 15 mm and gap width at column top of 0 mm is shown.

It is seen that in the vicinity of an excitation frequency causing 'maximum' impact force, the frequency of a maximum occurring is small, and occurrence is spontaneous. On the other hand, at an excitation frequency away from the 'maximum' frequency, causing a lower impact force (2.5 Hz in Table 3.2) , the frequency of a maximum occurring is large, and it occurs respeatedly. The spontaneous nature is accentuated at high input accelerations (large impact forces) . The above may be partly due to the fact that under excitation conditions where the impact becomes violent and impact mode varies due to the rotation of the block and whirling of the column.

3.3.3 Random wave response

The response characteristics of the column to seismic waves and beat waves were observed for comparison with that of sinusoidal waves. In Fig. 3.8, maximum impact velocity and force versus input acceleration for excitations by seismic, beat and sinusoidal waves are shown. It can be seen that the impact velocity and force have the same trend as input acceleration is varied. Since there is no impact for a low input acceleration, the impact values are zero. Beyond a certain input acceleration level, an impact occurs. The impact values then increase almost proportionally with input acceleration levels. The figure also compares impact forces with various excitation waves, i. e. sinusoidal waves, earthquake waves and beat waves. The maximum impact response values for earthquake waves are about 40 to 75% of those for sinusoidal waves. The maximum impact response for the beat waves are tke same as that for sinusoidal waves.

3.3.4 Core seismic response

(1) Effect of excitation direction

As already described on section 3.3.2, the impact forces become a mauimum when there is a seismic force in a direction such that impacts are between the sides of hexagonal blocks (i. e. in the X-direction) . The impact forces then become a minimum where a seismic force is in such a direction that impact is between V-shaped surfcaces (i. e. in the Y-direction) . In an intermediate direction between the two, the values are intermediate. Therefore, by considering the maximum impact values in the X-direction in the HTGR core design, the results will be the most conservative, compared with all other directions.

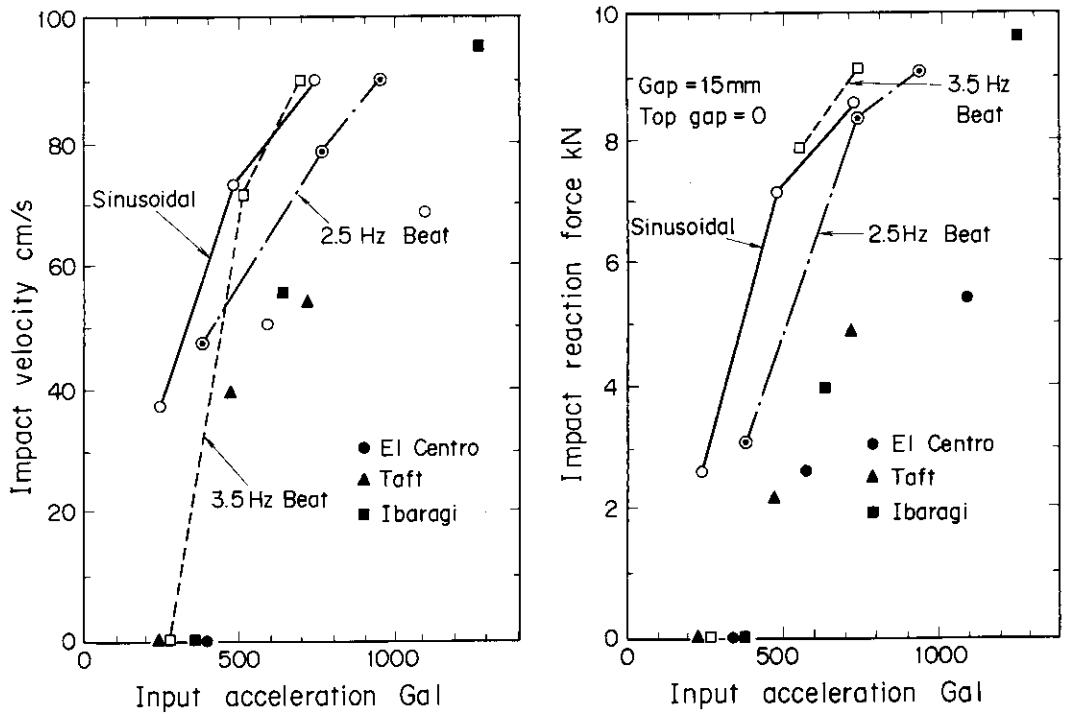

(a) Impact velocity

(b) Impact reaction force
1kN = 102kgf

Fig. 3.8 Effect of input wave on impact response

(2) Gap width at column top

As evident in section 3.3.1, by reducing the gap width at the column top, the column behaves in vibration as a beam supported at both ends. Compared tith a case of large gap width, the resonant frequency becomes high and the displacements of the column become small. Therefore, in the design of the HTGR core, reducing the top gap width as much as possible or restraining the column top while considering the requirements in construction and fuel exchange, will raise its aseismicity.

(3) Compressive force from column top

The downward force from the top to the bottom of the column due to such as a gas pressure difference increases apparent rigidity of the column. Therefore the column resonant frequency is increased and the displacements of the column are decreased.

3.4 Concluding remarks

Vibration tests were carried out on a single stacked blocks column which is a fundamental core elment of the block-type fuels HTGR. The vibration characteristics of the single stacked column was examined. The following were revealed by the vibration tests.

(1) The column resonant frequency decreases with excitation amplitude. The jump-up frequency of the column displacements is higher in sweep-up than in sweep-down. The column has a nonlinear resonance and exhibits a hysterisis response with jump points. These are the column softening charactersitics due to column rocking, interface friction between blocks and loose dowel connections. The column displacements also increase with increasing excitation levels.

(2) With an increase of the input acceleration, resonant frequency shifts to a higher frequency and the impact forces increase. Nonlinear hardening characteristics due to block impact are exhibited.

(3) By increasing a gap width, both jump-up and jump-down frequencies of the impact forces shift

to lower frequencies. The range of impact frequency gets smaller with increasing gap width. The impact forces rise with increasing gap width.

(4) The top block gap has effects on the column displacement mode. Increasing the top gap pushes the maximum displacement point of the column upwards and makes the motion more unstable.

(5) The effects of excitation direction on the resonant frequency are almost negligble, but a change in excitation direction results in a slight change of the displacements and impact forces.

(6) The column damping factor is about 30% of the critical factor. It increases slightly with increasing displacement amplitude.

(7) The maxium response of the column for seismic waves is about 40 to 75% of that for sinusoidal waves.

4. Seismic Analysis Method for a Single Stacked Column

4.1 Introduction

Excat modeling of the complete three-dimensional core array is not possible because of computational cost. It is realized however, that reasonable tools are needed; i. e. analytical methods and computer programs, which are conducted in parallel with experiments. The methods and computer programs can be verified and revised from experimental data. Then, the cmputer programs can be used for design purposes.

Since such a sytem of blocks dose not constitute a structure in the usual sense, existing structural theory and experimental data cannot be directly applied. Several special analytical methods have been developed for analysis of this unique system.

The analytical method presented in this Chapter takes into account the complex nonlinear vibration associated with multiple collisions and, in addition, the frictional forces between the block interfaces and between the dowel pins and their mating holes are accounted for. The method is applied to a column of blocks and the results obtained from the analysis are compared to results obtained from experiments. In the real core, the blocks and columns extend three-dimensionally. In the present study, the following two dimensional model is considered:

(1) each block is modeled as a rigid body,
(2) each block has three degrees-of-freedom, two translational displacements and one rotation around the block center of gravity,
(3) impact forces are represented by a spring and dashpot model located at impact points of each block,
(4) dowels are represented as deformable members and the slipping on interfaces between dowel pins and holes is allowed. and
(5) friction forces are calculated at horizontal interfaces between blocks.

4.2 Calculation equation

4.2.1 Equation governing motion

The forces involved in the analysis of a single stacked column of the HTGR core constrained within rigid boundaries are as shown in Fig. 4.1 (a) and 4.2.

Let the coordinate system by chosen as shown in Fig. 4.1 (b) . Each block has two translational coordinates, u and w, and one rotational coordinate θ. Figure 4.1 (b) shows the forces that act upon an individual block. The equations of motion for the i-th block of the single column may be written as:

$$m_i\ddot{u}_i = F_i^{TL} + F_i^{TR} + F_i^{BL} + F_i^{BR} + F_i^{F} + F_{i+1}^{F} + F_i^{DL} + F_i^{DR} + F_{i+1}^{DL} + F_{i+1}^{DR} + C_i^{C}\dot{u}_i , \quad (4.1)$$

$$m_i\ddot{w}_i = F_i^{VL} + F_i^{VR} + F_{i+1}^{VL} + F_{i-1}^{VR} - \mu F_i^{DL} + \mu F_i^{DR} + \mu F_{i+1}^{DL} + \mu F_{i+1}^{DR} + W_i^{U} + W_i^{L} , \quad (4.2)$$

$$I_i\ddot{\theta}_i = M(F_i^{TL}) + M(F_i^{TR}) + M(F_i^{BL}) + M(F_i^{BR}) + M(F_i^{F}) + M(F_{i+1}^{F}) + M(F_i^{DL})$$

$$+ M(F_i^{DR}) - M(F_{i+1}^{DL}) + M(F_{i+1}^{DR}) - M(F_i^{VL}) - M(F_i^{VR}) + M(F_{i+1}^{VL}) + M(F_{i+1}^{VR})$$

$$+ M(\mu F_i^{DL}) + M(\mu F_i^{DR}) + M(\mu F_{i+1}^{DL}) + M(\mu F_{i+1}^{DR}) - M(W_i^{U}) + M(W_i^{L}) , \quad (4.3)$$

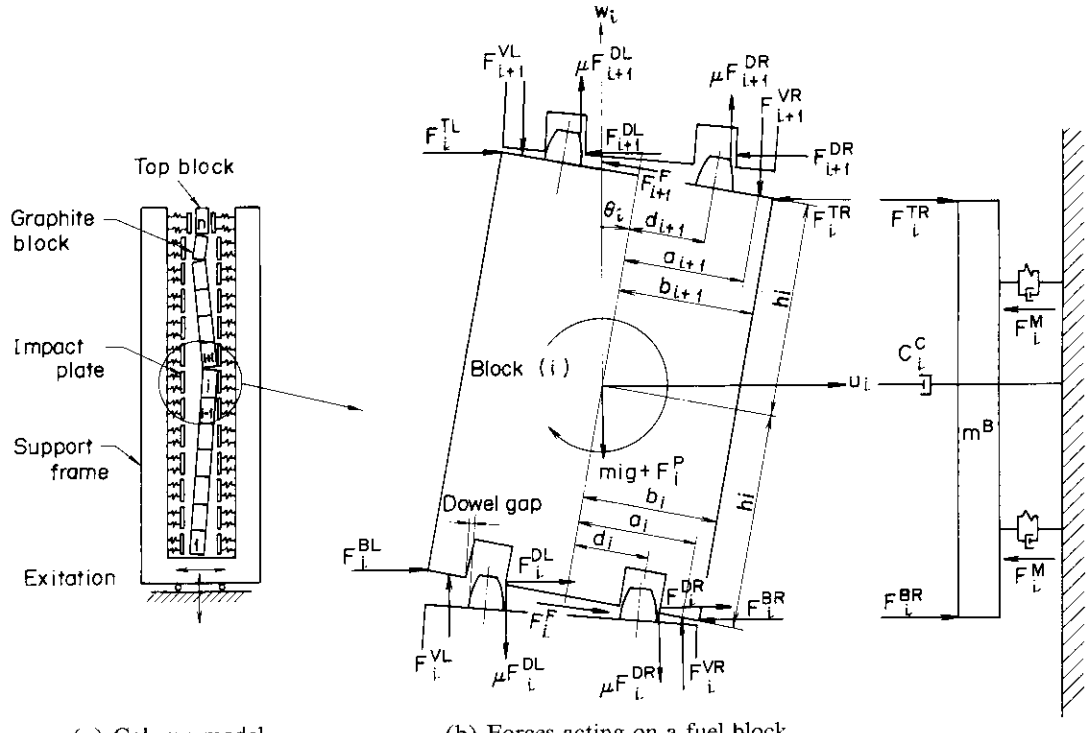

(a) Column model (b) Forces acting on a fuel block

Fig. 4.1 Column calculation model and forces acting on a fuel block

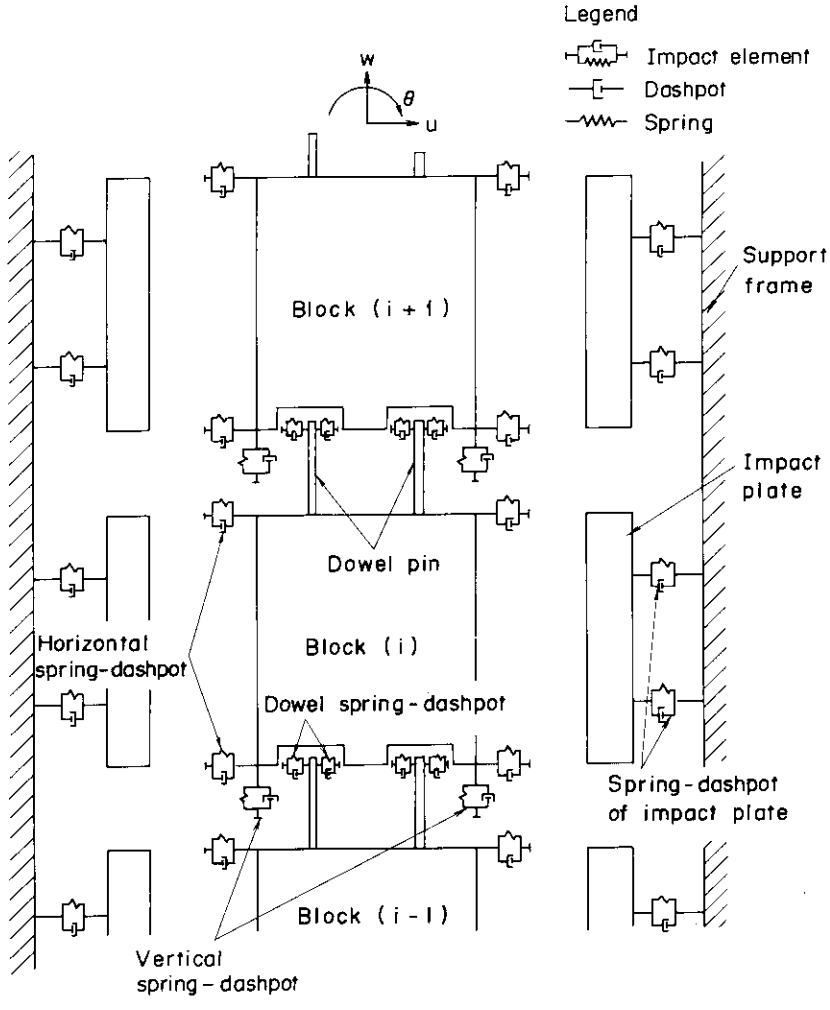

Fig. 4.2 Idealized spring–dashpot model

where, M(F) are moments caused by forces F. $W^U$and W^L are forces due to block weights and pressure differentials acting at the upper and lower parts of a block.

4.2.2 Friction force between blocks and its associated moment

The friction force due to surface sliding is represented by a nonlinear Coulomb element. The equations for the friction force F_i^F and its associated moment $M(F_i^F)$ acting on the i-th block, are as follows.

$$\left.\begin{aligned} F_i^F &= -\mathrm{sign}(v_i)F(v_i)\ , \\ M(F_i^F) &= F_i^F(-h_i\cos\theta_i - b_i\sin\theta_i)\ , \end{aligned}\right\} \tag{4.4}$$

and for the $i-1$ block

$$\left.\begin{aligned} F_{i-1}^F &= \mathrm{sign}(v_i)F(v_i)\ , \\ M(F_{i-1}^F) &= F_{i-1}^F(h_{i-1}\cos\theta_{i-1} - b_{i-1}\sin\theta_{i-1})\ , \end{aligned}\right\} \tag{4.5}$$

where

$$\begin{aligned} v_i = &\{\dot{u}_i - (h_i\cos\theta_i + b_i\sin\theta_i)\dot{\theta}_i\} \\ &- \{\dot{u}_{i-1} + (h_{i-1}\cos\theta_{i-1} - b_{i-1}\sin\theta_{i-1})\dot{\theta}_{i-1}\}\ . \end{aligned} \tag{4.6}$$

For $i=1$

$$v_1 = \dot{u}_1 - (h_1\cos\theta_1 + b_1\sin\theta_1)\dot{\theta}_1 - \dot{u}_0\ , \tag{4.7}$$

where u_i and $\dot{u}_i$ are the horizontal displacement and velocity of the center of gravity of the i-th block, respectively. $\dot{u}_0$ is the horizontal velocity of the support floor.

If sing $(\alpha_i) \leqq 0$, then

$$\left.\begin{aligned} F_i^F &= -\mathrm{sign}(v_i)\mathrm{F}(v_i)\ , \\ M(F_i^F) &= F_i^F(-h_i\cos\theta_i + b_i\sin\theta_i)\ , \end{aligned}\right\} \tag{4.8}$$

and for the $i-1$ block

$$\left.\begin{aligned} F_{i-1}^F &= \mathrm{sign}(v_i)F(v_i)\ , \\ M(F_{i-1}^F) &= F_{i-1}^F(h_{i-1}\cos\theta_{i-1} - b_{i-1}\sin\theta_{i-1})\ , \end{aligned}\right\} \tag{4.9}$$

where

$$\begin{aligned} v_i = &\{\dot{u}_i - (h_i\cos\theta_i - b_i\sin\theta_i)\dot{\theta}_i\} \\ &- \{\dot{u}_{i-1} + (h_{i-1}\cos\theta_{i-1}\cos\theta_{i-1} - b_i\sin\theta_{i-1})\dot{\theta}_{i-1}\}\ . \end{aligned} \tag{4.10}$$

For $i=1$

$$v_1 = \dot{u}_1 - (h_1\cos\theta_1 - b_1\sin\theta_1)\dot{\theta}_1 - \dot{u}_0\ , \tag{4.11}$$

where $\dot{u}_0$ is the horizontal velocity of the support floor. $\mathrm{F}(v_i)$ is a prescribed function for the friction characteristics which are related to the vertical contact force and the coefficients of both dynamical and statical frictions.

$$F(v_i) = F_i\{\mu_s + f(v_i) + f(v_i^2) + \mathrm{f}(v_i^3)\}\ , \tag{4.12}$$

and, the functions $\mathrm{f}(v_i, v_i^2, v_i^3)$ are related to the dynamical coefficient of friction μ_k. The vertical contact forces are obtained by summing blocks weights m_jg and the differential pressure of a unit block length, F_i^P.

$$F_i = \sum_{j-i}^{n} m_j g + F_i^P\ . \tag{4.13}$$

4.2.3 Vertical impact force and its associated moment

The forces acting on the interface between the i-th and the $i-1$ blocks as a result of impact are derived in term of deformation of each spring dashpot unit. When the gap is closing, the spring deformation γ_i and its time rate $\dot{\gamma}_i$ are

$$\gamma_i=\frac{1}{2}\{w_{i-1}-h_{i-1}(1-\cos\theta_{i-1})-a_i\sin\theta_{i-1}\}$$
$$-\frac{1}{2}\{w_i+h_i(1-\cos\theta_i)-a_i\sin\theta_i\}, \tag{4.14}$$

$$\dot{\gamma}_i=\frac{1}{2}\{\dot{w}_{i-1}-(h_{i-1}\sin\theta_{i-1}+a_i\cos\theta_{i-1})\dot{\theta}_{i-1}\}$$
$$-\frac{1}{2}\{\dot{w}_i+(h_i\sin\theta_i-a_i\cos\theta_i)\dot{\theta}_i\}. \tag{4.15}$$

For $i=1$

$$\gamma_1=\frac{1}{2}[w_0-\{w_1+h_1(1-\cos\theta_1)-a_1\sin\theta_1\}], \tag{4.16}$$

$$\dot{\gamma}_1=\frac{1}{2}[\dot{w}_0-\{\dot{w}_1+(h_1\sin\theta_1-a_1\cos\theta_1)\dot{\theta}_1\}], \tag{4.17}$$

whrer w_0 and $\dot{w}_0$ are the vertical displacement and velocity of the support floor, respectively. The vertical impact forces F_i^{VR} (or F_i^{VL}) and its associated moments $M(F_i^{VR})$ (or $M(F_i^{VL})$) acting on the i-th block are as follows.

If $\gamma_i>0$

$$\left.\begin{aligned}F_i^{VR}&=-K_i^V\gamma_i-C_i^V\dot{\gamma}_i,\\ M(F_i^{VR})&=-F_i^{VR}(h_i\sin\theta_i-a_i\cos\theta_i).\end{aligned}\right\} \tag{4.18}$$

For the $i-1$ block

$$\left.\begin{aligned}F_{i-1}^{VR}&=K_i^V\gamma_i+C_i^V\dot{\gamma}_i,\\ M(F_{i-1}^{VR})&=F_{i-1}^{VR}(h_{i-1}\sin\theta_{i-1}+a_i\cos\theta_{i-1}).\end{aligned}\right\} \tag{4.19}$$

When $\gamma_i\leqq 0$

$$\left.\begin{aligned}F_i^{VR}&=F_{i-1}^{VR}=0,\\ M(F_i^{VR})&=M(F_{i-1}^{VR})=0,\end{aligned}\right\} \tag{4.20}$$

where K_i^V and C_i^V are the vertical spring and damping coefficients, respectively, for a single unit. In the more general formulation, these quantities may be represented by a polynominal function.

$$\left.\begin{aligned}K_i^V&=\sum_{j=0}^{m}K_{ij}^V\gamma_i^j,\\ C_i^V&=\sum_{j=0}^{m}C_{ij}^V\dot{\gamma}_i^j.\end{aligned}\right\} \tag{4.21}$$

4.2.4 Boundary wall force and its associated moment

The forces acting on the i-th block as a result of impact on the boundary walls are derived by deformation of each spring dashpot unit which is located on the upper and lower, right and left-hand corners. During impact against the boundary wall on the upper right-hand corner the spring deformation ε_i and its time rate $\dot{\varepsilon}_i$ of the i-th block are

$$\varepsilon_i=u_i+h_i\sin\theta_i-b_i(1-\cos\theta_i)-u_i^B-\delta_i^B, \tag{4.22}$$

$$\dot{\varepsilon}_i=\dot{u}_i+(h_i\cos\theta_i-b_i\sin\theta_i)\dot{\theta}_i-\dot{u}_i^B, \tag{4.23}$$

where u_i^B is the lateral boundary displacement at the contact point and δ_i^B is the gap between the i–th block and its boundary wall. The boundary wall impact force F_i^{TR} and its associated moment $M(F_i^{TR})$ acting on the i–th block are as follows.

If $\varepsilon_i > 0$

$$\left.\begin{aligned} F_i^{TR} &= -\{K_i^B \varepsilon_i + C_i^B \dot{\varepsilon}_i\}, \\ M(T_i^{TR}) &= F_i^{TR}(h_i \cos\theta_i - b_i \sin\theta_i), \end{aligned}\right\} \tag{4.24}$$

where K_i^B and C_i^B are the boundary spring and damping coefficients, respectively and may be represented in the following general form.

$$\left.\begin{aligned} K_i^B &= \sum_{j=0}^{m} K_{ij}^B \varepsilon_i^j, \\ C_i^B &= \sum_{j=0}^{m} C_{ij}^B \dot{\varepsilon}_i^j. \end{aligned}\right\} \tag{4.25}$$

Similarly, on the upper left–hand corner

$$\varepsilon_i = -u_i - \{h_i \sin\theta_i - b_i(1-\cos\theta_i)\} + u_i^B - \delta_i^B, \tag{4.26}$$

$$\dot{\varepsilon}_i = -\dot{u}_i - (h_i \cos\theta_i + b_i \sin\theta_i)\dot{\theta}_i + \dot{u}_i^B, \tag{4.27}$$

if $\varepsilon_i > 0$

$$\left.\begin{aligned} F_i^{TL} &= K_i^B \varepsilon_i + C_i^B \dot{\varepsilon}_i, \\ M(F_i^{TL}) &= F_i^{TL}(h_i \cos\theta_i + b_i \sin\theta_i). \end{aligned}\right\} \tag{4.28}$$

On the lower right–hand corner

$$\varepsilon_i = u_i - \{h_i \sin\theta_i + b_i(1-\cos\theta_i)\} - u_i^B - \delta_i^B, \tag{4.29}$$

$$\dot{\varepsilon}_i = \dot{u}_i - (h_i \cos\theta_i + b_i \sin\theta_i)\dot{\theta}_i - \dot{u}_i^B, \tag{4.30}$$

if $\varepsilon_i > 0$

$$\left.\begin{aligned} F_i^{BR} &= -\{K_i^B \varepsilon_i + C_i^B \dot{\varepsilon}_i\}, \\ M(F_i^{BR}) &= -F_i^{BR}(h_i \cos\theta_i + b_i \sin\theta_i). \end{aligned}\right\} \tag{4.31}$$

On the lower left–hand corner

$$\varepsilon_i = -u_i + \{h_i \sin\theta_i - b_i(1-\cos\theta_i)\} + u_i^B - \delta_i^B, \tag{4.32}$$

$$\dot{\varepsilon}_i = -\dot{u}_i + (h_i \cos\theta_i - b_i \sin\theta_i)\dot{\theta}_i + \dot{u}_i^B, \tag{4.33}$$

if $\varepsilon_i > 0$

$$\left.\begin{aligned} F_i^{BL} &= -K_i^B \varepsilon_i + C_i^B \dot{\varepsilon}_i, \\ M(F_i^{BL}) &= -F_i^{BL}(h_i \cos\theta_i - b_i \sin\theta_i). \end{aligned}\right\} \tag{4.34}$$

When $\varepsilon_i \leq 0$

$$\left.\begin{aligned} F_i^{TR} &= F_i^{TL} = F_i^{BR} = F_i^{BL} = 0, \\ M(F_i^{TR}) &= M(F_i^{TL}) = M(F_i^{BR}) = M(F_i^{BL}) = 0. \end{aligned}\right\} \tag{4.35}$$

4.2.5 Dowel force in the horizontal direction and its associated moment

The dowel forces in the horizontal direction are derived from the contact condition between dowel pins and mating holes. When a dowel pin and its mating hole are in contact, the dowel spring deformation β_i and its time rate of deformation $\dot{\beta}_i$ for the i–th block interface are

$$\beta_i=\{u_{i-1}+h_{i-1}\sin\theta_{i-1}-d_{i-1}(1-\sin\theta_{i-1})\}-\{u_i-h_i\sin\theta_i-d_i(1-\cos\theta_i)\}\mp\delta_{R,L}\,, \tag{4.36}$$

$$\dot{\beta}_i=\dot{u}_{i-1}-(h_{i-1}\cos\theta_{i-1}-d_{i-1}\sin\theta_{i-1})\dot{\theta}_{i-1}-\{\dot{u}_i-(h_i\cos\theta_i+d_i\sin\theta_i)\dot{\theta}_i\}\,. \tag{4.37}$$

For $i=1$

$$\beta_1=u_0-\{u_1-h_1\sin\theta_1-d_1(1-\cos\theta_1)\}\mp\delta_{R,L}\,, \tag{4.38}$$

$$\dot{\beta}_1-\dot{u}_0-\{\dot{u}_1-(h_1\cos\theta_1+d_1\sin\theta_1)\dot{\theta}_1\}, \tag{4.39}$$

wkere δ_R and δ_L are the gap between dowel pin and hole on the right and left respectively. The dowel force F_i^{DR} and its associated moment $M(F_i^{DR})$ in the horizontal direction acting on the i-th right-hand dowel are as follows. If $\beta_i>0$ on the right gap and $\beta_i<0$ on the left gap

$$\left.\begin{aligned}&F_i^{DR}-K_i^D\beta_i+C_i^D\dot{\beta}_i\,,\\&M(F_i^{DR})=-F_i^{DR}(h_i\cos\theta_i+d_i\sin\theta_i)\,,\end{aligned}\right\} \tag{4.40}$$

for the $i-1$ block

$$\left.\begin{aligned}&F_{i-1}^{DR}=-K_i^D\beta_i-C_i^D\dot{\beta}_i\,,\\&M(F_{i-1}^{DR})=F_{i-1}^{DR}(h_{i-1}\cos\theta_{i-1}-d_i\sin\theta_{i-1})\,.\end{aligned}\right\} \tag{4.41}$$

If $\beta_i<0$ on the right gap and $\beta_i>0$ on the left gap

$$\left.\begin{aligned}&F_i^{DR}=F_{i-1}^{DR}=0\,,\\&M(F_i^{DR})=M(F_{i-1}^{DR})=0\,,\end{aligned}\right\} \tag{4.42}$$

where $K_i^D$and C_i^D are the dowel spring and damping coefficients, respectively and may be represented in the following general form.

$$\left.\begin{aligned}&F_i^D=\sum_{j=0}^{m}K_{ij}^D\beta_i^j\,,\\&C_i^D=\sum_{j-0}^{m}C_{ij}^D\dot{\beta}_i^j\,.\end{aligned}\right\} \tag{4.43}$$

Similarly, the dowel force F_i^{DL} and its associated moment $M(F_i^{DL})$ in the horizontal direction acting on the i-th left-hand dowel are the same as equations (4.40) through (4.43) above.

4.2.6 Dowel friction force in the vertical direction and its associated moment

The dowel friction forces in the vertical direction are derived from the dowel forces and the friction factor. When a dowel pin and mating hole are in sliding contact, the relative velocity between pin and hole on the i-th block interface is

$$\omega_i=\dot{w}_i+(h_i\sin\theta_i-d_i\cos\theta_i)\dot{\theta}_i-\{\dot{w}_{i-1}-(h_{i-1}\sin\theta_{i-1}+d_i\cos\theta_{i-1})\dot{\theta}_{i-1}\}\,. \tag{4.44}$$

For $i=1$

$$\omega_1=\dot{w}_1+(h_1\sin\theta_1-d_1\cos\theta_1)\dot{\theta}_1-\dot{w}_0\,. \tag{4.45}$$

The dowel friction force in the right-hand dowel in the vertical direction μF_i^{DR} and its associated moment $M(\mu F_i^{DR})$ for the i-th block are as follows.

$$\left.\begin{aligned}&\mu F_i^{DR}=-\mathrm{sign}(\omega_i)\cdot\mid F_i^{DR}\mid\cdot f(\mu)\,,\\&M(\mu F_i^{DR})=-\mu F_i^{DR}(h_i\sin\theta_i-d_i\cos\theta_i)\,,\end{aligned}\right\} \tag{4.46}$$

for the $i-1$ block

$$\left.\begin{aligned}\mu F_{i-1}^{DR}&=\mathrm{sign}(\omega_i)\cdot\mid F_i^{DR}\mid\cdot f(\mu)\ ,\\ M(\mu F_{i-1}^{DR})&=-\mu F_{i-1}^{DR}(-h_{i-1}\sin\theta_{i-1}+d_i\cos\theta_{i-1})\ ,\end{aligned}\right\} \tag{4.47}$$

whrer f(μ) is a function of both statical and dynamical friction factors. Similarly, the friction force μF_i^{DL} on the left-hand side and its moment $M(\mu F_i^{DL})$ are as follows.

For the i-th block

$$\left.\begin{aligned}\mu F_i^{DL}&=-\sin(\omega_i)\cdot\mid F_i^{DL}\mid\cdot f(\mu)\ ,\\ M(\mu F_i^{DL})&=-\mu F_i^{DL}(h_i\sin\theta_i+d_i\cos\theta_i)\ ,\end{aligned}\right\} \tag{4.48}$$

for the i-th block

$$\left.\begin{aligned}\mu F_{i-1}^{DL}&=\sin(\omega_i)\cdot\mid F_i^{DL}\mid\cdot f(\mu)\ ,\\ M(\mu F_{i-1}^{DL})&=-\mu F_{i-1}^{DL}(-h_{i-1}\sin\theta_{i-1}+d_i\cos\theta_{i-1})\ ,\end{aligned}\right\} \tag{4.49}$$

$$f(\mu)=f(\mu_k,\ \mu_s)\ . \tag{4.50}$$

4.2.7 Moment due to block weight and pressure difference

The moments acting on the i-th block as a result of the block weight and pressure difference are as follows. If $\alpha_{i-1}>0$

$$M(W_i^U)=W_i^U(h_i\sin\theta_i+b_i\cos\theta_i)\ . \tag{4.51}$$

If $\alpha_{i+1}=0$

$$M(W_i^U)=W_i^U h_i\sin\theta_i\ . \tag{4.52}$$

If $\alpha_{i-1}<0$

$$M(W_i^U)=W_i^U(h_i\sin\theta_i-b_i\cos\theta_i)\ . \tag{4.53}$$

where

$$W_i^U=\sum_{j=i+1}^{n}W_j-F_i^P. \tag{4.54}$$

when $j=n$, $M(W_n^U)=0$. Similarly, if $\alpha_i>0$

$$M(W_i^L)=W_i^L(h_i\sin\theta_i-b_i\cos\theta_i)\ . \tag{4.55}$$

If $\alpha_i=0$

$$M(W_i^L)=W_i^L h_i\sin\theta_i\ . \tag{4.56}$$

If $\alpha_i<0$

$$M(W_i^L)=W_i^L(h_i\sin\theta_i+b_i\cos\theta_i)\ . \tag{4.57}$$

where

$$W_i^L=\sum_{j=i}^{n}W_j+F_i^P. \tag{4.58}$$

4.2.8 Equation of motion for impact plate

For the i-th impact plate on the right hand side, the equations of motion are as:

$$m_i^{BR}\ddot{u}_i^{BR}=-F_i^{MR}+F_i^{TR}+F_i^{BR}, \tag{4.59}$$

where

$$F_i^{MR}=K_i^{MR}\phi_i+C_i^{MR}\dot{\phi}_i\,, \tag{4.60}$$

and for the left impact plate

$$m_i^{BL}\ddot{u}_i^{BL}=F_i^{ML}-F_i^{TL}-F_i^{BL}\,, \tag{4.61}$$

where

$$F_i^{ML}=K_i^{ML}\phi_i+C_i^{ML}\dot{\phi}_i\,, \tag{4.62}$$

$$\phi=u_B-u_0\,, \tag{4.63}$$

$$\left.\begin{aligned} K_i^M&=\sum_{j=0}^{m}K_{ij}^M\phi_j^j\,,\\ C_i^M&=\sum_{j\ 0}^{m}C_{ij}^M\dot{\phi}_j\,. \end{aligned}\right\} \tag{4.64}$$

4.3 Results and discussions

The governing equations given in section 4.2 can be numerically solved by using the Runge-Kutta integration schemes. The geometry data and mass of the blocks are shown in Table 4.1 in such a way that the system analyzed corresponds to the exmerimental HTGR fuel blocks with dimension scaled by 1/2 and weight scaled by 1/8. The computation time interval is 0.05 milli-seconds. The numerical results for both free vibration and forced vibration problems are compared with experimental results.

Table 4.1 Calculation data

Item		Block No. 1~12	Top block
a	(cm)	2.5	
b	(cm)	7.23	
d	(cm)	5.2	
h	(cm)	14.23	
I	(kN・m)	0.0514	0.133
m	(kg)	6.15	9.0
m_B	(kg)	6.15	9.0
δ_R, δ_L	(cm)	0.025	
μ_k	(−)	0.2	
μ_s	(−)	0.2	
C^B	(kN・s/m)	1.73	
C^C	(kN・s/m)	0.0196~0.118 (depend on dolumn defleftion)	
C^D	(kN・s/m)	4.12	
C^M	(kN・s/m)	1.73	
C^V	(kN・s/m)	1.73	
K^B	(kN・s/m)	2.45×10^4	
K^D	(kN/m)	1.52×10^4	
K^M	(kN/m)	2.45×10^4	
K^V	(kN/m)	2.45×10^4	
P	(MPa)	0.0	

(1 kN=102 kgf, 1 kN/m=1.02 kgf/cm)

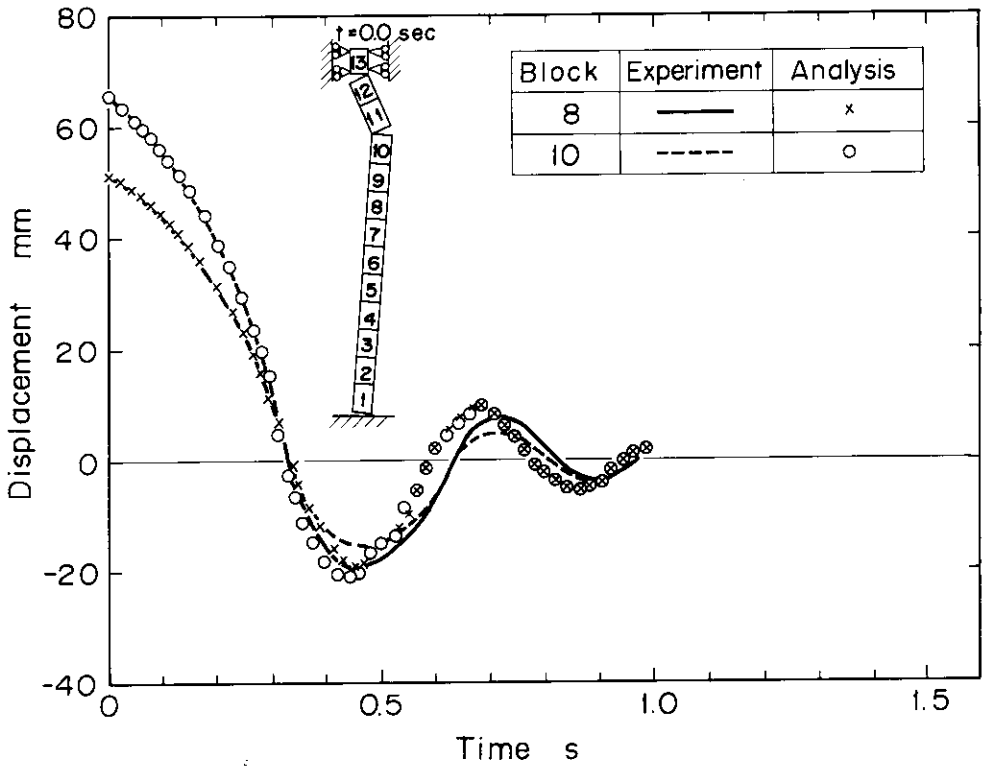

Fig. 4.3 Column free vibration

4.3.1 Free vibration of a single stacked column

Figure 4.3 shows a comparison of the calculated and experimental results of a single stacked column released from an initially displaced position. In the figure the time histories of the blck displacements were plotted. For this free vibration case there is good agreement between the expeirmental and analytical results. It is also seen that the oscillation periods are amplitude dependent.

Through proper adjustement of the physical parameters in the analytical model, a close correlation between the analytical results and experimental data can be achieved for free vibration problems. In the experiment the displacements were accurately measured by means of a differential transformer type displacement detector. In the analysis the damping coefficient of this detector was varied to align the analytical data to the experimental data.

4.3.2 Forced vibration without boundary impact

The forced vibration response of the single column under boundary excitation was also studied. The support floor was assumed to be connected with the boundary walls to form a rigid frame so that the movement of the walls is the same as that of the floor. Except at the top block, the side wall gap was large and as a result, no side wall impact occured. The column was excited by a sinusoidal floor motion at 3.5 Hz with 500 Gal maximum acceleration. The time histories of displacements of the blocks from both the experiment and analysis are shown in Fig. 4.4. Figure 4.5 shows the column displacements as function of input acceleration levels for sinusoidal excitation along the horizontal axis. It can be seen from the figure that there is satisfactory agreement between the analytical and experimental results.

4.3.3 Forced vibration with boundary impact

The forced vibration response of the single column impacting the boundary walls was studied for both sinusoidal and seismic wave input.

The blocks were subjected to impact loads due to periodic impact against the walls. The column to

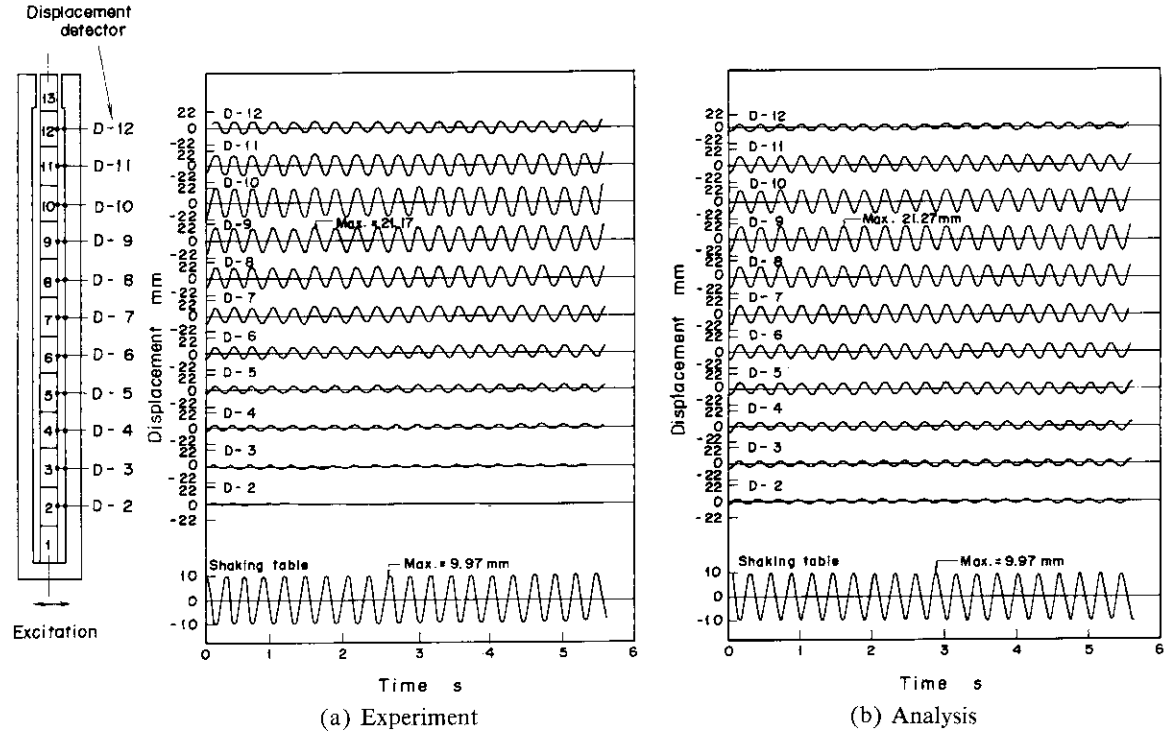

Fig. 4.4 Comparison between experiment and analysis displacement (Input wave sinusoidal 3.5 Hz, Max. acceleration 500 Gal)

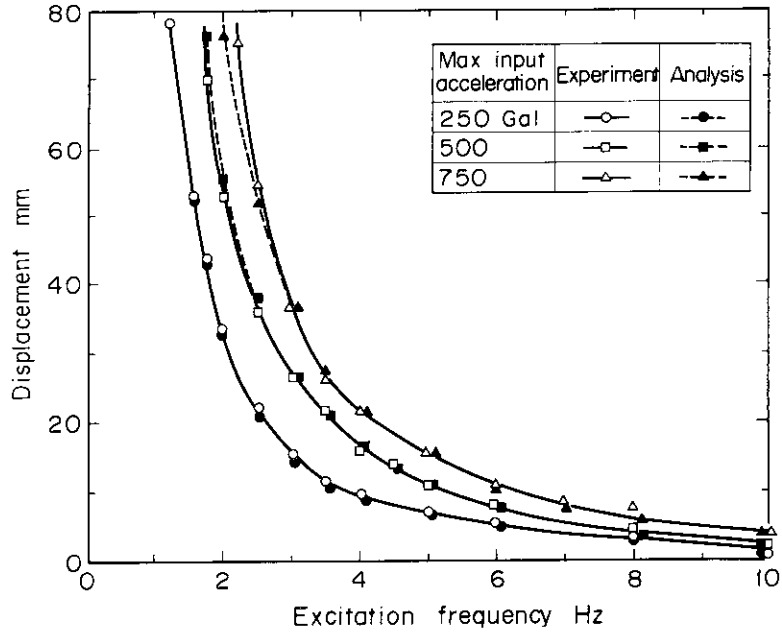

Fig. 4.5 Displacement vs. excitation frequency

wall gap in the test was taken to be 15 mm except at the top where a smaller gap of 0.5 mm was used.

(1) Sinusoidal wave excitation

Figure 4.6 shows the time histories of displacements and impact forces of the column for a 3.5 Hz, 500 Gal sinusoidal excitation. The results from analysis and experiment are compared. Figure 4.7 presents a sequential display of the motion of a thirteen blocks column. The blocks were subjected to impact loads due to periodic impact against the impact plates.

In this Fig. 4.8, it can be seen that the analytical results for both block displacements and impact

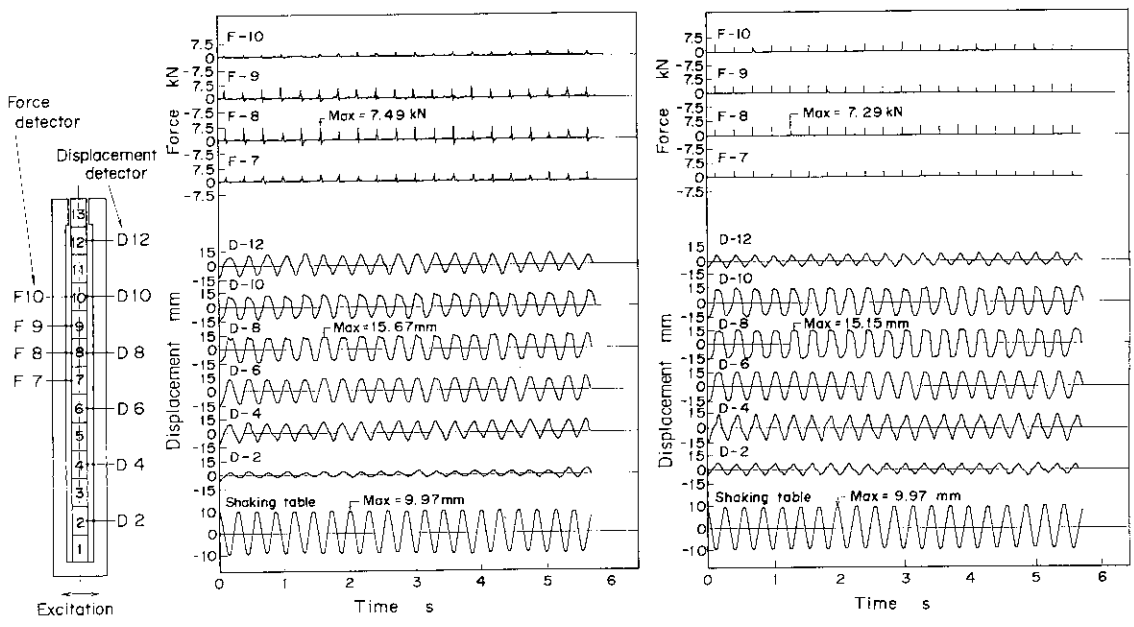

(a) Experiment (b) Analysis 1 kN = 102 kgf

Fig. 4.6 Comparison between experiment and analysis of displacement and impact reaction force (Input wave sinusoidal 3.5 Hz, Max. acceleration 500 Gal)

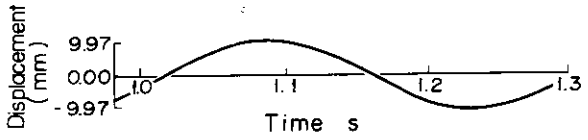

(a) Shaking table displacement

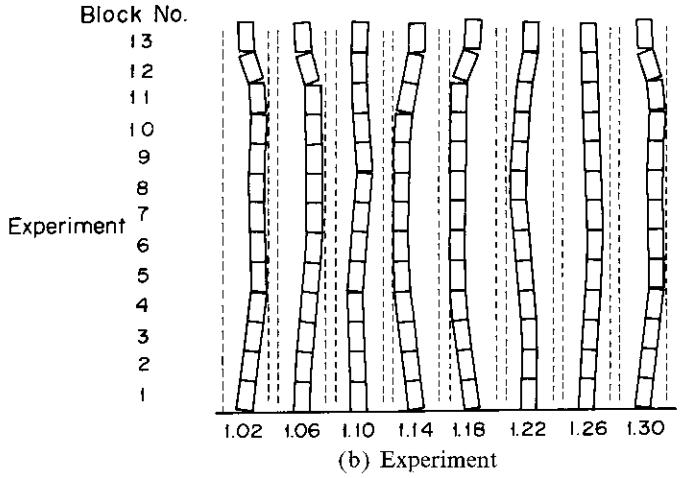

(b) Experiment

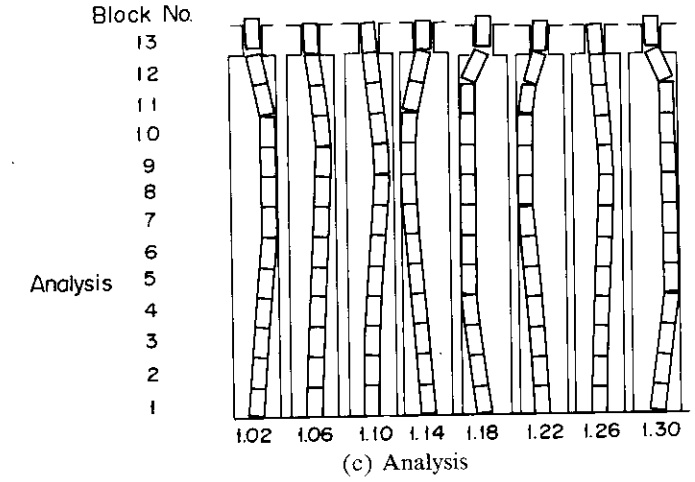

(c) Analysis

Fig. 4.7 Comparison between experiment and anatysis of columm vibration behavior (Input wave sinusoidal 3.5 Hz, Max. acceleration 500 Gal)

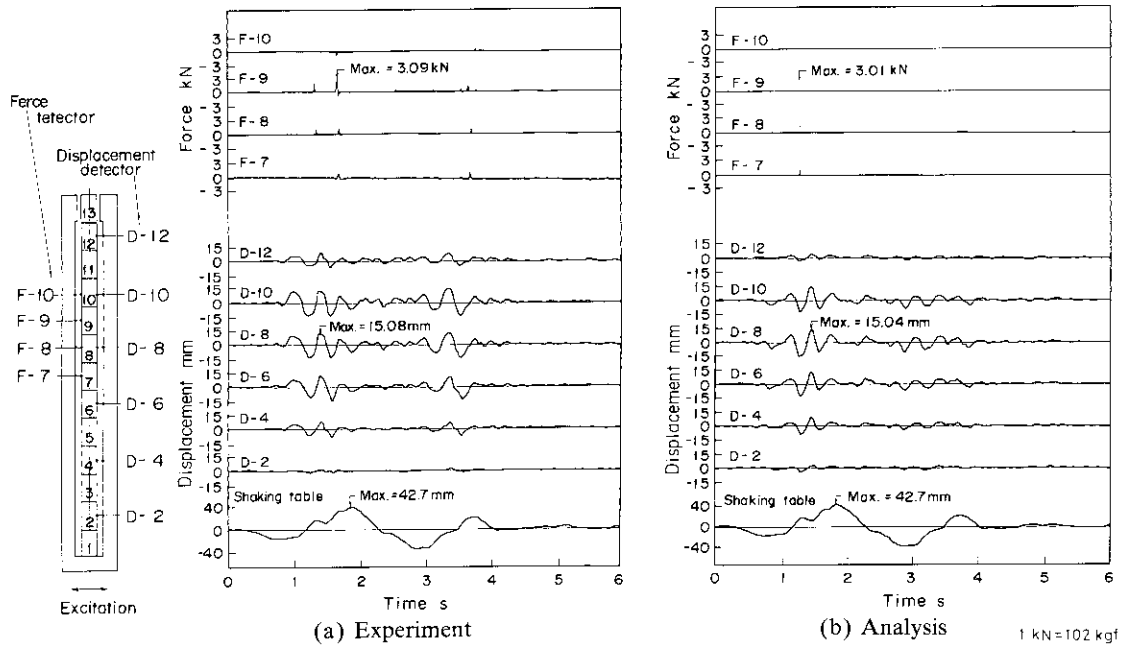

Fig. 4.8 Comparison between experiment and analysis of displacement and impact reaction force (Input wave El Centro 1940 NS, Max. acceleration 500 Gal)

forces are in good agreement with the experimental ones.

Figure 4.9(a) shows the distributions of the block impact forces along the column and compares analytical and experimental results. The analytical results show a favorable correlation with the results of the experimens.

(2) Random wave excitation

For a random input wave, the modified El Centro (1940 NS) was applied to the HTGR core. Since

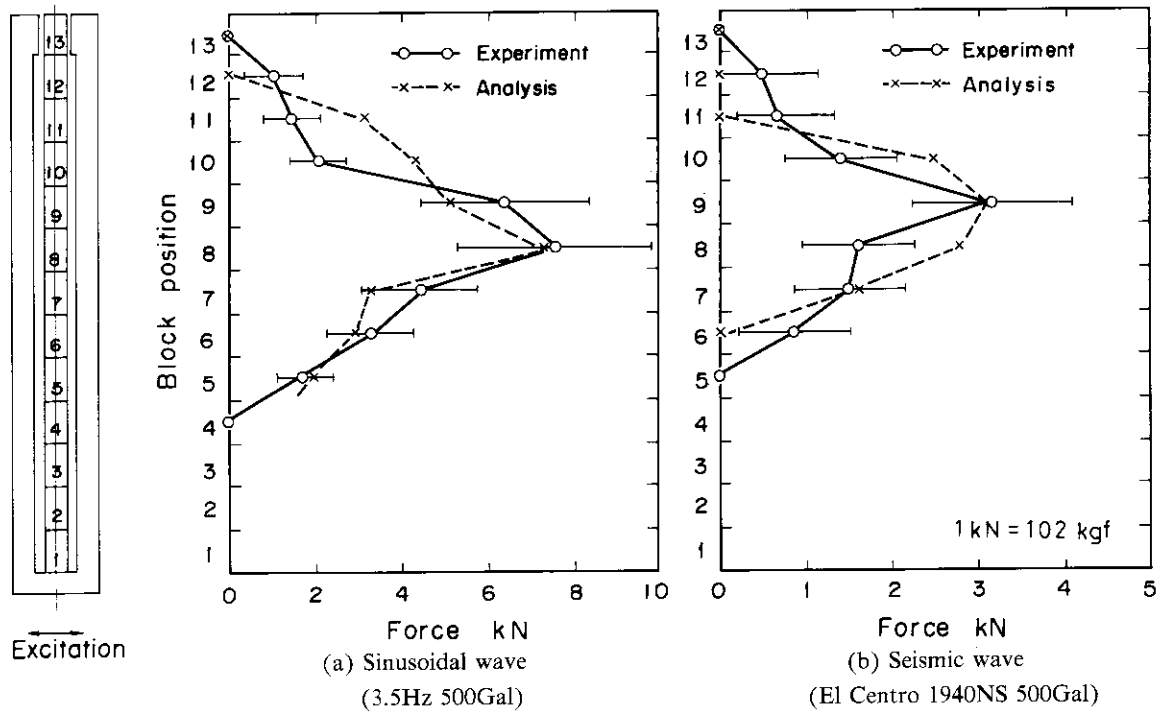

Fig. 4.9 Comparison between experiment and analysis value of impact reaction force distribution of block along column

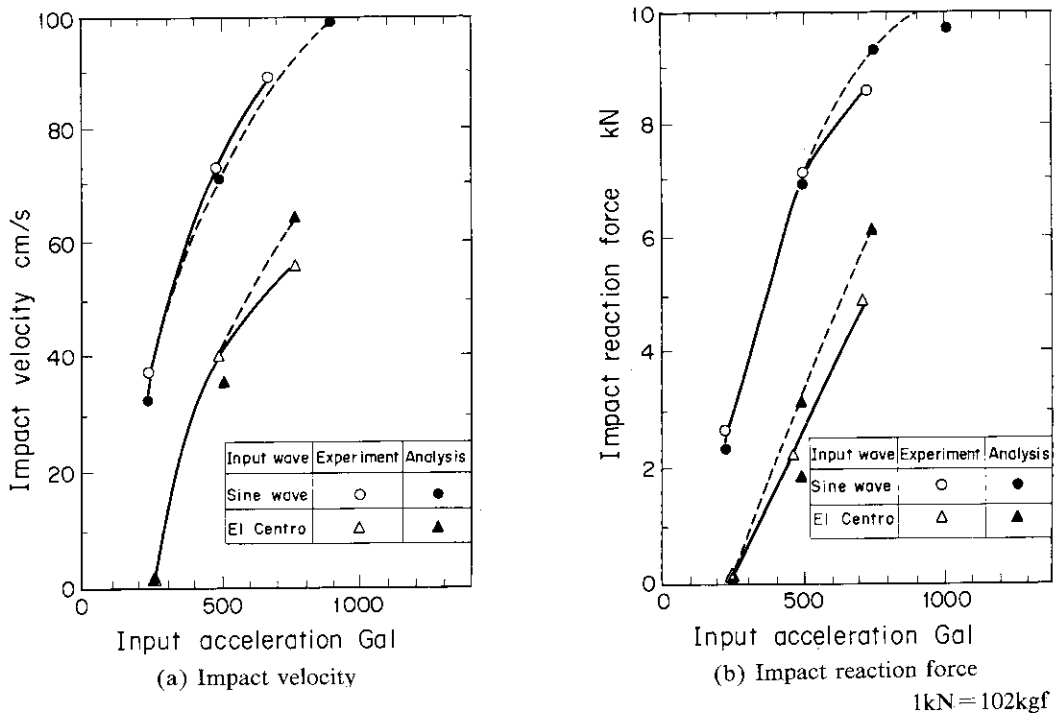

(a) Impact velocity (b) Impact reaction force

1kN=102kgf

Fig. 4.10 Impact reaction force and velocity vs. input acceleration

the column model was 1/2 scale the time scale was reduced by $1/\sqrt{2}$ according th the laws of similarity.

Figure 4.8 shows the time histories of the displacements and impact forces of the column for the modified E1 Centro wave of 500 Gal peak acceleration. The analytical and experimental results are compared. Figure 4.9(b) shows the distribution of block impact forces along the column. The analytical results show a favorable correlation with the results of the experiments. Figure 4.10 shows the impact forces as function of input acceleration level for sinusoidal and random excitaions. The analytical results show a favorable corrlation with the results of the experiments.

4.4 Concluding remarks

A seismic analysis method for the block column of the experimental HTGR core has been developed. The calculation equations and numerical results have been presented and were compared with the results of the experiments. The following conclusions have been drawn:

(1) The analytical results were compared with experimental data for both free and forced vibration of a single stacked column. Good agreement was obtained between analytical and experimental results.

(2) Using this method, forces of dowel pins and around the holes can be computed. In addition stresses of dowel pins and corresponding holes can slso be evaluated from forces. This is important since structural design of dowel pin and hole is often the most critical part of fuel block structural design.

(3) The method is capable of being extended to the plane motion problem of a series of many interacting stacked columns.

5. Column Response Characteristics in Three-dimensional Space

5.1 Introduction

Whirling of the columns and effects of a pressure difference between the top and bottom of the columns upon the vibration characteristics are not clarified yet. In a real core, cooling gas flows downward from the top, so that a pressure difference between the top and bottom of the reactor core occurs. Due to this gas pressure difference, each column is pressed down. In the core three-dimensional motion (whirling) of the columns may be expected. As seen, for an aseismic design of the reactor core, it is necessary to understand displacement and impact characteristics of the columns under a pressure difference from the top to the bottom as whirling characteristics. In the present study vibration characteristics of the column were examined by experiment.

5.2 Experimental apparatus and method

5.2.1 Experimental apparatus

In the HTGR core, seven columns form each fuel region. The fuel region (seven columns) was used in the experiment, as shown in Photo. 5.1. Each column was composed of twelve hexagonal graphite blocks and one steel block of the same shape giving a total of thirteen layers of blocks. The seven columns were assembled as a unit; the external six columns were fixed to support frame and the central column

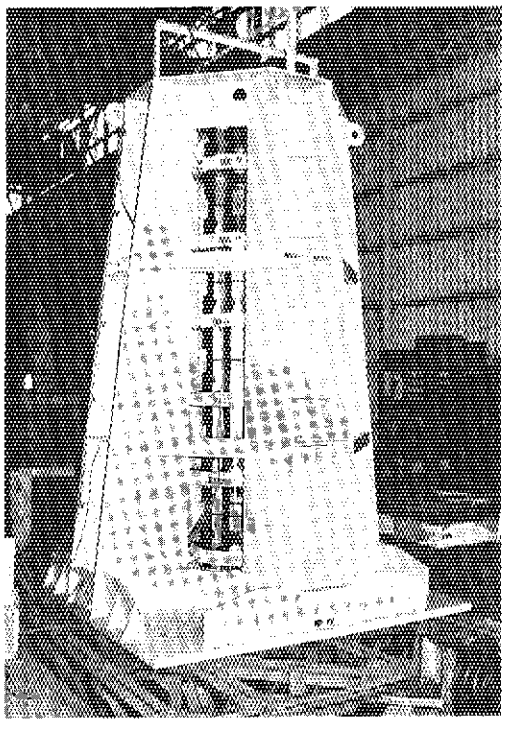

(a) Vertical view

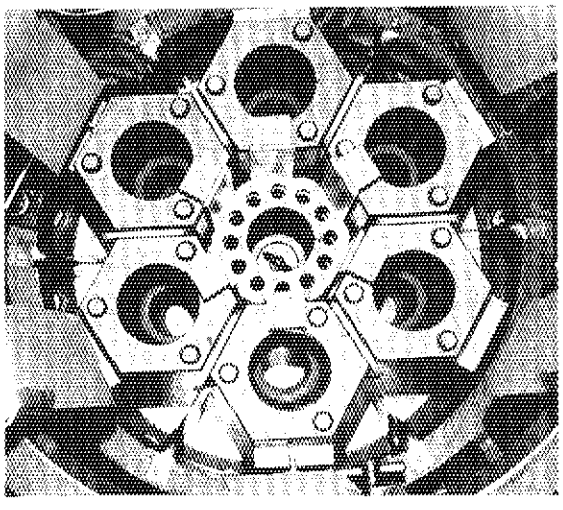

(b) Horizontal view

Photo. 5.1 External appearance of one region core model

stood by itself with some distance from the surrounding ones. The gap width was changed by changing the thickness of steel shims between the surrounding columns. In this way, motion of the column and impact characteristics, depending on the gap width, were examined. The gap pressure diffrence from the top to the bottom of the column was simulated by a compressive force (1.34 kN) of a spring attached to the top of the column, in order to examine effects of the pressure difference upon the column characteristics.

As indicated in Fig. 5.1, excitation (shaking) of the column was in two alternative directions, at right angles to each other. The vibration characteristics of the column, depending on exciation direction, were thus examined.

The support frame was a steel box type, having sufficient rigidity (primary natural frequency 24 Hz). As a unit with the group of columns inside, the frame was fixed on a shaking table.

The graphite fuel blocks, as shown in Fig. 5.2, were hexagonal prisms of 150 mm in width between

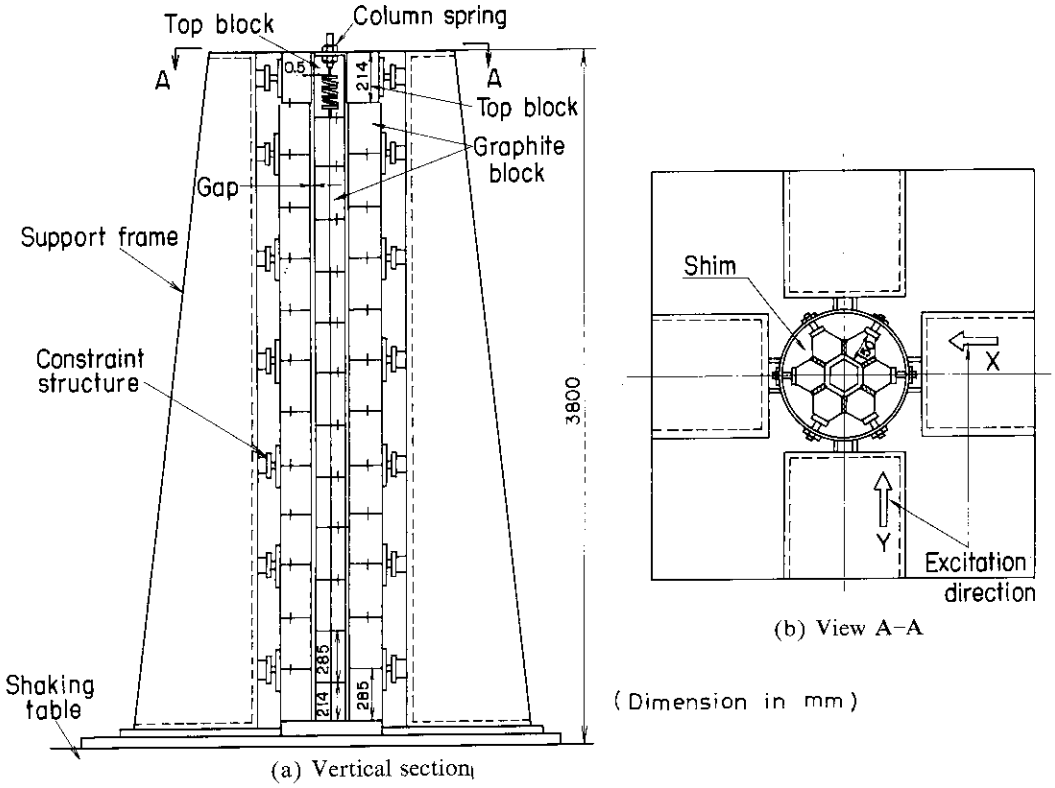

Fig. 5.1 Experimental apparatus for one region core model

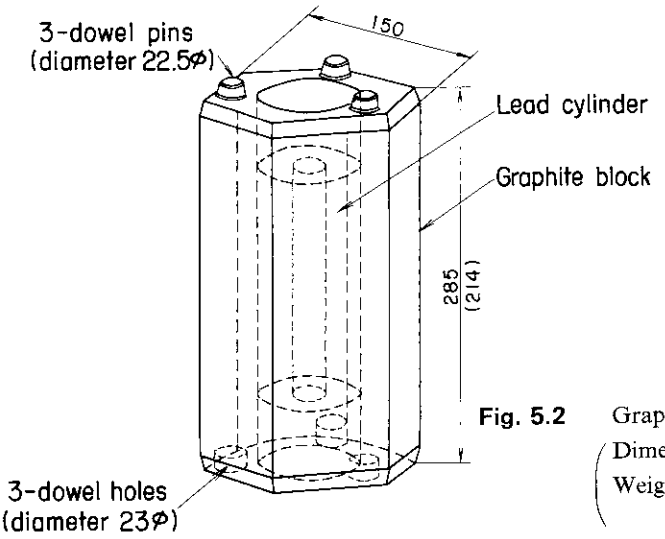

Fig. 5.2 Graphite fuel block
(Dimension: mm
Weight : 285mm, 19.1kg
214mm, 14.3kg)

Table 5.1 Detectors and measuring positions

Item	Detector	Detector position	Number
Block displacement	Eddy current type	Block No. 7, 9, 11, 13 (Horizontal) Block No. 7 (Vertical)	10
Impact acceleration	Piezoelectric type	Block No. 4, 6, 8, 10, 12, 13	12
Frame acceleration	Strain gauge type	Frame	3
Shaking table acceleration	Strain gauge type	Table	1

the sides and 285 mm in length (bottom block is 214 mm). Material was a nuclear grade graphite of apparent specific gravity 1.74 and Young's moduls about 8 GPa. In each block, there were three graphite dowel pins on the top face of each block which fit into mating holes in the bottom of the above block. The bottom block were connected to a base plate through dowels on the plate. The dowels work as shear connectors. The dowels restrict horizontal motion between block but not vertical or rocking motion. Compared with the experimental HTGR under design study in Japan Atomic Energy Research Institute, the graphite blocks were dimension scaled by 1/2 and weight scaled by 1/4 of those of the real fuel blocks (or about 1/2.5 the size and about 1/6.2 the weight of those of the large HTGR fuel block by General Atomic). To correct the weight, for adopting to the similarity laws, as indicated in Fig. 5.2, a lead cylinder was attached in the middle of a block as an additional mass. Consequently, the weight of graphite blocks was 19.1 kg (14.3 kg in the bottom block). The top steel block, though the same in size, was 17.4 kg in weight.

Measurements were made, as shown in Table 5.1, of displacements between blocks, and horizontal and vertical impact accelerations of blocks. Displacement detectors used were of the non-contact eddy current type. To measure whirling of the column, two detectors were set on two sides (120° apart) of each block, as shown in Fig. 5.3.

The impact accelerometer was piezoelectric type. In order to record the excitation conditions, strain gauge type accelerometers were set on the support frame and the shaking table. The positions of attached detectors were indicated in Fig. 5.3. Higher harmonic fraquencies were cut off from the impact acceleration data using a low pass filter with a cut-off frequency of 800 Hz.

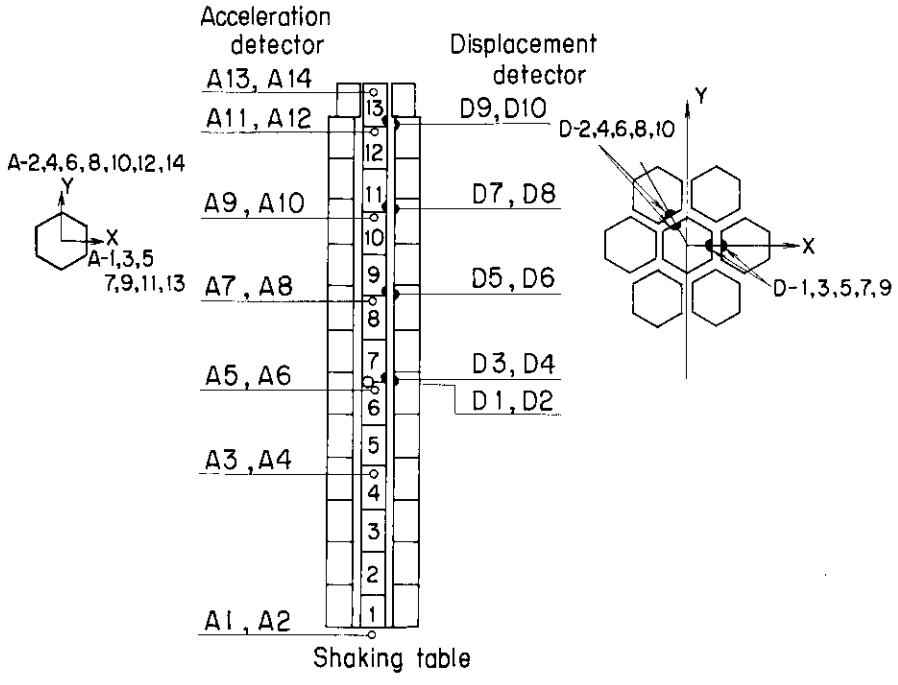

Fig. 5.3 Instrumentation

5.2.2 Experimental method

Uni-axial horizontal excitation tests were made on a group of columns on the shaking table. Excitation conditions were ranging in frequency from 1 to 20 Hz, acceleration from 50 to 500 Gal, input amplitude from 0.5 to 4 mm, gaps between the central column and surrounding ones, 2, 4, 7 and 80 mm, and two alternative excitation directions. Experiments were made with constant input amplitude. Effects on (1) column vibration and impact characteristics of gap width, (2) excitation frequency and acceleration, (3) excitation direction and (4) a gas pressure simulation column spring were examined.

5.3 Results and discussions

5.3.1 Displacement characteristics

(1) Vibration mode

Figure 5.4 describes vibration modes of the column in maximum displacement at each excitation frequency. At low excitation frequeny, the central column does not impact with the surrounding columns. With an increase of excitation frequency, the column displacements increase, and the central column impacts with the surrounding ones. Then, with further rise of frequency, the displacements decrease suddenly, with no impact any more. In the case of no impact, the column bends between blocks No. 8 to 9, i. e. at about two-thirds of the column length. In the case of an impact, it exhibits a vibration mode, with blocks attaching to the surrounding ones.

(2) Column whirling

In Fig. 5.5 is shown whirling of block No. 9 at each excitation frequency in the Y direction of column excitation (the supporting point in block rocking at one of the six hexagonal corners). The displacement locus of the block center is for a cycle of sinusoidal wave excitation in the figure. At low excitation frequency, whirling is not large. With a raise of frequency in increases. A maximum whiriling is exhibited at 7.5 Hz. Concerning the whiriling, Fig. 5.6 shows the displacement characteristics of the block in a 30° direction close to the excitation direction and Y direction. As seen in the figure, a peak displacement in the 30° direction appears at 7 Hz. After this has decreased, a peak displacement in the Y excitation direction appears at 7.5 Hz. Occurrence of block whirling is thus shown. With further increase of excitation frequency, displacements in both excitation direction decrease. In Table 5.2, the amlitude jump -down frequency for the condition of Fig. 5.6 is 7.0 Hz for the Y excitation dirction. It is seen, therefore,

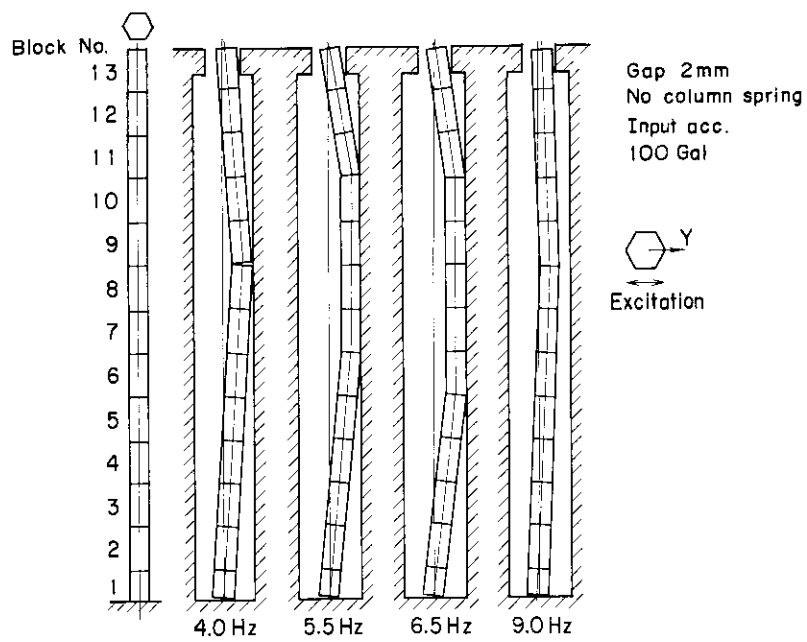

Fig. 5.4 Vibration mode of column

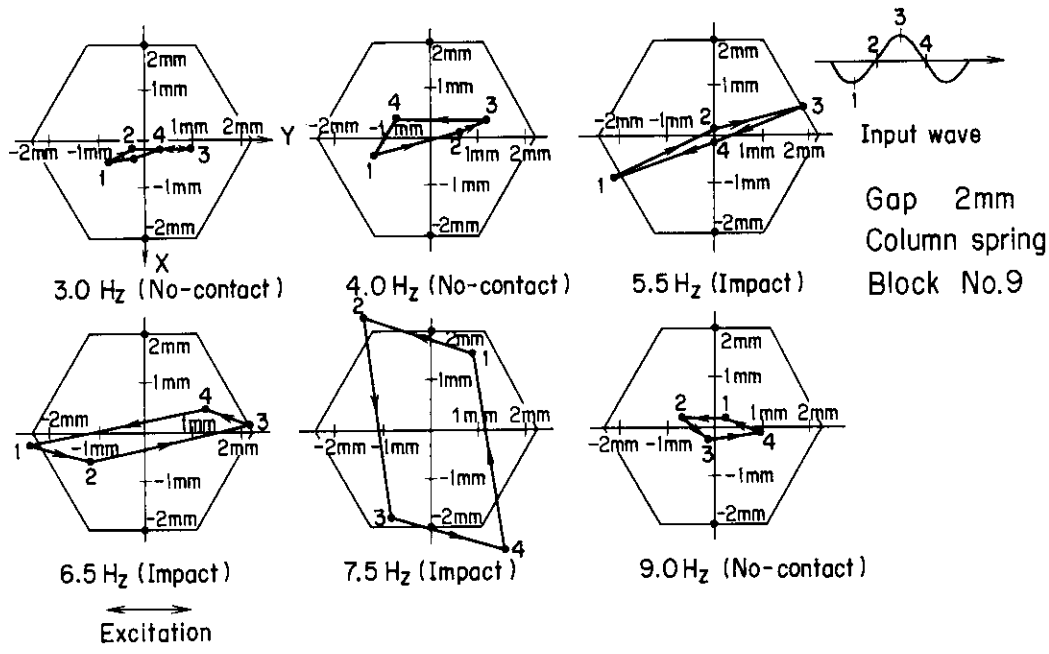

Fig. 5.5 Locus of block center

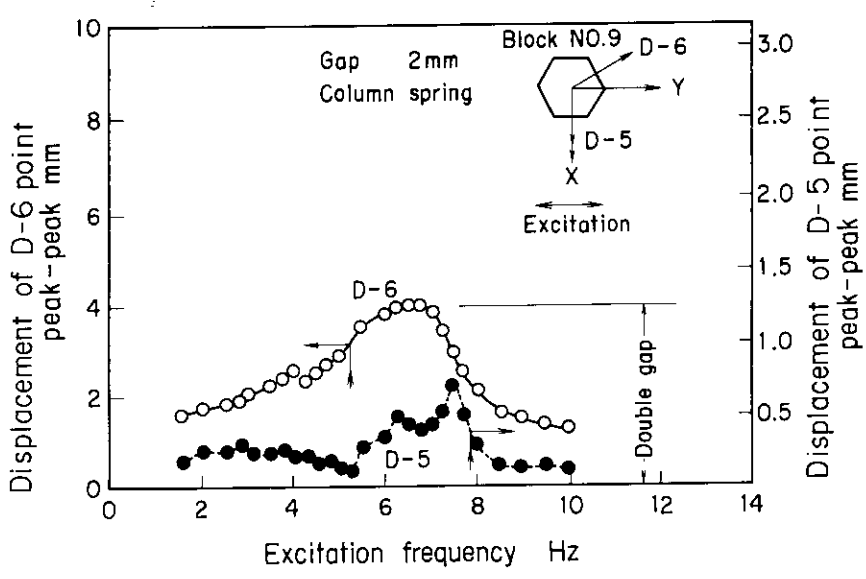

Fig. 5.6 Column whirling response

Table 5.2 Jump frequency (resonant frequency)

Model condition			Jump up frequency (Hz)				Jump down frequency (Hz)			
			Input displacement (mm)				Input acceleration (Gal)			
Excitation direction	Column spring	Gap (mm)	0.5	1	2	4	75	100	300	400
Y	With spring	2	5.5	5.5	4.5	3.5	7.0	7.0	9.0	9.5
X	With spring	2	8.0	6.5	5.5	3.6	—	7.5	—	13.5
X	Without spring	2	5.0	5.0	4.0	3.0	5.5	6.0	10.5	12.0
X	Without spring	4	4.0	3.3	2.8	2.5	4.5	4.5	7.0	7.5
X	Without spring	7	4.5	3.5	3.5	2.5	2.8	4.0	5.0	5.5

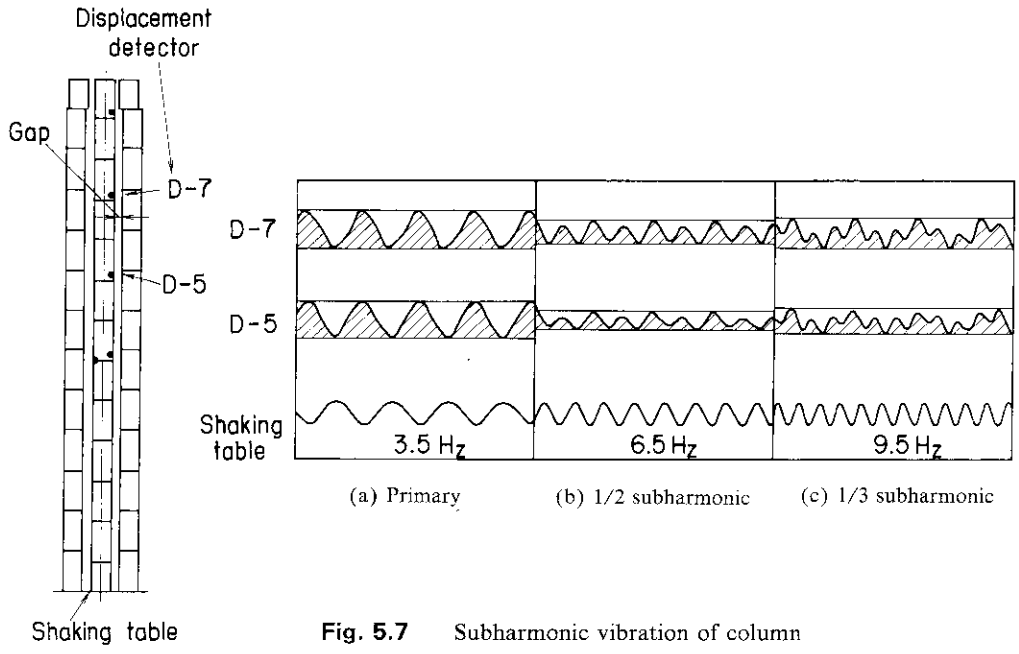

Fig. 5.7 Subharmonic vibration of column

that the conditions for whirling are a resonant frequency in the X direction in the Y excitation direction.

For the cause of whirilig, the following is plausible. In block rocking with a hexagonal corner as the supporting point, the potential energy is higher than in the case of a hexagonal side as the supporting point. The former rocking phenomenon thus tends toward the latter one, resulting in block whirling. Whilling is more likely to cocur in the Y direction than the X direction.

(3) Subharmonio vibration

Subharmonic vibration appears either with high excitation frequency at low acceleration levels or with low frequency at high acceleration levels. Figure 5.7 is an example of the former case, a one-half and a one-third subharmonic vibraion at frequencies 6.5 and 9.5 Hz respectively. The same results are also observed in analysis with a tracking filter, as shown in Fig. 5.8. Subharmonic vibration takes place due to the friction contact of the upper and lower blocks and to the unsymmetrical support in the upper column

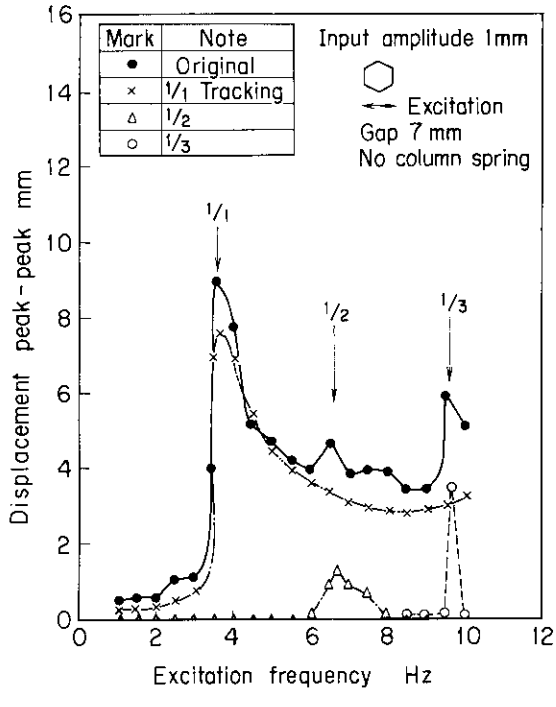

Fig. 5.8 Tracking analysis

gaps and uneven gaps horizontally.

(4) Displacement characterisitics

Figure 5.9 shows the displacement as function of excitation frequency under constant excitation levels. Figure 5.9 (a) is the displacements of the column under contant excitation amplitudes. The jump -up frequency, which suddenly increases the displacements, shifts to a lower frequency with an increase of excitation amplitude. These are a nonlinear spring characteristics due to block rocking and frictional force, i. e. the column softening characteristics.

Figure 5.9 (b) is the displacements under constant acceleration levels. It is seen that with an increase of acceleration level, the frequency for sudden drop of the displacements, i. e. the jump-down frequency shifts to a higher frequency. These are nonlinear spring characteistics of the column.

(5) Comparison between frequency sweep-up and sweep-down

Figure 5.10 shows the displacement response curves under excitation frequencies of sweep-up and

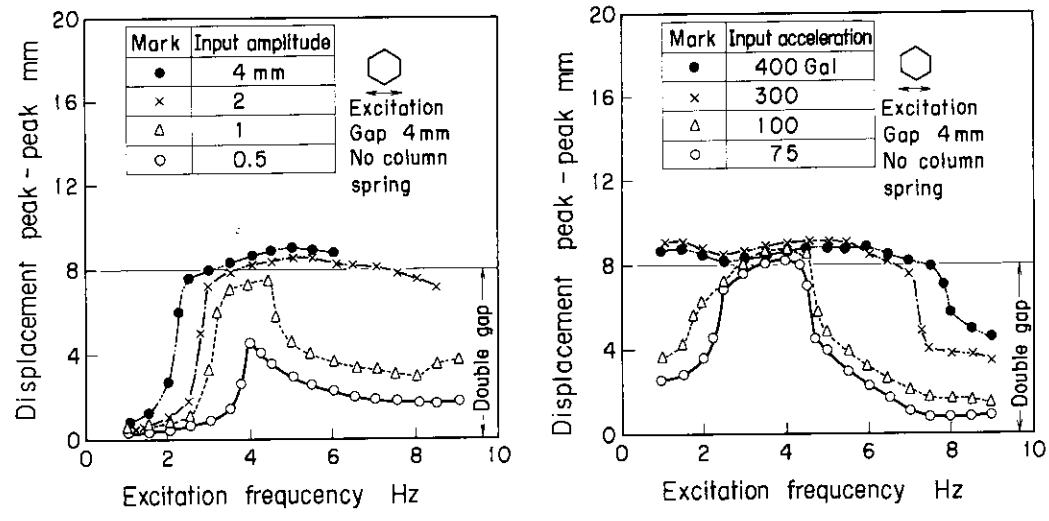

(a) Constant displacement input (b) Constant acceleration input

Fig. 5.9 Displacement response characteristics

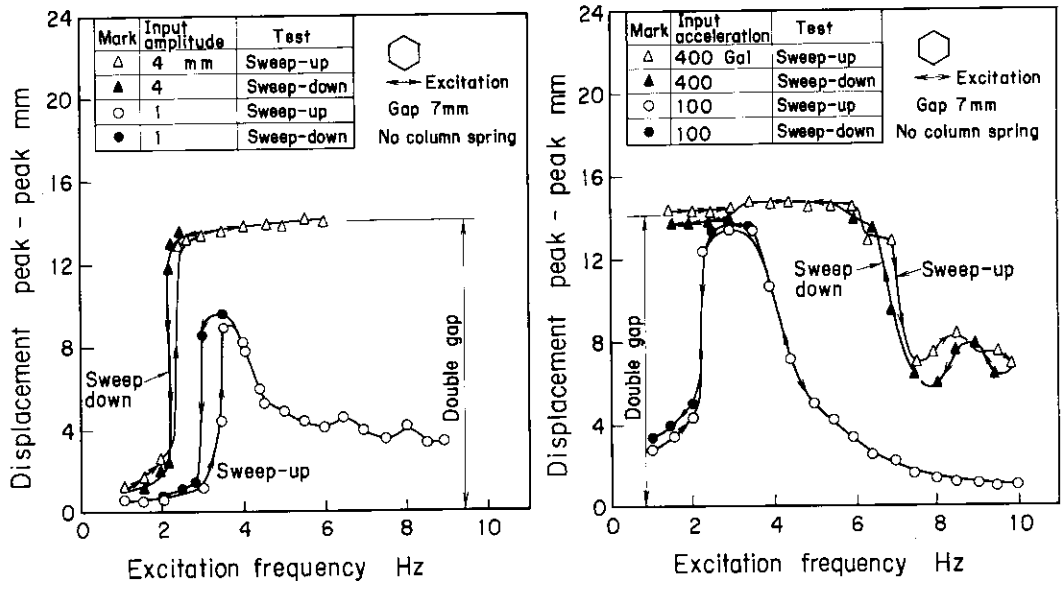

(a) Constant displacement input (b) Constant acceleration input

Fig. 5.10 Comparison between sweep-up and sweep-down response

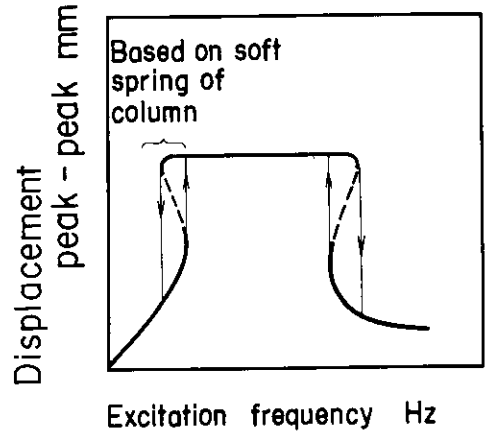

Fig. 5.11 Column nonlinear response of a system with softening characteristic and hardening characteristic

sweep-down. Figure 5.10 (a) is the case under constant excitation amplitude. The jump-up frequency is higher in sweep-up than in sweep-down. Figure 5.10 (b) is the case under constant acceleration level. The jump-down frequency is also higher in sweep-up than in sweep-down. As shown in Fig. 5.11, there is a hysteresis at low excitation frequency due to the column softening characteristics.

(6) Effect of gas pressure difference simulation spring

Figure 5.12 shows the displacement response of the column with and without a gas pressure

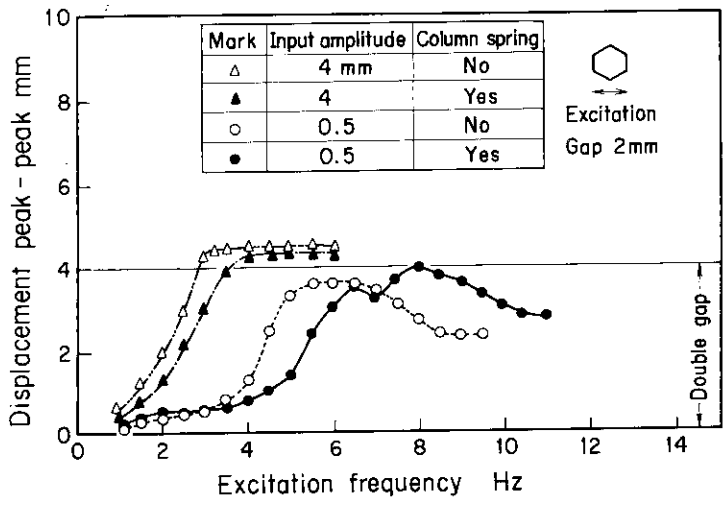

(a) Constant displacement input

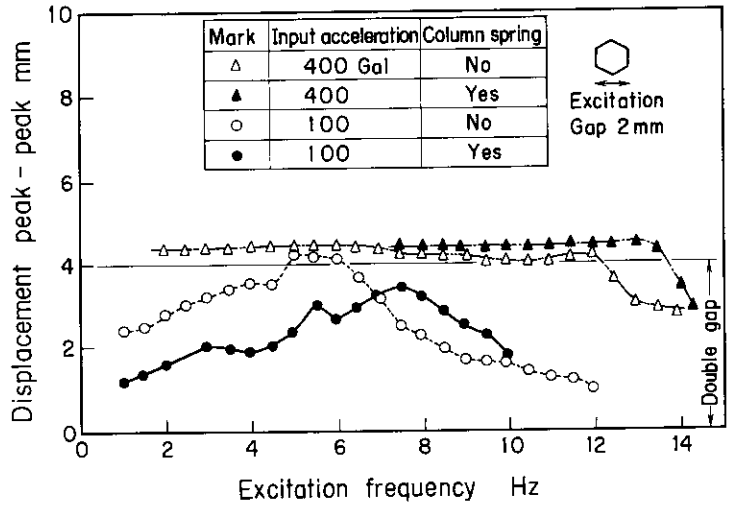

(b) Constant acceleration input

Fig. 5.12 Effect of column spring on displacement

Table 5.3 Column vibration characteristics

Input acceleration (Gal)	Response amplitude (−)	Resonant frequency (Hz)	Damping factor (%)
50	4.0	4	13
75	3.3	3	15
100	3.0	2.5	17

difference simulation spring. Figure 5.12 is the case under constant excitation amplitude. The jump-up frequency for the displacements is higher with the spring than without. The jump-down frequency for the displacements is also higher with the spring than without. These results are summarized in Table 5.2.

As seen above, with a gas pressure difference simulation spring the jump-up and jump-down frequencies for the displacements are both higher than that without it. The displacements at resonance are also smaller with the spring. The above is due to an increase in frictional force between the upper and lower blocks caused by the compressive force of the spring.

(7) Effect of excitation direction

In Table 5.2 are shown the jump-up and jump-down frequencies for the displacements in two alternaive excitation directions comparatively. Both the frequencies are higher in the X direction excitation than in the Y direction.

(8) Displacement amplification at column resonance and its damping constant

Table 5.3 shows the column response magnifications and the damping factors in resonance at low acceleration levels. The column resonant amplitude magnifications are about three to four. The damping factors increase with the column displacements.

5.3.2 Impact characteristics

(1) Effect of input acceleration level

In Fig. 5.13 are shown the impact accelerations and impact forces as function of input acceleration

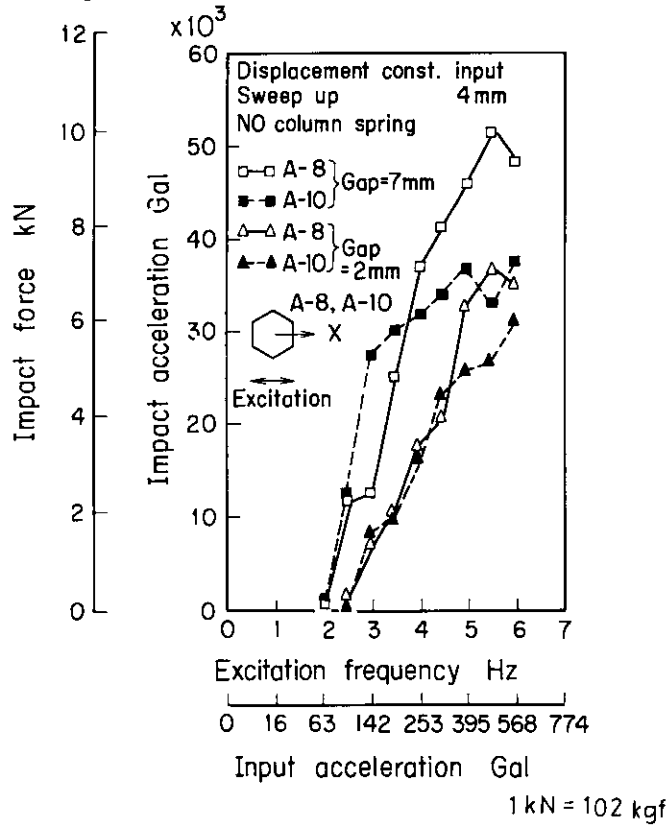

Fig. 5.13 Impact response as function of excitation level

under constant excitation amplitudes. The impact force is calculated as the product of block mass and impact acceleration. There is no impact at low input acceleration level, so the impact values are zero. Beyond a certain input acceleration level, an impact occurs. The impact values then increase almost proportionately with input acceleration. The peak values are exhibited at resonance 5.5 Hz under excitation conditions.

(2) Effect of gap width between columns

In Table 5.2 is indicated the variation of the column displacement jump-up and jump-down frequencies with gap width. At an increase of gap width, the jupp-up frequency shifts to lower frequency. With its increase, the jump-down frequency also shifts to lower frequency. Therefore, the range of impact frequency gets smaller with increasing gap width.

Figure 5.14 shows the impact accelerations and impact forces versus gap width as function of acceleration levels. The impact values increase with increasing gap width. This is because the velocity of the column berfore an impact increases with gap width.

(3) Contact duration

For the seismic simulation analysis of column behavior including impacts, it is necessary to make clear the contact duration in an impact and also to set an impact equivalent spring constant and an equivalent damping coefficient from the contact duration and coefficient of restitution. For this purpose, an experiment was made in the impact of two blocks, to measure the contact duration and coefficient of restitution for impact velocity and impact mode. Practically, however, the contact duration for blocks constituting the reactor core must be measured and an average value is to be introduced in simulation analysis. Therefore, the contact duration was estimated from the acceleration wave form in an impact between the upper and lower blocks.

Under the experimental conditions (such as impact velocity 5~15 cm/s), the contact durations are 2~4 milli-seconds. The effect of impact velocity on the contact duration could not be made clear because of the scattering in data. Nevertheless, an average value of the contact duration for analysis data could be obtained.

(4) column impact in only one direction

When the gaps between the central column and surrounding ones are not uniform, the column may

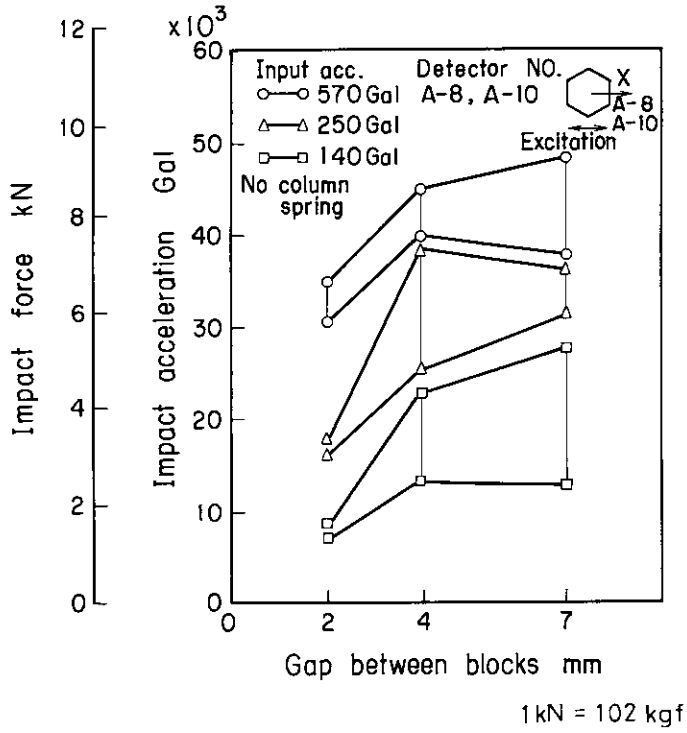

Fig. 5.14 Effect of gap width on impact response

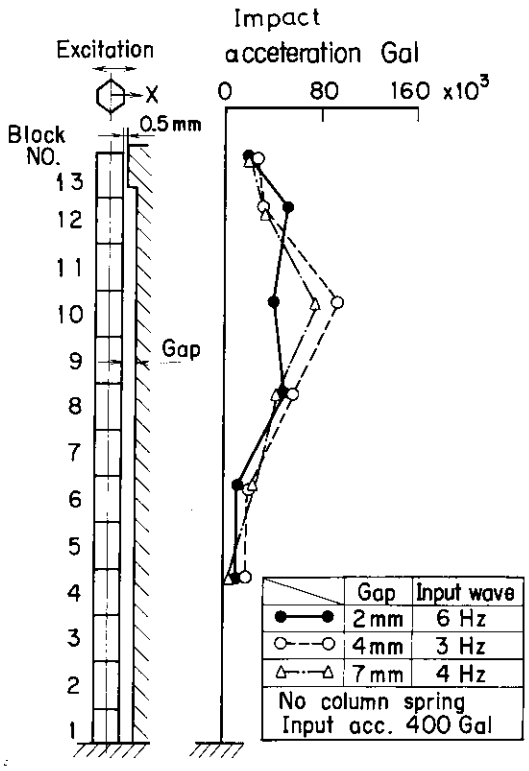

Fig. 5.15 Impact acceleration distribution of block along column

impact with the surrounding ones only in one direction. The case of impacting only in one direction and of a stronger impact in one direction than the other were observed.

(5) Impact acceleration distribution along the column

In Fig. 5.15 is indicated the impact accelerations along the column. At small gap width, the distributions are a broad peak along two-thirds of the column length. At large gap width, the distributions are a peak with a maximum at two-thirds of the column length. This distributions are similar to the vibration mode with a miximum column displacement as shown in Fig. 5.4.

5.4 Concluding remarks

Vibraiton tests were carried out on an one region core (seven stacked columns) which is a fundamental core element of the block type fuels HTGR. The vibration characteristics of a stacked block column were examined.

(1) In the experiment of vibration response of the stacked block column, it was observed that the column exhibits softening-hardening characteristics. The softening characteristics are caused by column rocking, block upper and lower faces friction and loose dowels connection.

(2) Whiriling phenomenon of the column appears under certain excitation conditions.

(3) The column vibrates in subharmonic frequency under certain excitation conditions.

(4) The compression spring simulating gas pressure difference between the top and bottom of the column has the effect of raising resonant frequency of the column.

(5) There is nearly pooportional relation between input acceleration and impact acceleration.

(6) The impact accelerations increase with an increase of both input accelaration level and gap width up to a certain level of impact acceleration.

6. Simplified Analytical Model for HTGR Core Seismic Response

6.1 Introduction

Seismic analysis of the high temperature gas-cooled reactor (HTGR) core consisting of graphite blocks is important from a safety point of view. However there is hardly any such established technology at present. Several analytical models and computer programs by Olsen et al.[2], Lee et al.[19]~[20] and Muto et al.[27]~[30], Bezler et al.[33], Merson and Bennett[45] and Ishizuka et al.[46]~[48] are available and they use an impulse-momentum model and a spring-dashpot model.

A large number of blocks are involved in the HTGR core. In the complete description of block motion, six degrees-of-freedom are required, so that several-ten-thousand degrees of freedom are necessary for full core blocks analyses. Integral times are within in the order of 0.05 milli-seconds, because the impacts between blocks occur in times of the order of milli-seconds. In several-seconds analysis of the time history core response, several ten thousand integral steps are necessary. Therefore, time history analysis of the core seismic response requires a considerable amount of computational cost. In order to reduce this cost, a simplified model for core seismic analysis is conceived.

In the simplified model, one degree-of-freedom mass with nonlinear column characteristics is used instead of the a single stacked column. Some problems are solved to show validity and applicability of the model in core seismic analysis. In the first problem, a single stacked column without side boundaries subjected to sinusoidal excitaiton is analyzed and the results are compared with the experiment and the detailed model. In the second problem, a single stacked column with boundary impact under sinusoidal exictation is analyzed. The results are also compared with the experiment and the detailed model.

6.2 Calculation model and formulae

Illustration of the simplified model for seismic behavior of the HTGR core requires discussions of the following three steps:

(1) detailed model,

(2) simplified model with nonlinear column characteristics, and

(3) simplified model with column boundary.

6.2.1 Detailed model

The dynamic models involving impacts can be divided into two categories; i. e. the impulse-momentum model and the spring-dashpot model. In the impulse-momentum model, the momentum conservation principle and collision theory are applied for block impacts. In the spring-dashpot model, the impact hehavior is represented by dynamic elements which have spring and dashpot elements (Voigt model). In the present study, the spring-dashpot model is used.

In the detatiled model the following assumptions are made, as shown in Fig. 6.1:

(1) each block is modeled as a rigid body,

(2) the calculation system is two-dimensional and each block has three degrees-of-freedom; two translational displacements and one rotation at block center of gravity,

(3) impact phenomenon is modeled with an impact spring-dashpot, and

(4) dowels are deformable and block interfaces have friction force.

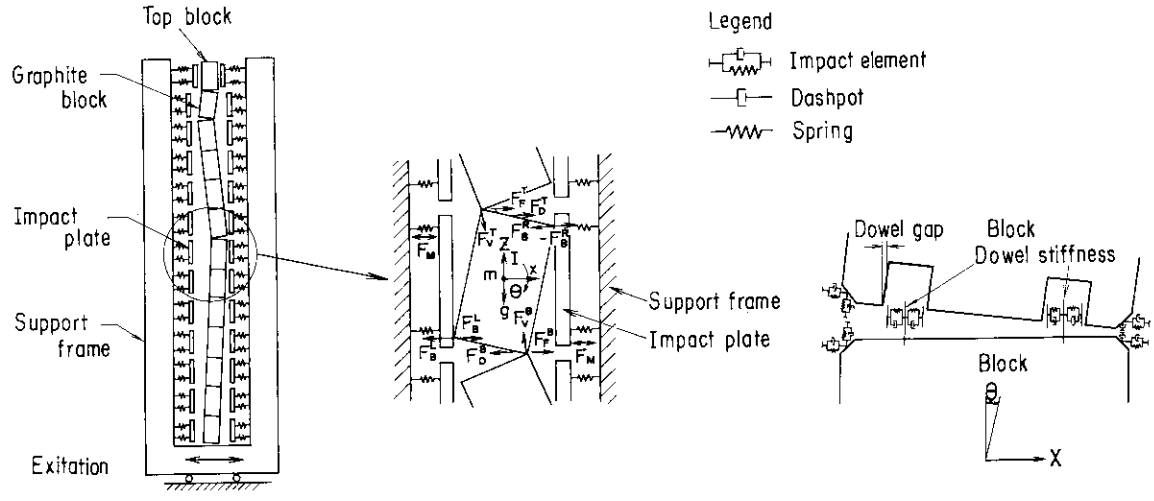

(a) Column model (b) Block rocking model

Fig. 6.1 Detailed model for column vibration

The equations of motion for an i-th block in the sigle column may be written as:

$$m\ddot{x}=F_D^B+F_D^T-F_F^B+F_F^T-F_B^R+F_B^L-m\ddot{x}_O\,, \tag{6.1}$$

$$m\ddot{z}=F_V^B+F_V^T+mg\,, \tag{6.2}$$

$$I\ddot{\theta}=M_D^B+M_D^T-M_F^B+M_F^T+M_B^R+M_B^L+M_V^B+M_V^T\,, \tag{6.3}$$

where F_B, M_B : boundary force and moment, F_D, M_D : dowel force and moment,

F_F, M_F : friction force and moment, F_V, M_V : vertical force and moment,

g : gravity constant, I : moment of inertia, m : mass of block,

x, $\ddot{x}$: lateral displacement and acceleration, $\ddot{x}_o$: base accelaration,

z, $\ddot{z}$: vertical displacement and acceleration, θ, $\ddot{\theta}$: rotation angle and angular acceleration.

Super scripts

B : lower, L : left, R : right, T : upper.

6.2.2 Simplified model

In the simplification, one degree-of-freedom mass with a nonlinear spring and dashpot is used instead of the stacked column, as shown in Fig. 6.2. The equation of motion of the mass is

$$m_e\ddot{x}+C_e\dot{x}+K_ex=m_e\ddot{x}_o, \tag{6.4}$$

where m_e : equivalent mass of column, C_e nonlinear damping coefficient dependent on velocity and displacement, and K_e nonlinear stiffness coefficient dependent on displacement.

The eqivalent column stiffness and damping coefficients and equivalent mass are derived from column static and dynamic experiments. The column stiffness and damping coefficients are generally defined in polynominal form.

$$K_e=\sum_{i-0}^{n}K_ix^i, \qquad C_e=\sum_{i-0}^{n}C_{1i}x^i+\sum_{i=0}^{n}C_{2i}\dot{x}^i.$$

According to the experiment. K_e and C_e are presented as

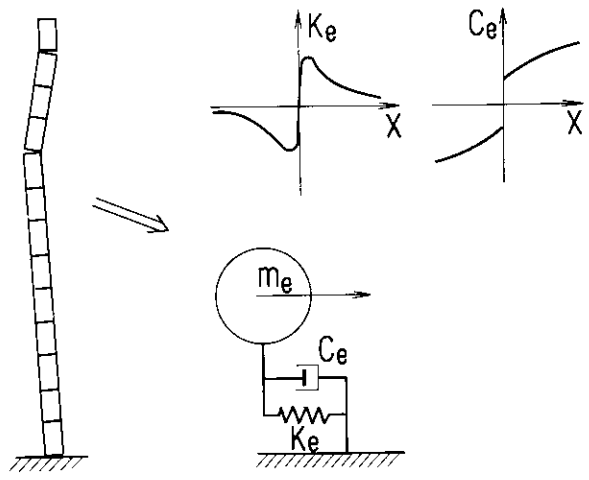

(a) Detailed model (b) Simplified model

Fig. 6.2 Detailed and simplified models for column vibration

$$K_e(x)=K_0+K_1x+K_2x^2, \qquad C_e(x)=C_0+C_1x\ .$$

An example of the equivalent column stiffness coefficient and damping factor (derived from experiment of a scale model) are shown in Fig. 6.3 and Fig. 6.4. (it is dimension scaled by 1/2 and weight acaled by 1/4 of a stacked column of the experimental HTGR.)

The equivalent stiffness coefficient was determined by the column restoring force and displacement curve which was obtained by the static loading test of the maximum deflection point of the column first order vibration mode. It is seen from Fig. 6.3 that equivalent stiffness is nearly linear at small displacement of the column and gradually decreases as a displacement increases (the column shows soft spring characteristics).

The equivalent damping coefficient was calculated by the measured resonant frequency and damping ratio in the vibration tests. The coefficient C_e can be calculated by the following equation.

$$C_e=C_0,\ C_0=2mh\ (2\pi f_n)\ , \tag{6.5}$$

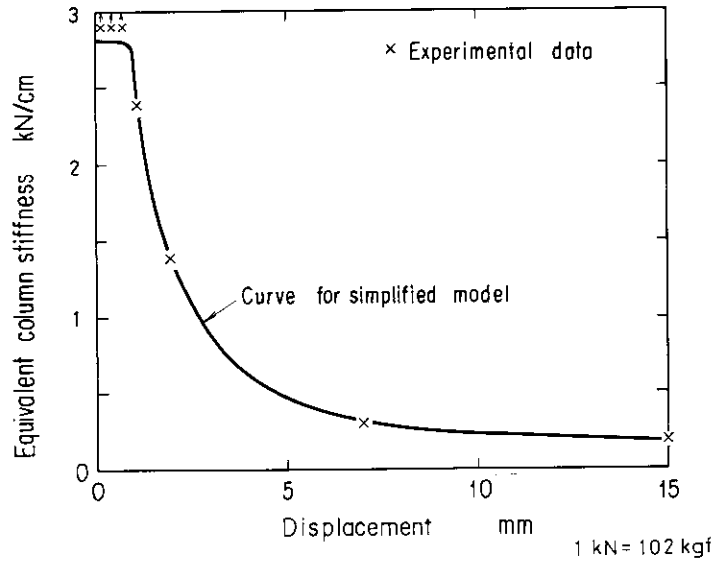

Fig. 6.3 Equivalent column stiffness vs. displacement

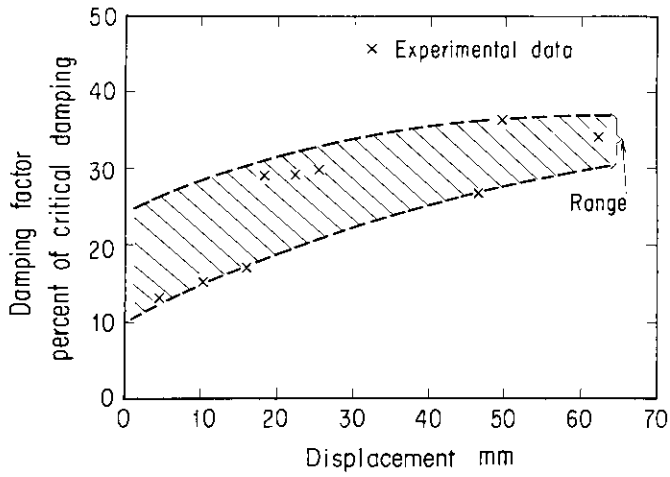

Fig. 6.4 Damping factor vs. displacement

where m is the mass calculated by Eq. (6.6) and h and f_n the damping ratio and natural angular frequency, respectively.

It is seen that the equivalent damping factor varies from 10 to 40 % of critical damping. The damping factor increases with an increase of column displacement.

The equivalent mass was calculated by the static deflection mode which was seasured by the static load tests. Mass m can be calculated by the following equation.

$$m=\Sigma\phi_i^2 m_i/\phi_l^2 , \tag{6.6}$$

where m_i and ϕ_i are the mass and deflection of the i-th block and ϕ_l the deflection of a loading block.

6.2.3 Simplified model with column boundary

Where a boundary exists, the impact element simulating impact behavior of the core blocks by spring and dashpot is attached to each column block with a gap between neighbor columns as shown in Fig. 6.5. The equation of motion is

$$m_e\ddot{x}+C_e\dot{x}+K_e x=m_e\ddot{x}_o+F_c , \tag{6.7}$$

where, F_c is the impact force between columns.

The initial gap between two adjacent columns is defined by parameter δ. The spring and damping forces as functions of relative displacement and velocity of two impacting bodies are:

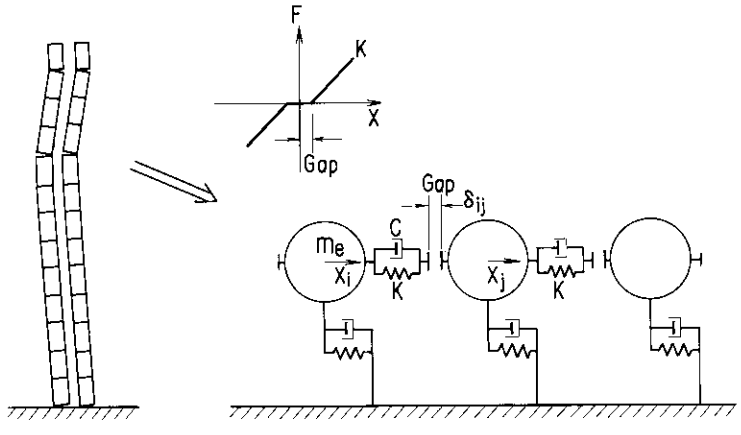

(a) Column array (b) Simptified model

Fig. 6.5 Simplified model for block impact

Spring force F_S

$$\left.\begin{aligned} F_S &= K(x_i - x_j - \delta_{ij}) \ ; \ \text{if} x_j < x_i - \delta_{ij} \ , \\ &= 0 \qquad\qquad\quad ; \ \text{if} \ x_j \geqq x_i - \delta_{ij} \ . \end{aligned}\right\} \tag{6.8}$$

Damping force F_D

$$\left.\begin{aligned} F_D &= C(\dot{x}_i - \dot{x}_j) \ ; \ \text{if} \ x_j < x_i - \delta_{ij} \ , \\ &= 0 \qquad\qquad ; \ \text{if} \ x_j \geqq x_i - \delta_{ij} \ . \end{aligned}\right\} \tag{6.9}$$

The impact force is then

$$F_C = F_S - F_D \ . \tag{6.10}$$

6.2.4 Damping coefficient in viscoelastic impact model

Let us consider the damping coefficient in the viscoelastic impact model. In the study, impact behavior is confined to elastic bodies impacting one another; and it is represented by the viscoelastic element as shown in Fig. 6.6. The kinematic energy of impact bodies, the potential energy of the elastic spring and the dissipation energy of the dashpot are as follows:

$$T = \frac{1}{2} m\dot{x}_1^2 + \frac{1}{2} m\dot{x}_2^2, \quad U = \frac{1}{2} K(x_1 - x_2 - \alpha_{12})^2, \quad F = \frac{1}{2} C(\dot{x}_1^2 - \dot{x}_2^2)^2 .$$

The Lagrange equations of motion are

$$\frac{d}{dt} \cdot \frac{\partial T}{\partial \dot{x}} + \frac{\partial U}{\partial x} + \frac{\partial F}{\partial \dot{x}} = 0 \ , \tag{6.11}$$

$$m\ddot{x}_1 + C(\dot{x}_1 - \dot{x}_2) + K(x_1 - x_2 - \delta_{12}) = 0 \ , \tag{6.12}$$

$$m\ddot{x} + C(\dot{x}_2 - \dot{x}_1) + K(x_2 - x_1 + \delta_{12}) = 0 \ . \tag{6.13}$$

Assume the following as the particular solutions of Eqs. (6.12) and (6.13)

$$x_1 = a_0 + a_1 t + a_2 e^{\lambda t}, \quad x_2 = b_0 + b_1 t - b_2 e^{\lambda t}, \tag{6.14}$$

where a_0, a_2, b_0, b_1, b_2 and λ are constants. And the initial conditions are

$$x_1 = 0, \ x_2 = -\delta_{12}, \ v_1 = \dot{x}_1 = 0, \ v_2 = \dot{x}_2 = 0, \ t = 0 \ . \tag{6.15}$$

We have the following equations from Eqs. (6.14) and (6.15)

$$a_0 = 0, \ a_1 = a_2\lambda = 0, \ b_0 = -\delta_{12}, \ b_1 - b_2\lambda = v_2 \ . \tag{6.16}$$

Substituting Eq. (6.16) into Eq. (6.14) gives

$$x_1 = a_1 t - a_2 e^{\lambda t}, \quad x_2 = -\delta_{12} + b_1 t + b_2 e^{\lambda t}. \tag{6.17}$$

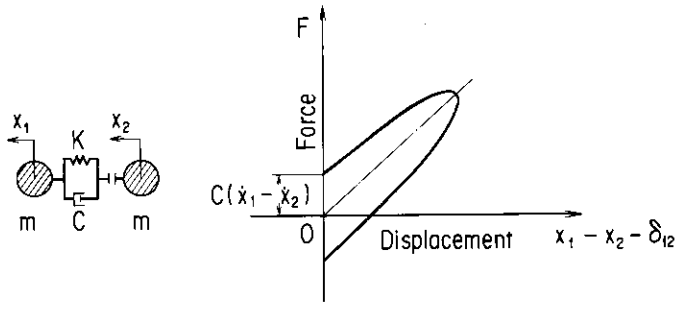

(a) Mass impacting model (b) Hysteresis loop for impact

Fig. 6.6 Viscoelastic model with two impacting bodies

Substituting Eq. (6.17) into Eqs. (6.12) and (6.13) yields

$$\left.\begin{aligned}&(C+Kt)(a_1-b_1)+e^{\lambda t}\{ma_2\lambda^2+C(a_2-b_2)\lambda+K(a_2-b_2)\}=0\ ,\\&(C+Kt)(b_1-a_1)+e^{\lambda t}\{mb_2\lambda^2+C(b_2-a_2)\lambda+K(b_2-a_2)\}=0\ .\end{aligned}\right\} \tag{6.18}$$

Since Eq. (6.18) is satisfied generally at all times, the equations below may be derived

$$a_1=b_1,\quad a_2+b_2=0,\quad a_2-b_2=-\frac{v_2}{\lambda}. \tag{6.19}$$

From Eqs. (6.16) and (6.19)

$$a_1=b_1=\frac{v_2}{2}. \tag{6.20}$$

Hence we obtain the so-called characteristic equation from Eqs. (6.18)

$$(m\lambda^2+2C\lambda+2K)a_2e^{\lambda t}=0\ \text{ or }\ \lambda^2+2\omega_n h+\omega_n^2=0, \tag{6.21}$$

where

$$\omega_n\equiv\sqrt{2K/m},\quad C_c\equiv\sqrt{2mK},\quad C/C_c\equiv h, \tag{6.22}$$

$$\lambda=\omega_n(-h\pm\sqrt{h^2-1})\,. \tag{6.23}$$

Since the impact takes place as an internal damping, the damping factor is smaller than 1. Equation (6.23) becomes

$$\lambda=\omega_n(-h\pm i\sqrt{1-h^2})\,, \tag{6.24}$$

or

$$\lambda=\omega_n(-h+\sqrt{1-h^2})\,. \tag{6.25}$$

Substituting Eqs. (6.20) and (6.25) into (6.17) gives

$$\left.\begin{aligned}x_1&=\frac{v_2}{2}t+a_2exp(-h\omega_n t+i\omega_n\sqrt{1-h^2}t)\ ,\\x_2&=-\delta_{12}+\frac{v_2}{2}t+b_2exp(-h\omega_n t+i\omega_n\sqrt{1-h^2}t)\,.\end{aligned}\right\} \tag{6.26}$$

$$\left.\begin{aligned}x_1&=\frac{v_2}{2}t+a_2exp(-h\omega_n t)sin\omega_n\sqrt{1-h^2}t\ ,\\x_2&=-\delta_{12}+\frac{v_2}{2}t+b_2exp(-h\omega_n t)sin\omega_n\sqrt{1-h^2}t\ .\end{aligned}\right\} \tag{6.27}$$

Applying the initial conditions, we obtain the relations

$$\left.\begin{aligned}&\frac{v_2}{2}+a_2\omega_n\sqrt{1-h^2}=0,\quad (t=0\ ;\ \dot{x}=0)\ ,\\&\frac{v_2}{2}+b_2\omega_n\sqrt{1-h^2}=v_2,\quad (t=0\ ;\ \dot{x}=v_2)\ .\end{aligned}\right\}$$

which are solved for a_2 and b_2 to give

$$a_2=-\frac{1}{\omega_n\sqrt{1-h^2}}\cdot\frac{v_2}{2}\ ,\quad b_2=\frac{1}{\omega_n\sqrt{1-h^2}}\cdot\frac{v_2}{2}\ .$$

Therefore after the impact Eq. (6.27) becomes with the initial conditions

$$\left.\begin{aligned}x_1&=\frac{v_2}{2}t-\frac{1}{\omega_n\sqrt{1-h^2}}\cdot\frac{v_2}{2}exp(-h\omega_n t)sin\omega_n\sqrt{1-h^2}t\ ,\\x_2&=-\delta_{12}+\frac{v_2}{2}t+\frac{1}{\omega_n\sqrt{1-h^2}}\cdot\frac{v_2}{2}exp(-h\omega_n t)\sin\omega_n\sqrt{1-h^2}t\ .\end{aligned}\right\} \tag{6.28}$$

Since $x_1-x_2=\delta_{12}$ when two bodies leave each other after impact, from Eq. (6.28) the contact time

is derived as

$$-\frac{1}{\omega_n\sqrt{1-h^2}}v_2 exp(-h\omega_n t)sin\omega_n\sqrt{1-h^2}t=0,$$

or

$$\omega_n\sqrt{1-h^2}t_c=\pi, \quad t_c=\frac{\pi}{\omega_n\sqrt{1-h^2}},$$

where t_c is the contact time.

Velocities of the two impacting bodies after impact are

$$(\dot{x}_1)_{t=t_c}=\frac{v_2}{2}+\frac{v_2}{2}exp(-h\omega_n t_c)=\frac{v_2}{2}(1+exp(-h\omega_n t_c)),$$

$$(\dot{x}_2)_{t=t_c}=\frac{v_2}{2}-\frac{v_2}{2}exp(-h\omega_n t_c)=\frac{v_2}{2}(1-exp(-h\omega_n t_c)).$$

The coefficient of restitution η is

$$\eta=-\frac{(\dot{x}_2)_{t=t_c}-(\dot{x}_1)_{t=t_c}}{v_2}, \tag{6.29}$$

or

$$\eta=exp(-h\omega_n t_c)=exp\left(-\frac{\pi h}{\sqrt{1-h^2}}\right). \tag{6.30}$$

In the model the relation between the damping factor h and the coefficient of restitution η is thus obtained, and from Eq. (6.22) the relation between the damping factor h and the damping coefficient C is also obtained

$$C=\sqrt{2mK}h, \tag{6.31}$$

or

$$C=2m\omega_n h=2mh(2\pi f_n). \tag{6.32}$$

Since the coefficient of restitution η, the contact time t_c and the natural frequency ω_n are obtained from the experimental data, the damping factor h is calculated from Eq. (6.30). Finally the damping coefficient can be calculated from Eq. (6.32).

6.3 Results and discussions

The governing equations were numerically solved by using the procedures of the Runge–Kutta integration schemes.

The numerical data presented for calculations were generated with $C_e=C_o=0.588$ kN • s/m, $m=120$ kg, and K_e from Fig. 6.3.

To confirm the validity of the simplified model, the analytical results are compared with those of the experiment and the detailed model. Figure 6.7 shows response characteristics for sinusoidal excitation which sweeps up in frequency. In the figure, circles show the experimental results and the solid line and broken line show those of the simplified and the detailed models, respectively. The results are in good agreement with those of the experiment and the detailed model. A nonlinear jump phenomenon is seen in the results of the simplified model.

The ratio of computer processing time of the simplified model to that of the detailed model is about 1 : 30 for the above problem.

Figure 6.8 shows relationship between excitation frequency and impact force in the simplified model, as compared to results from both the experiment and the detailed model. The results are in relatively good agreement with those of the evperiment and detailed model.

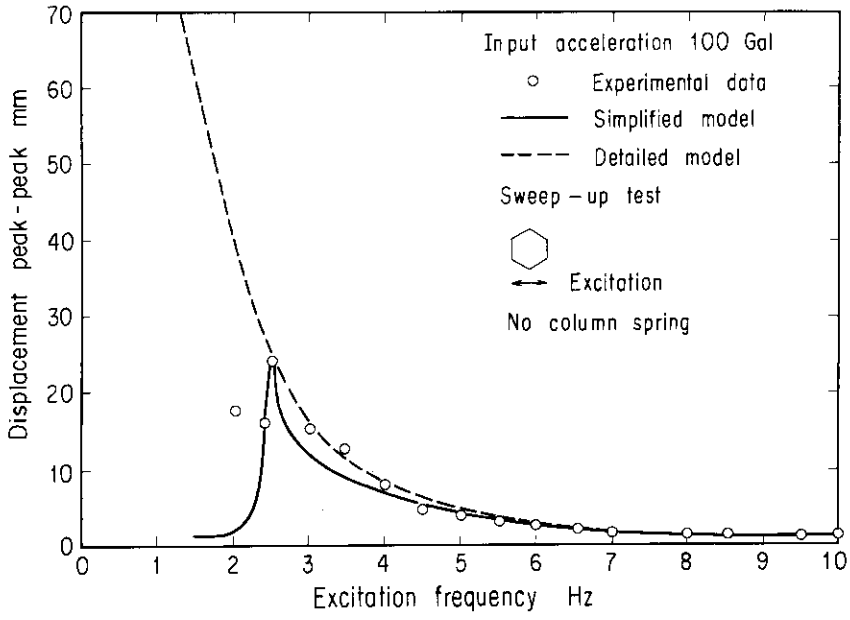

Fig. 6.7 Displacement vs. excitation frequency (Sweep–up test)

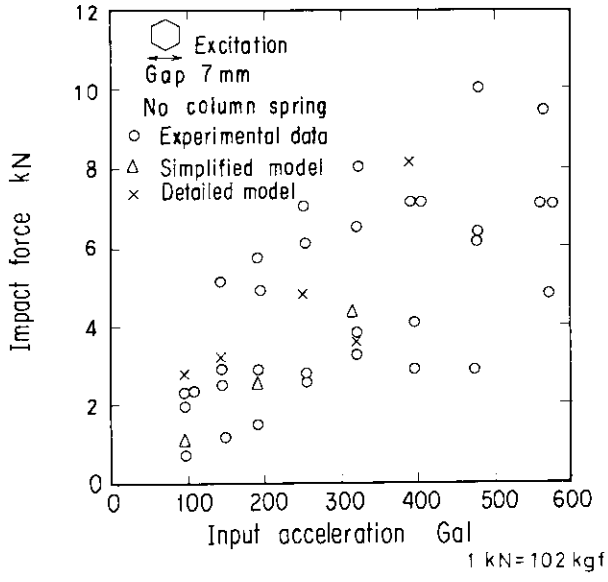

Fig. 6.8 Impact force vs. imput acceleration

6.4 Concluding remarks

Successful application of the simplified model which uses one degree–of–freedom mass with non-linear column stiffness and damping characteristics has been shown for the seismic response of a column.

By the analysis and in comparing with the results of experiment and datailed analysis, the following conclusions have been reached:

(1) The results of the test problems show validity of the simplified model in nonlinear core dynamic analysis.

(2) The computer cost of time history analysis of the HTGR core by the simplified model is signficantly lower than that of the detailed model.

7. Seismic Response of a Two-dimensional Vertical HTGR Core

7.1 Intorduction

The column vibration behavior and impact characteristics in two-dimensional elevation were clarified in the single column test. The softening and hardening characteristics of the stacked block column are revealed in the single column tests. The effects of the gap width between the column and lateral boundary on the impact forces and the effects of the excitation direction of the hexagonal column were also revealed. Whirling of the column and the effect of the pressure difference from the top of the column upon the vibration characteristics were clarified in the one region core tests. Subharmonic frequency due to the unsymmetrical support in the column upper gap were also determined.

However, multi-column interacting motion and impact forces, effects of the side support stiffness upon column displacments, impact forces and dowel forces are not clear yet. For this purpose, vibration tests of the two-dimensional vertical slice model were coducted. A vertical slice model (twelve stacked block columns and two permanent side reflector columns) across the center of the core was selected.

Uni-axial, horizental, sinusoidal and time history excitation tests of a half scale model were performed by using a shaking table to obtain the vibration mode, and dynamic properties; as function of frequency, such as acceleration level, side support stiffness and effects of gas pressure simulating spring, collision forces and distributions along the column and dowel forces.

7.2 Experimental apparatus and method

7.2.1 Experimental apparatus

A vertical slice across the core was selected and twelve fuel columns and two permanent side reflector columns were modeled as shown in Fig. 7.1 and photo. 7.1. Each column was composed of twelve graphite blocks and one steel block of the same shape, giving a total of thirteen layered blocks. The three columns were grouped to form simulating a one fuel exchange region. The blocks within the center column (simulating the control rod channel column) of each region were placed downward relative to the two surrounding columns. In each block, as shown in Fig. 7.2, there were three dowel pins in the top and three dowel holes in the bottm for alignment of the block column. The bottom block in each column was doweled to the core support plate. Therefore, in the column, the horizontal motion between layered blocks is restricted, but rocking or vertical motions are permitted. In the real core, each fuel region is joined together at the top blocks. Simulating the joined blocks, a tie plate of three columns each was adopted.

Each side reflector block (simulating a permanent side reflector) was fixed to the steel frame by side restraint structures. Three kinds of side support springs were provided, namely; hard support spring, combined bilinear soft support with hard stop, and intermediate support. The spring rates were as shown in Table 7.1; (1) hard spring support, 8134 kN/m. (2) intermediate spring support, 588 kN/m and (3) combined billinear soft spring and stop support, 39.2/784/8134 kN/m. The side support spring was changed to examine effects of support stiffness upon the core vibration response.

In the real core, a core support block is supported by graphite posts. In the test model roller bearings between the core support plate and the base plate in the steel frame were used. The roller bearing permitted lateral movement of the core floor without residual vertical travel that accompanied support post rocking motion in the real core.

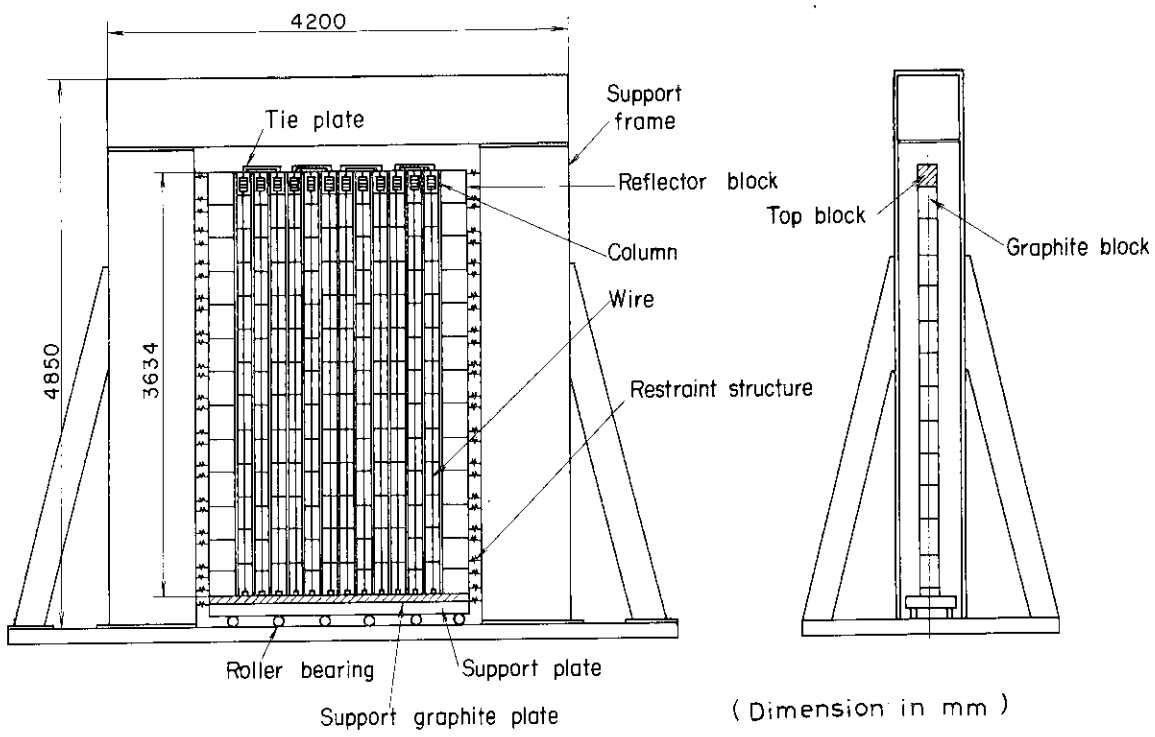

Fig. 7.1 Experimental apparatus of two-dimensional vertical core moddl

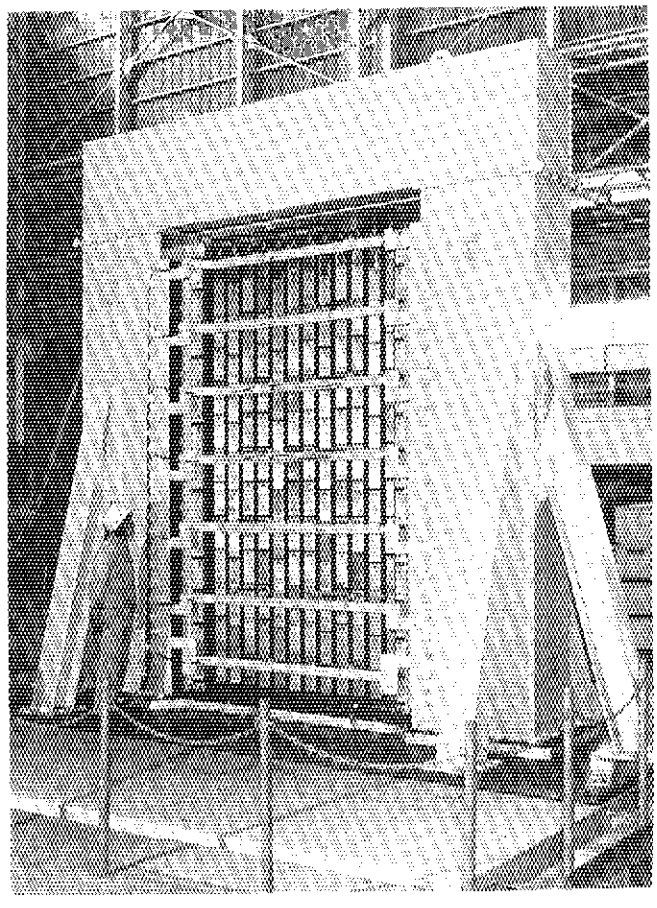

Photo. 7.1 External appearance of two-dimensional vertical core model

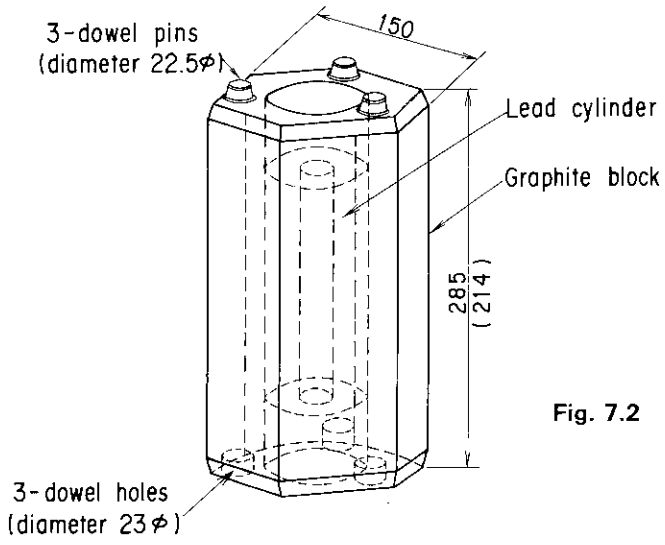

Fig. 7.2 Graphite fuel block
(Dimension: mm
Weight : 285mm, 19.1kg
214mm, 14.3kg)

Table 7.1 Spring constant of support structure

Support spring			Spring constant (kN/m)	
			Reflector block	Support plate
Hard			8134	5880
Intermediate			588	725
Soft	Displacement (cm)	$0<\delta<1.1$	39.2	39.2
		$1.1<\delta<5.5$	784	784
		$\delta<5.5$	8134	5880

(1 kN/m = 1.02 kgf/cm)

The model represented the reactor core in its cold and fully irradiated state so that the gap width between columns was 2 mm (4 mm in the real core) . This test condition was expected to have the most severe response, clarified in previous experiments. The total cross core gap of the model was constant at 26 mm, with the gap in the top block layer equal to 6.5 mm (each gap width 0.5 mm). The gap width between top blocks was changed from 0.5 mm to 2 mm by means of changing two different top blocks. In this way the motion of the column and its impact characteristics depending on the top gap width were examined.

The gas pressure defference along the column was then simulated by the compressive force of a spring attached to the top of the column, in order to examine effects of a pressure difference upon the column characteristics.

According to the similarity laws graphite fuel blocks were dimension scaled by 1/2 and weight scaled by 1/4 of the real fuel blocks of the experimental HTGR under design study in JAERI. To make a correction to the weight, as indicated in Fig. 7.2, a lead cylinder was inserted to in the middle of each block as an additional mass. The block material was a nuclear grade graphite of apparent spcific gravity 1.74, and Young's moduls 8 GPa,

The support frame was a steel box, having sufficient rigidity (primary natural frequency 20 Hz) . As a unit with the group of columns inside, the frame was fixed on a shaking table.

Measurements were made, as shown in Fig. 7.3, of relative displacements between blocks and support frame and hoizontal and vertical impact accelerations between the blocks and between the blocks and side reflector blocks. Impact reaction forces of the reflector blocks were measured by strain gauges attached to the side support structures.

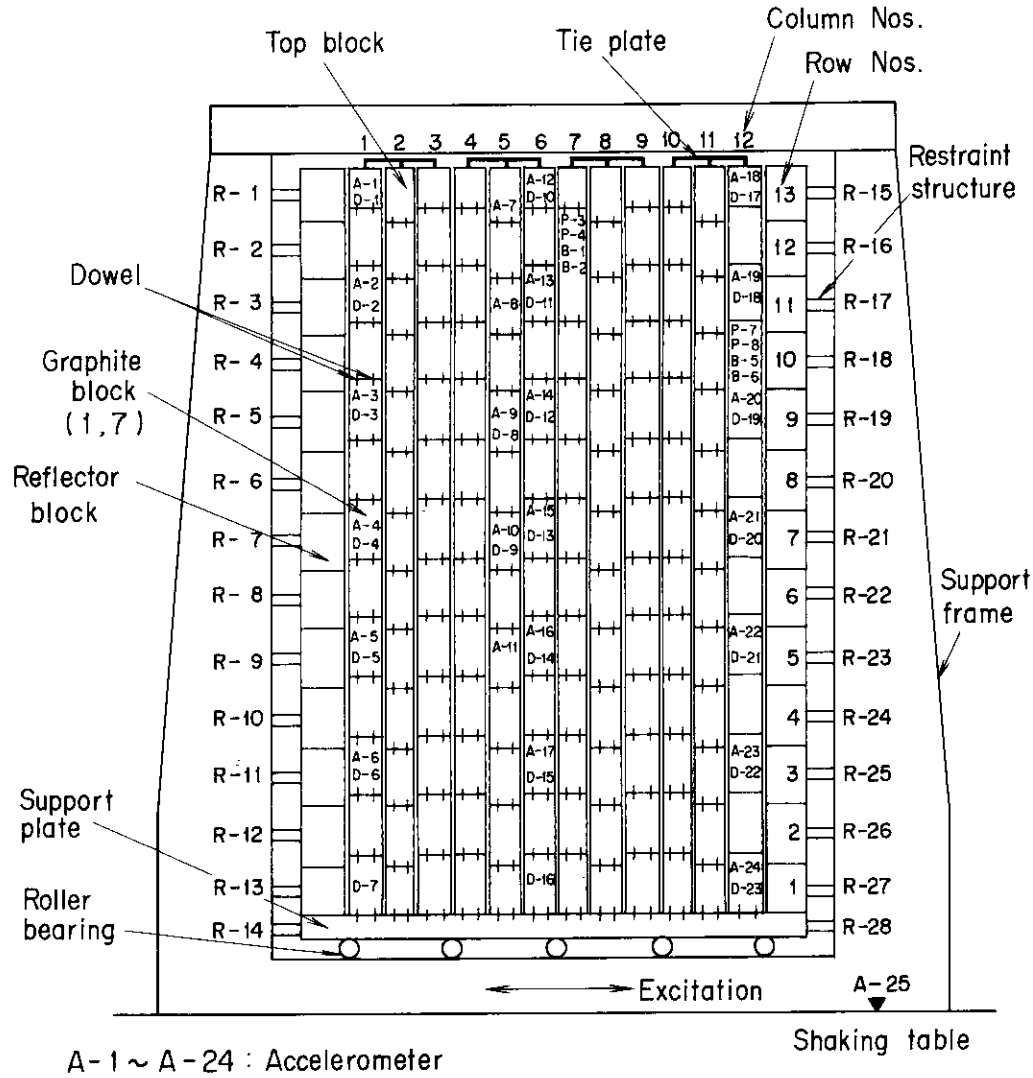

Fig. 7.3 Instrument location

The displacement detectors used were differential transformers. Piezoelectric impact accelerometers were used. In order to measure the dowel force strain gauges were set on dowel pins and dowel holes of selected graphite blocks.

7.2.2 Experimental method

Uni-axial horizontal excitation tests were made on a group of columns on a shaking table. Excitation conditions were ranging in frequencies from 1 to 10 Hz and accelerations from 50 to 50 Gal. The effects on column motion and impact charactersitics like excitation frequency and acceleration, side support stiffness, top blocks gap width and a gas pressure simulation spring were thus exmined.

Sinusoidal waves and random excitation waves such as the El Centro 1940 NS, the Ibaraki 1964 EW and a white noise wave were used to vibrate the shaking table. In the seismic wave, the time scale was reduced to $1/\sqrt{2}$ to fit the laws of similarity.

The sinusoidal frequency sweeps, sweeping up and down from 1 to 10 Hz range, were applied to study

the nonlinear resonance of the columns. The vibration tests of constant input acceleration levels from 50 to 500 Gal were carried out to obtain column motion and impact response as function of the acceleration levels. To estimate column damping, the shaking table was arrested abruptly and the damping factor was obtained from the free vibration column displacement decay.

7.3 Results and discussions

7.3.1 Displacement characteristics

(1) Vibration mode and distribution of side reflector reaction force along column

The vibration modes are classified into two categories, i. e. the low and high frequency ranges. In a low frequency range, where the primary vibration mode of the column is dominant, columns vibrate together and the reflector reaction forces are larger at the top layer of the column. Figure 7.4 shows an example of the column displacements and reflector reaction forces at a low excitation frequency. At the low excitation frequency, the core oscillates as a tightly lumped mass between the side reflector bundaries. The core lumping increases with increasing excitation frequency. At still higher frequency the core lumping rapidly decreases. At an high frequency range subharmonic vibration of the column was observed and each column vibrates in random collision with adjacent columns (see Fig. 7.6) . The reflector reaction forces and block displacements are large at around two-thirds of the column length.

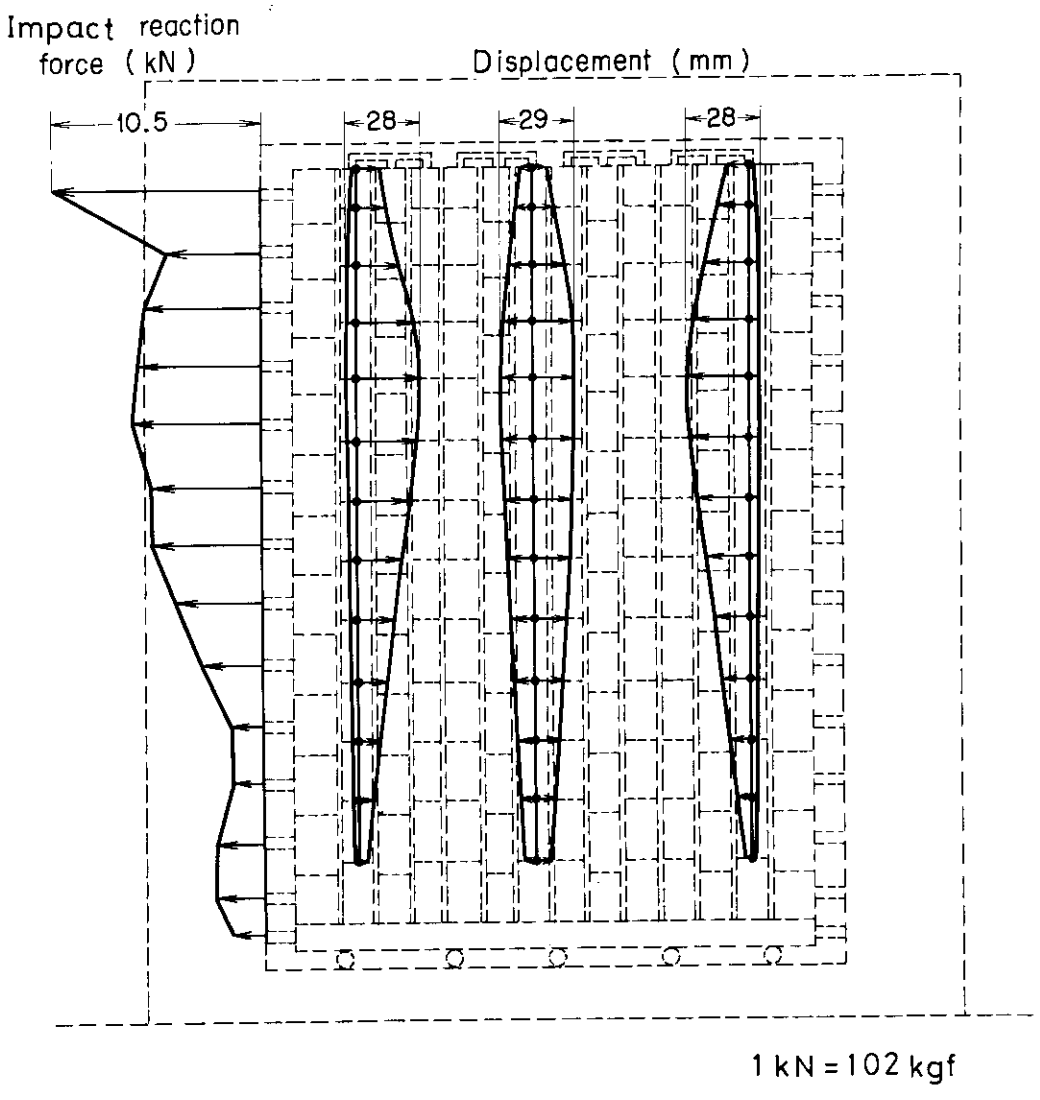

Fig. 7.4 Displacement and impact reaction force along column (Sinusoidal wave 3 Hz, Max. acceleration 250 Gal)

(2) Effect of acceleration level on column displacement

Figure 7.5 shows the column displacements versus excitation freauency as function of input acceleration levels. The curves are characteristics of the behavior a nonlinear and discontinuous structure such as the core vertical section tested. At a certain frequency, sudden drop-off in response occurs. This is clearly illustrated in the figure. With an increase in excitation level, the column displacements increase. It is seen that with an increase of the input accelerations, the frequency for rapid drop of the column displacements, i. e. the jump-down frequency shifts to an higher frequency.

(3) Effect of support stiffness on column displacement

Figure 7.6 shows effects of hard and soft support of the support structure on the column displacements. It is seen that with a decrease of the reflector side support stiffness, the column displacements

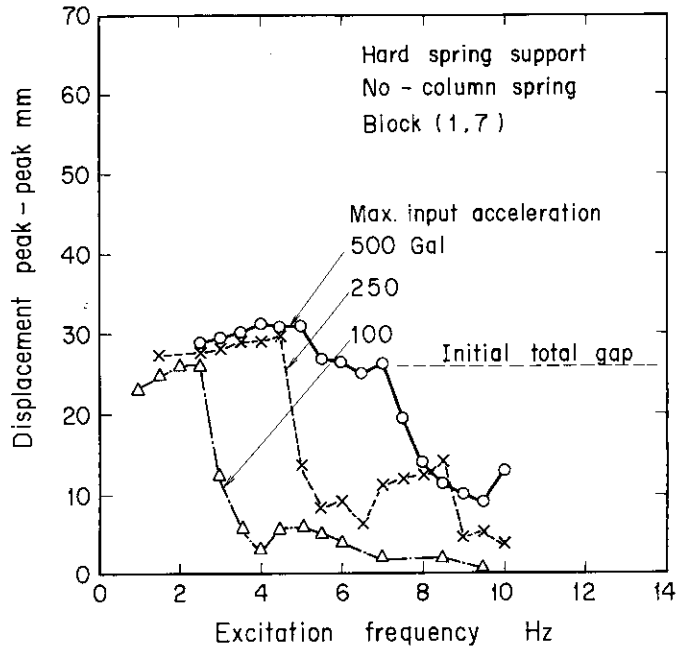

Fig. 7.5 Effect of input acceleration on displacement

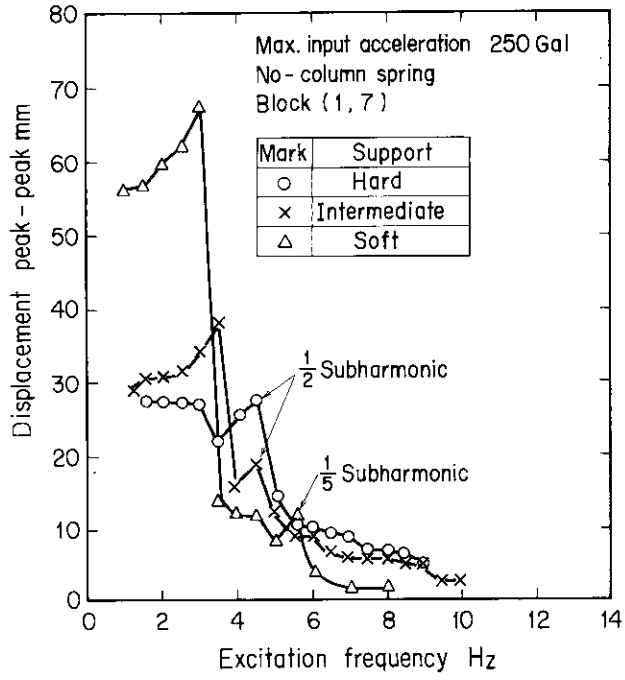

Fig. 7.6 Effect of support stiffness on displacement

displacements increase. The soft spring support results in large desplacements which affect the insertion of control rods.

(4) Effect of gas pressure difference simulation spring on column displacement

Figure 7.7 shows the column displcements with and without a spring simulating a gas pressure difference. It is seen that the jump-down frequency for the column displacements are higher with the spring than without it. The column displacements are also small with the spring. The above is due to an increase in the frictional force between the upper and lower blocks caused by compressive force of the spring.

(5) Comparion of column displacement between core periphery and core center

The column displacements are shown in Fig. 7.8, between the core periphery and the center. The

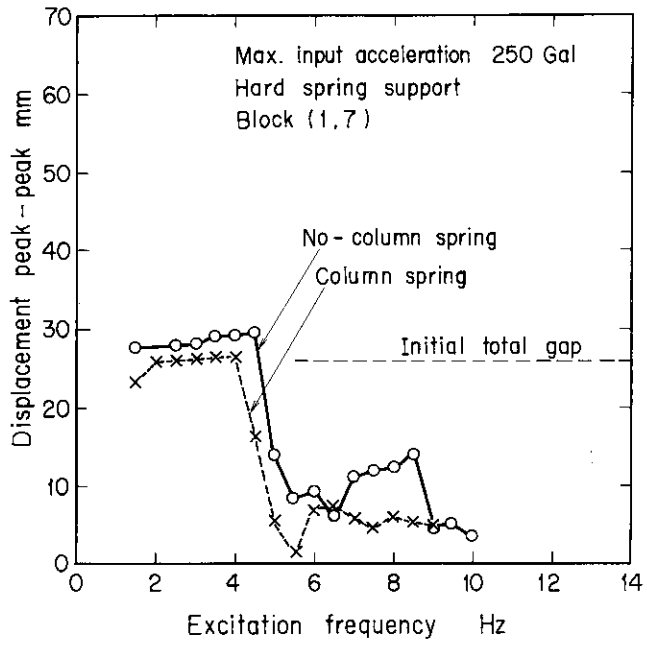

Fig. 7.7 Effect of spring simulating gas pressure on displacement

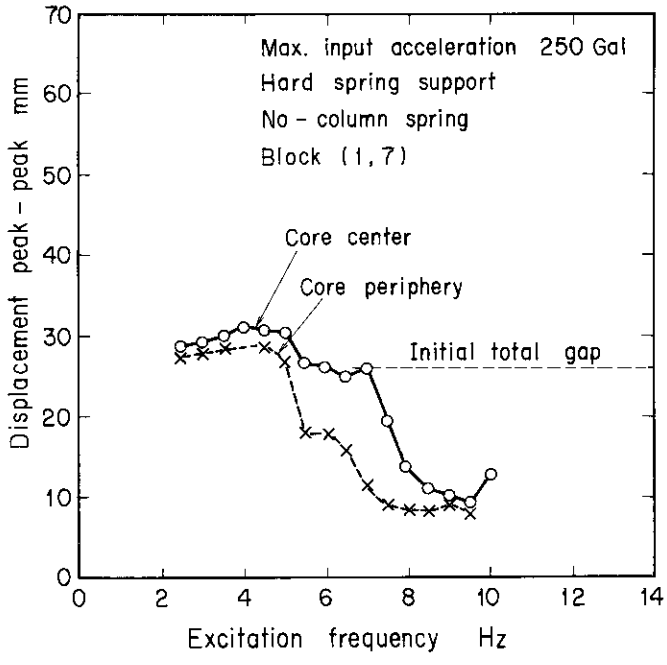

Fig. 7.8 Comparison between core periphery and core center on displacement

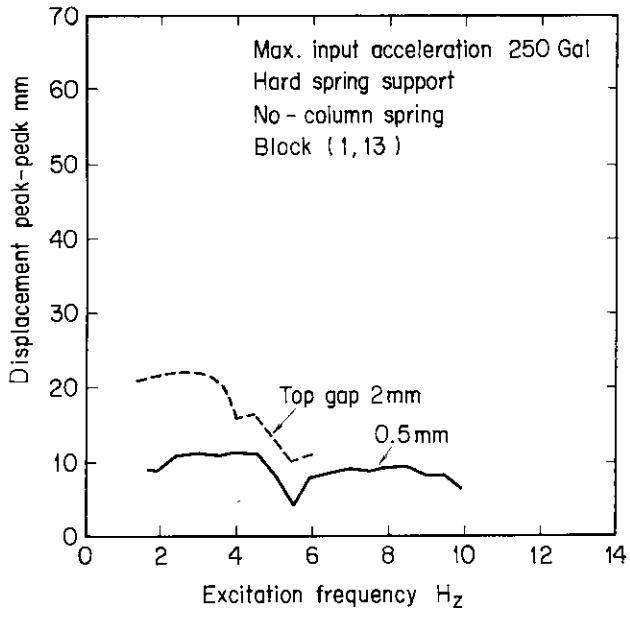

Fig. 7.9 Effect of top gap width on displacement

column displacements as shown in the figure, vary depending on both the position relative to the boundary and excitation frequency. The column displacements are larger in the core center than in the core periphery. It is seen that the column moves between two outermost columns. This makes sense since the outermost column travels only a short distance in the opposite direction to the rest of the core (the side reflector column) .

(6) Effect of gap width between column top blocks on column displacement

Figure 7.9 shows the displacements of the column top block versus excitation frequency, comparing 0.5 mm (standard case) and 2 mm of gap width between the column top blocks. It is seen that with decreasing gap width of the column top blocks, the column displacements decrease.

(7) Column damping factor

Overall column damping factors were obtained by sudden arrest of the shaking table motion (sinusoidal excitation) and the recording of the column amplitude decay motions. The displacements are observed to decay to less than measurable values after only several cycles following the apparatus shutdown. It is difficult to estimate the column damping expressed as equivalent viscous damping from the column displacement decay motions. It was estimated that the column damping factors are 4～10% of critical. The damping factor increases with increasing displacements. It this case the column displacements measured were small, so the damping factors are small.

(8) Contact duration

For the seismic simulation analysis of a HTGR core behavior including impacts, it is necessary to know the contact duration. The contact duration was measured using two blocks pendulum collision tests. The values are 0.60～0.65 milli-seconds when impact velocities are 10 to 200 cm/s. However, the actual contact duration for blocks in the core must be measured and the average value is to be introduced in simulation analysis. Therefore, the contact duration was estimated from the measured acceleration wave form of an impact between adjacent blocks. Under the experimental conditions (such as impact velocities 10～15 cm/s) , the contact durations are 1～2 milli-seconds.

7.3.2 Impact characteristics

(1) Effect of input acceleration level on impact reaction force

Figure 7.10 shows the impact reaction forces as function of input acceleration levels for excitation frequency. It is seen that the impact reaction force increases with an increase of the input acceleration

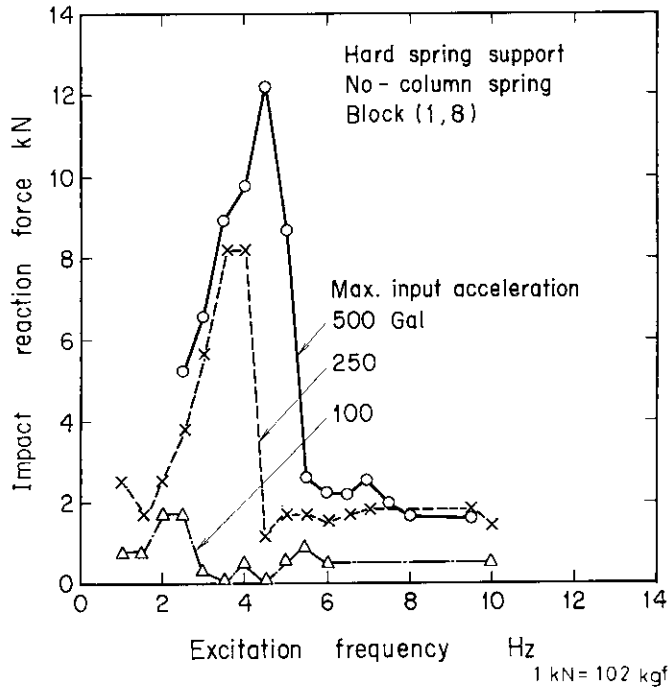

Fig. 7.10 Effect of input acceleretion on impact reaction force

levels. The resonant frequency is strongly excitation level dependent and shifts to high frequency with an increase of the input acceleration levels. These characteristics are typical of a nonlinear hardening spring mass system.

(2) Effect of support stiffness on impact reaction force

The effects of the reflector support stiffness on the impact reaction forces are shown in Fig. 7.11, comparing the hard spring support and the soft support. In the hard spring support, the impact reaction forces are larger than in the soft support and the resonant frequency shifts to a higher level. The soft spring support of the fixed side reflector block reduces the impact forces, but the large reflector

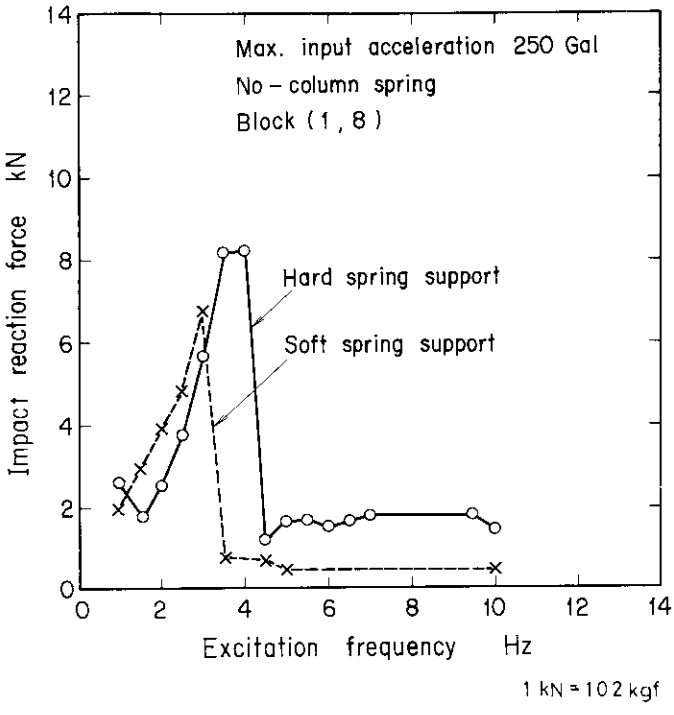

Fig. 7.11 Effect of support stiffness on impact reaction force

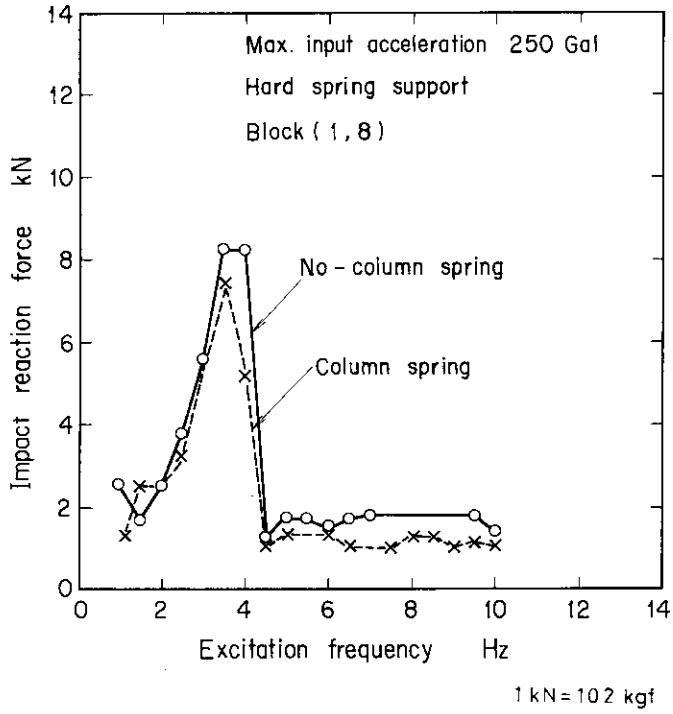

Fig. 7.12 Effect of spring simulating gas pressure on impact reaction force

displacements result in a large core displacement. A core design with the soft spring support is therefore not favorable for control rod insertion during seismic disturbance.

(3) Effect of gas pressure difference simulation spring on impact reaction force

Figure 7.12 shows the impact reaction forces of columns with and without a gas pressure difference simulating spring. The spring forces were chosen equivalent to a core gas pressure difference of 0.05 MPa.

In the figure, it is seen that the boundary reaction forces with the column spring are lower than without it. The above is due to the increase in friction force between the upper and lower blocks cused by the compressive force of the column spring. Since force caused by a gas pressure difference reduces the impact forces and the core displacements, the gas pressure difference favorably affects the core vibration

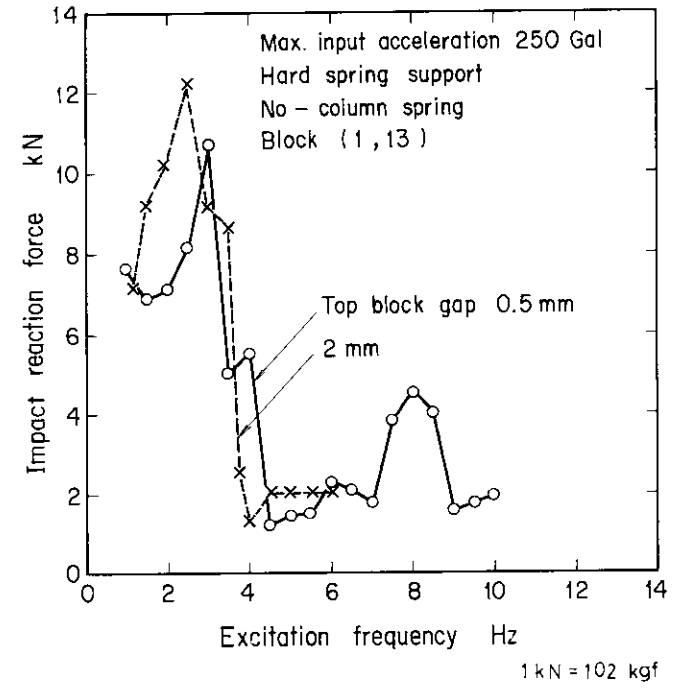

Fig. 7.13 Effect of support stiffness on impact reaction force

characersitics.

(4) Effect of gap width between top blocks on impact reaction force

Figire 7.13 shows the impact reaction forces of the column top block versus excitation frequency, comparing 0.5 mm and 2 mm of gap width between the column top blocks. It is seen that with a amall gap width between the column top blocks, the impact reaction forces decrease. Since a small gap width of the column top blocks reduces the core desplacements and the impact forces, the choice of a small gap width favourably affects the core aseismic design.

(5) Relationship between impact acceleration and impact reaction force

Figure 7.14 shows relation between the impact accelerations and impact reaction forces. It is seen that the impact acceleration and the impact reaction force have the same tendency with varying excitation frequency.

(6) Comparison of impact acceleration between core periphery and core center

The impact accelerations are shown in Fig . 7.15, between the core priphery and the core center

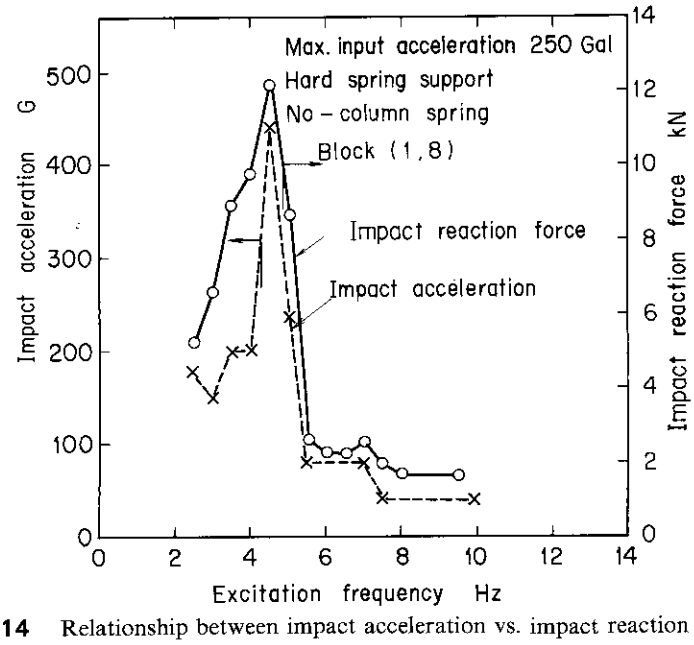

Fig. 7.14 Relationship between impact acceleration vs. impact reaction force

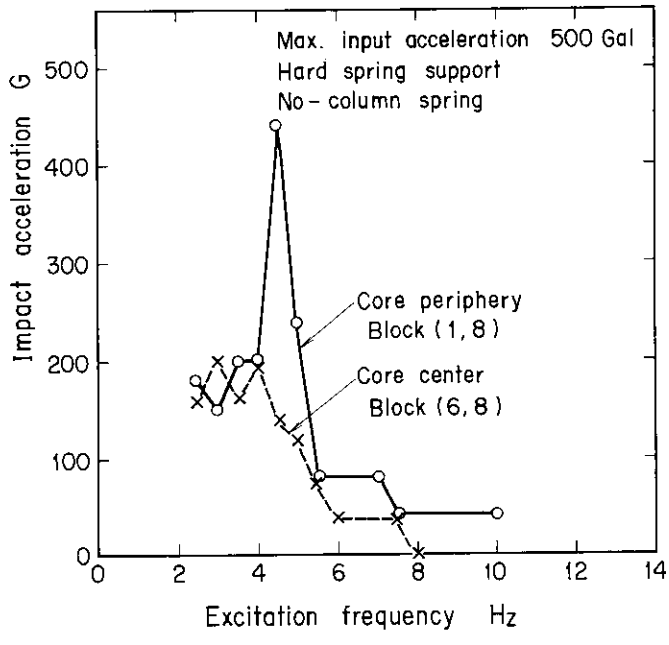

Fig. 7.15 Comparison between core periphery and core center on impact acceleration

comparatively. The impact forces, as shown in the figure, vary with both the positions in the core and excitation frequency. The impact forces are larger at core periphery than in core center. This causes core lumping which are larger at core periphery than in core center.

7.3.3 Dowel force

Since stresses of dowel pins and dowel holes are often most critical in a fuel block design under seismic load, it is important to obtain imformation for the dowel forces by experiment and/or analysis. The dowel forces were obtained from the vibration tests. The following are the results.

(1) Effect of input acceleration level on dowel force

The dowel forces versus excitation frequency as function of input acceleration levels are shown in Fig. 7.16. With an increase in excitation levels, dowel forces increase. It is seen that with the increase of the input accelerations, the resonant frequency of the dowel forces shifts to a higher values. This is caused by the hard spring characteristics of the dowel pins.

(2) Effect of support stiffness on dowel force

Effects of the reflector support stiffness on the dowel forces are shown in Fig. 7.17, comparing the

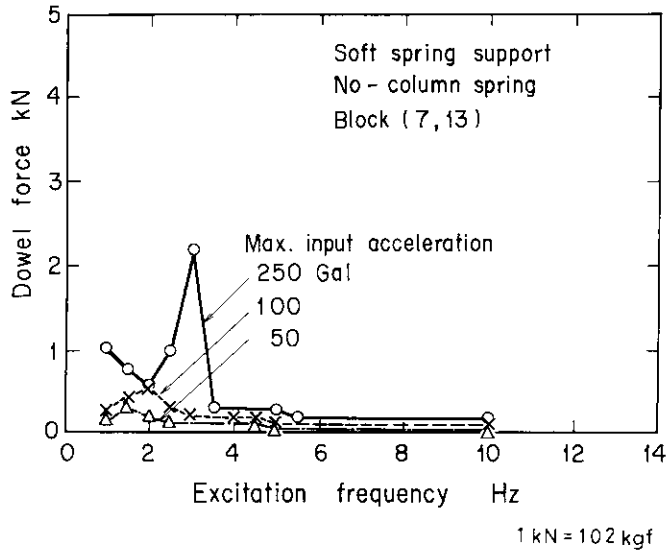

Fig. 7.16 Effect of input acceleration on dowel force

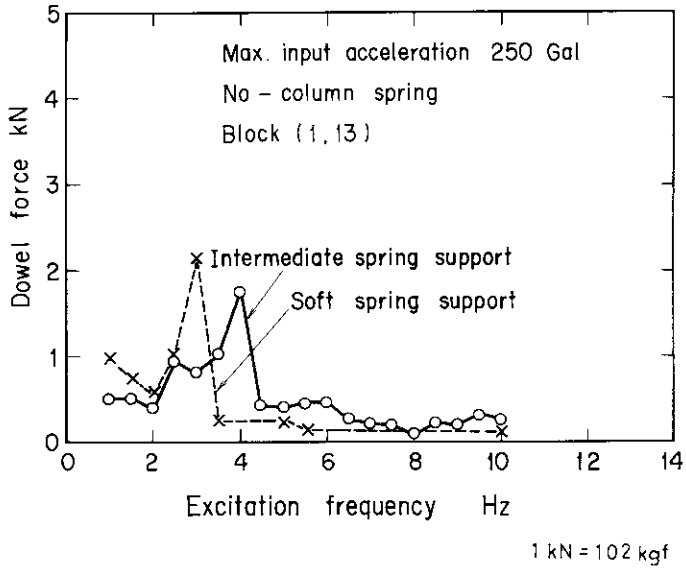

Fig. 7.17 Effect of support stiffness on dowel force

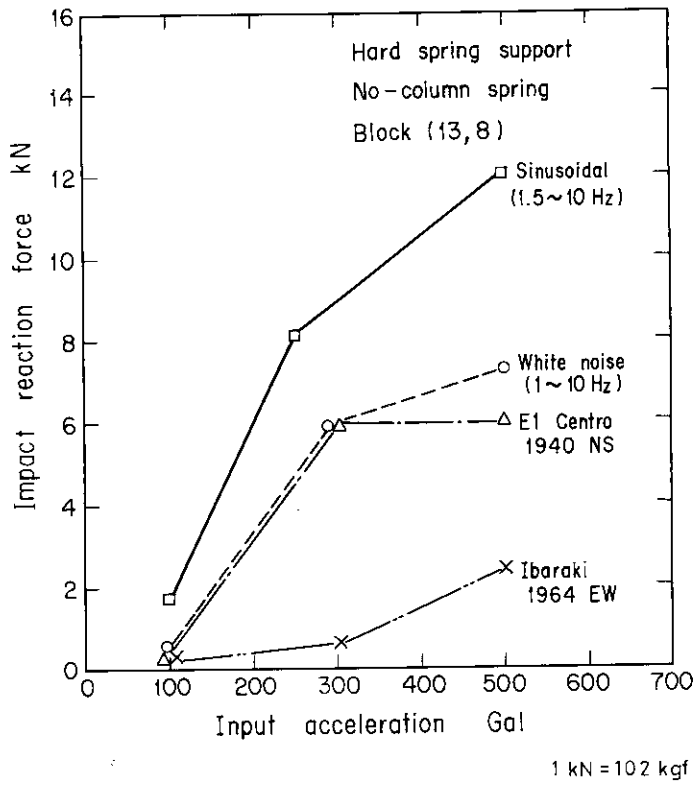

Fig. 7.18 Impact reaction force vs. input acceleration

intermediate spring support and the soft support. The figure illustrates that the dowel forces for the soft spring support are smaller than that for the intermediate support, since the columns are bent more with the soft support than with the hard support.

7.3.4 Random wave response

Maximum values of impact reaction forces from the El Centro earthquake, Ibaraki earthquake and white noise wave are given in Fig. 7.18, comparing with sinusoidal wave response values. These values represent the overall maximum for the indicated locations regardless of the time at which the maximum occurred. There is no impact at the low input acceleration level, so the impact forces are zero. Beyond a certain input acceleration level, there occurs an impact. The impact forces then increase almost proportionally with the input acceleration. The maximum impact forces for random waves are under 60% of that for sinusoidal waves.

7.4 Concluding remarks

An experimental study has been carried out with a two-dimensional core model which is a vertical silce along the axis of the experimental HTGR core. The forced vibration tests of a half scale model were performed by using a shaking table to obtain such dynamic properties as frequency response of the column displacements, the impact reaction forces and the dowel forces, vibration modes of core, accounting for effects of a gas pressure defference simulation spring, the reflector side support stiffness, and the column top gap width.

The more important experimental results and conclusions are the following.

(1) The column resonance curve shows typical nonlinear hardening characteristics. The resonant frequency increases with an increase of input acceleration and is strongly amplitude dependent.

(2) The column displacements and impact reaction forces increase with an increase of the input acceleration level.

reflector bondaries. The core lumping increases with increasing excitation frequency. At still higher frequency the core lumping rapidly decreases and subharmonic vibration occurs.

(4) The soft spring support of side reflector support structure causes large column displacements affecting the insertion of control rods. The soft spring support slightly reduces impact reaction forces but increases dowel forces. The resonant frequeucy decreases with a decrease of support stiffness.

(5) The column displacements at resonance are snaller with a spring simulating gas pressure difference than without one. The impact forces are also smaller with the spring than that without it.

(6) The column displacements are larger in the core center than in the core periphery. The impact accelerations(forces) in the center are smaller than in the periphery.

(7) The column damping factors are estimated to be 4～10% of the critical damping factor.

(8) The maximum impact forces for random waves are below 60% that for sinumoidal waves.

8. Seismic Analysis Method for a Two-dimensional Vertical HTGR Core

8.1 Introduction

An analytical method presented in this Chapter has taken into account the complex nonlinear vibration associated with multiple impacts and, addition, frictional forces between the block interfaces and between the dowel pins and their mating holes are also accounted for. The method is applied to a column of blocks and the results obtained from the analysis are compared to results obtained from experiments. In a real core, the blocks and columns extend three-dimensionally. In the present study, the following two -dimensional model is considered:

(1) each block is modeled as a rigid body,

(2) each block has three degrees-of-freedom; two translational displacements and rotational around the block center of gravity,

(3) impact forces are represented by a spring and dashpot model located at impact points of each block,

(4) dowels are represented as deformable members and slipping of interfaces between dowel pins and holes is allowed, and

(5) friction forces are calculated at the horizontal interfaces between blocks.

8.2 Calculation equation

8.2.1 Equation of governing motion

The forces involved in the analysis of multiple columns of the HTGR core constrained within boundaries are as shown in Fig. 8.1.

Let the coordinate system be chosen as shown in Fig. 8.2. Each block has two translational coordinates, u and w, and one rotational coordinate θ. Figure 8.3 shows the forces that act upon an individual block. The equations of motion for the block (k,ℓ), (the ℓ-th row block in the k-th column) may be written as:

$$\begin{aligned} m_{k,\ell}\ddot{u}_{k,\ell} &= F^{TL}_{k,\ell}+F^{ML}_{k,\ell}+F^{NL}_{k,\ell}+F^{BL}_{k,\ell}-F^{TR}_{k,\ell}+F^{MR}_{k,\ell}+F^{NR}_{k,\ell}+F^{BR}_{k,\ell} \\ &\quad -F^{F}_{k,\ell}+F^{F}_{k,\ell+1}+F^{DL}_{k,\ell}-F^{DR}_{k,\ell}-F^{DL}_{k,\ell+1}+F^{DR}_{k,\ell+1}+F^{OP}_{k,\ell} \\ &\quad +C^{C}_{k,\ell}\dot{u}_{k,\ell}\,, \end{aligned} \tag{8.1}$$

$$\begin{aligned} m_{k,\ell}\ddot{w}_{k,\ell} &= F^{VL}_{k,\ell}+F^{VR}_{k,\ell}+F^{VL}_{k,\ell+1}+F^{VR}_{k,\ell-1}+\mu F^{DL}_{k,\ell}+\mu F^{DR}_{k,\ell} \\ &\quad +\mu F^{DL}_{k,\ell+1}+\mu F^{DR}_{k,\ell+1}+W^{U}_{k,\ell}+W^{L}_{k,\ell}\,, \end{aligned} \tag{8.2}$$

$$\begin{aligned} I_{k,\ell}\ddot{\theta}_{k,\ell} &= M(F^{TL}_{k,\ell})+M(F^{ML}_{k,\ell})-M(F^{NL}_{k,\ell})-M(F^{BL}_{k,\ell})-M(F^{TR}_{k,\ell}) \\ &\quad +M(F^{MR}_{k,\ell})-M(F^{NR}_{k,\ell})+M(F^{BR}_{k,\ell})+M(F^{F}_{k,\ell})+M(F^{F}_{k,\ell+1}) \\ &\quad -M(F^{DL}_{k,\ell})+M(F^{DR}_{k,\ell})+M(F^{DL}_{k,\ell+1})+M(F^{ER}_{k,\ell+1})+M(F^{VL}_{k,\ell}) \\ &\quad +M(F^{VR}_{k,\ell})+M(F^{VL}_{k,\ell+1})-M(F^{VR}_{k,\ell+1})+M(\mu F^{DL}_{k,\ell})+M(\mu F^{DR}_{k,\ell}) \\ &\quad +M(\mu F^{DL}_{k,\ell-1})+M(\mu F^{DR}_{k,\ell+1})-M(W^{U}_{k,\ell})+M(W^{L}_{k,\ell})\,, \end{aligned} \tag{8.3}$$

where, $M(F)$ are moments caused by the force F. W^{u} and W^{L} are the forces due to block weights and pressure differentials acting at the upper and lower parts of the block.

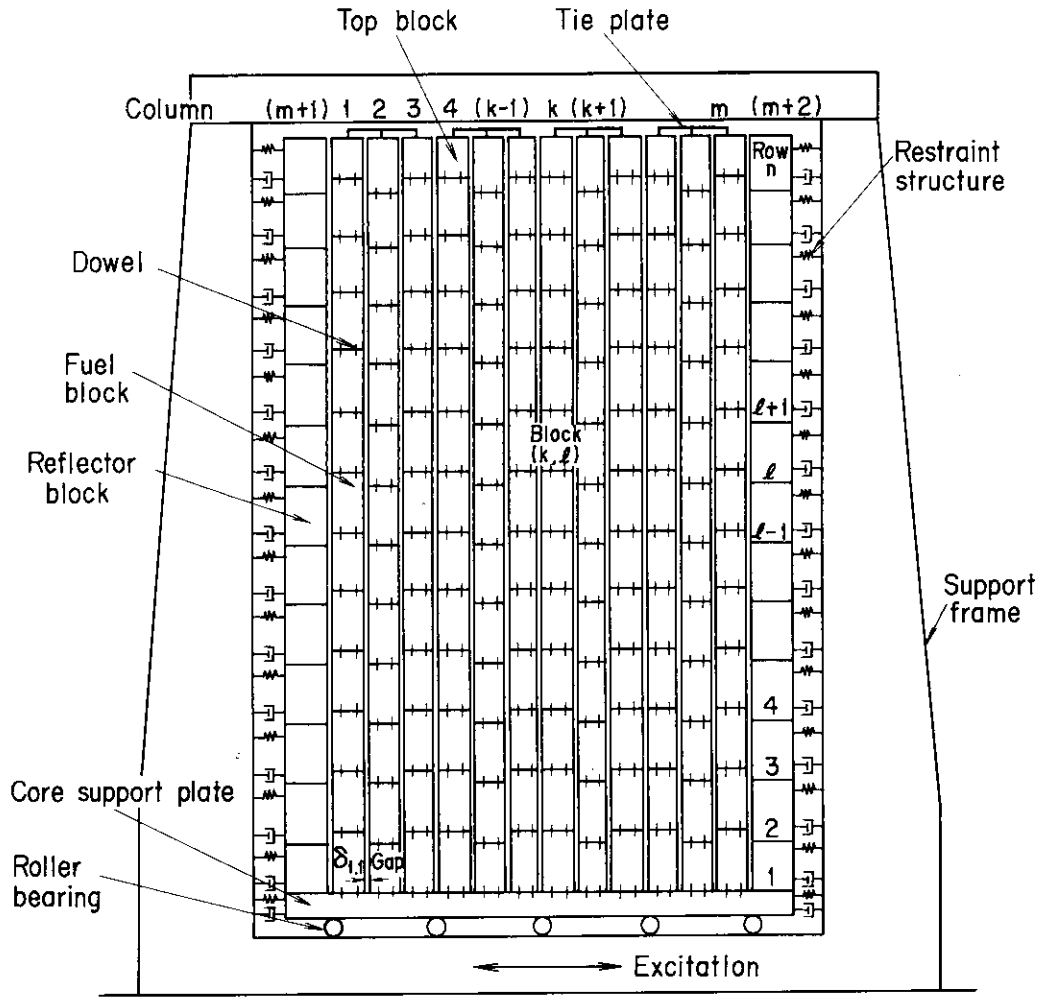

Fig. 8.1 Calculation model

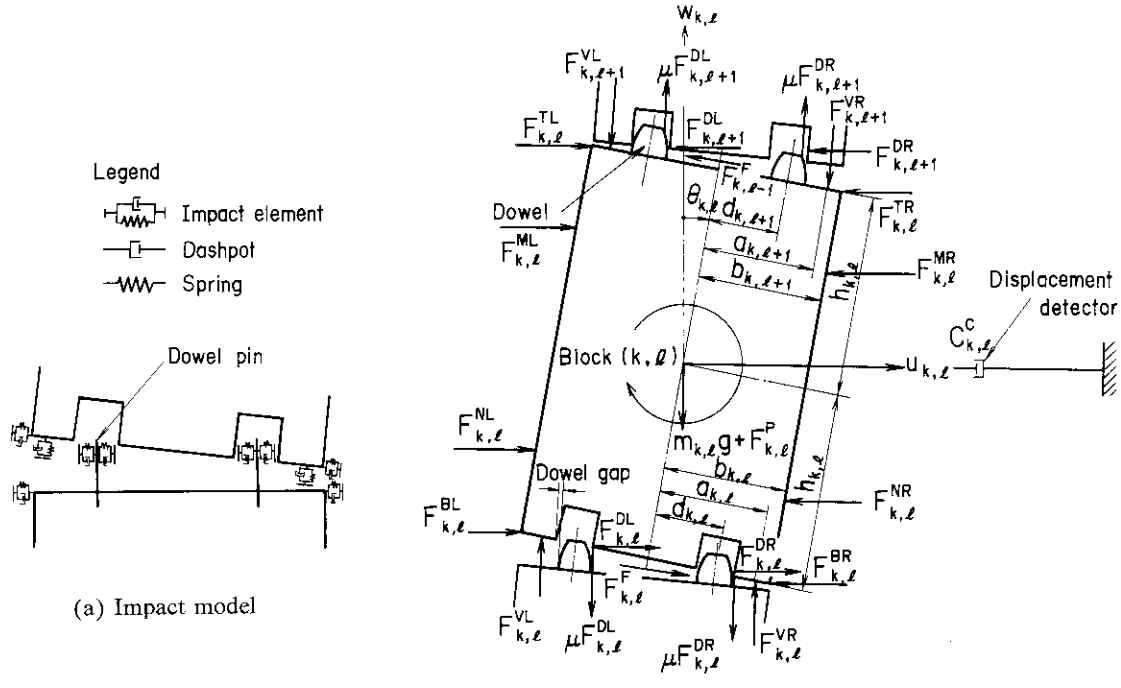

(a) Impact model

(b) Forces acting on a fuel block

Fig. 8.2 Impact model and forces acting on a fuel block

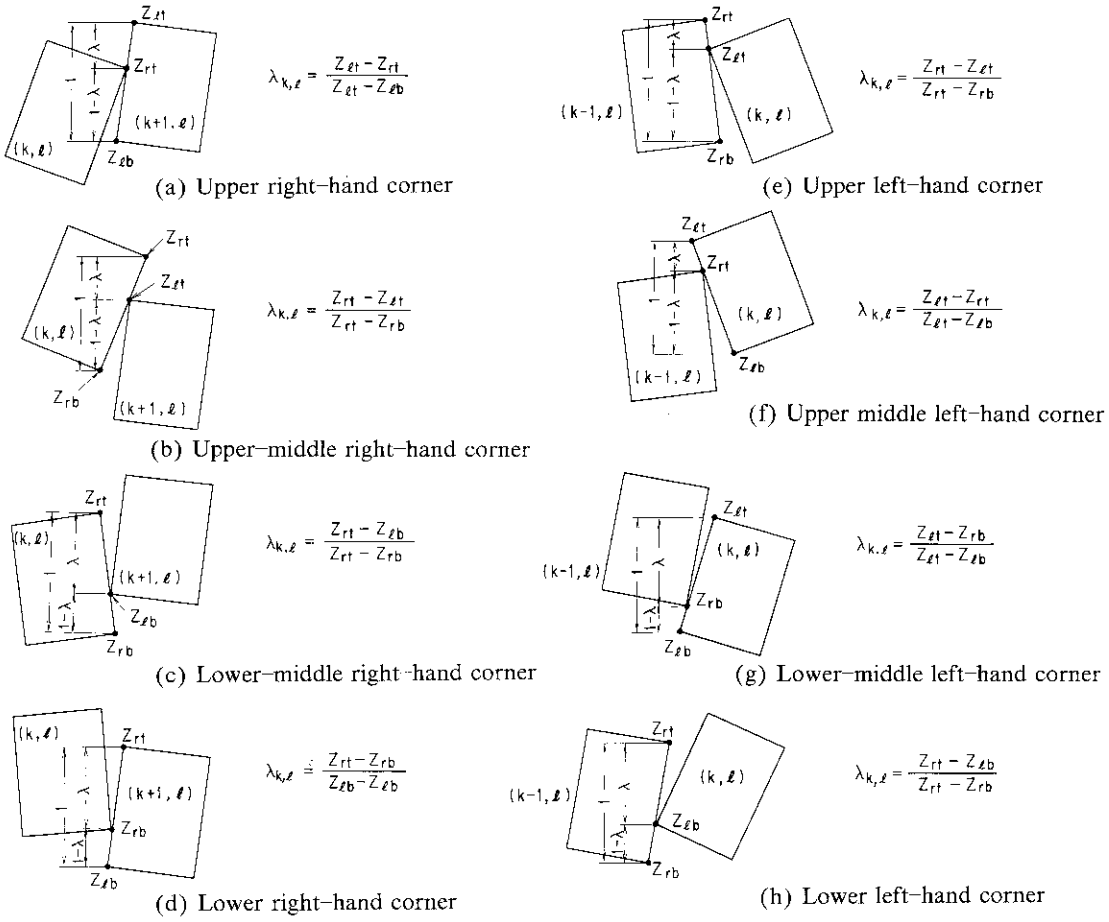

Fig. 8.3 Various blocks impact pattern

8.2.2 Friction force between blocks and its associated moment

The friction force due to surface sliding is represented by a nonlinear Coulomb element. The equations for the friction force $F^F_{k,\ell}$ and its associated moment $M(F^F_{k,\ell})$ acting on the block (k,ℓ), are as follows. Defining $\alpha_{k,\ell}$ as $(\theta_{k,\ell}, \theta_{k,\ell+1})$, then when $\alpha_{k,\ell}>0$

$$\left.\begin{aligned} F^F_{k,\ell} &= -\mathrm{sign}(v_{k,\ell})F(v_{k,\ell}), \\ M(F^F_{k,\ell}) &= F^F_{k,\ell}(-h_{k,\ell}\cos\theta_{k,\ell} - b_{k,\ell}\sin\theta_{k,\ell}), \end{aligned}\right\} \tag{8.4}$$

and for the block $(k,\ell-1)$

$$\left.\begin{aligned} F^F_{k,\ell-1} &= \mathrm{sign}(v_{k,\ell})F(v_{k,\ell}), \\ M(F^F_{k,\ell-1}) &= F^F_{k,\ell-1}(-h_{k,\ell-1}\cos\theta_{k,\ell-1} - b_{k,\ell-1}\sin\theta_{k,\ell-1}), \end{aligned}\right\} \tag{8.5}$$

where

$$\begin{aligned} v_{k,\ell} &= \{\dot{u}_{k,\ell} - (h_{k,\ell}\cos\theta_{k,\ell} + b_{k,\ell}\sin\theta_{k,\ell})\dot{\theta}_{k,\ell}\} \\ &\quad - \{\dot{u}_{k,\ell-1} - (h_{k,\ell-1}\cos\theta_{k,\ell-1} - b_{k,\ell-1}\sin\theta_{k,\ell-1})\dot{\theta}_{k,\ell-1}\}. \end{aligned} \tag{8.6}$$

For $\ell=1$

$$v_{k,1} = \dot{u}_{k,1} - (h_{k,1}\cos\theta_{k,1} + b_{k,1}\sin\theta_{k,1})\dot{\theta}_{k,1} - \dot{u}_0, \tag{8.7}$$

where $u_{k,\ell}$ and $\dot{u}_{k,\ell}$ are the horizontal displacement and velocity of the center of gravity of the block (k, ℓ), respectively $\dot{u}_0$ is the horizontal velocity of the support floor.

If sign $(\alpha_{k,\ell}) \leqq 0$, then

$$\left.\begin{aligned} F^F_{k,\ell} &= -\text{sign}(v_{k,\ell}) F(v_{k,\ell}), \\ M(F^F_{k,\ell}) &= F^F_{k,\ell}(-h_{k,\ell}\cos\theta_{k,\ell} + b_{k,\ell}\sin\theta_{k,\ell}), \end{aligned}\right\} \tag{8.8}$$

and for the block $(k,\ell-1)$

$$\left.\begin{aligned} F^F_{k,\ell-1} &= \text{sign}(v_{k,\ell}) F(v_{k,\ell}), \\ M(F^F_{k,\ell-1}) &= F^F_{k,\ell\ \ 1}(h_{k,\ell-1}\cos\theta_{k,\ell-1} + b_{k,\ell-1}\sin\theta_{k,\ell-1}), \end{aligned}\right\} \tag{8.9}$$

where

$$\begin{aligned} v_{k,\ell} = &\{\dot{u}_{k,\ell} - (h_{k,\ell}\cos\theta_{k,\ell} - b_{k,\ell}\sin\theta_{k,\ell})\dot{\theta}_{k,\ell}\} \\ &- \{\dot{u}_{k,\ell-1} - (h_{k,\ell-1}\cos\theta_{k,\ell-1} + b_{k,\ell}\sin\theta_{k,\ell-1})\dot{\theta}_{k,\ell-1}\}. \end{aligned} \tag{8.10}$$

For $\ell = 1$

$$v_{k,1} = \dot{u}_{k,1} - (h_{k,1}\cos\theta_{k,1} - b_{k,1}\sin\theta_{k,1})\dot{\theta}_{k,1} - \dot{u}_0, \tag{8.11}$$

where $\dot{u}_0$ the horizontal velocity of the support floor. $F(u_{k,\ell})$ is a prescribed function for the friction characterics which is related to the vertical contact force and the coefficients of both dynamic and statical frictions.

$$F^F(v_{k,\ell}) = F^Q_{k,\ell}\{u_s + f(v_{k,\ell}) + f(v^2_{k,\ell}) + f(v^3_{k,\ell})\}, \tag{8.12}$$

and the functions $f(v_{k,\ell},\ v^2_{k,\ell},\ v^3_{k,\ell})$ are related to the kinematic coefficient of friction μ_k. The vertical contact forces are obtained by summing the block weights $m_{k,\ell}g$ and the differential pressure of a unit block length, $F^P_{k,\ell}$.

$$F^Q_{k,\ell} = \sum_{j=\ell}^{n} m_{k,\ell,j}g + F^P_{k,\ell}. \tag{8.13}$$

8.2.3 Vertical impact force and its associated moment

The forces acting on the interface between the block (k,ℓ) and the block $(k,\ell-1)$ as a results of impact are derived in term of deformation of each spring dashpot unit. When the gap is closing, the spring deformation of $\gamma_{k,\ell}$ and its time rate $\dot{\gamma}_{k,\ell}$ are

$$\begin{aligned} \gamma_{k,\ell} = &\frac{1}{2}\{w_{k,\ell-1} - h_{k,\ell-1}(1-\cos\theta_{k,\ell\ -1}) - a_{k,\ell}\sin\theta_{k,\ell\ \ 1}\} \\ &-\frac{1}{2}\{w_{k,\ell} - h_{k,\ell}(1-\cos\theta_{k,\ell}) - a_{k,\ell}\sin\theta_{k,\ell}\}, \end{aligned} \tag{8.14}$$

$$\begin{aligned} \dot{\gamma}_{k,\ell} = &\frac{1}{2}\{\dot{w}_{k,\ell-1} - (h_{k,\ell-1}\sin\theta_{k,\ell-1} + a_{k,\ell}\cos\theta_{k,\ell-1})\dot{\theta}_{k,\ell-1}\} \\ &-\frac{1}{2}\{\dot{w}_{k,\ell} + (h_{k,\ell}\sin\theta_{k,\ell} - a_{k,\ell}\cos\theta_{k,\ell})\dot{\theta}_{k,\ell}\}. \end{aligned} \tag{8.15}$$

For $\ell = 1$

$$\gamma_{k,\ell} = \frac{1}{2}[w_0 - \{w_{k,\ell} + h_{k,\ell}(1-\cos\theta_{k,\ell}) - a_{k,\ell}\sin\theta_{k,\ell}\}], \tag{8.16}$$

$$\dot{\gamma}_{k,\ell} = \frac{1}{2}[\dot{w}_0 - \{\dot{w}_{k,\ell} + (h_{k,\ell}\sin\theta_{k,\ell} - a_{k,\ell}\cos\theta_{k,\ell})\dot{\theta}_{k,\ell}\}], \tag{8.17}$$

where w_0 and $\dot{w}_0$ are vertical displacement and velocity of the support floor, respectively. The vertical impact forces $F^{VR}_{k,\ell}$ (or $F^{VL}_{k,\ell}$) and its associated moments $M(F^{VR}_{k,\ell})$ (or $M(F^{VL}_{k,\ell})$) acting on the block (k,ℓ) are as follows.

If $\gamma_{k,\ell} > 0$

$$\left.\begin{aligned} F^{VR}_{k,\ell} &= -K^{V}_{k,\ell}\gamma_{k,\ell} - C^{V}_{k,\ell}\dot{\gamma}_{k,\ell}\ , \\ M(F^{VR}_{k,\ell}) &= -F^{VR}_{k,\ell}(h_{k,\ell}\sin\theta_{k,\ell} - a_{k,\ell}\cos\theta_{k,\ell})\ . \end{aligned}\right\} \tag{8.18}$$

For the block $(k,\ell-1)$

$$\left.\begin{aligned} F^{VR}_{k,\ell-1} &= K^{V}_{k,\ell}\gamma_{k,\ell} + C^{V}_{k,\ell}\dot{\gamma}_{k,\ell}\ , \\ M(F^{VR}_{k,\ell-1}) &= F^{VR}_{k,\ell-1}(h_{k,\ell-1}\sin\theta_{k,\ell-1} + a_{k,\ell}\cos\theta_{k,\ell-1})\ . \end{aligned}\right\} \tag{8.19}$$

When $\gamma_{k,\ell}\leqq 0$

$$\left.\begin{aligned} F^{VR}_{k,\ell} &= F^{VR}_{k,\ell-1} = 0, \\ M(F^{VR}_{k,\ell}) &= M(F^{VR}_{k,\ell-1}) = 0\ . \end{aligned}\right\} \tag{8.20}$$

Where $K^{v}_{k,\ell}$ and $C^{v}_{k,\ell}$ are the vertical spring and damping coefficients, respectively, for a single unit. In the more general formulation, these quantities may be represented by a polynominal function.

$$\left.\begin{aligned} K^{v}_{k,\ell} &= \sum_{j=0}^{m} K^{v}_{k,\ell,j}\gamma^{j}_{k,\ell}\ , \\ C^{v}_{k,\ell} &= \sum_{j=0}^{m} C^{V}_{k,\ell,j}\dot{\gamma}^{j}_{k,\ell}\ . \end{aligned}\right\} \tag{8.21}$$

8.2.4 Horizontal impact force and its associated moment between columns

The forces acting on the block (k,ℓ) as a result of impact on the adjacent column's blocks are derived by deformations of the spring dashpot units which are located on the upper, middle and lower, and right and left-hand corners.

(1) Impact on the upper right-hand corner

During impact against an adjacent block on the upper-right hand corner, the spring deformation $\varepsilon_{k,\ell}$ and its time rate $\dot{\varepsilon}_{k,\ell}$ of the block (k,ℓ) are

If $\varepsilon_{k,\ell}>0$

$$\begin{aligned} \varepsilon_{k,\ell} &= u_{k,\ell} + \{h_{k,\ell}\sin\theta_{k,\ell} - b_{k,\ell}(1-\cos\theta_{k,\ell})\} - u_{k+1,\ell} \\ &\quad - \{(1-2\lambda_{k,\ell})h_{k+1,\ell}\sin\theta_{k+1,\ell} + b_{k-1,\ell}(1-\cos\theta_{k+1,\ell})\} - \delta_{k,\ell}\ , \end{aligned} \tag{8.22}$$

$$\begin{aligned} \dot{\varepsilon}_{k,\ell} &= \dot{u}_{k,\ell} + (h_{k,\ell}\cos\theta_{k,\ell} - b_{k,\ell}\sin\theta_{k,\ell})\dot{\theta}_{k,\ell} - \dot{u}_{k,\ell+1} \\ &\quad - \{(1-2\lambda_{k,\ell})h_{k+1,\ell}\cos\theta_{k+1,\ell} + b_{k-1,\ell}\sin\theta_{k+1,\ell}\}\dot{\theta}_{k+1,\ell}\ , \end{aligned} \tag{8.23}$$

where $\lambda_{k,\ell}$ is of the following form as shown in Fig. 8.4

$$\lambda_{k,\ell} = \frac{Z_{\ell t} - Z_{rt}}{Z_{\ell t} - Z_{\ell b}}\ . \tag{8.24}$$

$u_{k,\ell-1}$ is the adjacent block displacement at the contact point and $\delta^{B}_{k,\ell}$ is the gap between the block (k,ℓ) and block $(k+1,\ell)$. The impact force $F^{TR}_{k,\ell}$ and its associated moment $M(F^{TR}_{k,\ell})$ acting on the block (k,ℓ) are as follows.

If $\varepsilon_{k,\ell}>0$

$$\left.\begin{aligned} F^{TR}_{k,\ell} &= -\{K^{B}_{k,\ell}\varepsilon_{k,\ell} + C^{B}_{k,\ell}\dot{\varepsilon}_{k,\ell}\}\ , \\ M(T^{TR}_{k,\ell}) &= F^{TR}_{k,\ell}(h_{k,\ell}\cos\theta_{k,\ell} - b_{k,\ell}\sin\theta_{k,\ell})\ , \end{aligned}\right\} \tag{8.25}$$

where $K^{B}_{k,\ell}$ and $C^{B}_{k,\ell}$ are the boundary spring and damping coefficients, respectively and may be represented in the following general form.

$$\left.\begin{aligned} K^{B}_{k,\ell} &= \sum_{j-0}^{m} K^{B}_{k,\ell,j}\varepsilon^{j}_{k,\ell}\ . \\ C^{B}_{k,\ell} &= \sum_{j=0}^{m} C^{B}_{k,\ell,j}\dot{\varepsilon}^{j}_{k,\ell}\ . \end{aligned}\right\} \tag{8.26}$$

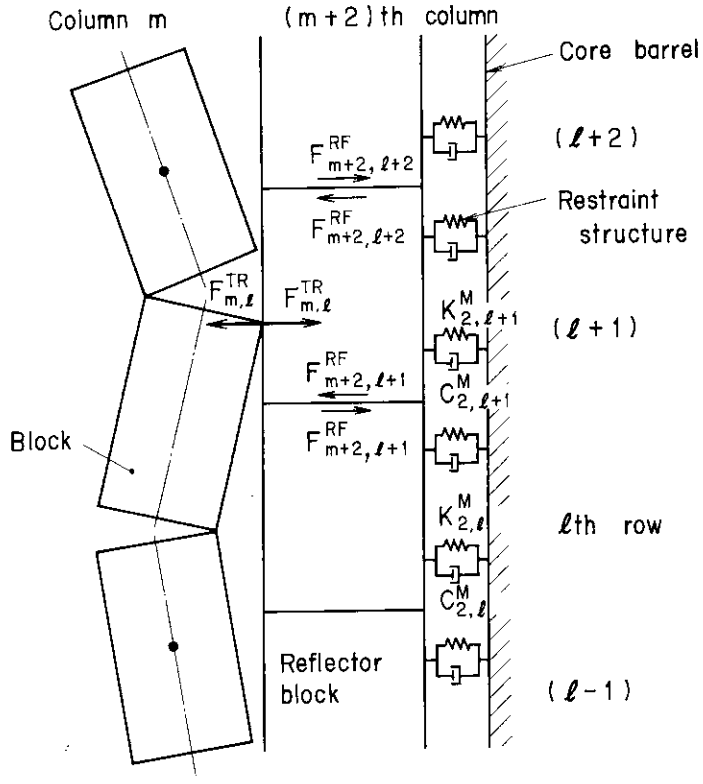

Fig. 8.4 Side reflector block model

(2) Impact on the upper-middle right-hand corner

Similarly, $\varepsilon_{k,\ell}$ and $\dot{\varepsilon}_{k,\ell}$ are

$$\varepsilon_{k,\ell}=u_{k,\ell}+\{(1-2\lambda_{k,\ell})h_{k,\ell}\sin\theta_{K,\ell}-b_{k,\ell}(1-\cos\theta_{k,\ell})\}-u_{k+1,\ell}$$
$$-\{h_{k-1,\ell}\sin\theta_{k+1,\ell}-b_{k+1,\ell}(1-\cos\theta_{k+1,\ell})\}-\delta_{k,\ell}\,, \tag{8.27}$$

$$\dot{\varepsilon}_{k,\ell}=\dot{u}_{k,\ell}+\{(1-2\lambda_{k,\ell})h_{k,\ell}\cos\theta_{k,\ell}-b_{k,\ell}\sin\theta_{k,\ell}\}\dot{\theta}_{k,\ell}$$
$$-\dot{u}_{k+1,\ell}-(h_{k-1,\ell}\cos\theta_{k+1,\ell}+b_{k-1,\ell}\sin\theta_{k-1,\ell})\dot{\theta}_{k+1,\ell}\,, \tag{8.28}$$

$$\lambda_{k,\ell}=\frac{Z_{rt}-Z_{\ell t}}{Z_{rt}-Z_{rb}}\,. \tag{8.29}$$

If $\varepsilon_{k,\ell}>0$, the force and moment are

$$\left.\begin{aligned}&F^{MR}_{k,\ell}=-(K^{B}_{k,\ell}\varepsilon_{k,\ell}-C^{B}_{k,\ell}\dot{\varepsilon}_{k,\ell})\,,\\&M(F^{MR}_{k,\ell})=F^{MR}_{k,\ell}\{(1-2\lambda_{k,\ell})h_{k,\ell}\cos\theta_{k,\ell}-b_{k,\ell}\sin\theta_{k,\ell}\}\,.\end{aligned}\right\} \tag{8.30}$$

(3) Impact on the lower-middle right-hand corner

$\varepsilon_{k,\ell}$ and $\dot{\varepsilon}_{k,\ell}$ are

$$\varepsilon_{k,\ell}=u_{k,\ell}+\{(1-2\lambda)_{k,\ell})h_{k,\ell}\sin\theta_{k,\ell}-b_{k,\ell}(1-\cos\theta_{k,\ell})\}-u_{k-1,\ell}$$
$$-\{-h_{k+1,\ell}\sin\theta_{k+1,\ell}+b_{k-1,\ell}(1-\cos\theta_{k+1,\ell})\}-\delta_{k,\ell}\,, \tag{8.31}$$

$$\dot{\varepsilon}_{k,\ell}=\dot{u}_{k,\ell}-\{1-2\lambda_{k,\ell})h_{k,\ell}\cos\theta_{k,\ell}-b_{k,\ell}\sin\theta_{k,\ell}\}\dot{\theta}_{k,\ell}-\dot{u}_{k+1,\ell}$$
$$-(-h_{k+1,\ell}\cos\theta_{k+1,\ell}-b_{k+1,\ell}\sin\theta_{k+1,\ell})\dot{\theta}_{k+1,\ell}\,, \tag{8.32}$$

$$\lambda_{k,\ell}=\frac{Z_{rt}-Z_{\ell b}}{Z_{rt}-Z_{rb}}\,. \tag{8.33}$$

If $\varepsilon_{k,\ell}>0$, the force and moment are

$$\left.\begin{aligned}&F^{NR}_{k,\ell}=-(K^{B}_{k,\ell}\varepsilon_{k,\ell}+C^{B}_{k,\ell}\dot{\varepsilon}_{k,\ell})\,,\\&M(F^{NR}_{k,\ell})=F^{NR}_{k,\ell}\{(1-2\lambda_{k,\ell})h_{k,\ell}\cos\theta_{k,\ell}+b_{k,\ell}\sin\theta_{k,\ell})\,.\end{aligned}\right\} \tag{8.34}$$

(4) Impact on the lower right-hand corner

$\varepsilon_{k,\ell}$ and $\dot{\varepsilon}_{k,\ell}$ are

$$\begin{aligned}\varepsilon_{k,\ell}&=u_{k,\ell}+\{-h_{k,\ell}\sin\theta_{k,\ell}-b_{k,\ell}(1-\cos\theta_{k,\ell})\}-u_{k-1,\ell}\\&\quad-\{(1-2\lambda_{k,\ell})h_{k-1,\ell}\sin\theta_{k+1,\ell}+b_{k+1,\ell}(1-\cos\theta_{k+1,\ell})\}\\&\quad-\delta_{k,\ell}\ ,\end{aligned}\tag{8.35}$$

$$\begin{aligned}\dot{\varepsilon}_{k,\ell}&=\dot{u}_{k,\ell}+\{-h_{k,\ell}\cos\theta_{k,\ell}-b_{k,\ell}\sin\theta_{k,\ell}\}\dot{\theta}_{k,\ell}-\dot{u}_{k-1,\ell}\\&\quad-\{(1-2\lambda_{k,\ell})h_{k+1,\ell}\cos\theta_{k+1}+b_{k+1,\ell}\sin\theta_{k+1,\ell}\}\dot{\theta}_{k+1,\ell}\ ,\end{aligned}\tag{8.36}$$

$$\lambda_{k,\ell}=\frac{Z_{\ell t}-Z_{rb}}{Z_{\ell t}-Z_{\ell b}}\ .\tag{8.37}$$

If $\varepsilon_{k,\ell}>0$, the force and moment are

$$\left.\begin{aligned}F_{k,\ell}^{BR}&=-(K_{k,\ell}^{B}\varepsilon_{k,\ell}+C_{k,\ell}^{B}\dot{\varepsilon}_{k,\ell})\ ,\\M(F_{k,\ell}^{BR})&=-F_{k,\ell}^{BR}(h_{k,\ell}\cos\theta_{k,\ell}+b_{k,\ell}\sin\theta_{k,\ell})\ .\end{aligned}\right\}\tag{8.38}$$

(5) Impact on the upper left-hand corner

$\varepsilon_{k,\ell}$ and $\dot{\varepsilon}_{k,\ell}$ are

$$\begin{aligned}\varepsilon_{k,\ell}&=u_{k-1,\ell}+\{(1-2\lambda_{k,\ell})h_{k-1,\ell}\sin\theta_{k-1,\ell}-b_{k-1,\ell}(1-\cos\theta_{k-1,\ell})\}\\&\quad-u_{k,\ell}-\{h_{k,\ell}\sin\theta_{k,\ell}+b_{k,\ell}(1-\cos\theta_{k,\ell})\}-\delta_{k-1,\ell}\ .\end{aligned}\tag{8.39}$$

$$\begin{aligned}\dot{\varepsilon}_{k,\ell}&=\dot{u}_{k-1,\ell}+\{(1-2\lambda_{k,\ell})h_{k-1,\ell}\cos\theta_{k-1,\ell}-b_{k-1,\ell}\sin\theta_{k-1,\ell}\}\dot{\theta}_{k-1,\ell}\\&\quad-\dot{u}_{k,\ell}-(h_{k,\ell}\cos\theta_{k,\ell}+b_{k,\ell}\sin\theta_{k,\ell})\dot{\theta}_{k,\ell}\ ,\end{aligned}\tag{8.40}$$

$$\lambda_{k,\ell}=\frac{Z_{rt}-Z_{\ell t}}{Z_{rt}-Z_{rb}}\ .\tag{8.41}$$

If $\varepsilon_{k,\ell}>0$, the force and moment are

$$\left.\begin{aligned}F_{k,\ell}^{TB}&=K_{k,\ell}^{B}\varepsilon_{k,\ell}+C_{k,\ell}^{B}\dot{\varepsilon}_{k,\ell}\ ,\\M(F_{k,\ell}^{TB})&=F_{k,\ell}^{TB}(h_{k,\ell}\cos\theta_{k,\ell}+b_{k,\ell}\sin\theta_{k,\ell})\ .\end{aligned}\right\}\tag{8.42}$$

(6) Impact on the upper-middle left-hand corner

$\varepsilon_{k,\ell}$ and $\dot{\varepsilon}_{k,\ell}$ are

$$\begin{aligned}\varepsilon_{k,\ell}&=u_{k-1,\ell}+\{h_{k-1,\ell}\sin\theta_{k-1,\ell}-b_{k-1,\ell}(1-\cos\theta_{k-1,\ell})\}\\&\quad-u_{k,\ell}-\{(1-2\lambda_{k,\ell})h_{k,\ell}\sin\theta_{k-1,\ell}+b_{k-1,\ell}(1-\cos\theta_{k-1,\ell})\}\\&\quad-\delta_{k-1,\ell}\ ,\end{aligned}\tag{8.43}$$

$$\begin{aligned}\dot{\varepsilon}_{k,\ell}&=\dot{u}_{k-1,\ell}+(h_{k-1,\ell}\cos\theta_{k-1,\ell}-b_{k-1,\ell}\sin\theta_{k-1,\ell})\dot{\theta}_{k-1,\ell}\\&\quad-\dot{u}_{k,\ell}-\{(1-2\lambda_{k,\ell})\cos\theta_{k,\ell}+b_{k,\ell}\sin\theta_{k,\ell}\}\dot{\theta}_{k,\ell}\ ,\end{aligned}\tag{8.44}$$

$$\lambda_{k,\ell}=\frac{Z_{\ell t}-Z_{rt}}{Z_{\ell t}-Z_{\ell b}}\ .\tag{8.45}$$

If $\varepsilon_{k,\ell}>0$, the force and moment are

$$\left.\begin{aligned}F_{k,\ell}^{MB}&=K_{k,\ell}^{MB}\varepsilon_{k,\ell}+C_{k,\ell}^{MB}\dot{\varepsilon}_{k,\ell}\ ,\\M(F_{k,\ell}^{MB})&=F_{k,\ell}^{MB}\{(1-2\lambda_{k,\ell})h_{k,\ell}\cos\theta_{k,\ell}+b_{k,\ell}\sin\theta_{k,\ell}\}.\end{aligned}\right\}\tag{8.46}$$

(7) Impact on the lower-middle left-hand corner

$\varepsilon_{k,\ell}$ and $\dot{\varepsilon}_{k,\ell}$ are

$$\begin{aligned}\varepsilon_{k,\ell}&=u_{k-1,\ell}+\{-h_{k-1,\ell}\sin\theta_{k-1,\ell}-b_{k-1,\ell}(1-\cos\theta_{k-1,\ell})\}\\&\quad-u_{k,\ell}+\{(1-2\lambda_{k,\ell})h_{k,\ell}\sin\theta_{k,\ell}-b_{k,\ell}(1-\cos\theta_{k,\ell})\}\\&\quad-\delta_{k-1,\ell}\ ,\end{aligned}\tag{8.47}$$

$$\dot{\varepsilon}_{k,\ell}=\dot{u}_{k-1,\ell}-(h_{k-1,\ell}\cos\theta_{k-1,\ell}+b_{k-1,\ell}\sin\theta_{k-1,\ell})\dot{\theta}_{k-1,\ell}$$
$$-\dot{u}_{k,\ell}+\{(1-2\lambda_{k,\ell})h_{k,\ell}\cos\theta_{k,\ell}-b_{k,\ell}\sin\theta_{k,\ell}\}\dot{\theta}_{k,\ell}\ , \tag{8.48}$$

$$\lambda_{k,\ell}=\frac{Z_{\ell t}-Z_{rb}}{Z_{\ell t}-Z_{\ell b}}\ . \tag{8.49}$$

If $\varepsilon_{k,\ell}>0$, the force and moment are

$$\left.\begin{aligned}&F_{k,\ell}^{NB}=K_{k,\ell}^{B}\varepsilon_{k,\ell}+C_{k,\ell}^{B}\dot{\varepsilon}_{k,\ell}\ ,\\&M(F_{k,\ell}^{NB})=F_{k,\ell}^{NB}\{(1-2\lambda_{k,\ell})h_{k,\ell}\cos\theta_{k,\ell}+b_{k,\ell}\sin\theta_{k,\ell}\}\ .\end{aligned}\right\} \tag{8.50}$$

(8) Impact on the lower left-hand corner

$\varepsilon_{k,\ell}$ and $\dot{\varepsilon}_{k,\ell}$ are

$$\varepsilon_{k,\ell}=u_{k-1,\ell}+(1-2\lambda_{k,\ell})h_{k-1,\ell}\sin\theta_{k-1,\ell}-b_{k-1,\ell}(1-\cos\theta_{k-1,\ell})\}$$
$$-u_{k,\ell}-\{h_{k,\ell}\sin\theta_{k,\ell}+b_{k,\ell}(1-\cos\theta_{k,\ell})\}$$
$$-\delta_{k-1,\ell}\ , \tag{8.51}$$
$$\dot{\varepsilon}_{k,\ell}=\dot{u}_{k-1,\ell}\{(1-2\lambda_{k,\ell})h_{k-1,\ell}\cos\theta_{k-1,\ell}-b_{k-1,\ell}\sin\theta_{k-1,\ell}\}\dot{\theta}_{k-1,\ell}$$
$$-\dot{u}_{k,\ell}-(h_{k,\ell}\cos\theta_{k,\ell}+b_{k,\ell}\sin\theta_{k,\ell})\dot{\theta}_{k,\ell}\ , \tag{8.52}$$

$$\lambda_{k,\ell}=\frac{Z_{rt}-Z_{\ell b}}{Z_{rt}-Z_{rb}}\ . \tag{8.53}$$

If $\varepsilon_{k,\ell}>0$

$$\left.\begin{aligned}&F_{k,\ell}^{BL}=-K_{k,\ell}^{B}\varepsilon_{k,\ell}-C_{k,\ell}^{B}\dot{\varepsilon}_{k,\ell}\ ,\\&M(F_{k,\ell}^{BL})=-F_{k,\ell}^{BL}(h_{k,\ell}\cos\theta_{k,\ell}-b_{k,\ell}\sin\theta_{k,\ell})\ .\end{aligned}\right\} \tag{8.54}$$

(9) No-impact case

When $\varepsilon_{k,\ell}\leq 0$

$$\left.\begin{aligned}&F_{k,\ell}^{TR}=F_{k,\ell}^{MR}=F_{k,\ell}^{NR}=F_{k,\ell}^{BR}=0,\\&F_{k,\ell}^{TL}=F_{k,\ell}^{ML}=F_{k,\ell}^{NL}=F_{k,\ell}^{BL}=0,\\&M(F_{k,\ell}^{TL})=M(F_{k,\ell}^{ML})=M(F_{k,\ell}^{NL})=M(F_{k,\ell}^{BL})=0,\\&M(F_{k,\ell}^{TR})=M(F_{k,\ell}^{MR})=M(F_{k,\ell}^{NR})=M(F_{k,\ell}^{BR})=0.\end{aligned}\right\} \tag{8.55}$$

8.2.5 Horizontal impact force and its associated moment between column and side reflector

The forces acting on the block of the m-th column and the first column as a result of impact on the adjacent reflector blocks are derived by deformations of the springs dashpot units which are located on the upper and lower, right and left corners (see Fig. 8.4).

(1) Impact on the upper right-hand corner of the ℓ-th block in the m-th column

During impact against the adjacent reflector block on the upper right-hand corner, the spring deformation $\varepsilon_{m,\ell}$ and its time rate $\dot{\varepsilon}_{m,\ell}$ of the block (m,ℓ) are

$$\varepsilon_{m,\ell}=u_{m,\ell}+\{h_{m,\ell}\sin\theta_{m,\ell}-b_{m,\ell}(1-\cos\theta_{m,\ell})\}$$
$$-u_{m-2,\ell}-\delta_{m,\ell}\ , \tag{8.56}$$
$$\dot{\varepsilon}_{m,\ell}=\dot{u}_{m,\ell}+(h_{m,\ell}\cos\theta_{m,\ell}-b_{m,\ell}\sin\theta_{m,\ell})\dot{\theta}_{m,\ell}-\dot{u}_{m-2,\ell}\ , \tag{8.57}$$

$u_{m+2,\ell}$ and $\dot{u}_{m-2,\ell}$ are the adjacent block displacements of the right reflector column and its velocity at the contact point, respectively. $\delta_{m,\ell}$ is the gap between the block (m,ℓ) and the reflector block. The impact force $F_{m,\ell}^{TR}$ and its associated moment $M(F_{m,\ell}^{TR})$ acting on the block (m,ℓ) are as follows.

If $\varepsilon_{m,\ell}>0$,

$$\left.\begin{aligned} F^{TR}_{m,\ell} &= -(K^{B}_{m,\ell}\varepsilon_{m,\ell} + C^{B}_{m,\ell}\dot{\varepsilon}_{m,\ell}) \ , \\ M(F^{TR}_{m,\ell}) &= F^{TR}_{m,\ell}(h_{m,\ell}\cos\theta_{m,\ell} - b_{m,\ell}\sin\theta_{m,\ell}) \ . \end{aligned}\right\} \tag{8.58}$$

(2) Impact on the lower right-hand corner of the ℓ-th block in the m-th column

$\varepsilon_{m,\ell}$ and $\dot{\varepsilon}_{m,\ell}$ are

$$\varepsilon_{m,\ell} = u_{m,\ell} - \{h_{m,\ell}\sin\theta_{m,\ell} + b_{m,\ell}(1-\cos\theta_{m,\ell})\} - u_{m+2,\ell} - \delta_{m,\ell} \ , \tag{8.59}$$

$$\dot{\varepsilon}_{m,\ell} = \dot{u}_{m,\ell} - (h_{m,\ell}\cos\theta_{m,\ell} + b_{m,\ell}\sin\theta_{m,\ell})\dot{\theta}_{m,\ell} - \dot{u}_{m+2,\ell} \ . \tag{8.60}$$

If $\varepsilon_{m,\ell} > 0$, the force and moment are

$$\left.\begin{aligned} F^{BR}_{m,\ell} &= -(K^{B}_{m,\ell}\varepsilon_{m,\ell} + C^{B}_{m,\ell}\dot{\varepsilon}_{m,\ell} \ , \\ M(F^{BR}_{m,\ell}) &= -F^{BR}_{m,\ell}(h_{m,\ell}\cos\theta_{m,\ell} + b_{m,\ell}\sin\theta_{m,\ell}) \ . \end{aligned}\right\} \tag{8.61}$$

(3) Impact on the upper left-hand corner of the ℓ-th block in the first column

$\varepsilon_{1,\ell}$ and $\dot{\varepsilon}_{1,\ell}$ are

$$\varepsilon_{1,\ell} = -u_{1,\ell} - \{h_{1,\ell}\sin\theta_{1,\ell} + b_{1,\ell}(1-\cos\theta_{1,\ell})\} + u_{m+1,\ell} + \delta_{1,\ell} \ , \tag{8.62}$$

$$\dot{\varepsilon}_{1,\ell} = -\dot{u}_{1,\ell} - (h_{1,\ell}\cos\theta_{1,\ell} + b_{1,\ell}\sin\theta_{1,\ell})\dot{u}_{1,\ell} - \dot{\theta}_{m+1,\ell} \ . \tag{8.63}$$

$u_{m+1,\ell}$ and $\dot{u}_{m+1}$ are the adjacent block displacements of the left reflector column and its velocity at the contact point, respectively. $\delta_{1,\ell}$ is the gap between the block $(1,\ell)$ and the reflector block.

If $\varepsilon_{1,\ell} > 0$, the force and moment are

$$\left.\begin{aligned} F^{TL}_{1,\ell} &= K^{B}_{1,\ell}\varepsilon_{1,\ell} + C^{B}_{1,\ell}\dot{\varepsilon}_{1,\ell} \ , \\ M(F^{TR}_{1,\ell}) &= F^{TL}_{1,\ell}(h_{1,\ell}\cos\theta_{1,\ell} + b_{1,\ell}\sin\theta_{1,\ell}) \ . \end{aligned}\right\} \tag{8.64}$$

(4) Impact on the lower left-hand corner of the ℓ-th block in the first column

$\varepsilon_{1,\ell}$ and $\dot{\varepsilon}_{1,\ell}$ are

$$\varepsilon_{1,\ell} = -u_{1,\ell} + \{h_{1,\ell}\sin\theta_{1,\ell} - b_{1,\ell}(1-\cos\theta_{1,\ell})\} + u_{m+1,\ell} - \delta_{1,\ell} \ , \tag{8.65}$$

$$\dot{\varepsilon}_{1,\ell} = -\dot{u}_{1,\ell} + (h_{1,\ell}\cos\theta_{1,\ell} - b_{1,\ell}\sin\theta_{1,\ell})\dot{\theta}_{1,\ell} + \dot{u}_{m+1,\ell} \ . \tag{8.66}$$

If $\varepsilon_{1,\ell} > 0$, the force and moment are

$$\left.\begin{aligned} F^{BL}_{1,\ell} &= K^{B}_{1,\ell}\varepsilon_{1,\ell} + C^{B}_{1,\ell}\dot{\varepsilon}_{1,\ell} \ , \\ M(F^{BL}_{1,\ell}) &= -F^{BL}_{1,\ell}(h_{1,\ell}\cos\theta_{1,\ell} - b_{1,\ell}\sin\theta_{1,\ell}) \ . \end{aligned}\right\} \tag{8.67}$$

(5) No-impact case

When $\varepsilon_{1,\ell} = \varepsilon_{m,\ell} = 0$

$$\left.\begin{aligned} &F^{TR}_{m,\ell} = F^{BR}_{m,\ell} = F^{TL}_{1,\ell} = F^{BL}_{1,\ell} = 0, \\ &M(F^{TR}_{m,\ell}) = M(F^{BR}_{m,\ell}) = M(F^{TL}_{1,\ell}) = M(F^{BL}_{1,\ell}) = 0. \end{aligned}\right\} \tag{8.68}$$

8.2.6 Dowel force in the horizontal direction and its associated moment

The dowel forces in the horizontal direction are derived by the contact condition between dowel pins and mating holes. When a dowel pin and its mating hole are in contact, the dowel spring deformation $\beta_{k,\ell}$ and its time rate $\dot{\beta}_{k,\ell}$ of the (k,ℓ) block interface are

$$\beta_{k,\ell} = \{u_{k,\ell-1} + h_{k,\ell-1}\sin\theta_{k,\ell-1} - d_{k,\ell-1}(1-\cos\theta_{k,\ell-1}) - \{u_{k,\ell} - h_{k,\ell}\sin\theta_{k,\ell} - d_{k,\ell}(1-\cos\theta_{k,\ell})\} \mp \delta_{R,L} \ , \tag{8.69}$$

$$\dot{\beta}_{k,\ell}=\dot{u}_{k,\ell-1}+(h_{k,\ell-1}\cos\theta_{k,\ell-1}-d_{k,\ell-1}\sin\theta_{k,\ell-1})\dot{\theta}_{k,\ell-1}$$
$$-\{\dot{u}_{k,\ell}-(h_{k,\ell}\cos\theta_{k,\ell}+d_{k,\ell}\sin\theta_{k,\ell})\dot{\theta}_{k,\ell}\}. \tag{8.70}$$

For $\ell=1$

$$\beta_{k,1}=u_0-\{u_{k,1}-h_{k,1}\sin\theta_{k,1}-d_{k,1}(1-\cos\theta_{k,1})\}\mp\delta_{R,L}\,, \tag{8.71}$$
$$\dot{\beta}_{k,1}=\dot{u}_0-\{\dot{u}_{k,1}-(h_{k,1}\cos\theta_{k,1}+d_{k,1}\sin\theta_{k,1})\dot{\theta}_{k,1}\}, \tag{8.72}$$

where δ_R and δ_L are the gaps between dowel pin and hole on the right and left, respectively. The dowel force $F_{k,\ell}^{DR}$ and its associated moment $M(F_{k,\ell}^{DR})$ in the horizontal direction acting on the right-hand dowel are as follows. If $\beta_{k,\ell}>0$ on the right gap and $\beta_{k,\ell}<0$ on the left gap

$$\left.\begin{aligned}F_{k,\ell}^{DR}&=K_{k,\ell}^{D}\beta_{k,\ell}+C_{k,\ell}^{D}\dot{\beta}_{k,\ell}\,,\\ M(F_{k,\ell}^{DR})&=-F_{k,\ell}^{DR}(h_{k,\ell}\cos\theta_{k,\ell}+d_{k,\ell}\sin\theta_{k,\ell})\,,\end{aligned}\right\} \tag{8.73}$$

for the block $(k,\ell-1)$

$$\left.\begin{aligned}F_{k,\ell-1}^{DR}&=-K_{k,\ell}^{D}\beta_{k,\ell}-C_{k,\ell}^{D}\dot{\beta}_{k,\ell}\,,\\ M(F_{k,\ell-1}^{DR})&=F_{k,\ell-1}^{DR}(h_{k,\ell-1}\cos\theta_{k,\ell-1}-d_{k,\ell}\sin\theta_{k,\ell\ \ 1})\,.\end{aligned}\right\} \tag{8.74}$$

If $\beta_{k,\ell}<0$ on the right gap and $\beta_{k,\ell}>0$ on the left gap

$$\left.\begin{aligned}F_{k,\ell}^{DR}&=F_{k,\ell-1}^{DR}=0,\\ M(F_{k,\ell}^{DR})&=M(F_{k,\ell-1}^{DR})=0,\end{aligned}\right\} \tag{8.75}$$

where $K_{k,\ell}^{D}$ and $C_{k,\ell}^{D}$ are the dowel spring and damping coefficients, respectively and may be represented in the following generalized form.

$$\left.\begin{aligned}K_{k,\ell}^{D}&=\sum_{j=0}^{m}K_{k,\ell,j}^{D}\beta_{k,\ell}^{j}\,,\\ C_{k,\ell}^{D}&=\sum_{j-0}^{m}C_{k,\ell,j}^{D}\dot{\beta}_{k,\ell}^{j}\,.\end{aligned}\right\} \tag{8.76}$$

Similarly, the dowel forces $F_{k,\ell}^{DL}$ and its associated moments $M(F_{k,\ell}^{DL})$ in the horizontal direction acting on the (k,ℓ) left-hand dowel are the same as in equations (8.73) through (8.76) above.

8.2.7 Dowel friction force in the vertical direction and its associated moment

The dowel friction forces in the vertical direction are derived from the dowel forces and the friction factor. When dowel pin and mating hole are in sliding contact, the relative velocity between pin and hole on the block (k,ℓ) interface is

$$\omega_{k,\ell}=\dot{w}_{k,\ell}+(h_{k,\ell}\sin\theta_{k,\ell}-d_{k,\ell}\cos\theta_{k,\ell})\dot{\theta}_{k,\ell}$$
$$-\{\dot{w}_{k,\ell\ \ 1}-(h_{k,\ell-1}\sin\theta_{k,\ell-1}+d_{k,\ell}\cos\theta_{k,\ell-1})\dot{\theta}_{k,\ell-1}\}, \tag{8.77}$$

For $\ell=1$

$$\omega_{k,1}=\dot{w}_{k,1}+(h_{k,1}\sin\theta_{k,1}-d_{k,1}\cos\theta_{k,1})\dot{\theta}_{k,1}-\dot{w}_0\,. \tag{8.78}$$

The dowel friction force on the right-hand dowel in the vertical direction $\mu F_{k,\ell}^{DR}$ and its associated moment $M(\mu F_{k,\ell}^{DR})$ for the block (k,ℓ) are as follows.

$$\left.\begin{aligned}\mu F_{k,\ell}^{DR}&=-\mathrm{sign}(\omega_{k,\ell})\cdot\mid F_{k,\ell}^{DR}\mid\cdot f(\mu)\,,\\ M(\mu F_{k,\ell}^{DR})&=-\mu F_{k,\ell}^{DR}(h_{k,\ell}\sin\theta_{k,\ell}-d_{k,\ell}\cos\theta_{k,\ell})\,,\end{aligned}\right\} \tag{8.79}$$

for the block $(k,\ell-1)$

$$\left.\begin{aligned}\mu F^{DR}_{k,\ell-1} &= \mathrm{sign}(\omega_{k,\ell}) \cdot \mid F^{DR}_{k,\ell} \mid \cdot f(\mu) \ , \\ M(\mu F^{DR}_{k,\ell-1}) &= -\mu F^{DR}_{k,\ell-1}(-h_{k,\ell-1}\sin\theta_{k,\ell-1} - \mathrm{d}_{k,\ell}\cos\theta_{k,\ell-1}) \ ,\end{aligned}\right\} \tag{8.80}$$

where $f(\mu)$ is function of both statical and dynamical friction factors. Similarly, the friction force $\mu F^{DL}_{k,\ell}$ on the left-hand side and its moment $M(\mu F^{DL}_{k,\ell})$ are as follows.

For the block (k,ℓ)

$$\left.\begin{aligned}\mu F^{DL}_{k,\ell} &= -\mathrm{sign}(\omega_{k,\ell}) \cdot \mid F^{DL}_{k,\ell} \mid \cdot f(\mu) \ , \\ M(\mu F^{DL}_{k,\ell}) &= -\mu F^{DL}_{k,\ell}(h_{k,\ell}\sin\theta_{k,\ell} + d_{k,\ell}\cos\theta_{k,\ell}) \ ,\end{aligned}\right\} \tag{8.81}$$

for the block $(k,\ell-1)$

$$\left.\begin{aligned}\mu F^{DL}_{k,\ell-1} &= \mathrm{sign}(\omega_{k,\ell}) \cdot \mid F^{DL}_{k,\ell} \mid \cdot f(\mu) \ , \\ M(\mu F^{DL}_{k,\ell-1}) &= -\mu F^{DL}_{k,\ell-1}(-h_{k,\ell-1}\sin\theta_{k,\ell-1} + d_{k,\ell}\cos\theta_{k,\ell-1}) \ ,\end{aligned}\right\} \tag{8.82}$$

$$f(\mu) = f(\mu_k, \mu_s) \ . \tag{8.83}$$

8.2.8 Moment due to block weight and pressure difference

The moments acting on the block as a result of the block weight and pressure difference are as follows;

If $\alpha_{k,\ell+1} > 0$

$$M(W^U_{k,\ell}) = W^U_{k,\ell}(h_{k,\ell}\sin\theta_{k,\ell} + b_{k,\ell}\cos\theta_{k,\ell}) \ . \tag{8.84}$$

If $\alpha_{k,\ell-1} = 0$

$$M(W^U_{k,\ell}) = W^U_{k,\ell} h_{k,\ell}\sin\theta_{k,\ell} \ . \tag{8.85}$$

If $\alpha_{k,\ell+1} < 0$

$$M(W^U_{k,\ell}) = W^U_{k,\ell}(h_{k,\ell}\sin\theta_{k,\ell} - b_{k,\ell}\cos\theta_{k,\ell}) \ , \tag{8.86}$$

where

$$W^U_{k,\ell} = \sum_{j=i+1}^{n} w_{k,\ell,j} + F^P_{k,\ell} \ . \tag{8.87}$$

When $j=n$, $M=(W^u_{n,\ell})=0$. Similarly, if $\alpha_{k,\ell} > 0$

$$M(W^L_{k,\ell}) = W^L_{k,\ell}(h_{k,\ell}\sin\theta_{k,\ell} - b_{k,\ell}\cos\theta_{k,\ell}) \ . \tag{8.88}$$

If $\alpha_{k,\ell} = 0$

$$M(W^L_{k,\ell}) = W^L_{k,\ell} h_{k,\ell}\sin\theta_{k,\ell} \ .$$

If $\alpha_{k,\ell} < 0$

$$M(W^L_{k,\ell}) = W^L_{k,\ell}(h_{k,\ell}\sin\theta_{k,\ell} + b_{k,\ell}\cos\theta_{k,\ell}) \ , \tag{8.89}$$

where

$$W^L_{k,\ell} = \sum_{j=1}^{n} W_{k,\ell,j} + F^P_{k,\ell} \ . \tag{8.90}$$

8.2.9 Restraint force between top orifice blocks

The top blocks of columns restrain each other regionally as shown in Fig. 8.1. The restraint force $F^{OP}_{k,\ell}$ is

$$F^{OP}_{k,\ell} = K^{OP}_{k,\ell}(u_{k+1,\ell} - u_{k,\ell}) - K^{OP}_{k-1,\ell}(u_{k,\ell} - u_{k-1,\ell}) \ , \tag{8.91}$$

where $K^{OP}_{k,\ell}$ is the spring constant of the tie plate between the block $(k+1,\ell)$ and the block (k,ℓ).

8.2.10 Equation of motion for side reflector block

Eack reflector block has one translational coordinate u. For the reflector block on the right-hand side, the equation of motion is

$$m_{m+2,\ell}\ddot{u}_{m+2,\ell}=F^{RF}_{m+2,\ell}+F^{RF}_{m+2,\ell-1}+F^{TR}_{m,\ell}+F^{MR}_{m,\ell}+F^{NR}_{m,\ell}+F^{BR}_{m,\ell}+F^{M}_{2,\ell}\ , \tag{8.92}$$

where $F^{RF}_{m+2,\ell}$ is the friction force between block surfaces. F^{M} is the force of the core restraint mechanism.

$$\left.\begin{aligned}
&F^{M}_{i,\ell}=K^{M}_{i,\ell}\Psi_{i,\ell}+C^{M}_{i,\ell}\dot{\Psi}_{i,\ell}\ ,\\
&\Psi_{i,\ell}=u_o-u_{i,\ell}\ ,\\
&\dot{\Psi}_{i,\ell}=\dot{u}_o-\dot{u}_{i,\ell}\ ,\\
&K^{M}_{i,\ell}=\sum_{j=0}^{m}K^{M}_{i,\ell,j}\Psi^{j}_{i,\ell}\ ,\\
&C^{M}_{i,\ell}=\sum_{j=0}^{m}C^{M}_{i,\ell,j}\dot{\Psi}^{j}_{i,\ell}\ ,\\
&(i=m-1,\ m+2)\ .
\end{aligned}\right\} \tag{8.93}$$

The friction force acting on the ℓ-th row reflector block is as follows.

$$\left.\begin{aligned}
&F^{RF}_{i,\ell}=-\mathrm{sign}(v_{i,\ell})F(v_{i,\ell})\ ,\\
&v_{i,\ell}=\dot{u}_{i,\ell}-\dot{u}_{i,\ell-1}\ ,\\
&F(v_{i,\ell})=F_{i,\ell}\{\mu_s+f(v_{i,\ell})+f(v^{v}_{i,\ell})+f(v^{3}_{i,\ell})\}\ ,\\
&(i=m+1,\ m+2)\ ,
\end{aligned}\right\} \tag{8.94}$$

and for the $(\ell-1)$th row reflector block

$$F^{RF}_{i,\ell-1}=\mathrm{sign}(v_{i,\ell})F(v_{i,\ell})\ , \tag{8.95}$$

velocity $v_{i,1}$ for $\ell=1$

$$v_{i1}=\dot{u}_{i1}-\dot{u}_{O}\ .$$

Similarly, for the reflector block on the left-hand side, the equation of motion is

$$m_{m-1,\ell}\ddot{u}_{m-1,\ell}=F^{RF}_{m-1,\ell}+F^{RF}_{m+1,\ell+1}+F^{TL}_{1,\ell}+F^{ML}_{1,\ell}+F^{NL}_{1,\ell}+F^{BL}_{1,\ell}+F^{M}_{1,\ell}\ . \tag{8.96}$$

8.2.11 Equation of motion for core support block

The core support block has one translational coordinate u. For the core support block, the equation of motion is

$$m_S\ddot{u}_S=F^{MR}_S+F^{D}_S+F^{F}_S\ , \tag{8.97}$$

where F^{MR}_S, F^{D}_S and F^{F}_S are the side support forces, dowel forces and friction forces, respectively.

$$\left.\begin{aligned}
&F^{MR}_S=2K^{M}_{1,1}\Psi_{1,1}+2C^{M}_{1,1}\dot{\Psi}_{1,1}\ ,\\
&\Psi_{1,1}=u_S-u_o\ ,\\
&\dot{\Psi}_{1,1}=\dot{u}_s-\dot{u}_o\ ,
\end{aligned}\right\} \tag{8.98}$$

$$F^{D}_S=\sum_{k=1}^{m}(F^{DR}_{k,1}-F^{DL}_{k,1})\ , \tag{8.99}$$

$$F^{F}_S=\sum_{k=1}^{m}F^{F}_{k,1}+\sum_{k=1}^{2}F^{RF}_{k,\ell}\ . \tag{8.100}$$

8.3 Results and discussions

The governing equations given in section 8.2 can be numerically solved by using the Runge–Kutta integration schemes. The geometry data and mass of the blocks (shown in Table 8.1) are such that the system analyzed corresponds to the experimental HTGR fuel column with dimension scaled by 1/2 and weight scaled by 1/4. The computation time interval was 0.05 milli–seconds. The numerical results are compared with experimental results.

Figure 8.5 shows displacement of fuel blocks and side reflectors motion at 3.0 Hz frequency sinusoidal, peak acceleration 250 Gal, uni–axial excitation. The lumpimg motion is observed in the figure as illustrated in the previous section 7.3.

8.3.1 Effect of input acceleration level

Figure 8.6 shows the displacements of analysis and experiment as function of the input acceleration levels for harmonic excitation. In the figure, it can be seen that the analytical results are in good agreement with the experimental results at input acceleration 100 and 500 Gal, but not at for 250 Gal. At 250 Gal level excitation, the analytical results are lower than the experimental ones, especially at excitation frequencies between 3 and 6 Hz. This frequency region is considered to be an unstable one. Concerning with unstable frequency, Fig. 8.7 shows the resonance curves comparing sweep–up with sweep–down.

The sweep–down response is also presented in Fig. 8.7 to verify the nonlinear behavior of the multiple column vibration. As illustrated, the limit frequency for lumping in the down sweep was slightly lower than in the up sweep, defining an unstable region.

The fact that the sweep–down frequency is lower than the sweep–up frequancy indicates that the system exhibits a nonlinear spring effect, which means that the response curve shows a hysterisis characteristic. In the unstable region, the analytical values of response displacements are slightly different from the experimental ones.

Table 8.1 Calculation data

Item			Column		Reflector column
			Block Nos. 1~12	Top block	
Block rocking spring half width	a	(m)	2.5×10^{-2}	2.5×10^{-2}	–
Block geometric half width	b	(m)	7.25×10^{-2}	7.25×10^{-2}	–
Damping coefficient of horizontal impact	C^B	(kN • s/m)	7.85	7.85	7.85
Damping coefficient of displacement detector	C^C	(kN • s/m)	0.0	0.0	–
Damping coefficient of dowel pin	C^D	(kN • s/m)	5.1	5.1	–
Damping coefficient of restraint structure	C^M	(kN • s/m)	–	–	1.96×10^{-2}
Damping coefficient of vertical block impact	C^V	(kN • s/m)	9.81	9.81	–
Distance of dowel from block center line	d	(m)	5.2×10^{-2}	5.2×10^{-2}	–
Block half height	h	(m)	14.25×10^{-2}	14.25×10^{-2}	14.25×10^{-2}
			(10.7×10^{-2})	(10.7×10^{-2})	(10.7×10^{-2})
Block mass moment of inertia	I	(kN • m)	9.06×10^{-2}	1.76×10^{-2}	–
			(2.96×10^{-2})	(6.08×10^{2})	
Spring constant of horizontal impact	K^B	(kN/m)	1.24×10^{4}	1.24×10^{4}	1.24×10^{4}
Spring constant of dowel pin	K^D	(kN/m)	1.23×10^{4}	1.23×10^{4}	–
Spring constant of top block restraint	K^{OP}	(kN/m)	–	–	8.3×10^{3}
Spring constant of vertical block impact	K^V	(kN/m)	2.45×10^{4}	2.45×10^{4}	–
Block mass	m	(kg)	19.1	15.4	52.8
			(14.3)	(10.2)	(39.0)
Gap between column	δ	(mm)	2.0×10^{-3}	5.0×10^{-4}	–
Gap between dowel pin and hole	δ_L, δ_R	(mm)	5.0×10^{-4}	5.0×10^{-4}	5.0×10^{-4}
Coefficient of friction	μ_k, μ_s	(–)	0.2	0.2	0.2

(( ) means short length block, 1 kN=102 kgf, 1 kN/m=1.02 kgf/cm)

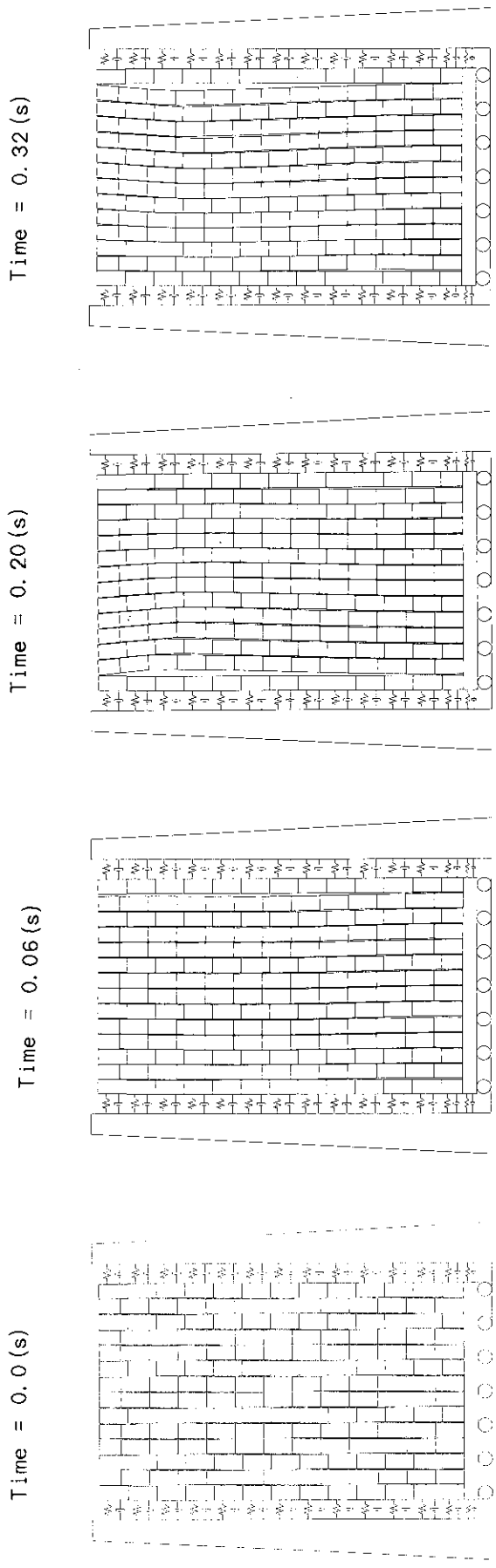

Fig. 8.5 Seismic behavior of two-dimensional vertical slice core model (Excitation 3.0Hz, Max. accleration 250 Gal)

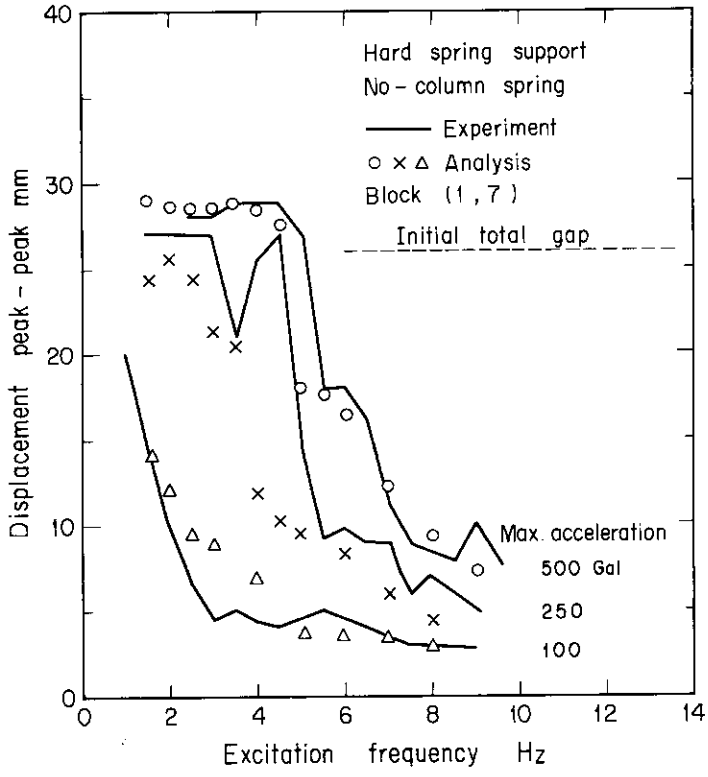

Fig. 8.6 Effect of input acceleration on displacement

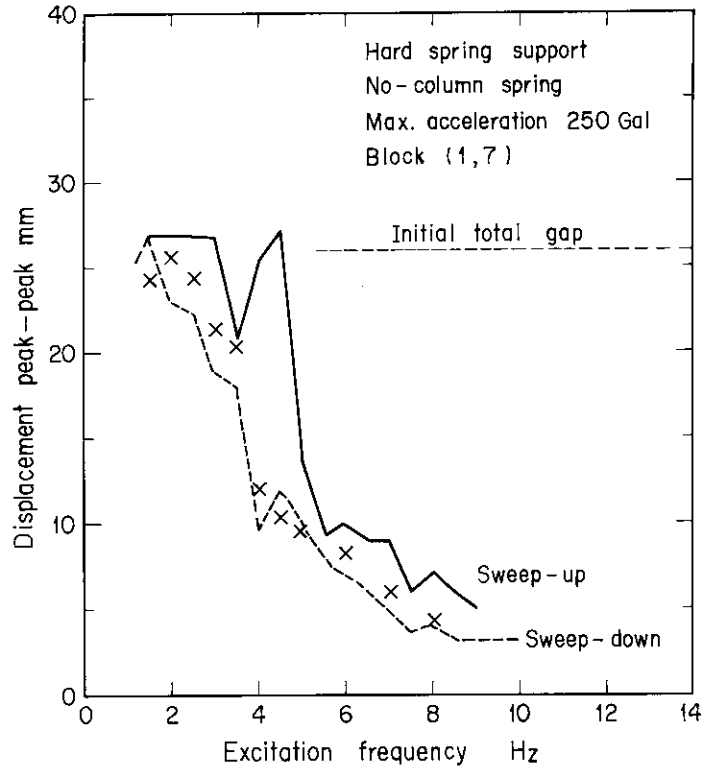

Fig. 8.7 Comparison sweep-up and sweep-down response

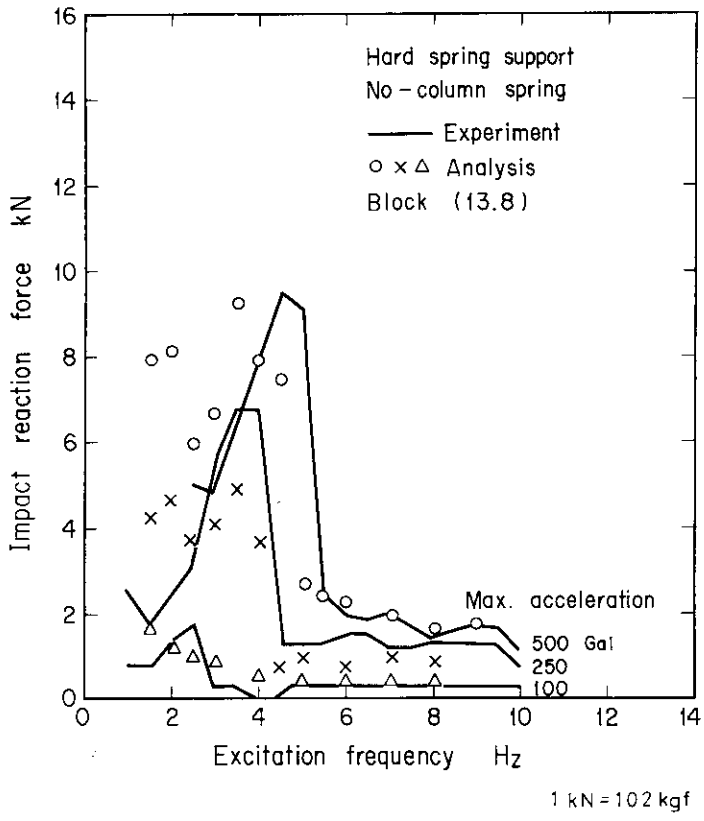

Fig. 8.8 Effect of input acceleration on impact reaction force

Figure 8.8 shows comparison between the experiment and analysis of the boundary reaction forces as function of input acceleration levels for harmonic excitation. The correlation is good for the lower reaction forces, but less satisfasctory for a strong reaction force.

It is seen that resonant frequency is strongly amplitude dependent and increases with an increase in excitation level.

The system exhibits a spring hardeing effect, which means that the jump frequency will increase with an increase in input acceleration level.

8.3.2 Impact reaction force along the column

Figure 8.9 shows distributions of the impact reaction forces along the column and compares the analytical and experimental results. The analytical results show a favorable correlation with the results of the experiments.

8.3.3 Effect of side reflector support stiffness

The displacement response characteristics of three kinds of the side support stiffness, (hard, intermediate and soft spring support) are shown in Fig. 8.10. These spring constants are shown in Table 8.2. At low excitation frequency, maximun column displacements decrease with increasing the side support stiffness, while the opposite is observed at high excitation frequency. In the figure, it can be seen that the analytical results are in good agreement with the experimental ones. The harder the side support stiffness, becomes the smaller colmn displacements.

Figure 8.11 shows the impact reaction force characteristics comparing analysis and experiment with the side support stiffness as parameters. The hard support stiffness is found to given a large impact force in comparison with the soft or intermediate stiffness. At low excitation frequency, a side support with the intermediate stiffness affords a smaller impact force than with the soft support. In the figure, it can be seen that the analytical results are in fairly good agreement with the experimental ones.

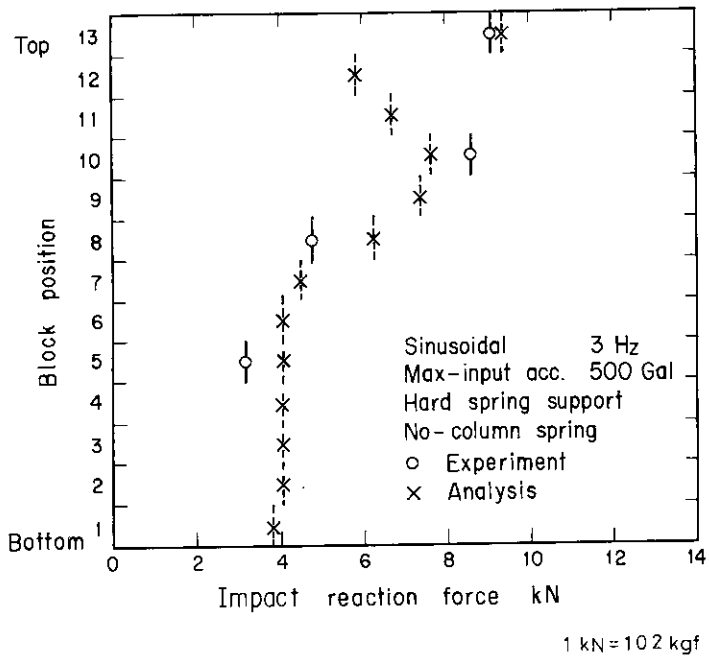

Fig. 8.9 Impact reaction force distribution along column

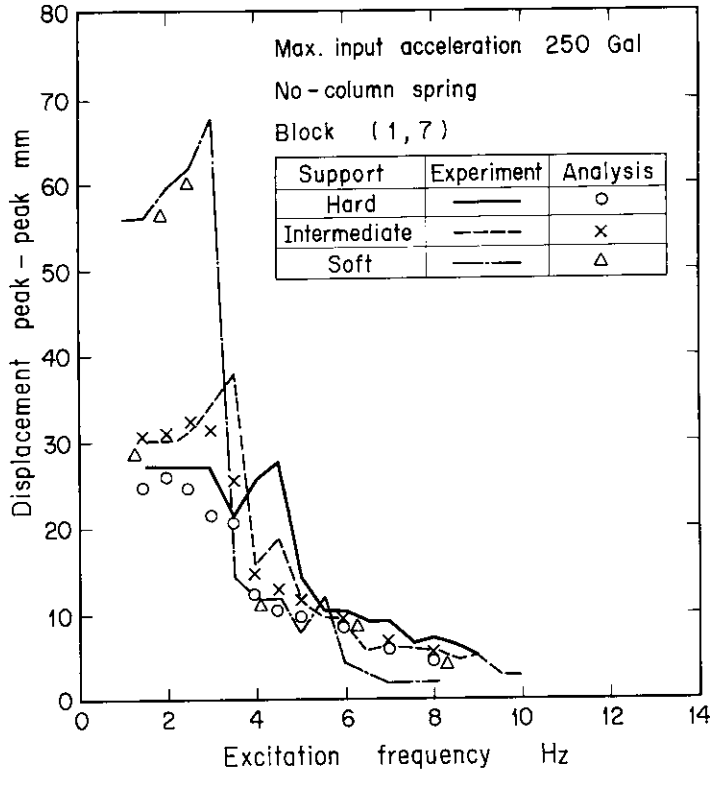

Fig. 8.10 Effect of support stiffness on displacement

Table 8.2 Spring constant of side support structure

Support spring			Spring constant (kN/m)	
			Reflector block	Support plate
Hard			8134	5880
Intermediate			588	725
Soft	Displacement (cm)	$0<\delta\leqq 1.1$	39.2	39.2
		$1.1<\delta\leqq 5.5$	784	784
		$\delta>5.5$	8134	5880

(1 kN/m = 1.02 kgf/cm)

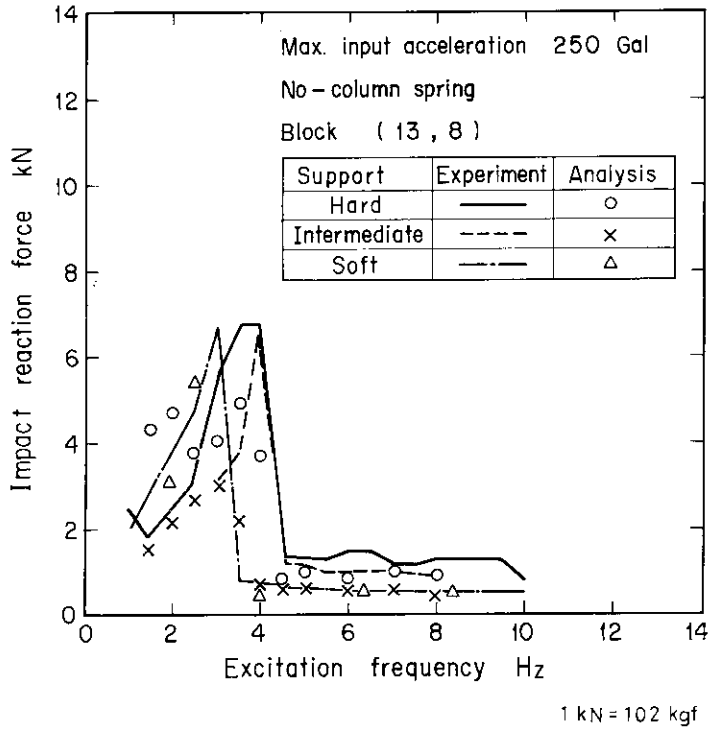

Fig. 8.11 Effect of support stiffness on impact reaction force

8.3.4 Dowel force

It is important to evaluate stresses of dowel pins and holes since the dowel pins and holes are often the weakest part of a fuel block in the structural design for seismic load. In the experiment, measurements of dowel forces were made.

The curves in Fig. 8.12 illustrate that the block dowel force frequancy response is compared for the analytical and experimental values. The analytical values show a favorable correlation with the experimental ones.

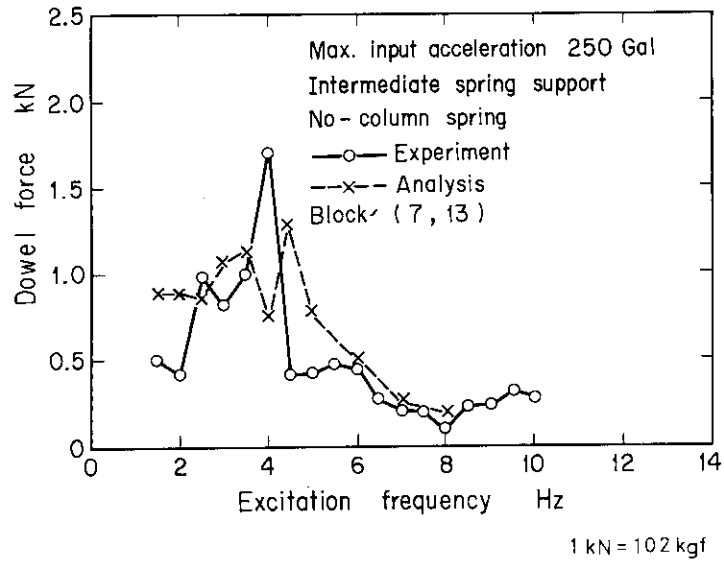

Fig. 8.12 Dowel force

8.4 Concluding remarks

A seismic analysis method for the block columns of the HTGR core has been developed. The calculation equations and numerical results have been presented and were compared with the results of the experiments. The following conclusions have been drawn:

(1) The analytical results were compared with the experimental data for horizontal forced vibration of the series of many interacting stacked columns. Good agreement was obtained between the analytical and experimantal results.

(2) Using this method, the forces in the dowel pins and around holes can be computed. The dowel pin forces from analysis were compared with the experimental data. The analytical values were in good agreement with the experimental ones.

9. Seismic Response of a Two-dimensional Horizontal HTGR Core

9.1 Introduction

In order to obtain the dynamic behavior of the HTGR core in a three-dimensional space under seismic disturbance, it is advisable to carry out a seismic test of a three-dimensional model. Howerver, seismic tests of the three-dimensional model take tremendous cost. It is difficult to measure displacements of the fuel blocks in the core in the excitation tests. For this reason, it is desirable to predict a real core dynamic behavior from two-dimensional core model tests. For this purpose the following seismic tests of the two core models were performed: a model seismic test of two-dimensional vertical slice core and a model seismic test of the two-dimensional horizontal slice core.

Olsen et al.[4] made seismic tests of uni-axial excitation and simultaneous bi-axial excitations, using a 1/5 scale model and a 1/2 scale model of a two-dimensional HTGR core. Studies were carried out in order to determine the fuel block displacement and impact characteristics, differences of excitation directions such as uni-axial and simultaneous bi-axial excitations. Muto et al.[30] made uni-axial seismic tests of a two-dimensional horizontal core model to obtain the displacement and the reaction force characteristics and developed a seismic analysis method.

In the above studies, however, the fuel block displacement and impact reaction characteristics due to the side support stiffness are not yet made clear. In order to clarify the effects of the side support stiffness and excitation directions on the fuel block displacements and impact reaction forces, the seismic tests were carried out.

9.2 Experimental apparatus and method

9.2.1 Experimental apparatus

An experimental apparatus was a horizontal two-dimensional slice core that was taken from a one fuel block row across the HTGR core as shown in Fig. 9.1. Graphite fuel blocks were an one half scale of a real fuel block which is the experimental HTGR under design study in JAERI. The experimental apparatus is shown in Fig. 9.2. and Photo. 9.1. They, apparatus shown consisted of 139 fuel blocks and 18 sourronding side reflector blocks. These blocks were graphite blocks. According to the similarity laws the fuel blocks were dimension scaled by 1/2 and weight scaled by 1/4 of those of the experimental HTGR

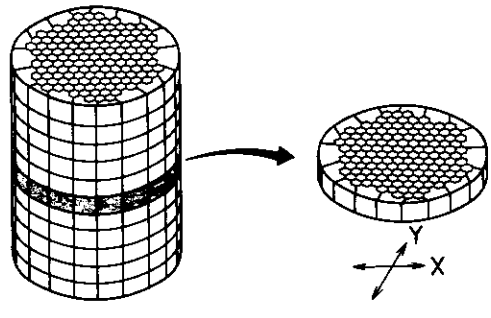

(a) Core (b) Test model

Fig. 9.1 Two-dimensional horizontal core model

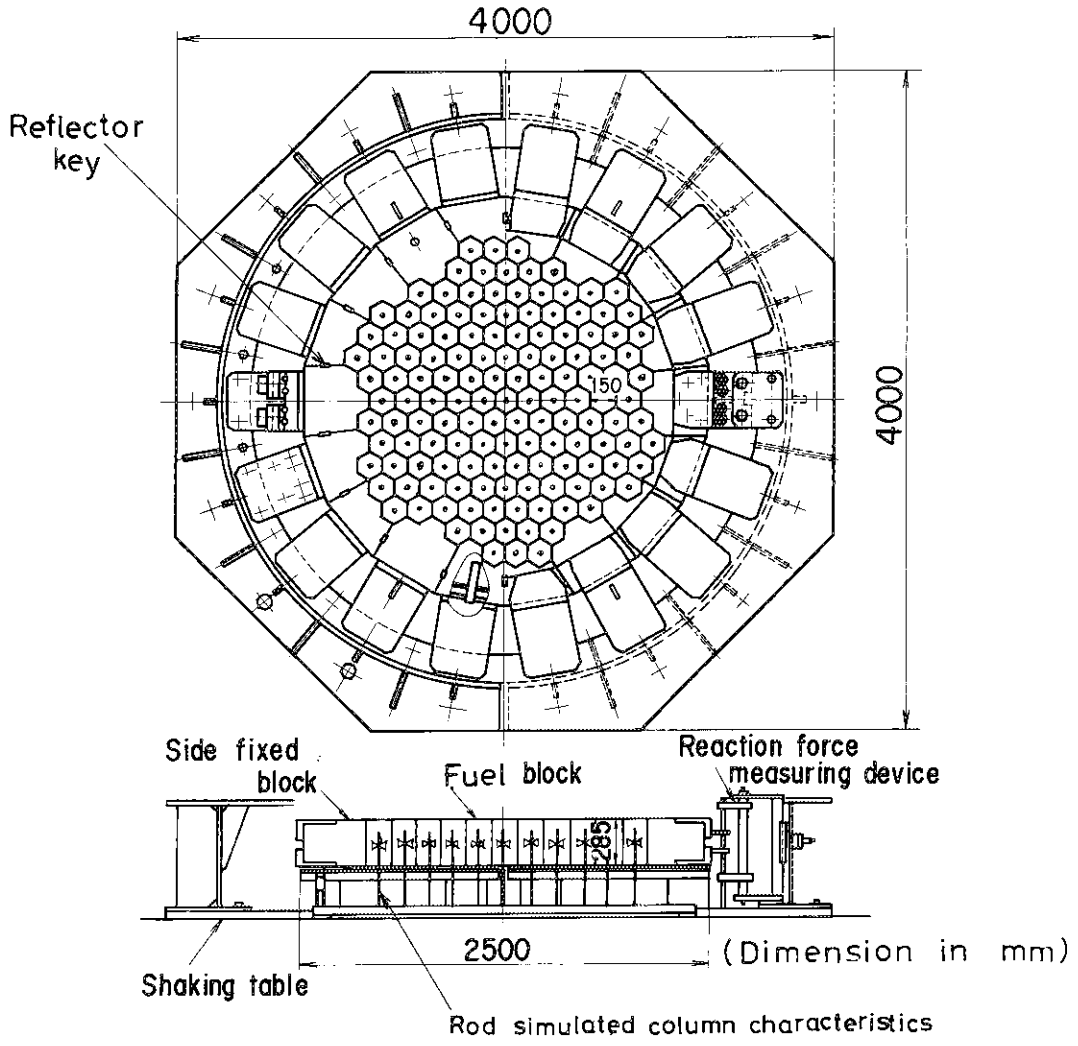

Fig. 9.2 Experimental apparatus of two-dimensional horizontal core model

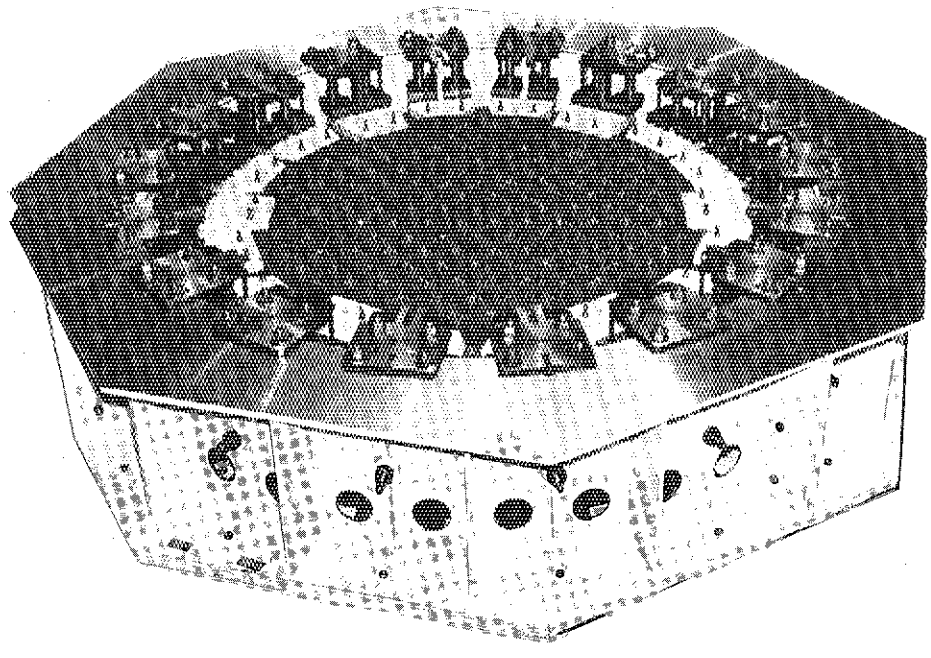

Photo. 9.1 External appearance of two-dimensional horizontal core model

fuel blocks. To make a correction of the weight, as indicated in Fig. 9.3, a lead cylinder was inserted into middle of each block as an additional mass.

The column restoring characteristics were simulated by a rod inserted into the block center as shown in Fig. 9.3. The spring characteristics of the center rod were made linear for simplicity of the experimental apparatus. The spring constant was 4.7 kN/m, being decided according to the natural frequency of the fuel block 2.5 Hz. The spring rod through the fuel block attached to the base plate of the apparatus. Three ball bearings, attached to the bottom of the fuel block, reduce friction between the fuel block and base plate. The displacements between the block and base plate were measured with strain gauges attached to the bottom of the spring rod at right angles to each other.

The eighteen side reflector blocks were made of three different kinds of graphite blocks. The weights of those blocks of the experimental apparatus were 142.8, 115.5 and 97.2kg. Each side reflector block (simulating a permanent side reflector) was fixed to the steel frame by the side restraint structure which consisted of two support bars. The impact reaction forces were measured with strain gauges attached to the restraint support bars. The strain gauges were attached to the support bars at right angles to each other (radial and circumferential reaction forces were measured). The four ball bearings attached to the bottom of the side reflector block reduce friction between the side reflector block and base plate.

In order to know effects of the side support stiffness on the fuel block displacements and the side reaction forces, three kinds of side support rods were provided. The spring constants were (1) hard spring support, 4160 kN/m, (2) intermediate spring support, 260 kN/m and (3) combined trilinear soft intermediate and hard spring support, 15 kN/m (displacement from 0 to 16 mm), 97 kN/m (displacement

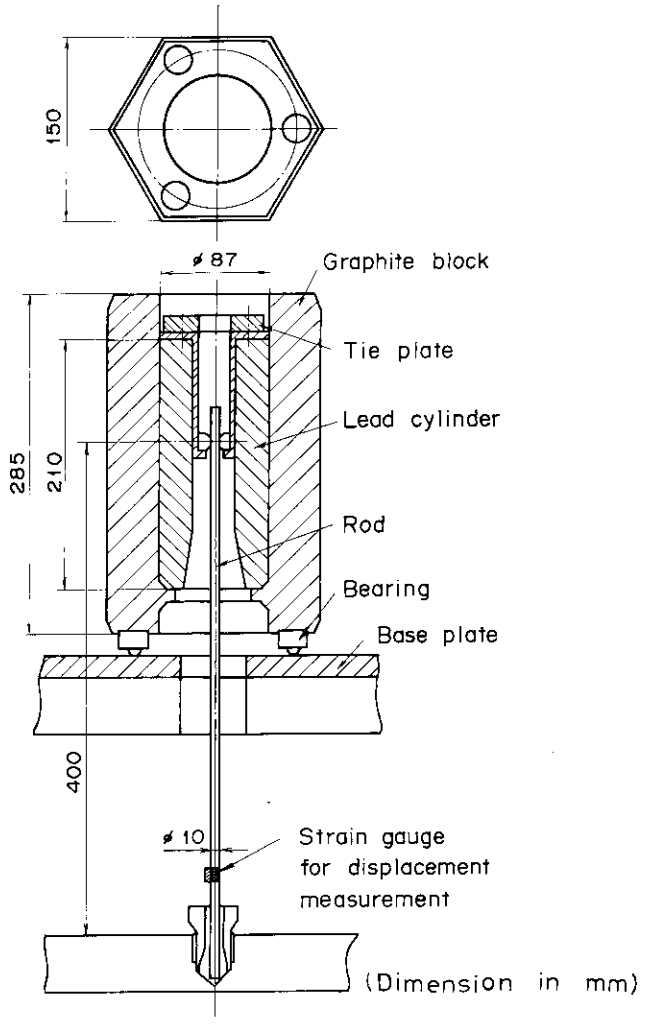

Fig. 9.3 Graphite fuel block

from 16 to 25.4 mm) and 4160 kN/m (displacement above 25.4 mm).

In addition to intermediate support stiffness, the apparatus was so designed as to apply a force from surroundings to the core center, to clarify effects of preload on the displacements and forces.A tied key (the reflector key) between side reflector blocks was also installed to compare effects of the reflector key on the displacements and forces.

9.2.2 Experimental method

Uni-axial and simultaneous bi-axial borizontal excitation tests were performed on the apparatus on a shaking table using sinusoidal and random waves. In the case of uni-axial sinusoidal excitations, tests were performed with the X direction excitation (flat-to-flat direction) and the Y direction excitation (corner-to-corner direction) as indicated in Fig. 9.4. In the case of the simultaneous bi-axial excitations, four kinds of excitation modes were selected for combined actuated X and Y direction displacements and phase change between two axes (the X and Y directions as shown in Fig. 9.4). Those excitation loci are (1) the X-Y circular excitation, (2) the X-Y axes elliptical excitation, (3) the X-Y 45° elliptical excitation and (4) the X-Y 45° axial excitation. Sinusoidal frequencs sweeps, sweeping up and down from 1 to 10 Hz range, peak acceleration levels of 50, 100 and 250 Gal were applied in the excitation tests.

It the case of the random excitation tests, two kinds of seismic waves and a white noise wave with frequency components ranging from 1 to 10 Hz were used. In the case of the uni-axial seismic tests, the E1 Centro 1940 NS wave and Ibaraki 1964 EW wave were used. In the case of the simultaneous two dimensional seismic tests, the E1 Centro 1940 NS wave for the X direction and the E1 Centro 1940 EW wave for the Y direction, and the Ibaraki 1964 NS wave for the X direction and the Ibaraki 1964 EW wave for the Y direction excitations were used. According to the similarity laws, the time axis was compressed to $1/\sqrt{2}$ times the actual seismic waves in the seismic tests. The peak acceleration levels of 100, 250 and 500 Gal were applied in the random excitation tests.

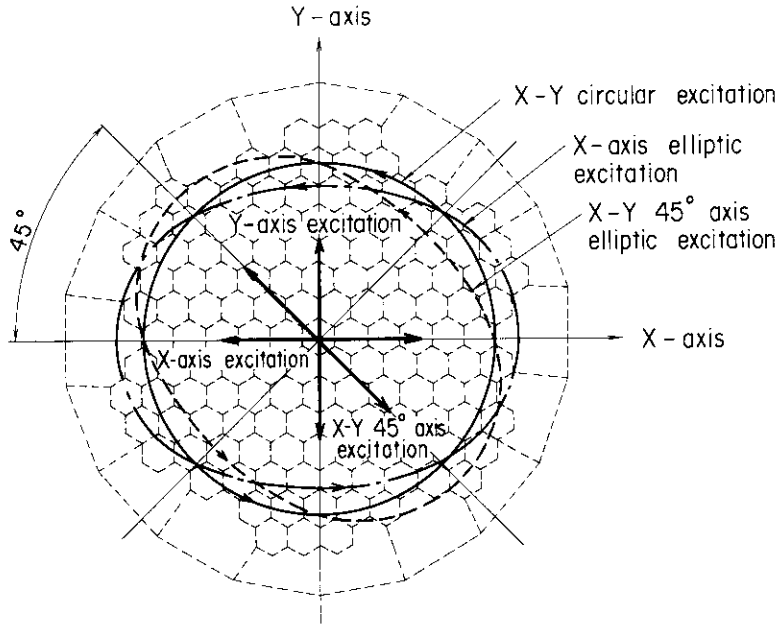

Fig. 9.4 Excitation modes

9.3 Results and discussions

9.3.1 Gap in block rows

The total gaps in each block row in the X and Y directions are shown in Fig. 9.5 and the total gaps are closely related to the fuel block displacements. Each gap between the fuel blocks was 2 mm. As shown in Fig. 9.5, the total gaps in each block row in the Y direction are greater than in the X direction and the total gaps in each block row in the core center region are greater than on the core periphery. In Fig. 9.5, fuel blocks and side reflector blocks are numbered for illustration of the experimental results.

9.3.2 Effect of acceleration level on response

Figure 9.6 shows the displacements vesus excitation frequency as function of input acceleration levels. It is seen that with an increase of input acceleration levels, the frequency for rapid drop of the displacements, i.e. the jump-down frequency shifts to a higher frequency. Figure 9.7 shows the displace-

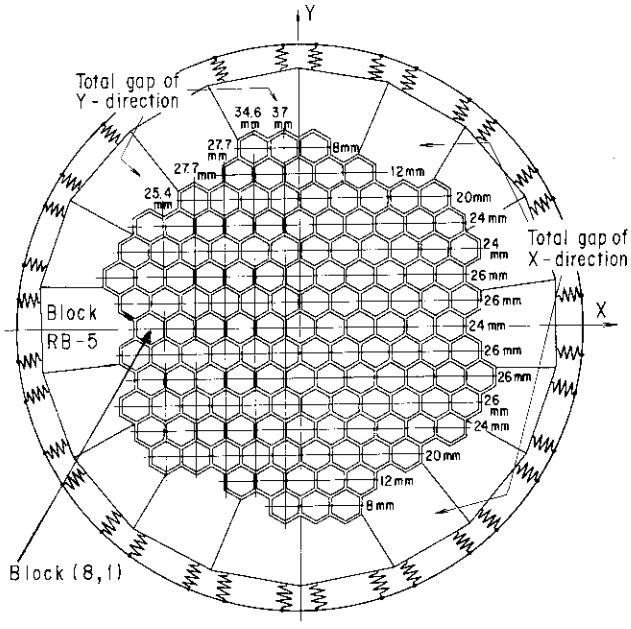

Fig. 9.5 Total gap of each row of core

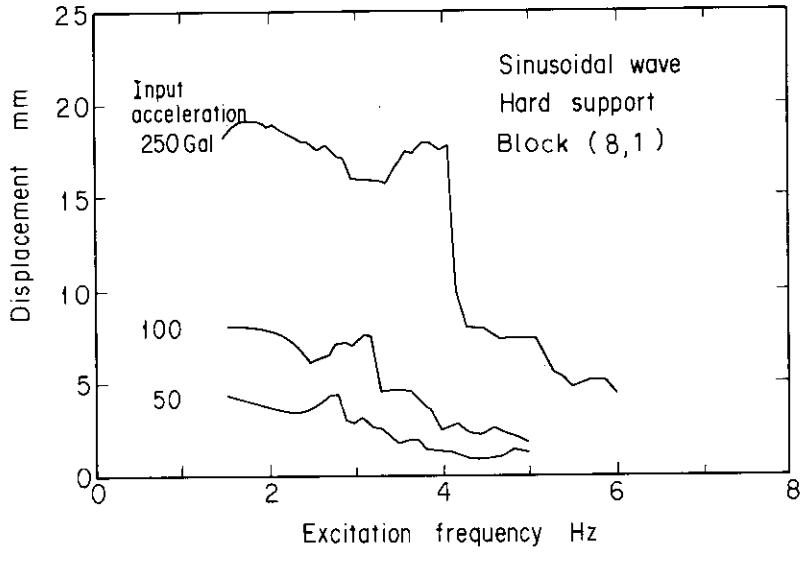

Fig. 9.6 Effect of input acceleration on displacement frequency characteristics

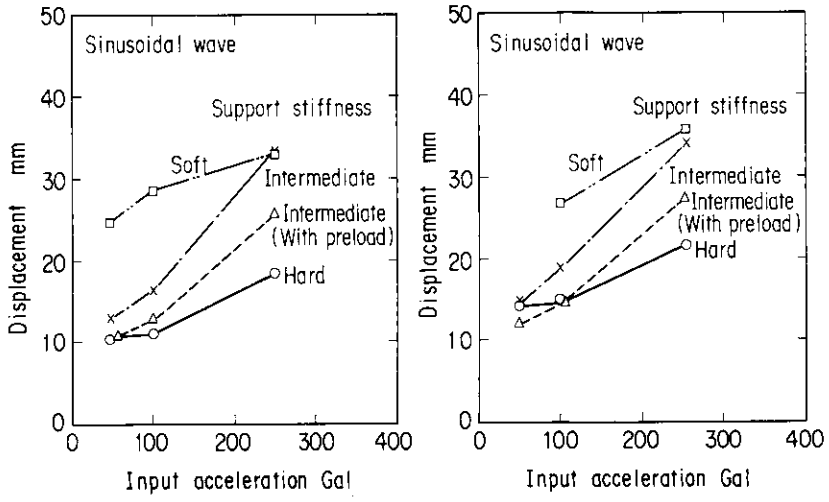

(a) Excitation (X-direction) (b) Excitation (Y-direction)

Fig. 9.7 Maximum displacement vs. input acceleration

ments versus input acceleration levels as function of side support stiffness. In Fig. 9.7 (b) are the maximum displacements for the case of uni-axial X direction and Y direction excitations, respectively. The displacements increase with input acceleration levels in all side support stiffness. In a region of low input acceleration, differences between the displacements in the X direction excitation and that in the Y direction excitation are negligible. With an increase of input acceleration levels the displacements in the Y direction excitation becomes slightly larger than the displacements in the X direction excitation. Since the total gaps in the Y direction are larger than in the X direction, the Y direction displacement occur more easily than the X direction displacement.

Figure 9.8 shows the impact reaction forces versus excitation frequency as function of input acceleration levels, in the case of uni-axial X direction excitation under a hard support condition. It is seen that the impact reaction forces increase with increase of input acceleration levels. The resonant frequency strongly depends on the input acceleration and shifts to a higher frequency with increase of input

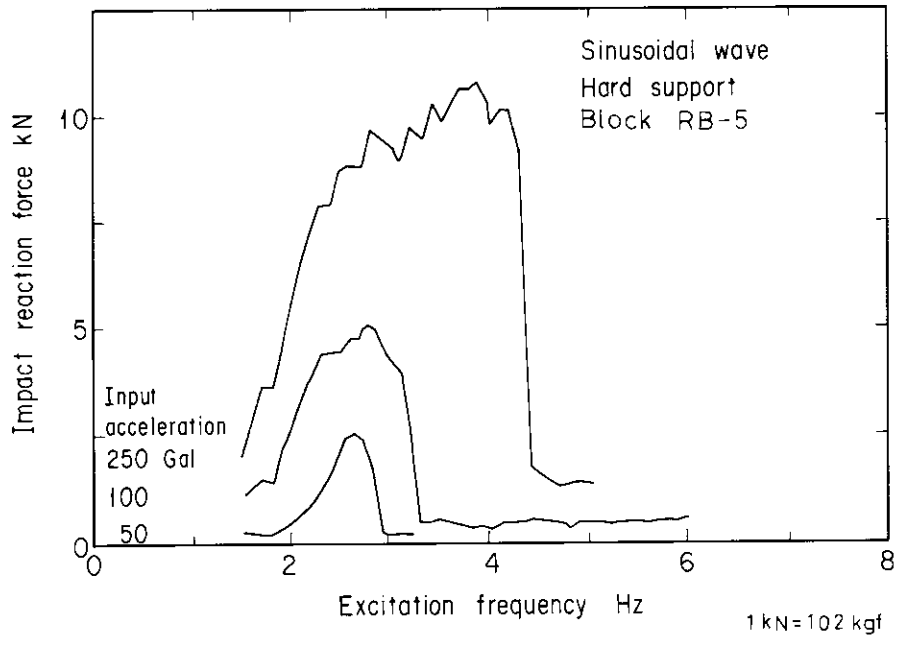

Fig. 9.8 Effect of input acceleration on force frequency characteristics

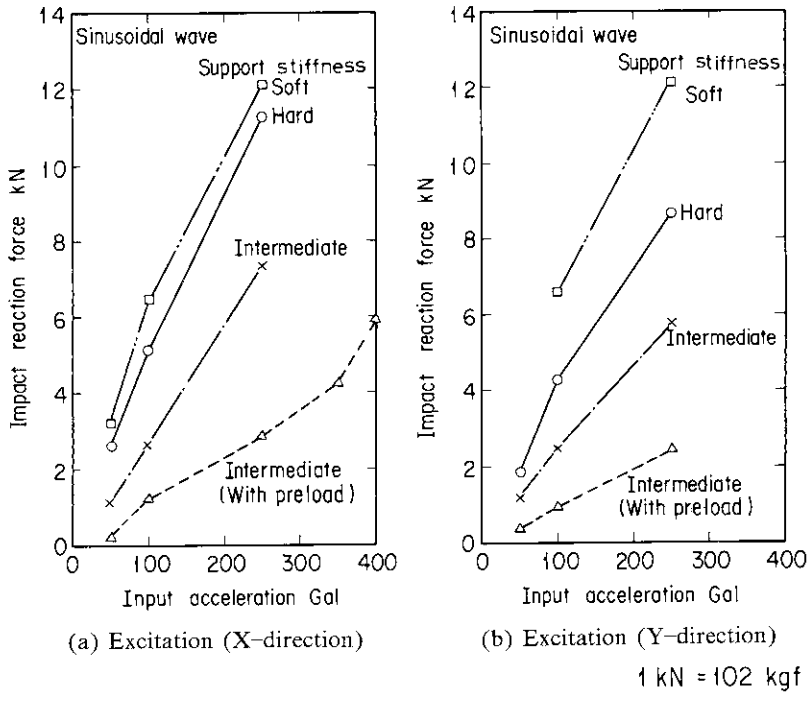

Fig. 9.9 Maximum force vs. input acceleration

acceleration levels. Figure 9.9 shows the impact reaction forces versus input acceleration levels as function of side support stiffness. Figure 9.9 (a) and 9.9 (b) show maximum forces for the cases of the uni-axial X direction and Y direction excitations, respectively.

The impact reaction forces increase with the input acceleration levels which all side support stiffnesses. In the region of the low input acceleration, differences between the force for the X direction excitation and that in the Y direction excitation are negligible. With an increase of input acceleration, the impact reaction force for the X direction excitation becomes slightly larger than the impact force for the Y derection excitation. The flat-to-flat collision of fuel blocks occur during the X direction excitation, while during the Y direction excitation, sliding side collision of fuel blocks occurs, converting impact energy to friction, so that the impact reaction force becomes smaller than that during the X direction excitation.

9.3.3 Effect of excitation direction on response

Figure 9.10 shows the displacements and impact reaction forces in the core at sinusoidal peak acceleration of 250 Gal, for uni-axial and simultaneous bi-axial excitations. In Fig. 9.10 are shown the displacements and forces at frequencies of around 4 Hz, in the maximum response regions. In the simultaneous bi-axial excitation, values of maximum acceleration of 250 Gal are vectors. In the case of the uni-axial X direction excitation, the fuel block moves not only in the X direction but also in the Y direction. The displacement locus of the block center has an elliptic shape with the line of apsides in the X direction. In the case of the uni-axial Y direction excitation, the fuel block moves not only in the Y direction but also in the X direction. The displacement locus of the block center has an elliptic shape with the line of apsides in the Y direction. In the case of X-Y circular excitation, the displacement locus of the block center does not have a circular shape but an elliptic shape with the line of apsides in the Y direction. In the case of the X-Y axis elliptic excitation, the displacement locus of the block center does not have an elliptic shape with the line of apsides in the X direction but an elliptic shape with the line of apsides as the axis inclined $20^\circ \sim 30^\circ$ from the X-axis. In the case of the X-Y 45° elliptic exitation, the displacement locus of the block center has an elliptic shape with the line of apsides inclined $70^\circ \sim 80^\circ$ from the X-axis. In the case of the X-Y 45° axis excitation, the displacement locus of the block center has an elliptic shape

with the line of apsides as the axis inclined 60° from the X-axis.In the simultaneous bi-axial excitations, the locus of the block center differs from the excitation locus. It is because the total gaps in the Y direction are larger than that in the X direction and the fuel blocks are easily displaced in the Y direction than in the X direction. Among the six different excitation conditions, the displacement in the case of the X-Y 45° elliptic excitation are the largest and subsequently becomes smaller in the following order; the X-Y 45° axis excitation, the X-Y axis elliptic excitation, the Y direction excitation, the X-Y circular excitation and the X direction excitation.

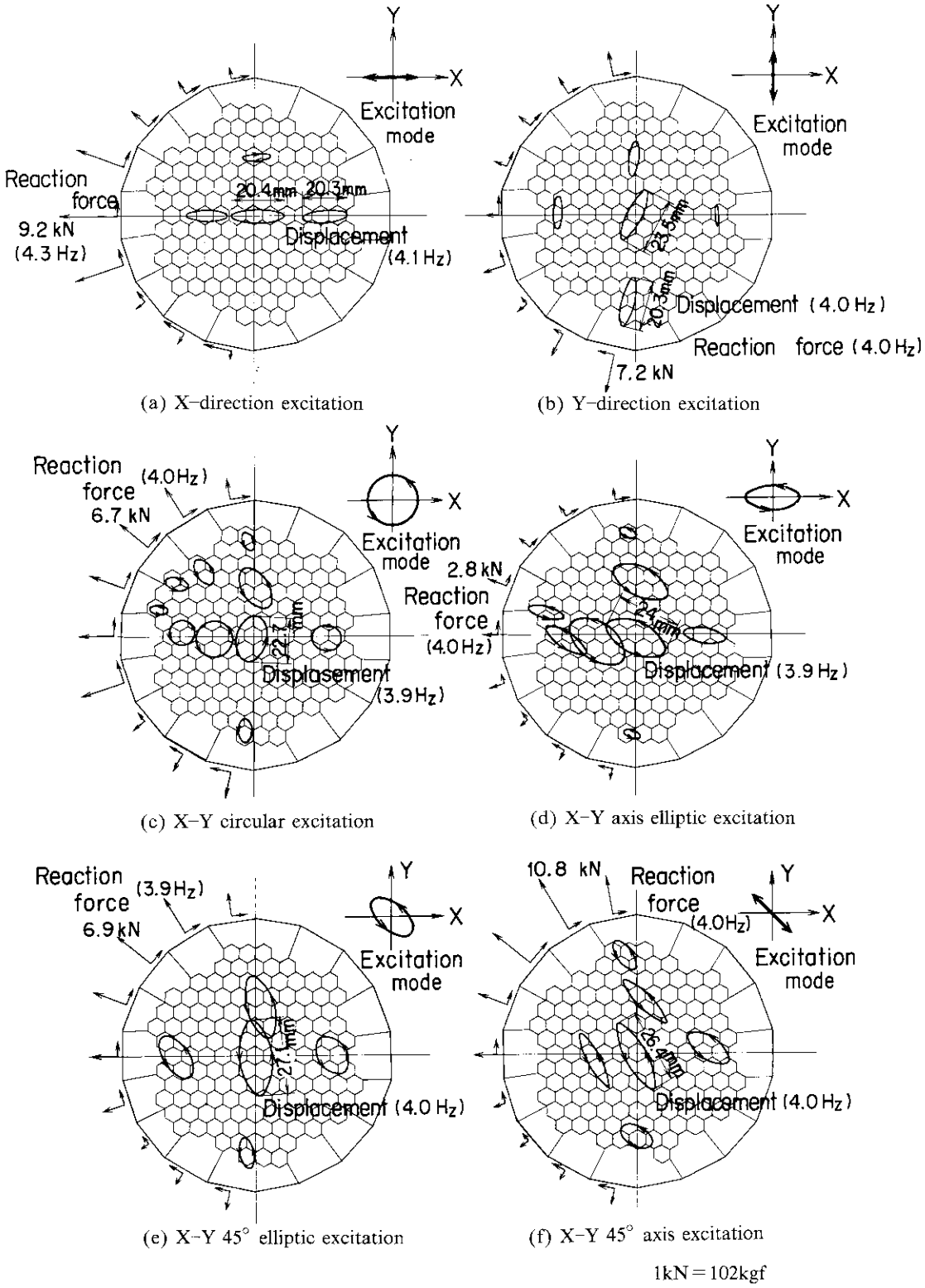

Fig. 9.10 Effect of excitation mode on displacement and force in core

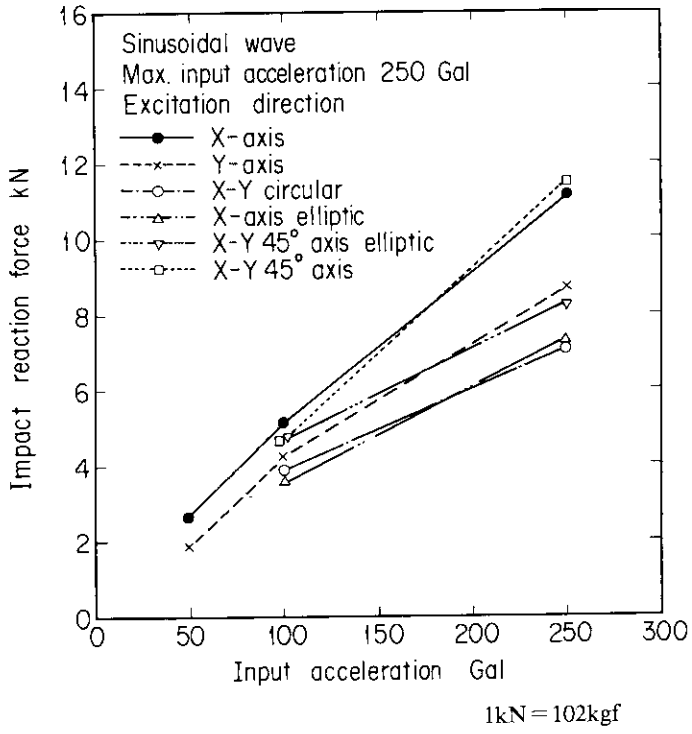

Fig. 9.11 Effect of excitation mode on maximum force

It is seen in Fig. 9.10 that the maximum reaction forces in the radial direction component are larger than that of the tangential component.

Figure 9.11 shows the maximum reaction forces versus input acceleration levels with excitation conditions as a parameter. The impact reaction forces increase with increasing input acceleration. It is seen that the impact reaction forces in the cases of the X direction and X–Y 45° axis excitation are larger than for the other excitation conditions.

9.3.4 Effect of side support stiffness on response

Figure 9.12 shows the fuel block displacements as function of the side support stiffness for the case of uni-axial X and Y direction excitations using a sinusoidal wave, and for the uni-axial X direction

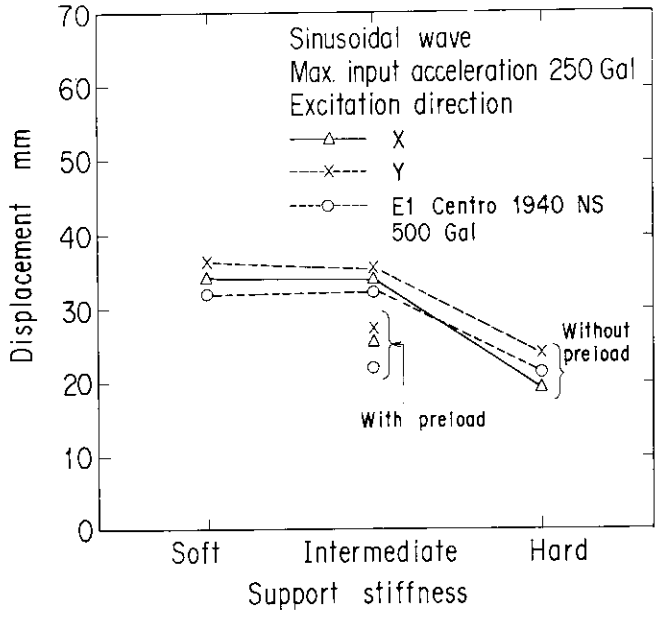

Fig. 9.12 Maximum displacement vs. side support stiffness

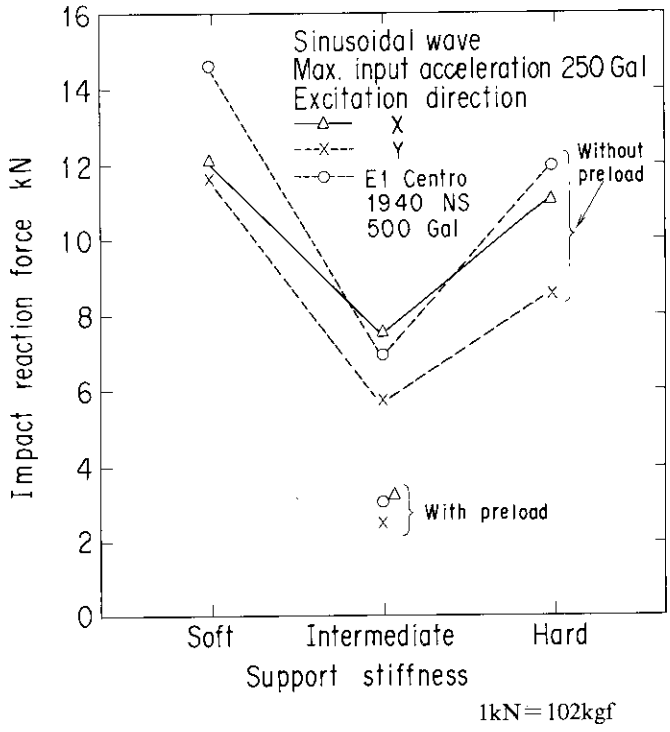

Fig. 9.13 Maximum force vs. side support stiffness

excitation using the El Centro 1940 NS wave. The maximum input accelerations of the sinusoidal wave were 250 Gal and 500 Gal for the El Centro 1940 NS wave. The displacements decrease with an increase of the side support stiffness. It is seen that the fuel block displacements are larger with preload than without preload in the case of the intermediate support condition. Preload from the core periphery to the core center could reduce the displacements of fuel blocks.

Figure 9.13 shows relationship between side support stiffness and the impact reaction force for same condition of Fig. 9.12. The impact reaction forces for the hard support are larger than for the soft support and the forces for the intermediate support condition are smaller than for the hard support. It is seen that the impact reaction forces are smaller with preload than without preload in the case of the intermediate support. There is a favorable support stiffness in the HTGR core design. Furthermore, preload from the core periphery to the core center could reduce the impact reaction forces.

9.3.5 Effect of Key between side reflector blocks

As shown in Fig. 9.2, there exists connection keys between side reflector blocks. The following are effects of the connection keys on response. Figure 9.14 shows the frequency characteristics curves of the impact reaction forces comparing effects of connection key between reflector blocks in the case of a hard support using the uni-axial X direction excitation with the maximum acceleration 250 Gal sinusoidal wave. Differences of the impact reaction forces between cases with the keys and without the keys are small. The impact reaction force with the keys are a little larger than without the keys. Moreover differences of the fuel block displacements between cases with the keys and without the keys are negligible. This is for the following reason. The side reflector blocks are supported by the side support structure and being in contact, may restrain each other. Even if impact occur between one fuel block and one reflector block, the impact force transfers from one reflector block to neighbouring reflector blocks, due to side contact of the reflector blocks. Whether there are connection keys or not, the reflector blocks affect one other, so that the connection keys slightly affect the response values. Nevertheless, when the side support stiffness becomes soft, each support stiffness of the reflector block decreases and the restraint effects between the reflector blocks become relatively large. Both the fuel block displacements and the impact

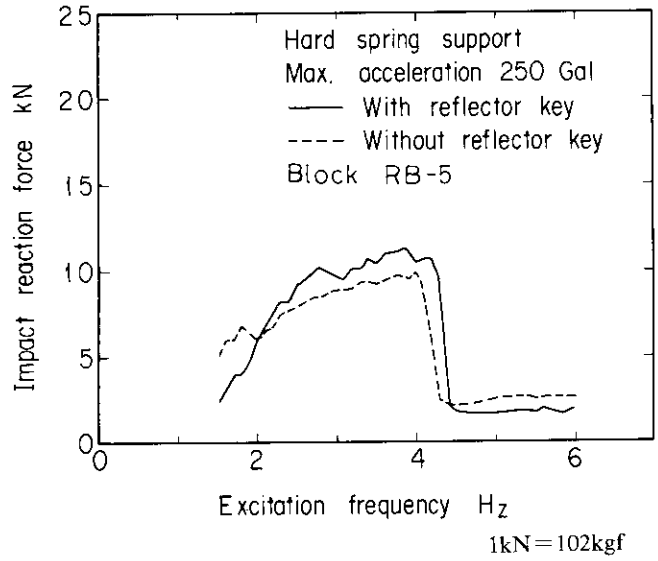

Fig. 9.14 Effect of reflector block key on force frequency characteristics

reaction forces with the connection keys are smaller than without the keys.

9.3.6 Random wave response

Figure 9.15 shows the displacements versus the side support stiffness with three kinds of random waves, of which the maximum acceleration is 500 Gal, as parameters. The maximum displacements of the El Centro 1940 NS wave and the white noise wave are the same. The displacements of the Ibaraki 1964 EW wave are smaller than those of the two other random waves. The resonant frequencies of the El Centro 1940 NS wave range from 2.8 to 9.1 Hz, and those of the Ibaraki 1964 EW wave range from 4.5 to 7.8 Hz. On the other hand the responant frequency, which is determined from the weight of a fuel block and a support rod simulating column stiffness, is 2.5 Hz. Consequently, the El Centro 1940 NS wave exists in the resonant frequency of the fuel block while the Ibaraki 1964 EW wave does not exist in the resonant frequency of the fuel block.

As shown in Figs. 9.12 and 9.15, effects of the side support stiffness on the displacements and the impact reaction forces due to sinusoidal waves and random waves have the same tendency.

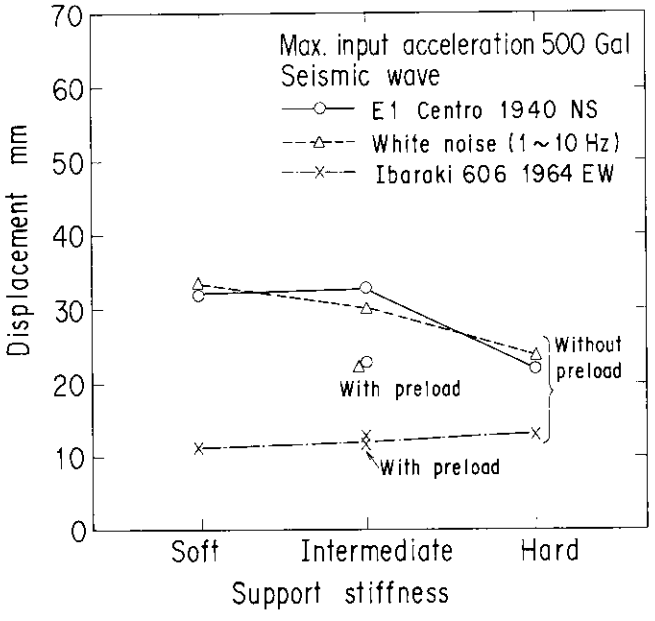

Fig. 9.15 Maximum displacement vs. input wave

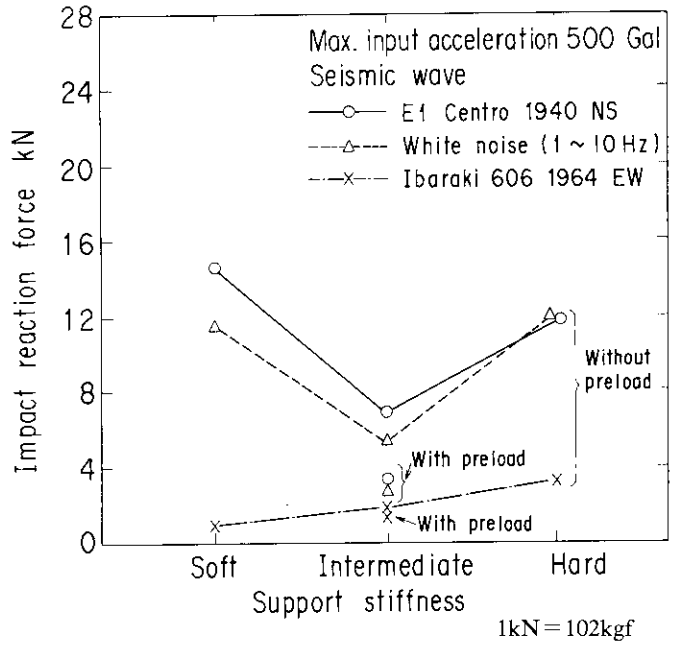

Fig. 9.16 Maximum force vs. input wave

Figure 9.16 shows the maximum reaction forces versus side support stiffness with three kinds of random waves as parameters. The test condition was the same as that of Fig. 9.15. The maximum reaction forces of the E1 Centro 1940 NS wave and the white noise wave are almost the same. The maximum reaction forces of the Ibaraki 1964 EW wave are smaller than that of the two other random waves. This tendency is the same as with the maximum displacement response as illustrated in Fig. 9.15 and it is considered to be due to the same reason.

As shown in Figs. 9.13 and 9.16, the maximum reaction forces dependent on the side support stiffness have almost the same response values for sinusoidal and random waves. The response values of random waves are one half times those of sinusoidal waves for the same input acceleration condition.

Table 9.1 shows the maximum reaction forces comparing the response values of three kinds of random waves and excitation directions. The impact reaction forces of the uni-axial X direction excitation are larger than that of the uni-axial Y direction and simultaneous bi-axial excitation. It is the same tendency as in the case of the sinusoidal wave response. For the above reason, the response values of random waves are estimated from those of the sinusoidal waves and the maximum response values are estimated from those of the uni-axial sinusoidal X direction excitation.

Table 9.1 Effect of input wave on maxium force

Seismic wave		Excitation	Force (kN)
E1 Centro 1940	NS wave	X-axis	11.8
	NS wave	Y-axis	7.5
	NS, EW waves	X-, Y-two axes	6.9
Ibaraki 1964	EW wave	X-axis	3.2
	EW wave	Y-axis	3.4
	NS, EW waves	X-, Y-two axes	2.5
White noise		X-axis	12.0
		Y-axis	7.3

(Maximum acceleration 500 Gal, 1 kN = 102 kgf)

9.4 Concluding remarks

In order to obtain seismic response characteristics and seismic design data for the HTGR core, an experimental study has been carried out using the two-dimensional core model which is a horizontal slice along the axis of the experimental HTGR core consisting of graphite blocks.

The important experimental results are as follows:

(1) The column resonance curve shows typical nonlinear hardening characteristics. The resonant frequency increases with an increase of the input acceleration level and strongly amplitude dependent.

(2) The displacements and impact reaction forces increase with an increase of input acceleration level.

(3) The displacements in the excitation of the corner-to-corner direction are larger than that in the excitation of the flat-to-flat direction. On the other hand, the impact reaction forces in the excitation of the flat-to-flat direction are larger than that in the excitation of the corner-to-corner direction.

(4) The displacements decrease with an increase of side support stiffness. It is seen that the fuel block displacements are larger with preload than without preload in case of the intermediate support condition. Preload from the core periphery to the core center could reduce the displacements of fuel blocks. The impact reaction forces for the hard support condition are larger than for soft support and the forces for the intermediate support condition are smaller than for hard support. It is seen that the impact reaction forces are smaller with preload than without preload in case of the intermediate support condition. There is a favorable support stiffness in the HTGR core design. Furthermore, preload from the core periphety to the core center could reduces the impact reaction forces.

(5) The following are effects of connection keys on response. Differences of the impact reaction forces between cases with the keys and without the keys are small. The impact reaction forces with the keys are a little larger than without the keys. Moreover differences of the fuel block displacements between cases with the keys and without the keys are negligible.

10. Seismic Analysis Method for a Two-dimensional Horizontal HTGR Core

10.1 Introduction

A HTGR core consists of more than several thousand individual graphite blocks of various shapes. It wuold be most difficult, if not impossible, to construct a mathematical model of such a large array of core blocks installed in the configuration of three dimensions, where each block can have six degrees-of -freedom. A three-dimensional analysis of the dynamics of the large array of core blocks would be economically unfeasible with respect to computional cost. A two-dimensional analysis would, on the other hand, seem to be one of of the best ways if it can adequately describe the major dynamic characteristics of the three-dimensional core blocks.

Since the system of blocks such as the HTGR core is a very different structure from the usual ones, conventional theory to analyze the structure and experimental data can not be applied directly.

Muto et al.[30] proposed a two-dimensional analytical method of a horizontal slice model of a HTGR core using a rigid body to simplify the model and to save computer calculation time. The model used impulse momentum conservation laws. However, the column (piled up with blocks) characteristics such as the column rotation was not considered. Tow [23] developed an analytical method for this problem and a computer program using a simplified model.

The author has developed a numerical method for analyzing the dynamic behavior of the two-dimensional horiznotal slice HTGR core under seismic excitation. The method is relatively general, based on a two-dimensional model capable of handling a wide range of core blocks, core restraint structures and the core support structure coupled with uni-axial or bi-axial horizontal excitations. The HTGR core is modeled as a multiple mass system consisting of an entire horizontal section of the core at a single elevation.

10.2 Calculation equation

10.2.1 Analytical model

A HTGR core consists of several thousand hexagonal graphite blocks stacked in columns and separated by small gaps. The core blocks are surrounded by both replaceable reflector blocks with the same hexagonal cross section as the fuel blocks, and fixed side reflector blocks which are of varying shapes.

An one fuel block height of a horizontal layer of the experimental HTGR core is modeled as shown in Figs. 10.1 and 10.2. Impacts of blocks are modeled by using interblock springs and dashpots as shown in Fijs. 10.3 and 10.4.

The basic assumptions of this analytical model are:

(1) each block is modeled as a rigid body,

(2) each block has three degrees-of-freedom; two translational displacements and one rotation around block center axis,

(3) block forces are normal to the faces and friction or other moment producing loads are allowed,

(4) impact forces are represented by a spring and dashpot model located an impact points of each block,

(5) each block is connected to the core support block by means of column springs and dashpots,

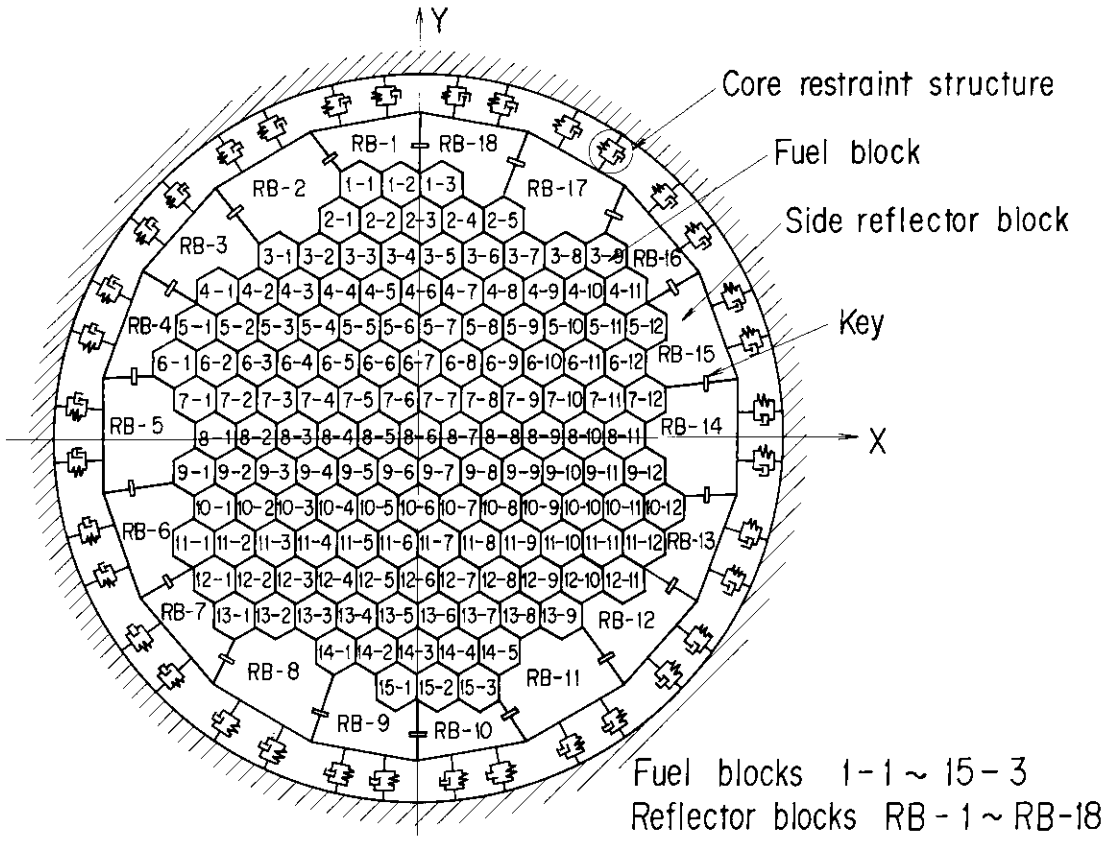

Fig. 10.1 Analytical model of two-dimensional horizontal core (I)

(6) each side reflector block is connected to a core outer structure (such as a core barrel, a reactor vessel or PCRV) by means of the core restraint springs and dashpots,

(7) the core support block is modeled as a single mass and has two degrees-of-freedom; two translational displacements, and

(8) the motion of the core outer structure is specified to be in two horizontal (translation) directions.

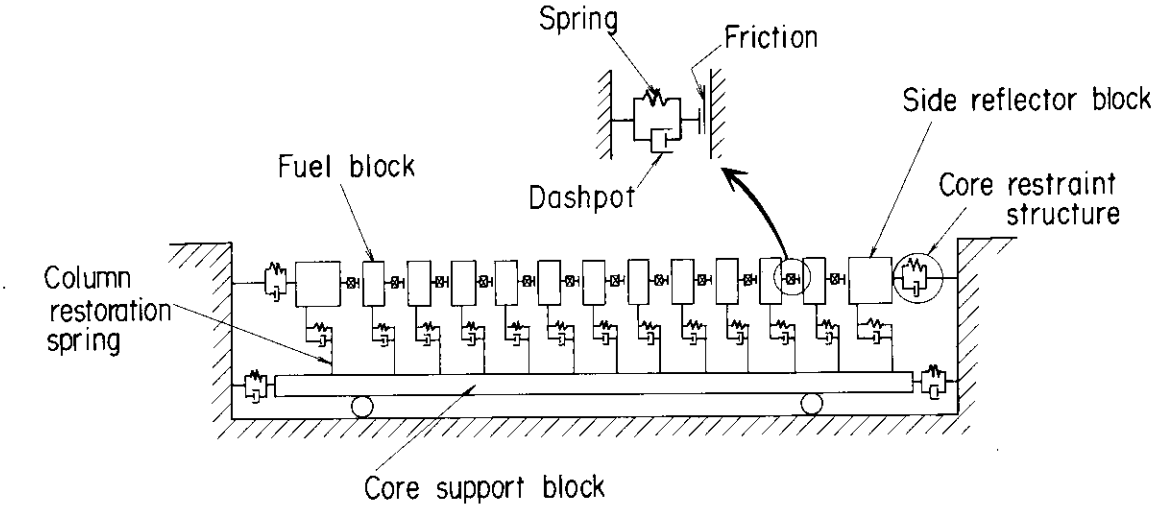

Fig. 10.2 Analytical model of two-dimensional horizontal core (II)

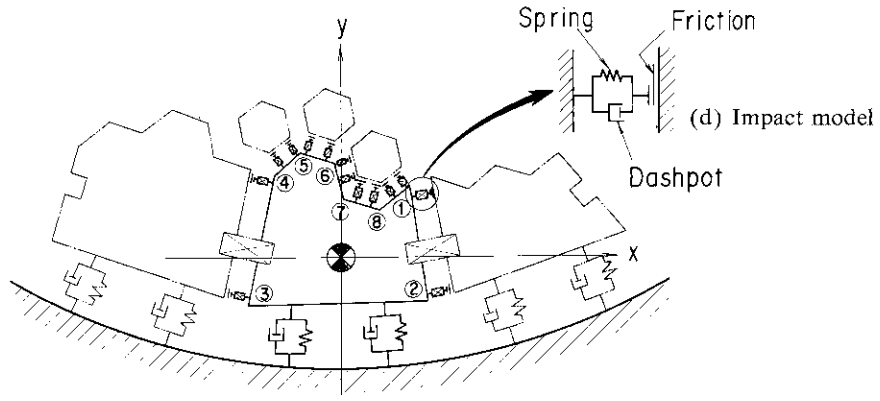

(a) Side block A

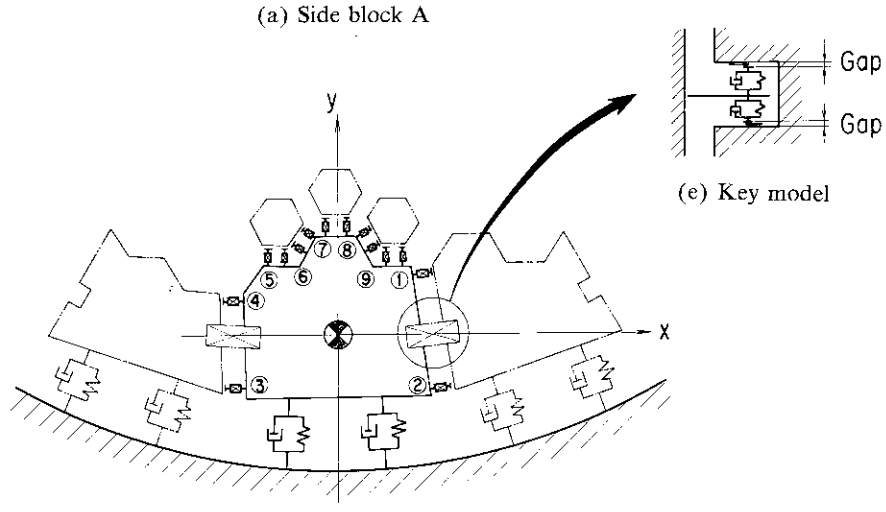

(b) Side block B

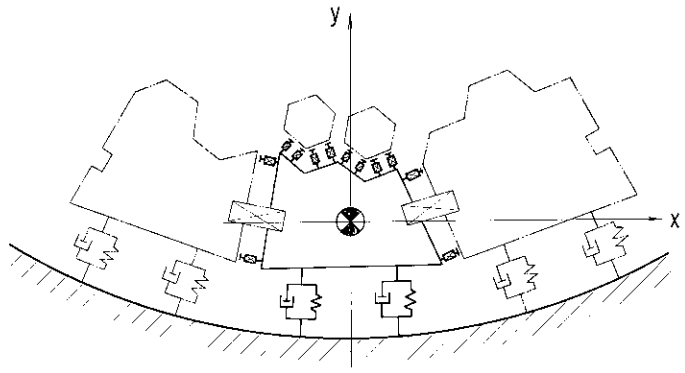

(c) Side block C

Fig. 10.3 Side reflector block model

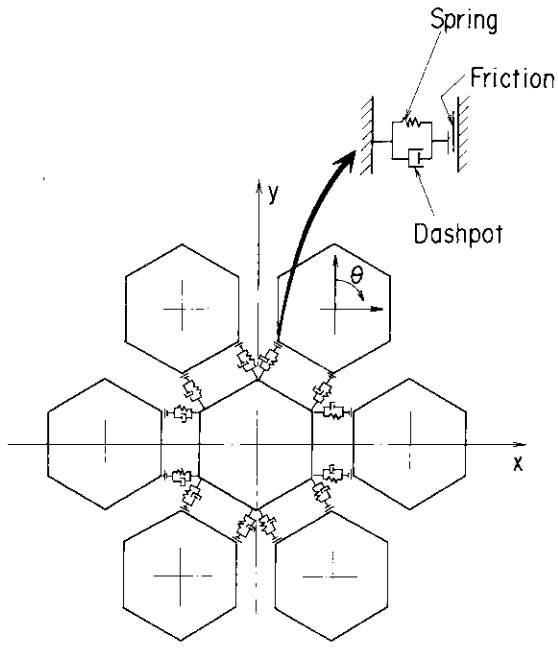

Fig. 10.4 Block arrangement and impact model

10.2.2 Representation of impact force

The impacts between blocks are modeled using the spring dashpot elements (alias a viscoelastic model) as shown in Fig. 10.5. At the instant of impact, when the gap between two blocks becomes zero or negative, the interblock spring and dashpot generate a force. The spring and damping forces are formulated as follows: The initial gap between two blocks (i. e. between the i-th and j-th biocks) is defined by parameter δ_{ij}, while the spring and damping forces are defined as function of relative displacement $x_i - x_j$, and relative velocity $\dot{x}_i - \dot{x}_j$ of the two impacting bodies,

Spring force F^S;

$$\left.\begin{aligned} F^S &= K_{ij}(x_i - x_j + \delta_{ij}), \quad if \mid x_i - x_j \mid \leqq \delta_{ij}, \\ &= 0, \qquad\qquad\quad if \mid x_i - x_j \mid > \delta_{ij}. \end{aligned}\right\} \tag{10.1}$$

Damping force F^D;

$$\left.\begin{aligned} F^D &= C_{ij}(\dot{x}_i - \dot{x}_j), \quad if \mid x_i - x_j \mid \delta_{ij}, \\ &= 0, \qquad\qquad if \mid x_i - x_j \mid > \delta_{ij}. \end{aligned}\right\} \tag{10.2}$$

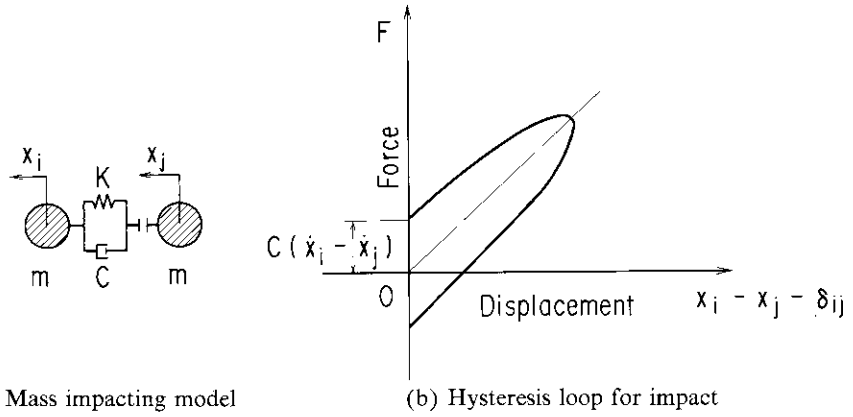

(a) Mass impacting model (b) Hysteresis loop for impact

Fig. 10.5 Viscoelastic model with two impacting bodies.

The impact force is then

$$F=F^S+F^D. \tag{10.3}$$

10.2.3 Global and local coordinate systems

One global coordinate system and three local coordinate systems are used for the convenience of the formulations. The coordinate systems of this analytical model are:

(1) global coordinate system with the origin (x, y) at the core center,

(2) local coordinate systems with the origin at the block center of gravity,

(a) initial coordinate system (x^L, y^L) ,

(b) coordinate system after displacement (x^Q, y^Q) , and

(3) local coordinate system for rotation (x^S, y^S) .

10.2.4 Equations of motion of fuel block

Let the coordinate system be chosen as shown in Fig. 10.6. The equations of motion for the n-th fuel block may be written as

$$\left.\begin{aligned} &m_n\ddot{x}_n+\sum_{i=1}^{6}\sum_{j=1}^{2}F_{nij}^{RX}+\sum_{i=1}^{6}F_{ni}^{SX}+F_n^{CX}=-m_n\ddot{x}_o\ , \\ &m_n\ddot{y}_n+\sum_{i=1}^{6}\sum_{j=1}^{2}F_{nij}^{RY}+\sum_{i=1}^{6}F_{ni}^{SY}+F_n^{CY}=-m_n\ddot{y}_o\ , \\ &I_n\ddot{\theta}_n+\sum_{i=1}^{6}\sum_{j=1}^{2}M_{nij}^{R}+\sum_{i=1}^{6}M_{ni}^{S}=0\ . \end{aligned}\right\} \tag{10.4}$$

10.2.5 Displacement and velocity of block

The displacements and velocities of the points on the surfaces of a hexagonal block and a fixed side reflector block are similar. Therefore, the case of the hexagonal block alone will be shown. As indicated in Fig. 10.7, when the center of gravity of the n-th block moves from O_2 to O_3 (displacement x_n, y_n) and the block rotates by an angle of θ_n, the surface point P of the n-th block in the global coordinate system is expressed by the following equations.

$$\left.\begin{aligned} x_{pn}^S&=x_n+y_{pn}^L\sin\theta_n-x_{pn}^L(1-\cos\theta_n)\ , \\ y_{pn}^S&=y_n-x_{pn}^L\sin\theta_n-y_{pn}^L(1-\cos\theta_n)\ . \end{aligned}\right\} \tag{10.5}$$

The velocity of the point P of the block is derived from equation (10.5) and expressed as follows

$$\left.\begin{aligned} \dot{x}_{pn}^S&=\dot{x}_n+(y_{pn}^L\cos\theta_n-x_{pn}^L\sin\theta_n)\dot{\theta}_n\ , \\ \dot{y}_{pn}^S&=\dot{y}_n-(x_{pn}^L\cos\theta_n+y_{pn}^L\sin\theta_n)\dot{\theta}_n\ . \end{aligned}\right\} \tag{10.6}$$

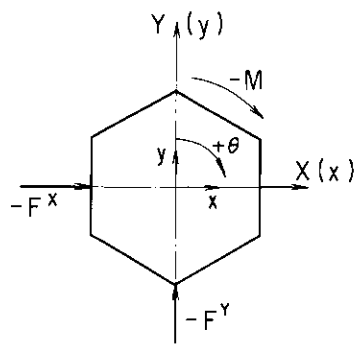

Fig. 10.6 Sign of displacement, force and moment

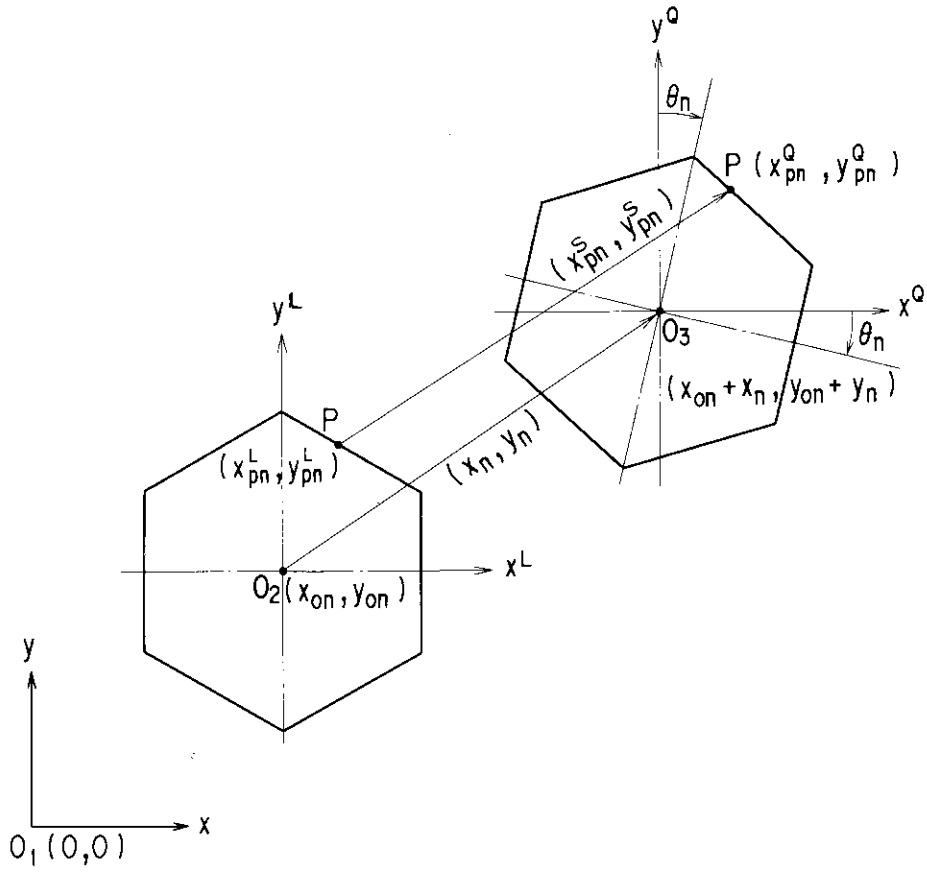

Fig. 10.7 Block displacement

The coordinates of the point P are expressed by the equations below

$$\left.\begin{aligned} x^{Q}_{npn} &= x^{S}_{pn} + x^{L}_{pn} - x_n \,, \\ y^{Q}_{npn} &= y^{S}_{pn} - y^{L}_{pn} - y_n \,. \end{aligned}\right\} \tag{10.7}$$

Substituting equation (10.5) into equation (10.7)

$$\left.\begin{aligned} x^{Q}_{npn} &= y^{L}_{pn}\sin\theta_n + x^{L}_{pn}\cos\theta_n \,, \\ y^{Q}_{npn} &= -x^{L}_{pn}\sin\theta_n + y^{L}_{pn}\cos\theta \,. \end{aligned}\right\} \tag{10.8}$$

The coordinates of the point P in the rotated local coordinate system can be expressed by the global coordinate system. Solving equation (10.8) for the coordinates (x^{L}_{pn}, y^{L}_{pn})

$$\left.\begin{aligned} x^{L}_{pn} &= x^{Q}_{npn}\cos\theta_n - y^{Q}_{npn}\sin\theta_n \,, \\ y^{L}_{pn} &= x^{Q}_{npn}\sin\theta_n + y^{Q}_{npn}\cos\theta_n \,, \end{aligned}\right\} \tag{10.9}$$

or

$$\left.\begin{aligned} x^{L}_{pn} &= x^{L}_{pno}\cos\theta_n - y^{L}_{pno}\sin\theta_n - x_n\cos\theta_n + y_n\sin\theta_n \,, \\ y^{L}_{pn} &= x^{L}_{pno}\sin\theta_n + y^{L}_{pno}\cos\theta_n - x_n\sin\theta_n - y_n\cos\theta_n \,, \end{aligned}\right\} \tag{10.10}$$

where

$$\left.\begin{aligned} x^{Q}_{npn} &= x^{L}_{pno} - x_n \,, \\ y^{Q}_{npn} &= y^{L}_{pno} - y_n \,. \end{aligned}\right\} \tag{10.11}$$

10.2.6 Gap between blocks

The calculations of the gap between hexagonal blocks, an hexagonal and a side reflector block, and side reflector blocks are carried out in a similar way. We will show only the calculation method for the gap between hexagonal blocks. The gap between a corner ①of the n-th block and the side ④–⑤ of the i-th block is shown in Fig. 10.8.

(1) Displacement coordinates of corners ① and ② of the n-th block

The coordinates of corners ① and ② of the displaced n-th block are expressed by the following equations.

(a) For the corner ①

$$\left.\begin{aligned} x^{Q}_{n1n} &= x^{L}_{1n} + x^{S}_{1n} - x_n \,, \\ x^{Q}_{n1n} &= y^{L}_{1n} + y^{S}_{1n} - y_n \,. \end{aligned}\right\} \tag{10.12}$$

(b) For the corner ②

$$\left.\begin{aligned} x^{Q}_{n2n} &= x^{L}_{2n} + x^{S}_{2n} - x_n \,, \\ y^{Q}_{n2n} &= y^{L}_{2n} + y^{S}_{2n} - y_n \,. \end{aligned}\right\} \tag{10.13}$$

(2) Displacement coordinates of corners ④ and ⑤ of the i-th block

The coordinates of corners ④ and ⑤ of the displaced i-th block are expressed by the following equations.

(a) For the corner ④

$$\left.\begin{aligned} x^{Q}_{i4n} &= x^{L}_{4i} + x^{S}_{4i} - x_n + (x_{oi} - x_{on}) \,, \\ y^{Q}_{i4n} &= y^{L}_{4i} + y^{S}_{4i} - y_n - (y_{oi} - y_{on}) \,. \end{aligned}\right\} \tag{10.14}$$

(b) For the corner ⑤

$$\left.\begin{aligned} x^{Q}_{i5n} &= x^{L}_{5i} + x^{S}_{5i} - x_n + (x_{oi} - x_{on}) \,, \\ y^{Q}_{i5n} &= y^{L}_{5i} + y^{S}_{5i} - y_n + (y_{oi} - y_{on}) \,. \end{aligned}\right\} \tag{10.15}$$

(c) Equation of the straight line of the side ①–② of the n-th block

Equation of the straight line of the side ①–② of the n-th block is the following.

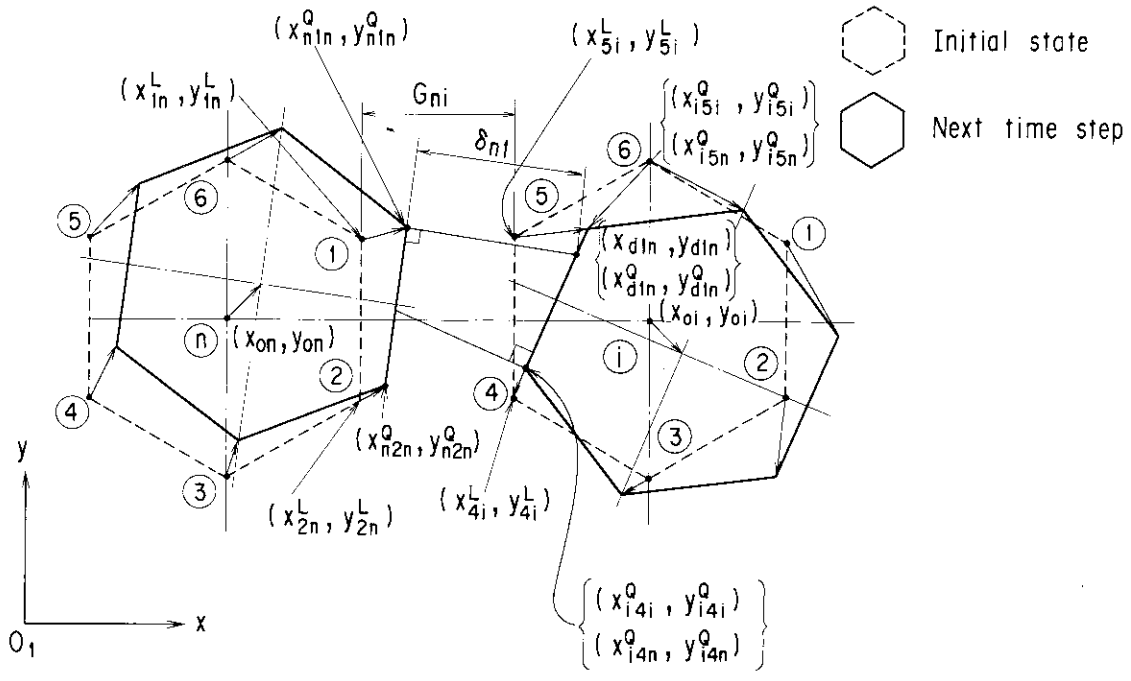

Fig. 10.8 Gap between blocks

$$y=a_1x+b_1\ , \tag{10.16}$$

where

$$a_1=\frac{A_2}{A_4}\ ,$$

$$b_1=y^Q_{n1n}-x^Q_{n1n}\frac{A_2}{A_4}\ ,$$

$$\left.\begin{aligned} A_1&=x^Q_{i4n}-x^Q_{i5n}\ ,\\ A_2&=y^Q_{n1n}-y^Q_{n2n}\ ,\\ A_3&=y^Q_{i4n}-y^Q_{i5n}\ ,\\ A_4&=x^Q_{n1n}-x^Q_{n2n}\ . \end{aligned}\right\} \tag{10.17}$$

(d) Equation of the straight line of the side ④–⑤ of the i–th block

$$y=a_2x+b_2\ , \tag{10.18}$$

whrer

$$a_2=\frac{A_3}{A1}\ ,$$

$$b_2=y^Q_{i4n}-x^Q_{i4n}\frac{A_3}{A_1}\ .$$

(e) Coordinates of block impact point

The coordinates of the point of intersection between a straight line passing through the corner ① of the n–th block and perpendicular to the side ①–② and the side ④–⑤ of the i–th block are give by the following.

Assuming that the side ①–② of the n–th block intersects the side ④–⑤ of the i–th block at a 90° angle, the condition under which a straight line passing through the corner ① of the n–th block and perpendicular to the side ①–② does not intersect the side ④–⑤ of the i–th block, i. e. , the corner ① of the n–th block does not impact the side ④–⑤ of the i–th block, is expressed by the equations below.

$$\left.\begin{aligned} &\text{i)}\ A_4\neq0,\ A_2\neq0 \text{ and } -\frac{A_4}{A_2}=\frac{A_3}{A_1}\ ,\\ &\text{ii)}\ A_4\neq0,\ A_2=0 \text{ and } A_1=0\ ,\\ &\text{iii)}\ A_4=0,\ A_2\neq0,\ A_1\neq0 \text{ and } A_3=0\ , \end{aligned}\right\} \tag{10.19}$$

where, A_1, A_2, A_3 and A_4 are given in equation (10.17).

(f) Impact point coordinates under conditions $A_4\neq0$ and $A_2\neq0$

i) Equation of the straight line of the side ①–② passing through the corner ①

The equation of a straight line passing through the corner ① of the n–th block and perpendicular to the side ①–②, which passes through the coordinates of the corner ① at a slope a_3, is given as follows.

$$y=a_3x+b_3\ , \tag{10.20}$$

where

$$a_3=\frac{A_4}{A_2}\ ,$$

$$b_3=y^Q_{n1n}+x^Q_{n1n}\frac{A_4}{A_2}\ .$$

ii) Coordinates of intersection point

The coordinates of the intersection point $(d^Q_{d1n},\ y^Q_{d1n})$ between the n–th block and the i–th block are obtained from equations (10.18) and (10.20).

ii-a) If $A_1 \neq 0$

$$\left.\begin{aligned} x^Q_{d1n} &= \left(-b_3 + y^Q_{i4n} - x^Q_{i4n}\frac{A_3}{A1_1} \right) \Big/ \left(a_3 - \frac{A_3}{A_1} \right), \\ y^Q_{d1n} &= (a_3 x^Q_{d1n} + b_3) . \end{aligned}\right\} \tag{10.21}$$

ii-b) If $A_1 = 0$

$$\left.\begin{aligned} x^Q_{d1n} &= x^Q_{i4n} , \\ y^Q_{d1n} &= a_3 x^Q_{i4n} + b_3 . \end{aligned}\right\} \tag{10.22}$$

(g) Impact point coordinates under the conditions $A_4 \neq 0$ and $A_2 = 0$

i) Equation of the straight line passing through the corner ① of the n-th block at right angle to the side ①-②.

Since the straight line of the side ①-② is parallel to the x axis, a straight line perpendicular to the straight line is given by the equation below.

$$X = x^Q_{n1n} . \tag{10.23}$$

ii) Coordinates of intersection point

The coordinates of the intersection point is obtained from equations (10.20), (10.21) and (10.22).

ii-a) If $A_1 \neq 0$

$$\left.\begin{aligned} x^Q_{d1n} &= x^Q_{n1n} , \\ y^Q_{d1n} &= \frac{A_3}{A_1} x^Q_{d1n} + \left\{ y^Q_{i4n} - x^Q_{i4n}\frac{A_3}{A_1} \right\} . \end{aligned}\right\} \tag{10.24}$$

ii-b) If $A_1 = 0$, there is no intersection under the condition ii) of dquation (10.19).

(h) Impact point coordinates under the conditions $A_4 = 0$ and $A_2 \neq 0$

i) Equation of the straight line passing through the corner ① of the n-th block at right angles to the side ①-②.

Since the straigt line of the side ①-② is parallel to the y axis, a straight line perpendicular to the straight line is given by the equation below.

$$y = y^Q_{n1n} . \tag{10.25}$$

ii) Coordinates of intersection point

The coordinates of the intersection point are obtained from equations (10.18) and (10.25).

ii-a) If $A_1 \neq 0$ and $A_3 \neq 0$

$$\left.\begin{aligned} x^Q_{d1n} &= \frac{A_1}{A_3}\left\{ y^Q_{d1n} - y^Q_{i4n} + x^Q_{i4n}\frac{A_3}{A_1} \right\} , \\ y^Q_{d1n} &= y^Q_{n1n} . \end{aligned}\right\} \tag{10.26}$$

ii-b) If $A = 0$

$$\left.\begin{aligned} x^Q_{d1n} &= x^Q_{i4n} , \\ y^Q_{d1n} &= y^Q_{i4n} . \end{aligned}\right\} \tag{10.27}$$

(i) Gap between the corner ① of the n-th block and the side ④-⑤ of the i-th block

The gap between the corner ① of the n-th block and the side ④-⑤ of the i-th block is given as follows.

$$\delta_{n1} = \{ (x^Q_{n1n} - x^Q_{d1n})^2 + (y^Q_{n1n} - y^Q_{d1n})^2 \}^{1/2} . \tag{10.28}$$

10.2.7 Judgment of impact between blocks

(1) Judgment of impact from geometrical arrangement of blocks

The judgment on the possibility of block impact is made by whether a corner of the block is facing a side of the adjacent block, or a straight line perpendicular to the side having a corner of the block intersects the side of its adjacent block. The condition under which this intersection does not exist is that, by reference to Fig. 10.9, there is no inersection between a corner ① of the n-th block and the side ④-⑤ of the i-th block, which is expressed by equations (10.17) and (10.19) . Under other conditions than the above, there is a possibility of block impact.

(2) Judgment of hexagonal block impact

When the conditions below are satisfied, block impact will occur.

(a) A corner ① of the n-th block is in between the side ④-⑤ of the i-th block (see Fig. 10.8)

$$\left.\begin{aligned}(x^Q_{d1n}-x^Q_{i4n})(x^Q_{d1n}-x^Q_{i5n})<0,\\(y^Q_{d1n}-y^Q_{i4n})(y^Q_{d1n}-y^Q_{i5n})<0.\end{aligned}\right\} \tag{10.29}$$

(b) The position of the intersection described above is within the hexagonal contours of the impacting n-th block (see Fig. 10.9),

$$R_2 \leqq R_1 .$$

where

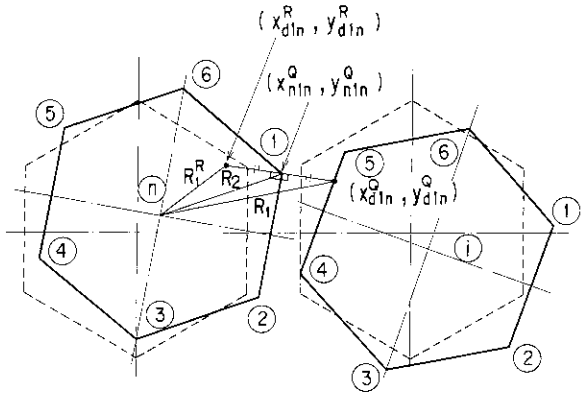

Fig. 10.9 Block impact

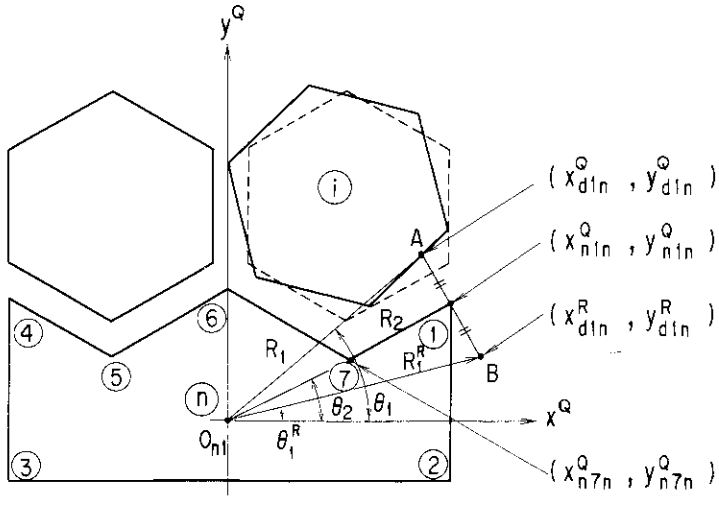

Fig. 10.10 Impact between hexagonal block and side reflector block

$$\left.\begin{aligned} R_1 &= \{(x_{d1n}^Q)^2+(y_{d1n}^Q)^2\}^{1/2}\ , \\ R_2 &= \{(x_{n1n}^Q)^2+(y_{n1n}^Q)^2\}^{1/2}\ . \end{aligned}\right\} \tag{10.30}$$

(3) Judgment of side reflector block impact

Additional judgment rules of block impact are applied as illustrated in Fig. 10.10. In the figure, the side ①–⑦ of the impact corner ① of the n–th block is on the line of passing point O_{n1} and if the following condition holds, impact occurs between blocks.

$$y_{n1n}^Q x_{n7n}^Q - x_{n1n}^Q y_{n7n}^Q = 0\ . \tag{10.31}$$

If it is not determined to judge impact under the condition as defined by the above equation, the following judgment rule is required for impact occurrence.

(a) Straight line of the side ①–⑦ of the n–th block

$$y = ax + b\ , \tag{10.32}$$

where

$$a = \frac{y_{n1n}^Q}{x_{n1n}^Q}\ ,$$

$$b = 0\ .$$

(b) Distance between the center of gravity and the corner ① of the n–th side reflector block is represented in equation (10.30).

(c) Judgment rule for impact is as follows.

$$\left.\begin{aligned} |\theta_1| &= \tan^{-1}\left|\frac{y_{d1n}^Q}{x_{d1n}^Q}\right|\ , \\ |\theta_2| &= \tan^{-1}\left|\frac{y_{n1n}^Q}{x_{n1n}^Q}\right|\ , \\ |\theta_1^R| &= \tan^{-1}\left|\frac{y_{d1n}^R}{x_{d1n}^R}\right|\ . \end{aligned}\right\} \tag{10.33}$$

i) If no–impact occurs between the n–th side reflector block and the i–th hexagonal block, the following equation exists.

$$\left|\frac{y_{n1n}^Q}{x_{n1n}^Q}\right| < \left|\frac{y_{d1n}^R}{x_{d1n}^R}\right| \quad \text{or} \quad |\theta_2| < |\theta_1^R|\ . \tag{10.34}$$

ii) If impact occurs between the n–th side reflector block and the i–th hexagonal block, the following equation exists.

$$\left|\frac{y_{n1n}^Q}{x_{n1n}^Q}\right| \geqq \left|\frac{y_{d1n}^R}{x_{d1n}^R}\right| \quad \text{or} \quad |\theta_2| \geqq |\theta_1^R|\ . \tag{10.35}$$

10.2.8 Impact forces and their associated moments of fuel blocks

(1) Inclination angle of impacting blocks

The inclination angle θ_{ln} at the corner of the n–th block in Fig. 10.11 i obtained. If the coordinates of the corner ⓘ of the block and of the corner (i+1) after the displacement of the block are (x_i^Q, y_i^Q) and (x_{i+1}^Q, y_{i+1}^Q) respectively, the equation of the straight line ⓘ – (i+1) becomes as follows.

(a) *If* $x_i^Q - x_{i+1}^Q \neq 0$

$$y = a_i x + b_i\ , \tag{10.36}$$

where

$$a_i = \frac{y_i^Q - y_{i+1}^Q}{x_i^Q - x_{i+1}^Q}\ ; \quad (i \neq 6)\ ,$$

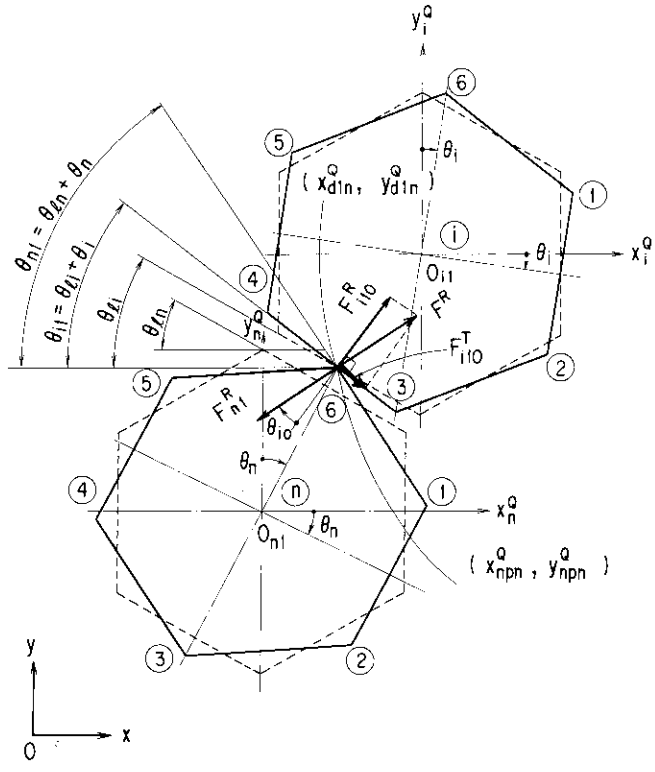

Fig. 10.11 Impact force components

$$a_6=\frac{y_1^Q-y_6^Q}{x_1^Q-x_6^Q} \quad ; \quad (i=6).$$

(b) *If* $x_i^Q-x_{i-1}^Q=0$

$$x=x_i^Q. \tag{10.37}$$

The inclination angle $\theta_{\ell n}$ is as follows.

(a) *If* $x_i^Q-x_{i-1}^Q\neq 0$

$$\theta_{\ell n}=\tan^{-1}a_i\,. \tag{10.38}$$

(b) *If* $x_i^Q-x_{i+1}^Q=0$

$$\left.\begin{aligned}\theta_{\ell n}&=-\frac{\pi}{2}\;;\;(y_i^Q-y_{i+1}^Q>0)\,,\\ \theta_{\ell n}&=\frac{\pi}{2}\;;\;(y_i^Q-y_{i+1}^Q<0)\,.\end{aligned}\right\} \tag{10.39}$$

(2) Relative velocity between impacting blocks

The velocity components, v_x and v_y, in the direction perpendicular to the impacting side having the impacting corner of the n-th block (the side ⑥-① of the n-th block in Fig. 10.11) are given by the following equations.

(a) velocity vector generated by x-direction velocity

$$\left.\begin{aligned}v_x&=|\dot{x}_p|\;|\sin(\theta_{\ell n}+\theta_n)|\;\frac{B}{|B|}\;;\;(y_1^Q-y_6^Q\neq 0)\,,\\ v_x&=0\;;\qquad\qquad\qquad\quad(y_1^Q-y_6^Q=0)\,.\end{aligned}\right\} \tag{10.40}$$

(b) velocity vector generated by y-direction velocity

$$\left.\begin{aligned} v_y &= |\dot{y}_p| \; |\cos(\theta_{\ell n}+\theta_n)| \; \frac{b}{|b|} \; ; \; (x_1^Q - x_6^Q \neq 0) \; , \\ v_y &= 0 \; ; \qquad\qquad\qquad\qquad (x_1^Q - x_6^Q = 0) \; , \end{aligned}\right\} \tag{10.41}$$

where

$$\dot{x}_p = \dot{x}_{pn} - \dot{x}_{pi} \; ,$$
$$\dot{y}_p = \dot{y}_{pn} - \dot{y}_{pi} \; ,$$
$$B = x_6^Q - y_6^Q \frac{x_1^Q - x_6^Q}{y_1^Q - y_6^Q} \; ,$$
$$b = y_6^Q - x_6^Q \frac{y_1^Q - y_6^Q}{x_1^Q - x_6^Q} \; .$$

The relative velocity in the direction perpendicular to the impacting side having the corner of the n-th block thus becomes tbe following.

$$v = v_x + v_y \; . \tag{10.42}$$

(3) Impact force of the n-th block

The impact force directed inward to the block is taken as positive. Impact force F_n^R of the n-th block is as follows.

$$F_n^R = F_n^S + F_n^D \; , \tag{10.43}$$

where

$$F_n^S = K_n^R \delta_{n1} \; ,$$
$$F_n^D = C_n^R v \; .$$

The judgment of block impact is carried out as in previous section 10.2.7, due to the viscoelastic model employed, it is necessary to consider also the following conditions.

$$\left.\begin{aligned} F_{n1}^R &\geqq 0; \text{ (impact case)} \; , \\ F_{n1}^R &= 0; \text{ (no-impact case)} \; . \end{aligned}\right\} \tag{10.44}$$

(4) Perpendicular and parallel forces to the impacting surface of the i-th block

As in Fig. 10.11 the force applied to the i-th block by the impact is divided into two components i. e. , the force F_{i10}^R in the direction perpendicular to the impacting surface and the force F_{i10}^T in the direction along the impacting surface, which are give by the equations below respectively.

$$\left.\begin{aligned} F_{i10}^R &= F_{n1}^R \cos\theta_{io} \; , \\ F_{i10}^T &= F_{n1}^R \sin\theta_{io} \; . \end{aligned}\right\} \tag{10.45}$$

where

$$\theta_{io} = \theta_{n1} - \theta_{i1} \; ,$$
$$\theta_{i1} = \theta_{li} + \theta_i \; ,$$
$$\theta_{n1} = \theta_{ln} + \theta_n \; .$$

(5) Parallel force to the impacting surface and friction force

The friction force F_{i10}^F of the impacting surface of the i-th block is

$$F_{i10}^F = \mu F_{i10}^R \; . \tag{10.46}$$

Where μ is the coefficient of static friction. The force F_{i10}^{TD}, parallel to the impacting surface, which exceeds the friction force F_{i10}^F, does not become larger than this friction force due to the slip. The following

conditions are, thus satisfied.

$$\left.\begin{aligned} F_{i10}^{TD}&=F_{i10}^{F}\ ;\ (\mid F_{i10}^{T}\mid \geqq F_{i10}^{F})\ ,\\ F_{i10}^{TD}&=F_{10}^{T}\ ;\ (\mid F_{i10}^{T}\mid < F_{i10}^{F})\ . \end{aligned}\right\} \tag{10.47}$$

The impact force of the n-th block, F_{ni}^{RD}, is modified as in the following,

$$F_{ni}^{RD}=F_{i10}^{R}\cos\theta_{io}+\mathrm{F}_{i10}^{TD}\sin\theta_{io}\ . \tag{10.48}$$

(6) x- and y-direction force components and their associated moments due to modified impact force

(a) impact force component in x- and y-direction for the n-th block

i) x-component force

$$\left.\begin{aligned} R_{ni}^{RX}&=F_{ni}^{RD}\mid \sin(\theta_{\ell n}+\theta_{n})\mid \frac{B}{\mid B\mid}\ ;\ (y_1^{Q}-y_6^{Q}\neq 0)\ ,\\ F_{ni}^{RX}&=0\ ;\qquad\qquad (y_1^{Q}-y_6^{Q}=0)\ . \end{aligned}\right\} \tag{10.49}$$

ii) y-component force

$$\left.\begin{aligned} F_{ni}^{RY}&=F_{ni}^{RD}\mid \cos(\theta_{\ell n}+\theta_{n})\mid \frac{b}{\mid b\mid}\ ;\ (x_1^{Q}-x_6^{Q}\neq 0)\ ,\\ F_{ni}^{RY}&=0\ ;\qquad\qquad (x_1^{Q}-x_6^{Q}=0)\ . \end{aligned}\right\} \tag{10.50}$$

(b) Moment around the n-th block center of gravity for the n-th block

$$M_{ni}^{R}=-x_{npn}^{Q}F_{ni}^{RY}+y_{npn}^{Q}F_{ni}^{RX}\ . \tag{10.51}$$

(c) x-and y-direction force component due to the modified impact force

F_{ni}^{RD} for the i-th block

i) x-component force

$$\left.\begin{aligned} F_{i10}^{RX}&=F_{ni}^{RD}\mid \sin(\theta_{io}+\theta_{i1})\mid \frac{B}{\mid B\mid}\ ;\ (y_3^{Q}-y_4^{Q}\neq 0)\ ,\\ F_{i10}^{RX}&=0\ ;\qquad\qquad (y_3^{Q}-y_4^{Q}=0)\ . \end{aligned}\right\} \tag{10.52}$$

ii) y-component force

$$\left.\begin{aligned} F_{i10}^{RY}&=F_{ni}^{RD}\mid \cos(\theta_{io}+\theta_{i1})\mid \frac{b}{\mid b\mid}\ ;\ (x_3^{Q}-x_4^{Q}\neq 0)\ ,\\ F_{i10}^{RY}&=0\ ;\qquad\qquad (x_3^{Q}-x_4^{Q}=0)\ . \end{aligned}\right\} \tag{10.53}$$

(d) Moment due to the modified impact force for the i-th block

$$M_{i10}^{R}=-x_{ipi}^{Q}F_{i10}^{RY}+y_{ipi}^{Q}F_{i10}^{RX}\ . \tag{10.54}$$

10.2.9 Restoring forces of fuel block

Restoring forces of the n-th fuel block are given by

$$\left.\begin{aligned} F_{n}^{CX}&=K_{n}^{CX}x_{n}^{Q}+C_{n}^{CX}\dot{x}_{n}\ ,\\ F_{n}^{CY}&=K_{n}^{CY}y_{n}^{Q}+C_{n}^{CY}\dot{y}_{n}\ . \end{aligned}\right\} \tag{10.55}$$

10.2.10 Restraint forces of side reflector blocks and their associated moment

Restraint forces of the side reflector blocks are written as

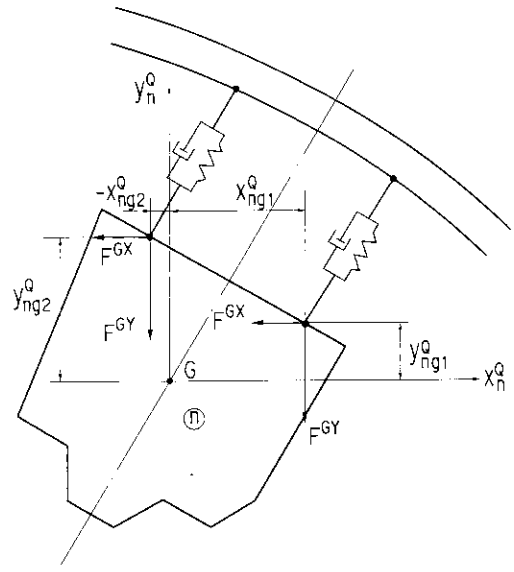

Fig. 10.12 Restraint forces of side reflector block

$$\left.\begin{aligned} F_n^{GX} &= K_n^{GX} x_n^Q + C_n^{GX} \dot{x}_n \,, \\ F_n^{GY} &= K_n^{GY} y_n^Q + C_n^{GY} \dot{y}_n \,. \end{aligned}\right\} \tag{10.56}$$

Moment M_n acting the n–th side reflector block caused by restraint forces is written as follows.

$$M_n^G = F_n^{GX}(y_{ng1}^Q + y_{ng2}^Q) - F_n^{GY}(x_{ng1}^Q + x_{ng2}^Q) \,. \tag{10.57}$$

where, x_{ng1}^Q, x_{ng2}^Q, y_{ng1}^Q and y_{ng2}^Q are shown in Fig. 10.12.

10.2.11 Key reaction force between side reflector blocks

The formulation of the reaction force due to shearing force in the key installed between two adjacent blocks is as follows. To simplify, the friction force between the key and keyway is ignored. Setting the origin of the coordinate system of the n–th block after displacement of the block to the center of gravity, the coordinates of the key corner are as follows (see Fig. 10.13) .

$$\left.\begin{aligned} x_{n1n}^Q &= x_{n1n}^L + x_{n1n}^S - x_n \,, \\ y_{n1n}^Q &= y_{n1n}^L + y_{n1n}^S - y_n \,, \\ x_{n2n}^Q &= x_{n2n}^L - x_{n2n}^S - x_n \,, \\ y_{n2n}^Q &= y_{n2n}^L + y_{n2n}^S - y_n \,. \end{aligned}\right\} \tag{10.58}$$

(1) Corrdinates of key after its displacement

Setting the origin of the coordinate system of the n–th block after its displacement as the center of gravity of the keyway are as follows.

i) For the n–th block

$$\left.\begin{aligned} x_{knn}^Q &= x_{knn}^L + x_{knn}^S - x_n \,, \\ y_{knn}^Q &= y_{knn}^L + y_{knn}^S - y_n \,. \end{aligned}\right\} \tag{10.59}$$

ii) For the i–th block

$$\left.\begin{aligned} x_{kin}^Q &= x_{kii}^L + x_{kii}^S - x_n + (x_{oi} - x_{on}) \,, \\ y_{kin}^Q &= y_{kii}^L + y_{kii}^S - y_n + (y_{oi} - y_{on}) \,. \end{aligned}\right\} \tag{10.60}$$

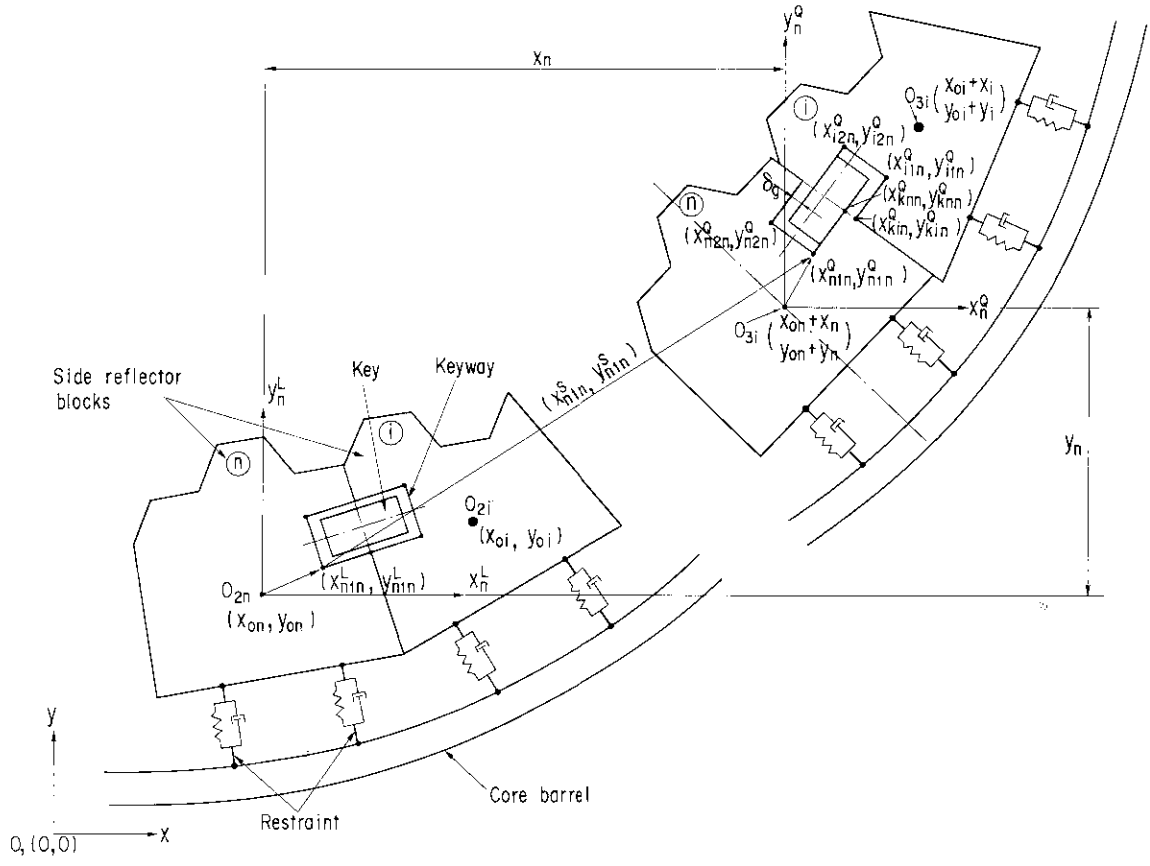

Fig. 10.13 Key and keyway displacements

(2) Inclination angles of side having the key

The inclination angles of the side having the key are as follows.

(a) For the n-th block

$$\left.\begin{aligned}\theta_{pn}&=\tan^{-1}\frac{y^Q_{n1n}-y^Q_{n2n}}{x^Q_{n1n}-x^Q_{n2n}}\ ;\ (x^Q_{n1n}-x^Q_{n2n}\neq 0)\ ,\\ \theta_{pn}&=\frac{\pi}{2}\ \frac{y^Q_{n1n}-y^Q_{n2n}}{|\ y^Q_{n1n}-y^Q_{n2n}\ |}\ ;\ (x^Q_{n1n}-x^Q_{n2n}=0)\ .\end{aligned}\right\}\tag{10.61}$$

(b) For the i-th block

$$\left.\begin{aligned}\theta_{pi}&=\tan^{-1}\frac{y^Q_{i1n}-y^Q_{i2n}}{x^Q_{i1n}-x_{i2n}}\ ;\ (x^Q_{i1n}-x^Q_{i2n}\neq 0)\ ,\\ \theta_{pi}&=\frac{\pi}{2}\ \frac{y^Q_{i1n}-y_{i2n}}{|\ y^Q_{i1n}-y^Q_{i2n}\ |}\ ;\ (x^Q_{i1n}-x^Q_{i2n}=0)\ .\end{aligned}\right\}\tag{10.62}$$

(3) x- and y-components of gap δ_{gx} and δ_{gy}

$$\left.\begin{aligned}\delta_{gx}&=\frac{\delta_g}{|\ \cos\theta_{pi}\ |}\ ,\\ \delta_{gy}&=\frac{\delta_g}{|\ \sin\theta_{pi}\ |}\ .\end{aligned}\right\}\tag{10.63}$$

where δ_g is gap between the key and the keyway.

(4) x- and y-components of spring constant K_n^{KX} and K_n^{KY}

$$\left.\begin{aligned}K_n^{KX}&=|\ K_n^K\cos\theta_{pn}\ |\ ,\\ K_n^{KY}&=|\ K_n^K\sin\theta_{pn}\ |\ .\end{aligned}\right\}\tag{10.64}$$

where K_n^K is spring constant of the key.

(5) x- and y-components of damping coefficient C_n^{KX} and C_n^{KY}

$$\left.\begin{aligned} C_n^{KX} &= \mid C_n^K \cos\theta_{pn} \mid , \\ C_n^{KY} &= \mid C_n^K \sin\theta_{pn} \mid . \end{aligned}\right\} \tag{10.65}$$

where C_n^K is damping coefficient of the key.

(6) x- and y-components of key reaction force F_n^{KX} and F_n^{KY}

(a) If $\mid x_{knn}^Q - x_{kin}^Q \mid \geq \delta_{gx}$

$$F_n^{KX} = \left\{ (x_{knn}^Q - x_{kin}^Q) - \frac{x_{knn}^Q - x_{kin}^Q}{\mid x_{knn}^Q - x_{kin}^Q \mid} \delta_{gx} \right\} K_n^{KX} + (v_{knx} - v_{kix}) C_n^{KX} . \tag{10.66}$$

(b) If $\mid y_{knn}^Q - y_{kin}^Q \mid \geq \delta_{gy}$,

$$F_n^{KY} = \left\{ (y_{knn}^Q - y_{kin}^Q) - \frac{y_{knn}^Q - y_{kin}^Q}{\mid y_{knn}^Q - y_{kin}^Q \mid} \delta_{gy} \right\} K_n^{KY} + (v_{kny} - v_{kiy}) C_n^{KY} . \tag{10.67}$$

(c) If $\mid x_{knn}^Q - x_{kin}^Q \mid < \delta_{gx}$

$$F_n^{KX} = 0 . \tag{10.68}$$

(d) If $\mid y_{knn}^Q - y_{kin}^Q \mid < \delta_{gy}$

$$F_n^{KY} = 0 . \tag{10.69}$$

(7) Key reaction forces

The shearing force in the key reaction is divided into two. One component is parallel to the side having the key, F_n^{KT}, and the other component is in the direction perpendicular to it, F_n^{KR}. These are given as follows.

$$\left.\begin{aligned} F_n^{KT} &= F_n^{KX} \cos\theta_{pn} + F_n^{KY} \sin\theta_{pn} , \\ F_n^{KR} &= -F_n^{KX} \sin\theta_{pn} + F_n^{KY} \cos\theta_{pn} . \end{aligned}\right\} \tag{10.70}$$

(8) Moment due to key reaction force

The moment around the center of gravity of the n-th side reflector block, due to the key reaction force, M_n^K is written as

$$M_n^K = F_n^{KX} y_{knn}^Q - F_n^{KY} X_{knn}^Q . \tag{10.71}$$

10.2.12 Equations of motion for side reflector block

The equations of motion for the n-th side reflector block may be written as

$$\left.\begin{aligned} &m_n \ddot{x}_n + \sum_{i=1}^{NCR} \sum_{j=1}^{2} F_{nij}^{RX} + \sum_{i=1}^{NCR} F_{ni}^{SX} + F_n^{CX} + \sum_{i=1}^{2} F_{ni}^{GX} + \sum_{i=1}^{2} F_{ni}^{KX} = -m_n \ddot{x}_o , \\ &m_n \ddot{y}_n + \sum_{i=1}^{NCR} \sum_{j=1}^{2} F_{nij}^{RY} + \sum_{i=1}^{NCR} F_{ni}^{SY} + F_n^{CY} + \sum_{i=1}^{2} F_{ni}^{GY} + \sum_{i=1}^{2} F_{ni}^{KY} = -m_n \ddot{y}_o , \\ &I_n \ddot{\theta}_n + \sum_{i=1}^{NCR} \sum_{j=1}^{2} M_{nij}^{R} + \sum_{i=1}^{NCR} M_{ni}^{S} + M_n^{C} + \sum_{i=1}^{2} M_{ni}^{G} + \sum_{i=1}^{2} M_{ni}^{K} = 0 . \end{aligned}\right\} \tag{10.72}$$

10.2.13 Equations of motion for core support block

The equations of motion of the core support block may be written as

$$\left.\begin{aligned} &m_b \ddot{x}_b - \sum_{i=1}^{NH} F_i^{CX} - \sum_{i=1}^{NR} F_i^{CX} + F_b^{GX} = -m_b \ddot{x}_o , \\ &m_b \ddot{y}_b - \sum_{i=1}^{NH} F_i^{CY} - \sum_{i=1}^{NR} F_i^{CY} + F_b^{GY} = -m_b \ddot{y}_o . \end{aligned}\right\} \tag{10.73}$$

10.2.14 Numerical integration method

A number of direct numerical integration methods have been considered for the calculation. Both implicit and explicit time integration methods and convergent characteristics as function of integration time step size and numerical stability have been investigated. The Runge-Kutta method was then selected for the calculation.

The integration time step used in the calculation should be large enough to reduce excessive computer run time but small enough to obtain an accurate convergent solution. In general, the recommended integration time step is based on the smaller value of 1/20 of the interblock contact time or 1/20 of the natural period of the highest natural frequency of the model. The numerical integration time step is automatically adjusted in the calculation.

10.3 Results and discussions

The governing equations given in section 10.2 can be numerically solved by using the Runge-Kutta integration schemes. The geometry data and mass of the blocks shown in Table 10.1 are chosen in such a way that the system corresponds to the experimental HTGR core with dimension scaled by 1/2 and weight scaled by 1/4. The computation time interval is 0.05 milli-seconds. The numerical results are compared with experimental ones. In the calculation the input acceleration wave is 4.1 Hz sinusoidal wave of maximum peak acceleration 250 Gal. The frequency 4.1 Hz was chosen because one of the maximum response values were observed during experiment under a sinusoidal excitation frequency of 4.1 Hz frequency.

10.3.1 Displacement response

Figure 10.14 shows the displacements of fuel blocks and side reflector blocks obtained under uni-axial sinusoidal excitation of 4.1 Hz and peak acceleration of 250 Gal. Fuel blocks move not in the X direction, same as excitation direction but also in the Y direction, perpendicular to the excitation direction. The displacement loci of fuel block centers have elliptic shapes. This phenomenon was observed by a seismic test illustrated in the previous section 5.3.

Figure 10.15 shows the comparison between analytical and exmerimental displacements of fuel blocks and side reflector blocks on the X-axis. The analytical results show a favorable correlation with the experimental ones.

Figure 10.16 shows the comparison between analytical and experimental displacements of fuel blocks and side reflector blocks on the Y-axis. In the figure, it can be seen that the analytical results are in good agreement with the experimental ones.

Table 10.1 Calculation data

Item		Unit	Fuel block	Fixed side reflector block			Core base plate
				Type A	Type B	Type C	
Mass		kg	19.1	97.2	115.5	142.8	—
Spring constant	Impact	kN/m	12400	12400			—
	support		4.71	7610			7610
Damping coefficient	Impact	kN • s/m	7.69	7.69			—
	Support		0.06	2.75	2.94	3.34	6.67
Spring constant of reflector key			kN/m	12400			
Damping coefficient of reflector key			kN • s/m	7.69			

(1 kN=102 kgf, 1 kN/m=1.02 kgf/cm)

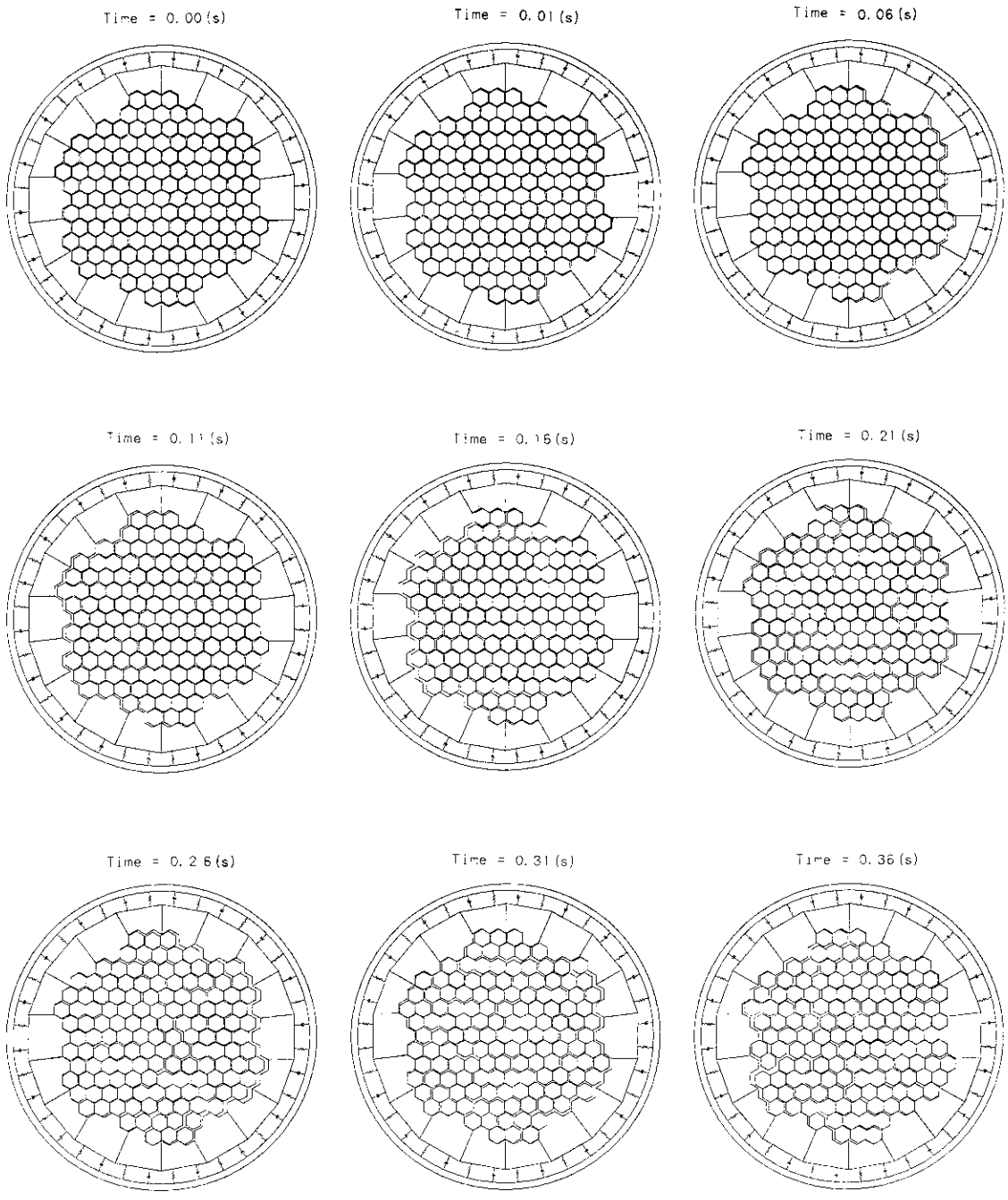

Fig. 10.14 Seismic behavior of two-dimensionai horizontal core model (Excitation X-direction, 4.1 Hz, Max. acceleration 250 Gal)

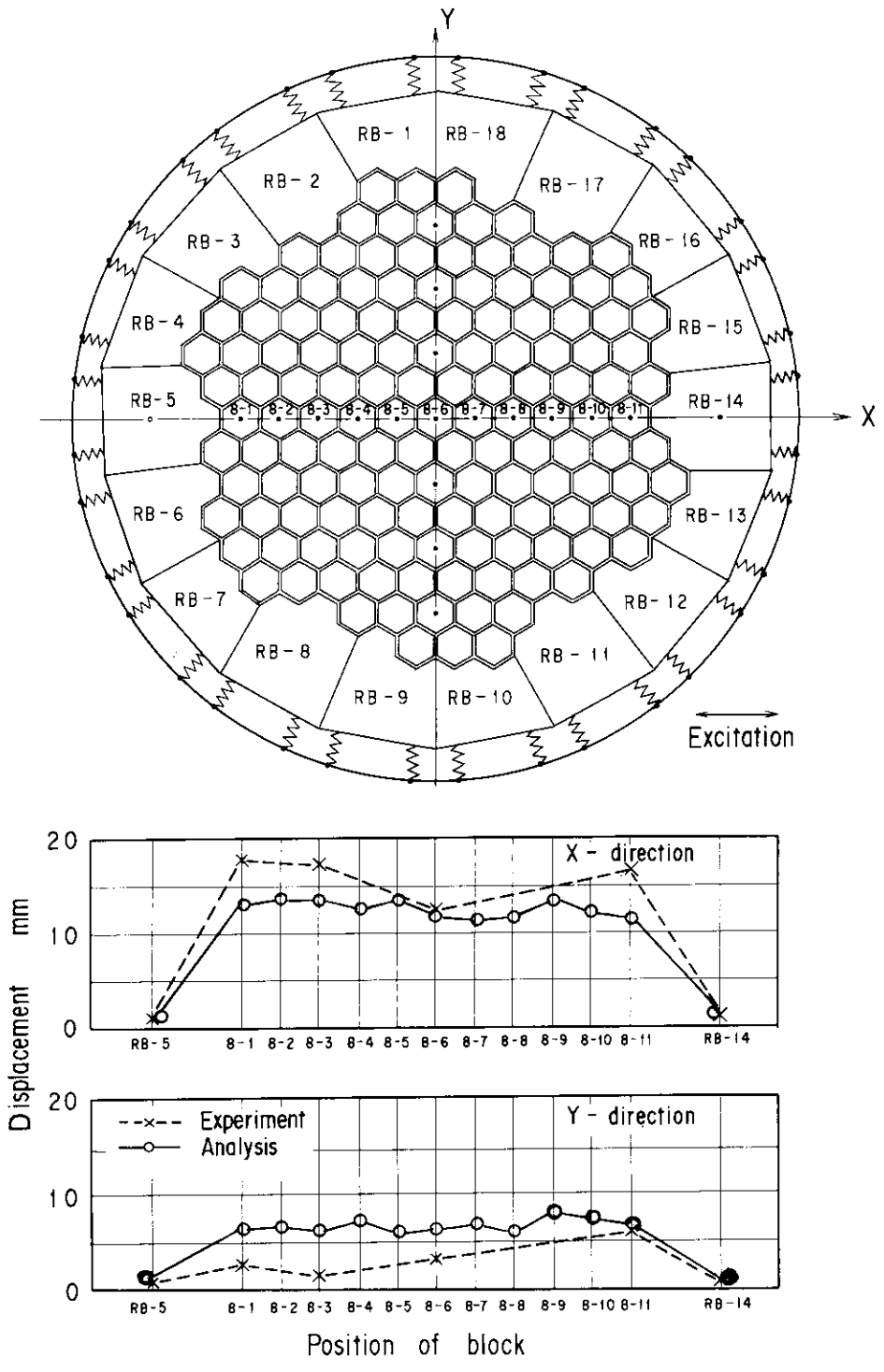

Fig. 10.15 Displacement of block on X–axis position
(Excitation X–direction, 4.1Hz, Max. acceleration 250 Gal)

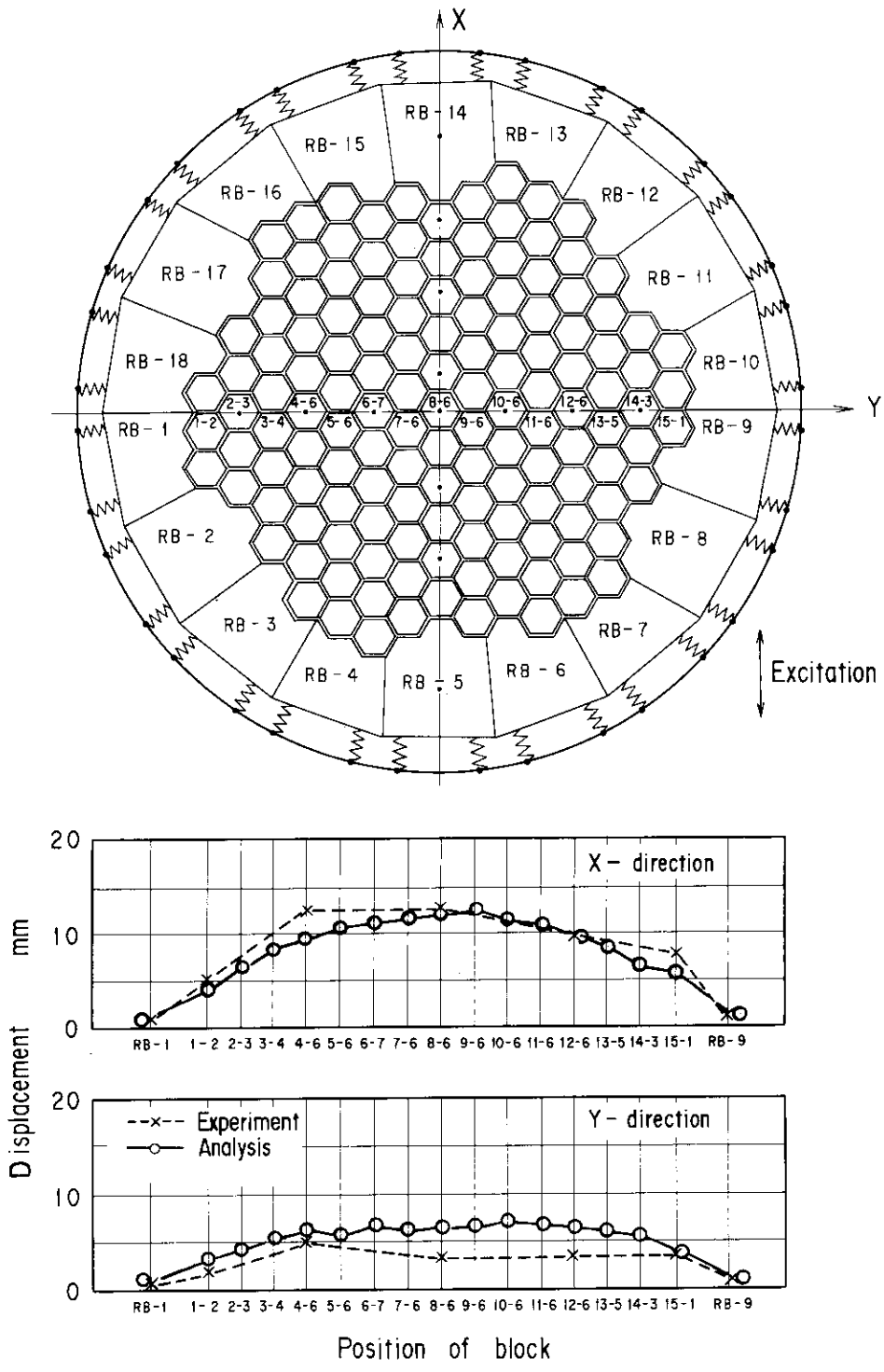

Fig. 10.16 Displacement of block on Y-axis position
(Excitation X-direction, 4.1Hz, Max. acceleration 250 Gal)

10.3.2 Impact acceleration response

Figure 10.17 shows the comparison between analysis and experiment of the accelerations of fuel blocks and side reflector blocks on the X-axis. The analytical results show a favorable correlation with the experimental ones.

Figure 10.18 shows the comparison between analysis and experiment of the impact accelerations of fuel blocks and side reflector biocks on the Y-axis. In the figure, it can be seen that the analytical results are in fairly good agreement with the experimental ones.

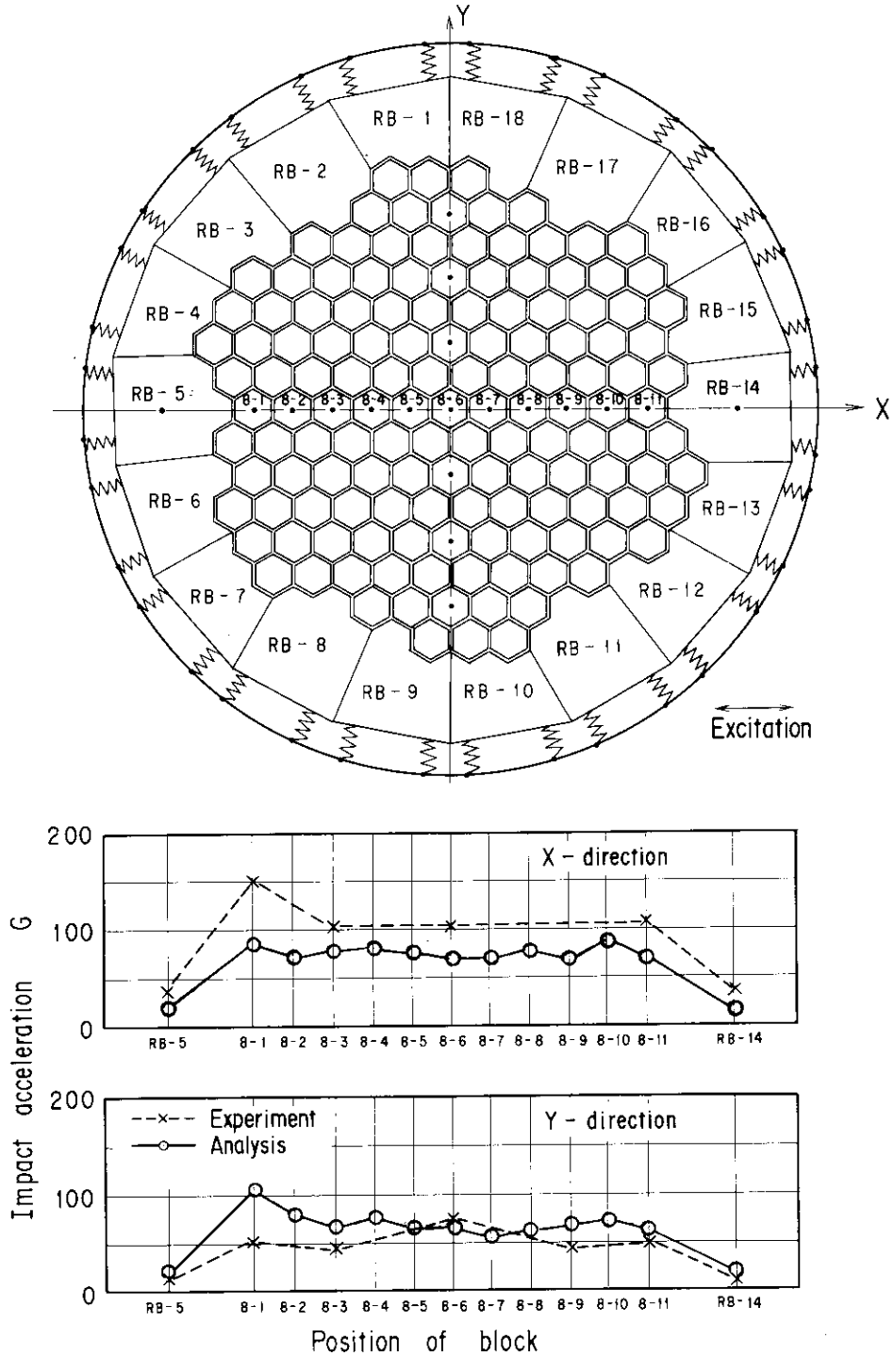

Fig. 10.17 Impact acceleration of block on X-axis position
(Excitation X-direction, 4.1Hz, Max. acceleration 250 Gal)

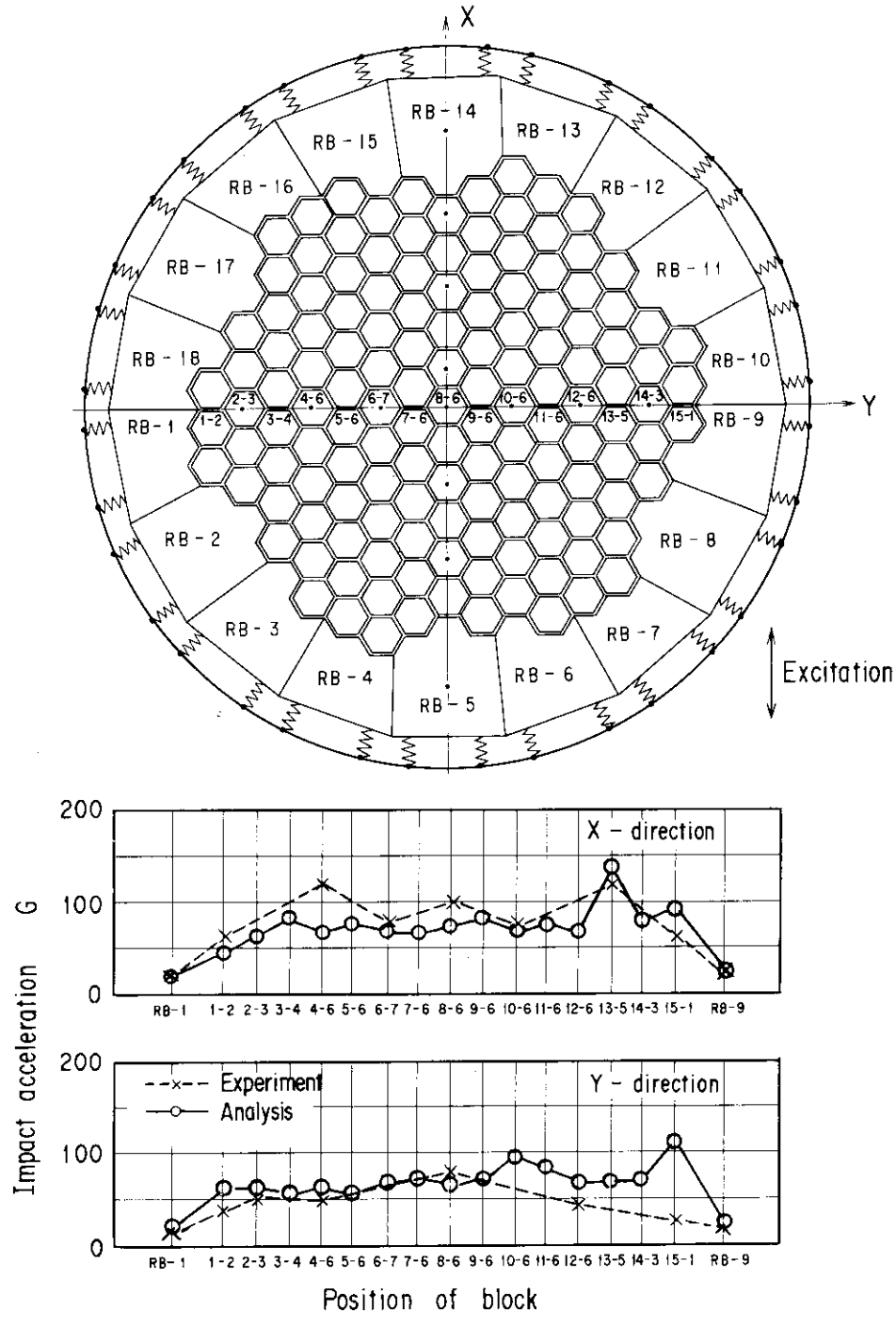

Fig. 10.18 Impact acceleration of block on Y-axis position
(Excitation X-direction, 4.1Hz Max. acceleration 250 Gal)

10.3.3 Impact reaction force response

Figure 10.19 shows the comparison between analysis and experiment of the impact reaction forces of side refiectors. In the figure, two kinds of reaction forces, namely radial and tangential, were shown. The analytical results show favorable correlation with the experimental ones.

10.3.4 Displacement characteristics

Figure 10.20 shows the displacements of analysis and experiment comparing the displacements at the core center and that of at the core periphery. The correlation is good for the displacements at the core center, but less satisfactory at tthe displacements at the core periphery.

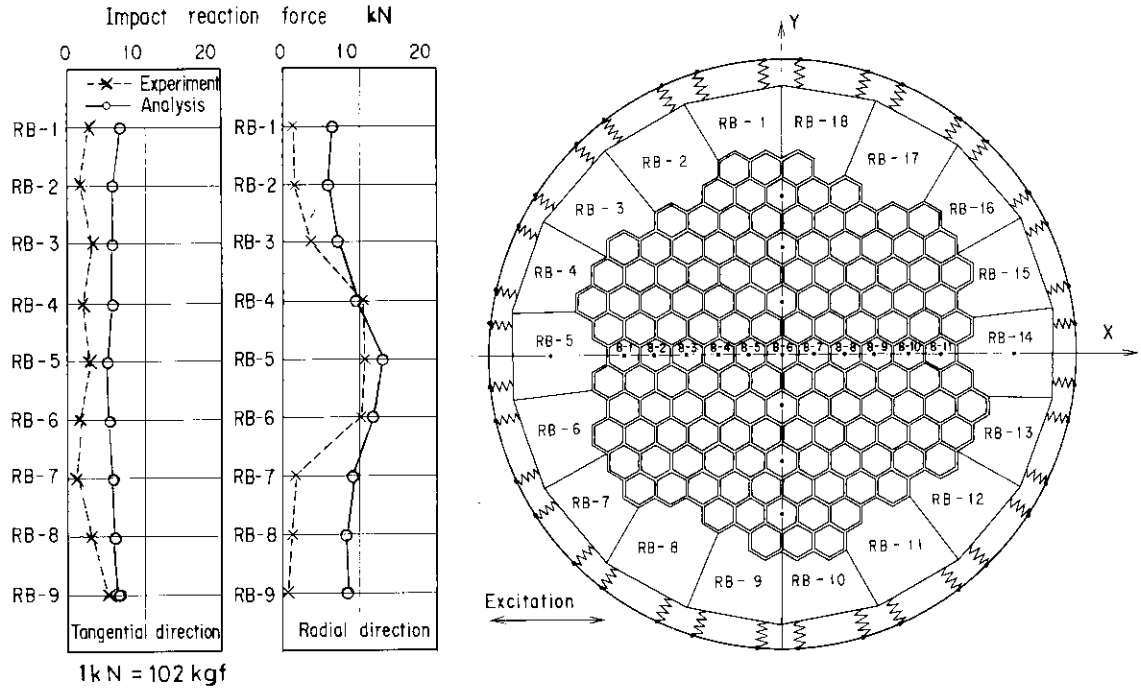

Fig. 10.19 Impact reaction force distribution of reflector block
(Excitation X-direction, 4.1Hz, Max. acceleration 250 Gal)

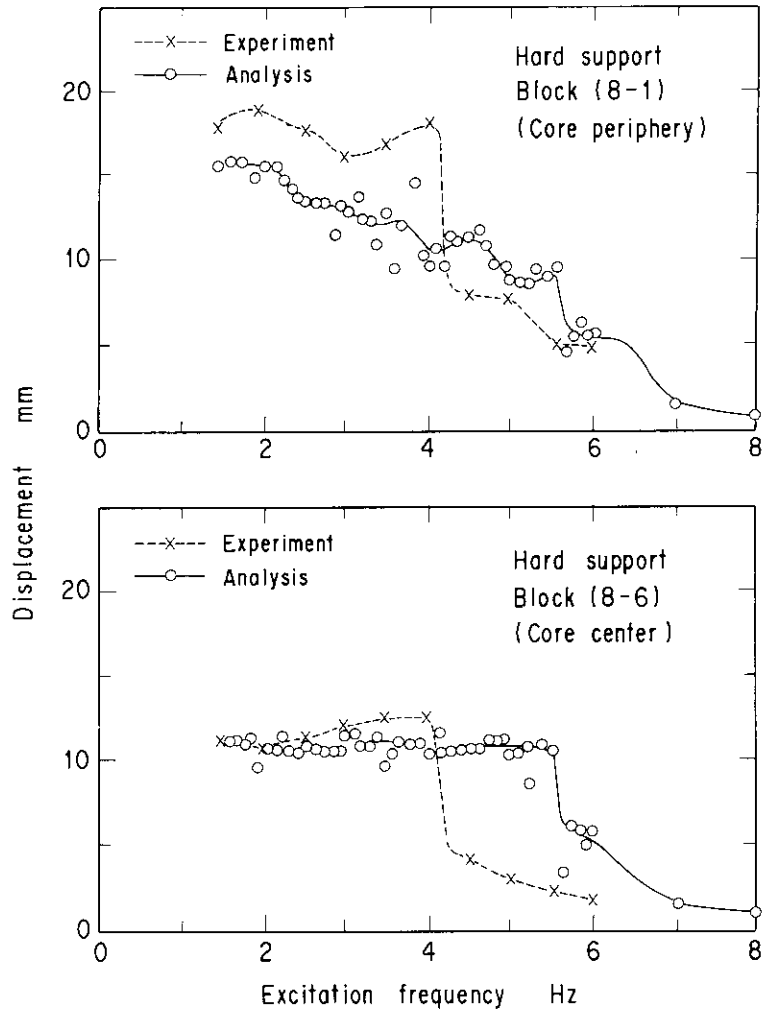

Fig. 10.20 Comparison between experiment and analysis on displacement
(Max. input acceleration 250 Gal)

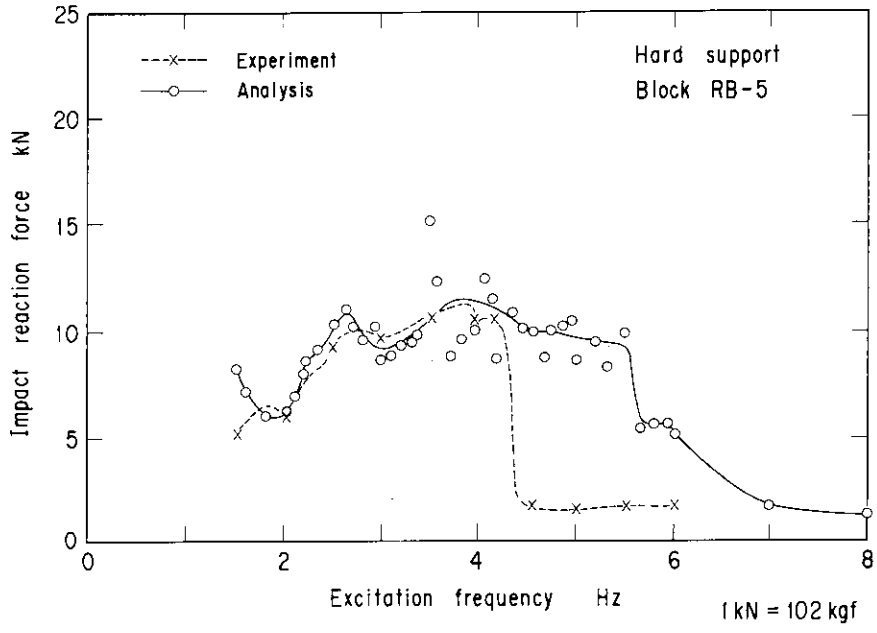

Fig. 10.21 Comparison between experiment and analysis on impact reaction force (Max. input acceleration 250 Gal)

10.3.5 Impact force characteristics

Figure 10.21 shows the impact reaction forces of analysis and experiment. As can be seen, the impact reaction forces can be fairly simulated by analysis.

10.4 Concluding remarks

A seismic analysis method for the two-dimensional slice HTGR core, which consits of block-type fuels, has been developed. The equations of motion for the core blocks used in the calculation and numerical results have been presented and were compared with the results obtained by experiments. The following conclusions have been derived:

(1) The analytical results were compared with experimental ones for horizontal vibration responses of the two-dimensional slice core model. Good agreement was obtained between analytical and experimental results.

(2) Using this method, impact forces of the fuel blocks and side reflector blocks, and support forces of side reflector blocks can be computed.

11. Estimation of a Real Core Response from Two-dimensional HTGR Core Response

11.1 Introduction

It is desirable to predict a real core dynamic behavior from experimental and analytical results of a two-dimensional vertical core model and a two dimensional horizontal core model.

This Chapter shows comparative studies of the two model experiments and analyses, to estimate the real core response under seismic excitation.

11.2 Displacement response characteristics

The displacement response curves in the vertical core and in the horizontal core are shown in Fig. 11.1. In the vertical core, the gaps between columns are 2 mm, and the total gap in the transverse direction is 26 mm. In the horizontal core, as indicated in Fig. 11.2, the total gap in the X-axis direction at the center is 24 mm. As seen in the displacement response curves of Fig. 11.1(a), at excitation frequencies below 5 Hz, the displacements exceed the total gap, so the vertical columns are in lumped vibration. On the other hand, in the horizontal core, as seen in Fig. 11.1(b), the displacement characteristics are similar to that in the vertical core but the displacements are smaller. For this difference, two causes are possible. The first is a difference in restoring forces between the column and the block. The second is the so-called mutual interference effects.

The difference in restoring forces will first be considered. Restoring characteristics in the column of the vertical column and in the block of the horizontal column are shown in Fig. 11.3. In the column, at small displacements the restoring force increases linearly, but beyond a certain displacement it drops rapidly. In the block, on the other hand, the restoring force is linear; with increasing displacement it increases in a straight line. Comparing the restoring force characteristics of the vertical and horizontal cores, in the small displacement region, the restoring forces are larger in the column of the vertical core, but at displacements beyond 28 mm the restoring forces in the block of the horizontal core becomes larger. The displacements in the horizontal core are up to 25 mm so that the core does not possess a large restoring force. Therefore, it is not due to a difference in the restoring forces that the displacements in the horizontal core are smaller than that in the vertical core.

Effects of the interference of the surrounding blocks will now be considered. In the vertical core, one column is merely adjoined to the columns on each of its sides. In the horizontal core, however, one block is surrounded by its neighboring from four to six blocks. In the vertical column, respective column has a similar restoring force, so they vibrate in group i.e. "lumped vibration", On the other hand, in the horizontal core, the surrounding blocks are in complex interference with the blocks, so that its lumped vibration is suppressed. Consequently, the displacements in the horizontal core become smaller than that in the vertical core.

In the verical core, the column receives interference only with its neighboring two columns. But in the real core, it is in interference with from four to six columns. Therefore, in the vertical column, effects of interference by the neighboring columns are less, so that the displacements become larger than in the real core. In the horizontal core, on the other hand, effects of interference by the neighboring blocks are similar to that in the real core. Consequently, taking into consideration that the restoring force at the maximum displacements (about 24 mm~26 mm) are close to that in the column, the displacements in the

real core may be taken as close to that in the horizontal core.

In aseismic design of the core, the maximum displacements will be the total gap in the columns and the displacements which will cause the maximum support reaction forces in the side fixed reflector blocks.

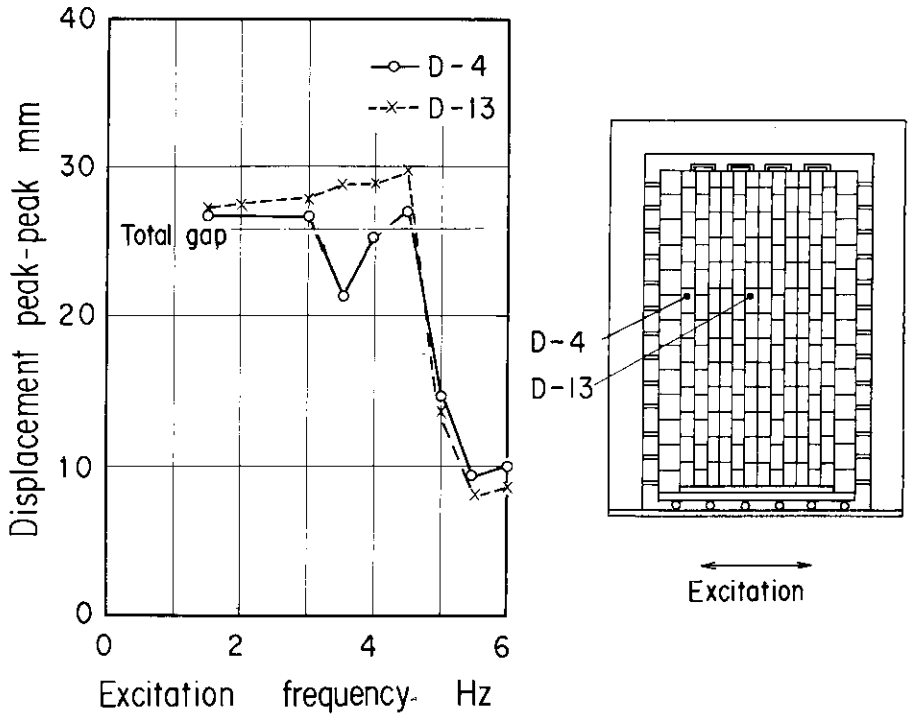

(a) Two-dimensional vertical core model

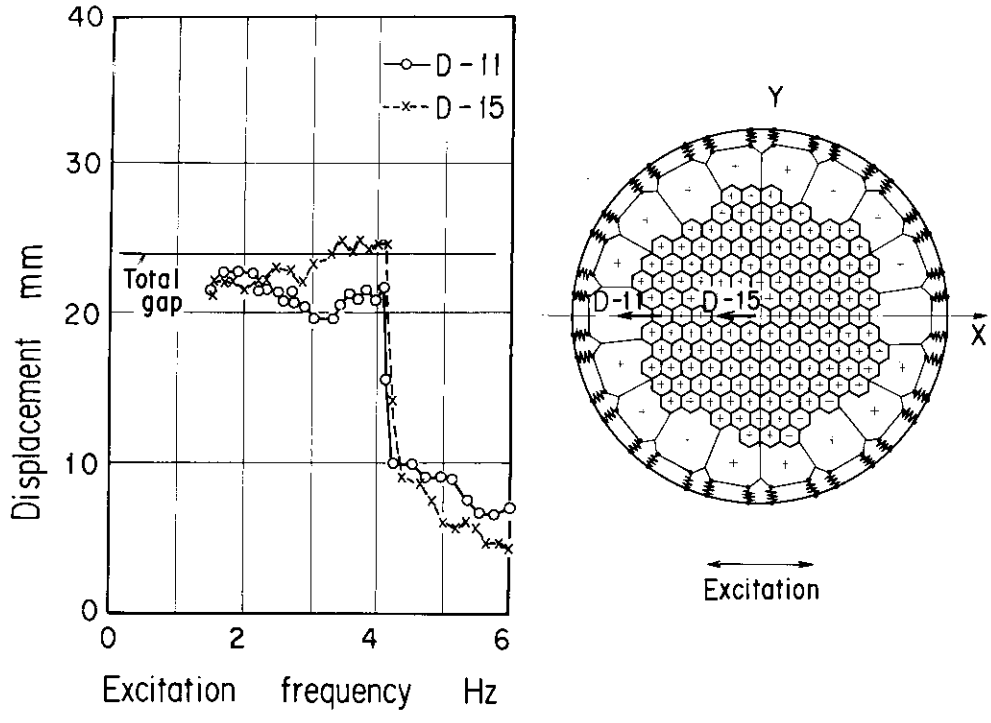

(b)Two-dimensional horizontal core model

Fig. 11.1 Comparison between vertical core and horizontal core models on displacement
(Excitation X-direction, Hard support, With reflector Key, Max. acceleration 250 Gal)

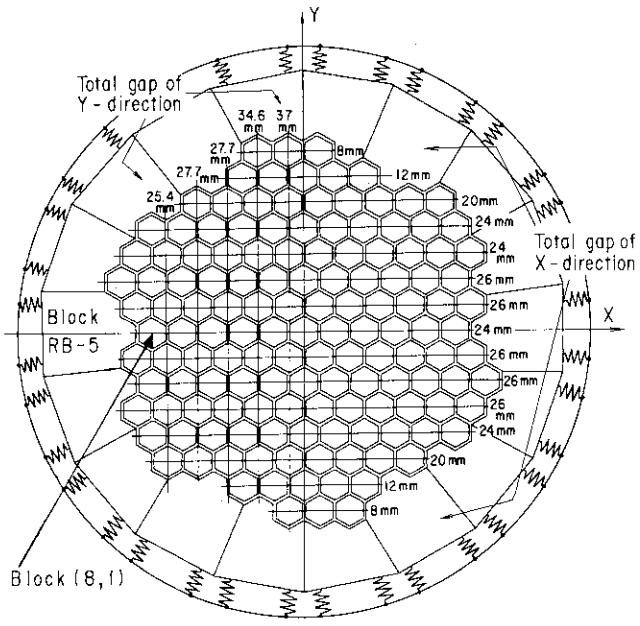

Fig. 11.2 Total gap of each row of core

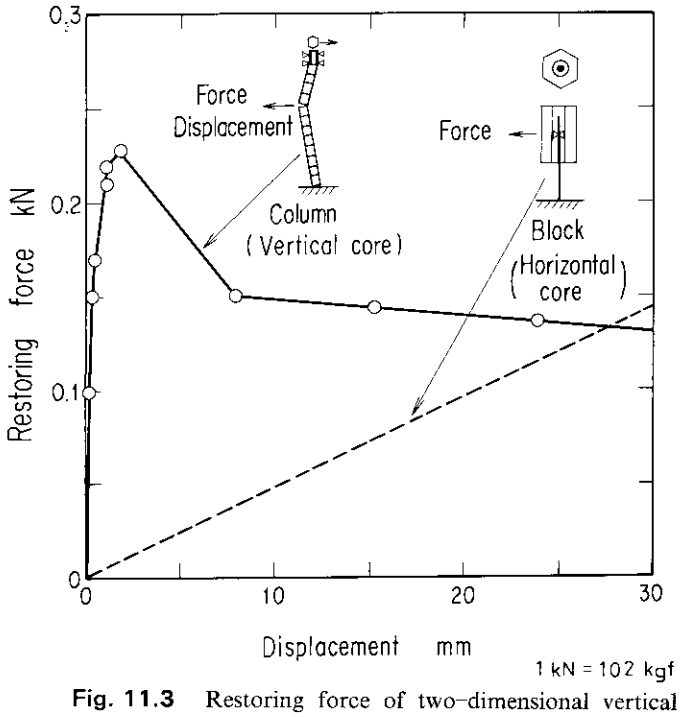

Fig. 11.3 Restoring force of two-dimensional vertical core column and two-dimensional horizontal core block

11.3 Acceleration response characteristics

The acceleration response curves in the vertical and horizontal cores are shown in Fig. 11.4. In the vertical core, as indicated in Fig. 11.4(a), the impact accelerations at the boundary positions are larger than that in center of the core. It is apparently in lumped vibration. Then, in the horizontal core, as seen in Fig. 11.4(b), the impact accelerations at the boundary positions and that in center of the core are nearly similar. This is possibly because the blocks in the core are in repeated impact with the neighboring blocks, rather than in lumped vibration. In the vertical core, the rotational forces imparted to the column on its

longitudinal axis due to the impacts between columns are small. In the horizontal core, however, in a block's collision with the surrounding four to six blocks, respective block receives mutual rotational force. And further, in the horizontal core, as shown in Fig. 11.2 the numbers of blocks in respective row are different, so the total gaps also differ. Consequently, the neighboring rows of blocks are in mutual interference, so that the lumped vibration is suppressed. The blocks are in mutual impacts not only in similar phase but also in dissimilar phase, thereby giving rise to large accelerations.

There is another cause for making the impact accelerations in the horizontal core larger than in the vertical core. That is, in the vertical core, each column is formed by stacking blocks. In the impacts between the core column and side fixed reflector column, the impact energy is partly absorbed by way of the friction between boundary faces of the upper and lower blocks. This may be the reason that the impact accelerations are smaller in the vertical core than in the horizontal core.

From the above, it is considered that the impact accelerations in the real core are close to that in the vertical core.

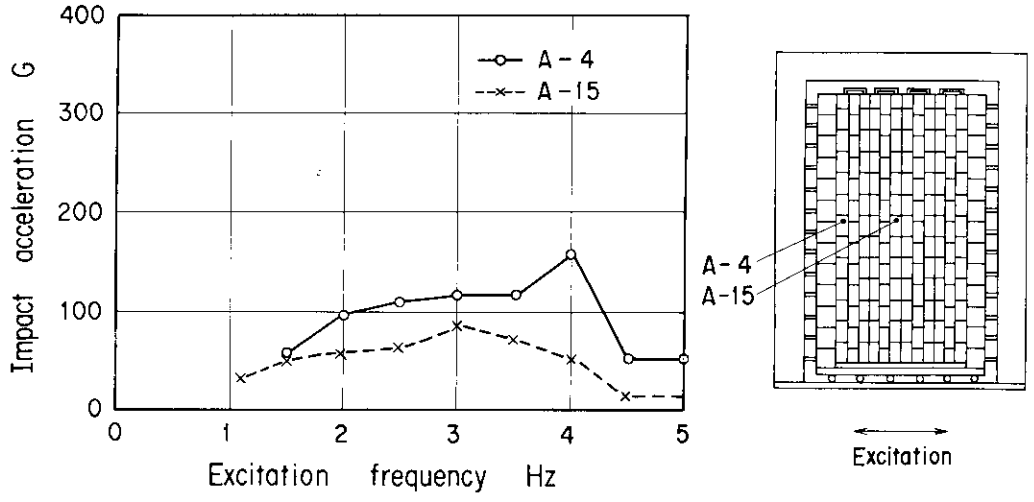

(a) Two-dimensional vertical core model

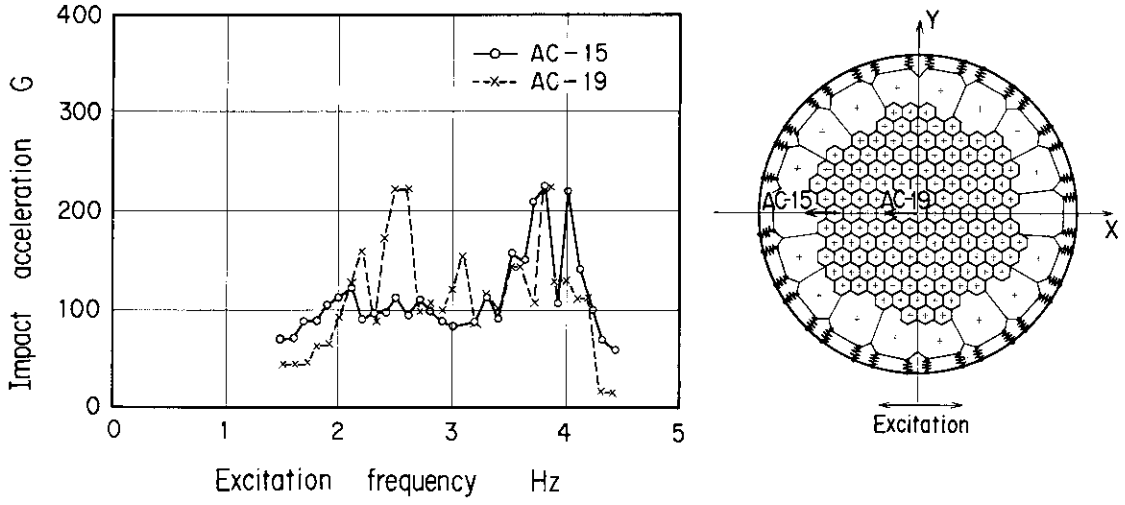

(b) Two-dimensional horizontal core model

Fig. 11.4 Comparison between vertical core and horizontal core models on impact acceleration (Excitation X-direction, Hard support, With reflector Key, Max. acceleration 250 Gal)

11.4 Side reaction force characteristics

The side support reaction forces in the vertical and horizontal cores are shown in Fig. 11.5. In the impact reaction force curves in the vertical core of Fig. 11.5(a), the peak values for the upper column end under excitation frequency 3 Hz are the resonant vibration with a steel block with a gap between the blocks at column top of 0.5 mm. Then, the peak values for the position of about two-thirds column height at excitation frequency 4 Hz are due to the resonant vibration with a graphite block with a gap between

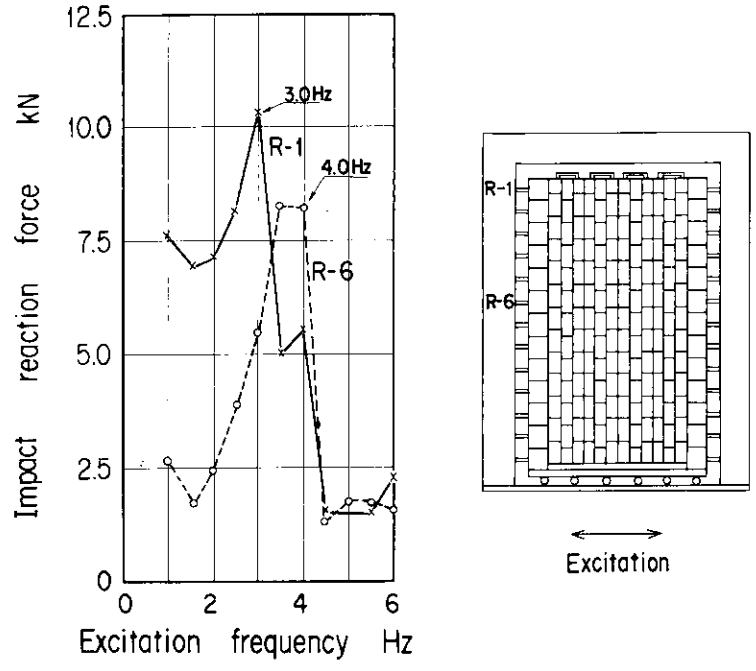

(a) Two-dimensional vertical core model

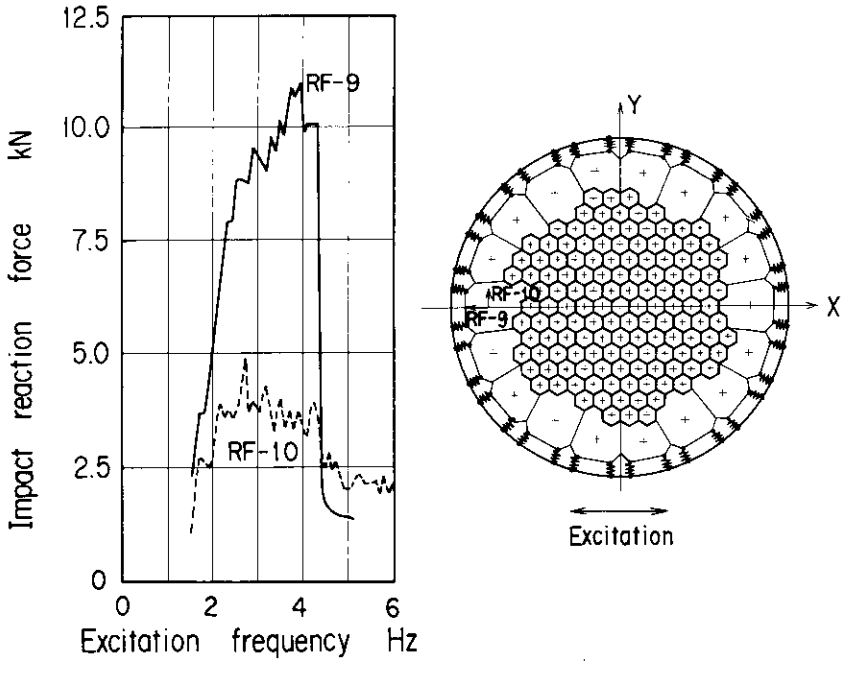

(b) Two-dimensional horizontal core model

1kN=102kgf

Fig. 11.5 Comparison between vertical core and horizontal core models on impact reaction force
(Excitation X-direction, Hard support, With reflector Key, Max. acceleration 250 Gal)

the blocks of 2 mm. Figure 11.5(b) shows the impact reaction force curves for the excitation reaction and the direction perpendicular to it the horizontal core.

In the comparison of the impact reaction forces in the horizontal core with the impact reaction forces at about two-thirds column height in the vertical core, it is seen that for peak values in the vicinity of excitation frequency 4 Hz, the latter is smaller than the former. As already described, this is because in the vertical core there occur friction forces between boundary faces of the upper and lower fixed reflector blocks, so that the impact forces are also dispersed into the upper and lower blocks.

From the above, it is considered that the impact forces in the real core are close to that in the vertical core.

11.5 Displacement, acceleration and impact reaction force distributions

In-core distributions of displacements, impact accelerations and impact reaction forces in the vertical and horizontal cores are shown in Fig. 11.6. In the horizontal core of Fig. 11.6(a), the response value

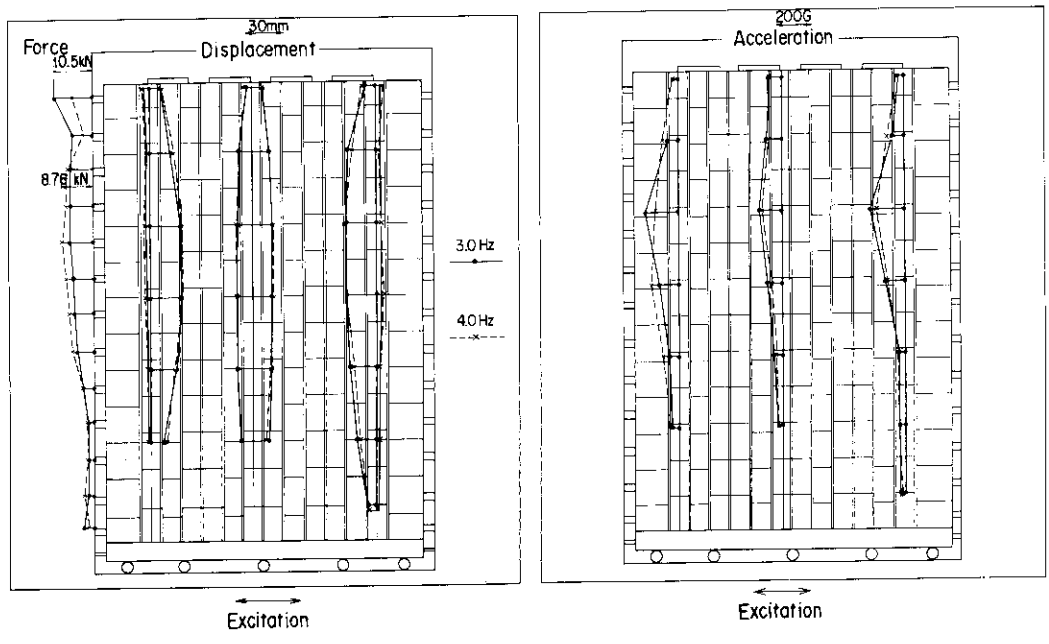

(a) Two-dimensional vertical core model

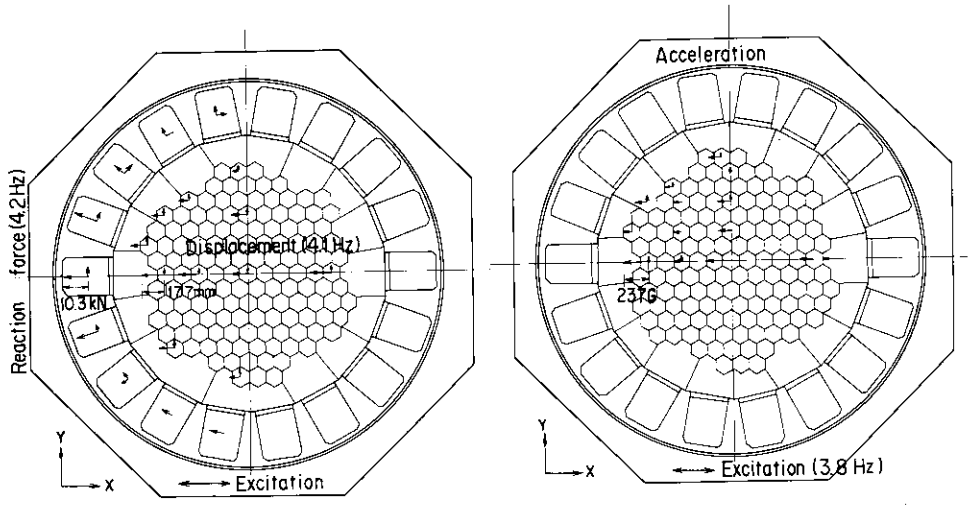

(b) Two-dimensional horizontal core model

1kN=102kgf

Fig. 11.6 Comparison between vertical core and horizontal core models
(Excitation X-direction, Hard support, With reflector Key, Max. acceleration 250 Gal)

distributions are for two vibration modes exhibiting peak values of impact accelerations and impact reaction forces, respectively, i.e., excitation frequencies of 3 Hz and 4 Hz. In the case of 3 Hz an uppermost block in the column is in resonant vibration, on the other hand in the case of 4 Hz a block at about two-thirds the column height is in resonant vibration. In the horizontal core of Fig. 11.6(b), the response value distributions are shown with an excitation frequency of 4.1 Hz corresponding to the maximum displacements, 3.8 Hz corresponding to the maximum impact accelerations and 4.2 Hz corresponding to the maximum impact reaction forces.

In the comparison between the vertical and horizontal cores, the displacements, impact accelerations and impact reaction forces in both cores are in mutual correspondence. The respective maximum values in both cores are also similar. The experimental results in the vertical and horizontal cores are thus in complementary relation for the purpose of predicting the response values in the real core.

11.6 Effect of the side support stiffness

Figure 11.7 shows change in the maximum displacements with change in the side support stiffness in the vertical and in the horizontal cores. As seen in the maximum displacement crves in the vertical column of Fig. 11.7(a), the displacements decrease with a softening of the support stiffness. In the horizontal core of Fig. 11.7(b), on the other hand, though the displacements decrease with a softening of the support stiffness, the decreases are not as marked as in the vertical core. The reason for this may be that the vibration in the vertical core is lumped vibration but in the horizontal core such lumped vibration is not so considerable, as already mentioned.

Figure 11.8 shows change in the maximum impact reaction forces with change in side support stiffness both in the vertical and horizontal cores comparatively. As seen in Fig. 11.8(a), in the vertical core, the impact reaction fores are smaller with the soft support stiffness than with the hard. It is also seen that there is a support stiffness which reduces the impact reaction forces. Also in the horizontal core, as seen in Fig. 11.8(b), the impact reaction forces are smaller with the soft than with the hard support stiffness. There is also a support siffness here, which reduces the impact reaction forces. The change in the impact reaction forces due to the existence of "preload" in the case of intermediate support stiffness will now be considered. That is, a side fixed reflector blocks are tightened toward the core center from the

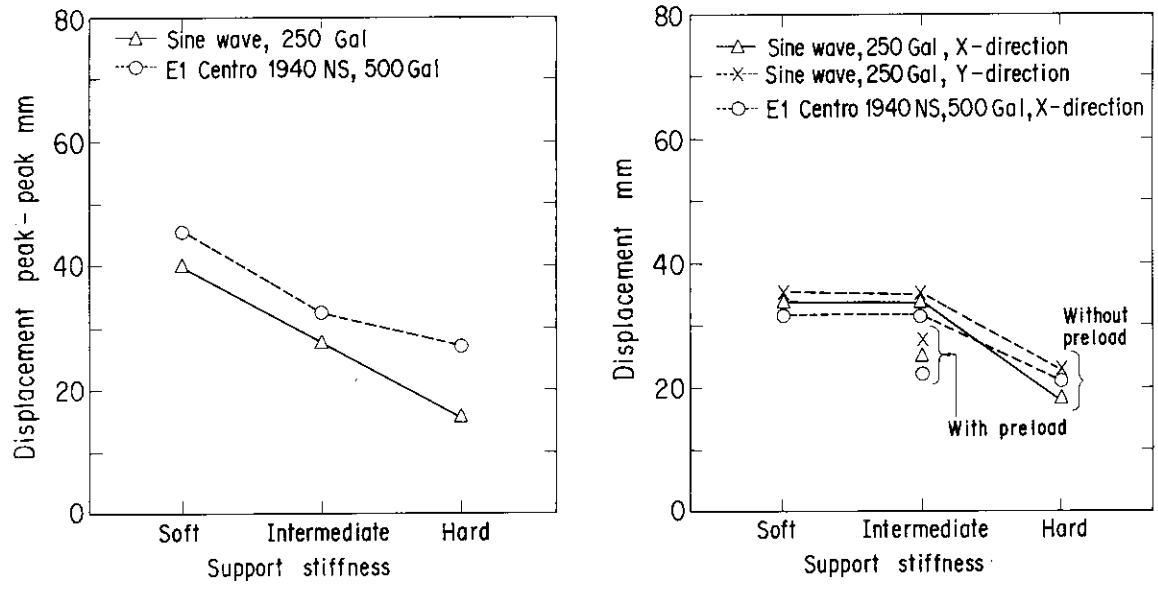

(a) Two-dimensional vertical core model

(b) Two-dimensional horizontal core model

Fig. 11.7 Effect of support stiffness on displacement

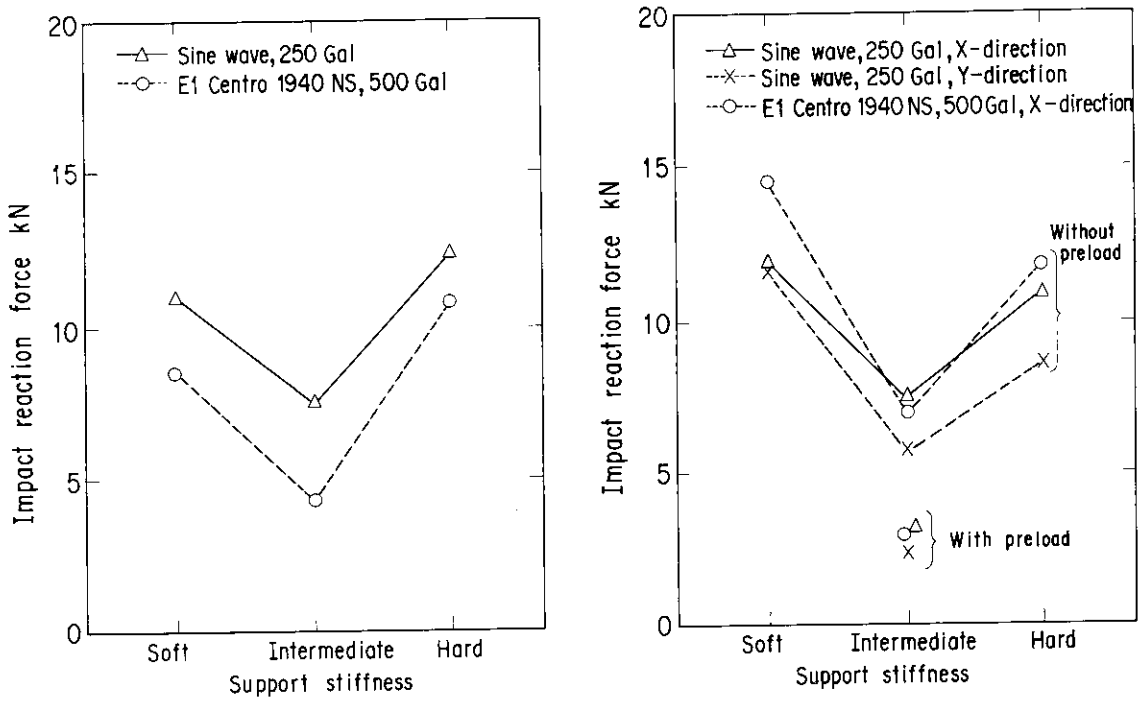

(a) Two-dimensional vertical core model

(b) Two-dimensional horizontal core model

1kN = 102kgf

Fig. 11.8 Effect of support stiffness on impact reaction force

peripheral region (i.e. pre-loading). In this case, the side impact reaction forces are reduced. By pre-loading, respective fixed reflector block is in loose coupling. It is now considered that a fuel block impacts with its adjoining fixed reflector block. In this case, the impact forces applied to this fixed reflector block are then diverted to its neighboring fixed reflector blocks. Consequently, the impact reaction forces in the first impact are reduced.

In the comparison of response values between the vertical and horizontal cores, the changes in response values with change in the support stiffness have similar trends for both cores. This may also apply to the real core.

In Figs. 11.7 and 11.8, together with the response values for sinusoidal waves and seismic waves are also shown. It is seen that the tendencies due to seismic waves are similar to those due to sinusoidal wave input.

11.7 Seismic wave response characteristics

The chages in the response values with sinusoidal waves and random waves such as seismic waves will be considered in the vertical and horizontal cores. The random waves are two different seismic waves and a white noise wave. The two seismic waves are the E1 Centro 1940 NS wave and the Ibaraki 1964 EW wave respectively. The former includes a long period component and the latter a short period component. The white noise wave is a random wave including a sinusoidal wave component of from 1 to 10 Hz.

Figure 11.9 shows effects of input waves on the displacement distribution and impact reaction force distributions in the vertical core. Figure 11.9(a) shows the response values for a sinusoidal wave of the maximum input acceleration 250 Gal and excitation frequency 4 Hz. Figures 11.9(b)~(d) show the response values for the E1 Centro 1940 NS wave, the Ibaraki 1964 EW wave and the white noise wave, each of the maximum input acceleration 500 Gal. As seen in Fig. 11.9, with exception of the response values to the Ibaraki 1964 EW wave, the maximum response values to the other three waves are almost the same. The reason is that the Ibaraki 1964 EW wave contain short period components, compared with

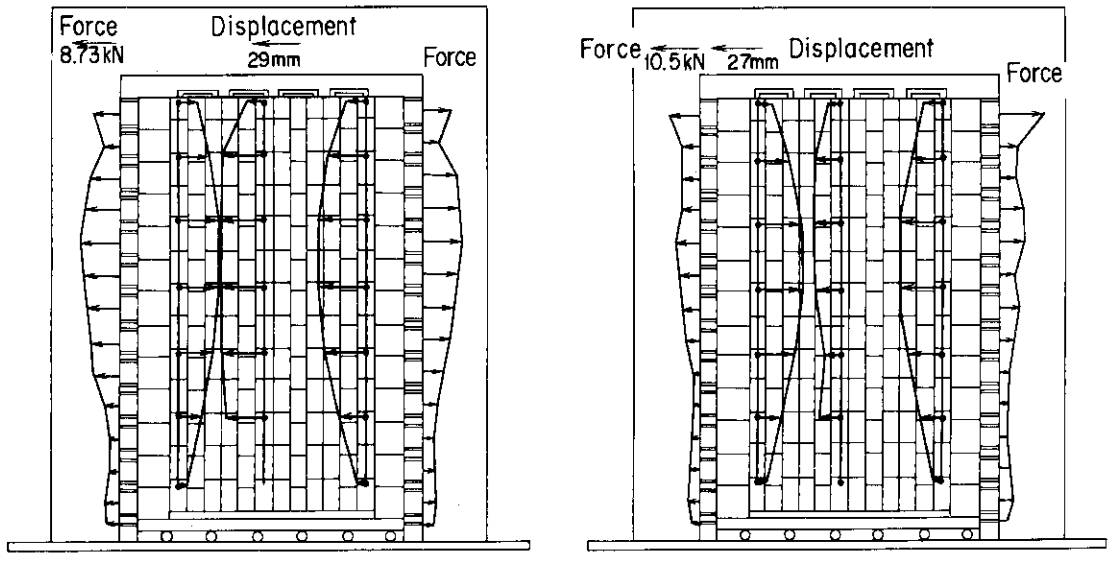

(a) Sinusoidal wave 4Hz
(Max. acceleration 250 Gal)

(b) El Centro 1940 NS wave
(Max. acceleration 500 Gal)

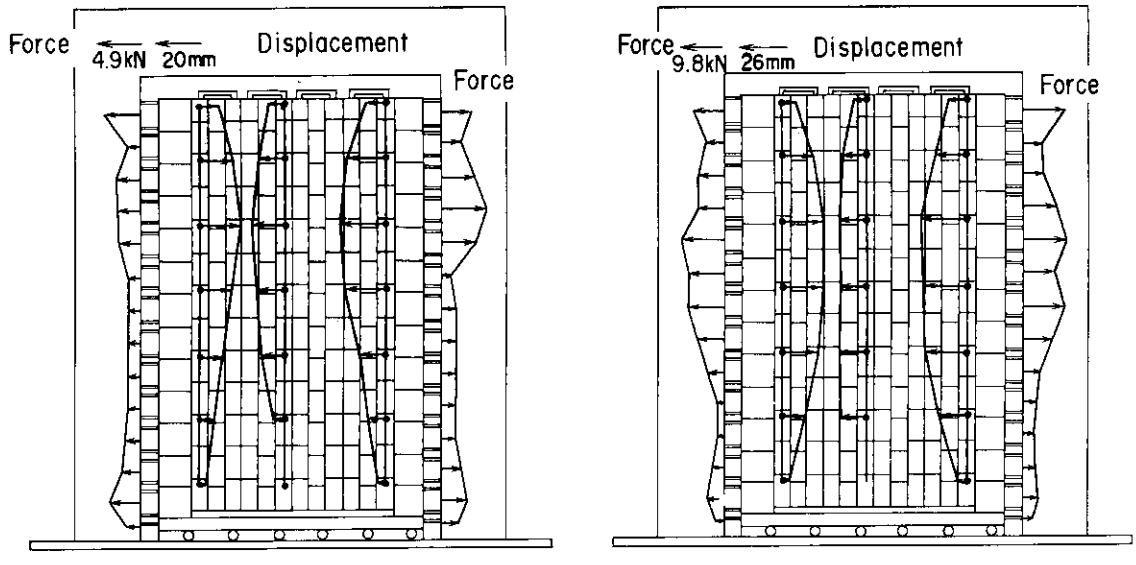

(c) Ibaraki 1964EW wave
(Max. acceleration 500 Gal)

(d) White noise wave
(Max. acceleration 500 Gal)

1kN = 102kgf

Fig. 11.9 Effecn of input wave on displacement, impact acceleration and impact reaction force distributions along column

the other three waves. This is also due to the fact, as indicated in Fig. 11.1 and Fig. 11.5, that beyond excitation frequency 5 Hz the response values drop rapidly.

The impact reaction forces for the sinusoidal wave of the maximum input acceleration 250 Gal, the El Centro 1940 NS wave of 500 Gal and the white noise wave of 500 Gal are similar. Between the input accelerations and the impact reaction forces there are proportional relation. Consequently, the impact reaction forces for the seismic waves are about 60 % of that for the sinusoidal waves. Therefore, from response values for the sinusoidal waves, the response values for a seimic wave are predictable.

Figure 11.10 shows effects of input waves on the displacement distributions and the impact reaction force distributions in the horizontal core. The input waves are those causing a maximum displacement and a maximum impact reaction force, respectively. Figure 11.10(a) shows the response values for the

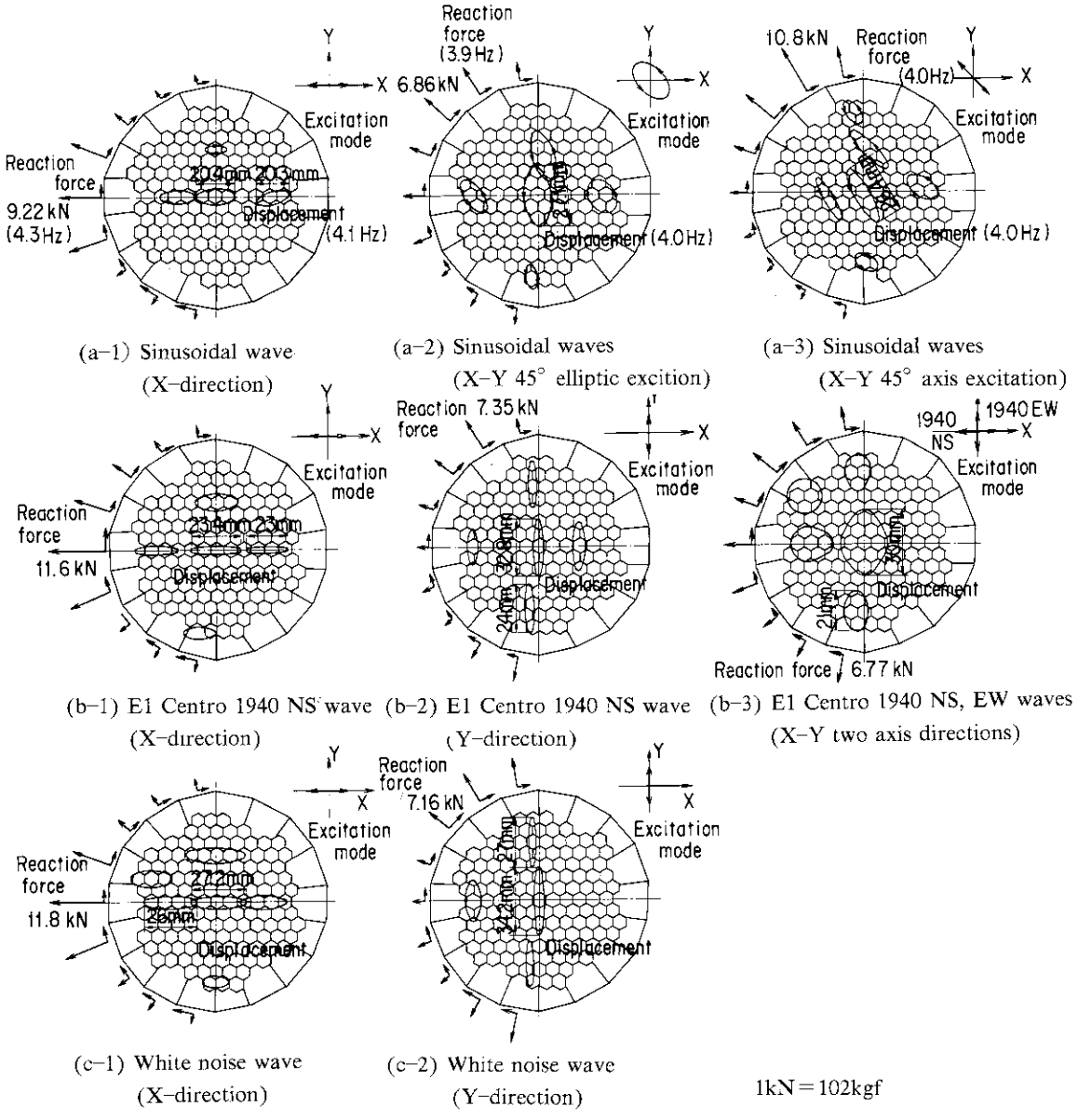

(a-1) Sinusoidal wave (X-direction)

(a-2) Sinusoidal waves (X-Y 45° elliptic excition)

(a-3) Sinusoidal waves (X-Y 45° axis excitation)

(b-1) El Centro 1940 NS wave (X-direction)

(b-2) El Centro 1940 NS wave (Y-direction)

(b-3) El Centro 1940 NS, EW waves (X-Y two axis directions)

(c-1) White noise wave (X-direction)

(c-2) White noise wave (Y-direction)

Fig. 11.10 Effect of input wave on displacement and impact reaction force distributions in core (Max. acceleration, Sinusoidal wave 250 Gal, El Centro wave 500 Gal, White noise wave 500 Gal)

sinusoidal wave of the maximum acceleration 250 Gal in uni-axial excitations in the X and Y directions, respectivity. Figure 11.10(b) shows response values for the E1 Centrol 1940 NS wave with the uni-axial exitation in the X and Y directions, respectivly, and the bi-axial excitation in the X and Y directions due to NS and EW waves. Figure 11.10(c) shows the response values for the white noise wave of the maximum input acceleration 500 Gal with uni-axial excitations in the X and Y directions, respectively, In the bi-axial simultaneous excitation, the maximum input excitation is a combined value of the vectors in the X and Y directions.

As seen in Fig. 11.10, the maximum displacements in the Y direction excitation occur in the Y axis with a large total gap. Then, the maximum impact reaction forces appear in the uni-axial excitation in the X direction. The maximum impact reaction forces for the sinusoidal waves of the maximum input acceleration and the maximum impact reaction forces for the E1 Centro 1940 NS wave of the maximum input acceleration 500 Gal and the white noise wave of 500 Gal are nearly the same.

From the above, the impact reaction forces in the real core be predicted from the response values for the sinusoidal waves. Its values are about 60% of the values for the sinusoidal waves. The impact reaction forces in the uni-axial excitation in the X direction are the same as or lower than that in the uni-axial excitation in the Y direction and in the bi-axial simultaneous excitation. Therefore, the response values in the real core can be predicted from the response values in the uni-axial excitation in the horizontal direction in the vertical core which is the uni-axial excitation in the Y direction.

11.8 Prediction of response values in the real core

From the results of a seismic experiment with a scale model, response values in the real core can be predicted in two ways. One is application of similarity laws to the experimental results, while another is the use of the computer programs, which are verified on the basis of the model experiments. It will be shown below that either method can predict the response values in the real core.

In the seismic experiment model shown far, as indicated in Fig. 11.11, the size of the core is 1/2 that

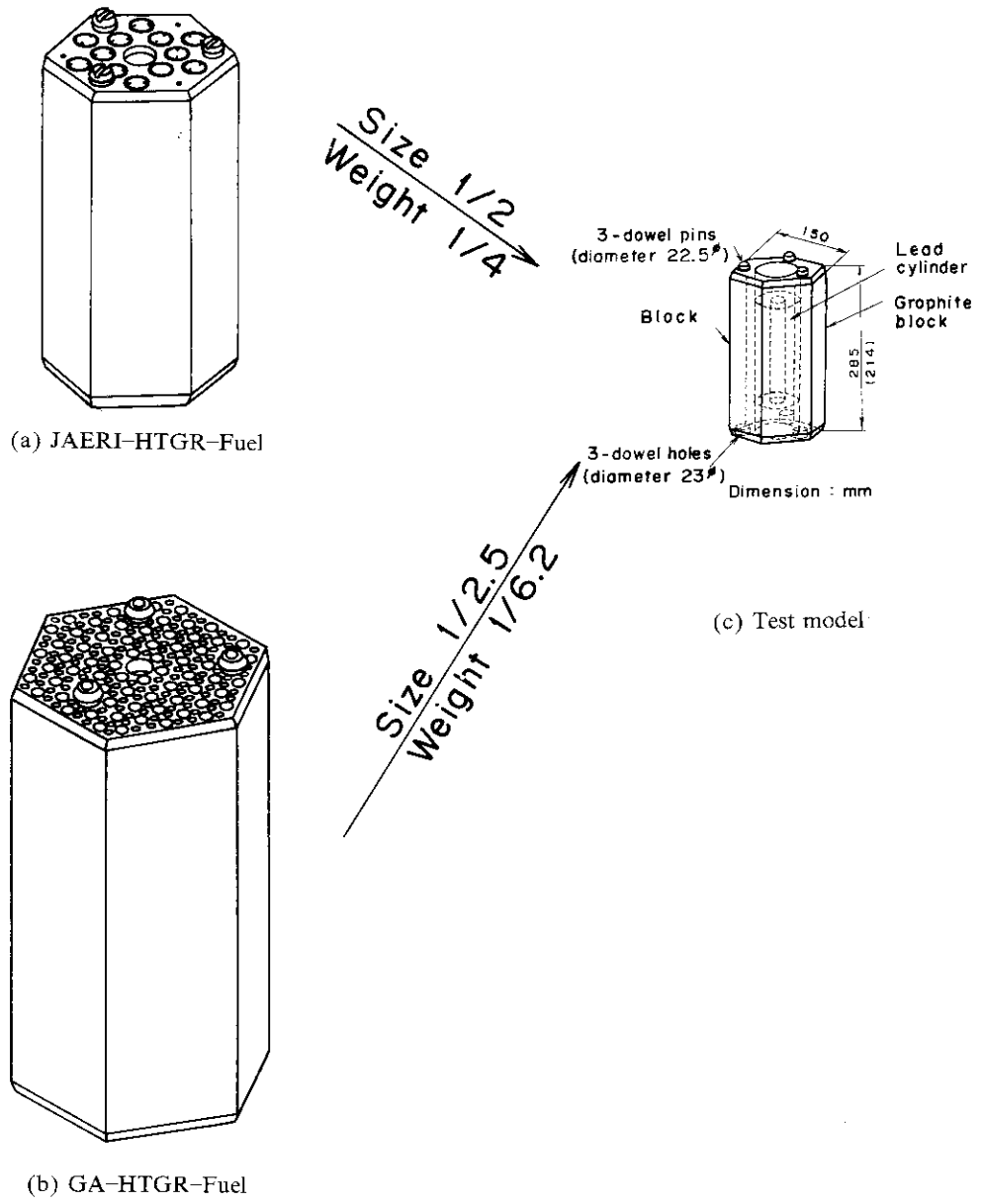

(a) JAERI-HTGR-Fuel

(b) GA-HTGR-Fuel

(c) Test model

Fig. 11.11 Fuel elements and test model

Table 11.1 Multiplication factor for predicting seismic response values of real HTGR core

Item	Multiplication factor		
	Experiment	JAERI-HTGR	GA-HTGR
Displacement	1	2	2.5
Force	1	4	6.2
Acceleration	1	1	1
Velocity	1	$\sqrt{2}$	$\sqrt{2.5}$
Frequency	1	$1/\sqrt{2}$	$1/\sqrt{2.5}$

of the small-scale experimental HTGR and the weight is 1/4 that of the same HTGR. And then, similarly, the core size is about 1/2.5 that of General Atomics power generating HTGR in the United States and the core weight is about 1/6.2 that of the same HTGR. In order to obtain response values in the real core from the experimental results with the models, as shown in Table 11.1, the experimental results are multiplied by the similarity multiplication factors. In the core of the experimental HTGR, for example, to obtain the displacement, the experimental result is multiplied by 2; to obtain the force, the result is multiplied by 4; to obtain the acceleration, the result is multiplied by 1; to obtain the velocity, the result is multiplied by $\sqrt{2}$; and to obtain the frequency, the result is multiplied by $1/\sqrt{2}$.

In Figs. 11.12 and 11.13 the displacement and the impact reaction force response curves in the fuel block of the experimental HTGR are shown. The two methods of using similarity laws and the computer program are compared. As can be seen in the figures, both values are almost in agreement. The two methods of predicting response values in the real core are thus seen to give adequate results.

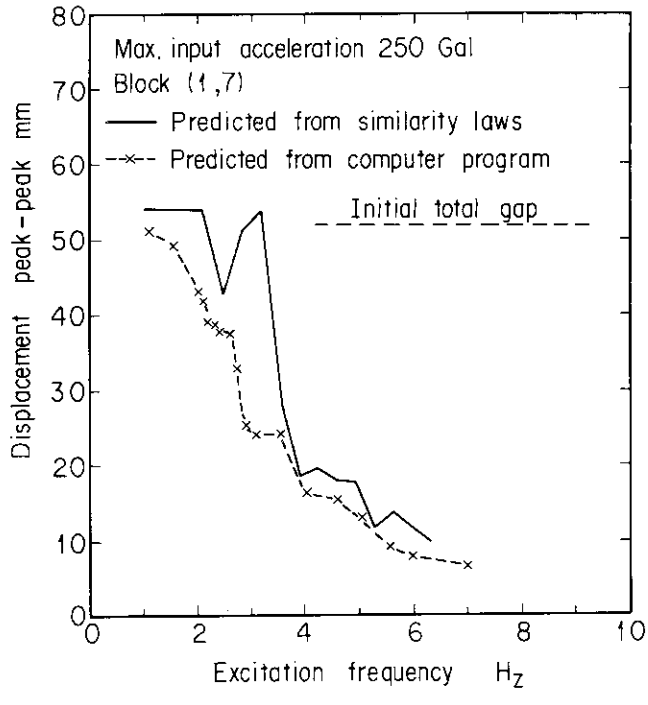

Fig. 11.12 Comparison between similarity laws and computer prediction on displacement

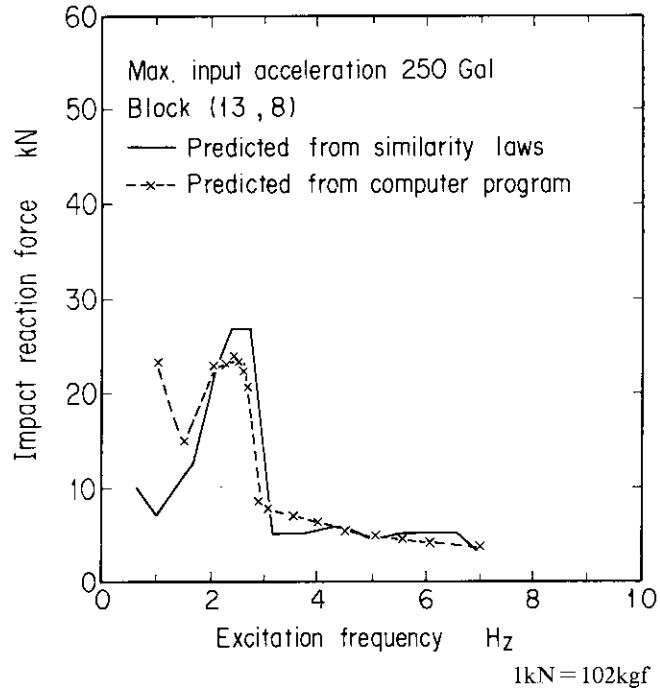

Fig. 11.13 Comparison between similarity laws and computer prediction on impact reaction force

11.9 Concluding remarks

In order to obtain seismic response characteristics of a real HTGR core, comparison of response characteristics of two-dimensional cores have been carried out. The more important results are as follows.

(1) From the results of the seismic experiments with the scale models, it is verified that the real core response can be predicted by the two following methods. These are the application of similarity laws to the experimental results and the use of the computer programs which are verified, on the basis of the model experiments.

(2) The response values of the real HTGR core could be estimated from the experimental and analytical results of the two-dimensional vertical and horizontal core models.

12. Seismic Response of HTGR Core and Aseismic Design Consideration for HTGR Core Structure Based on Previously Shown Study

The author has clarified the dynamic characteristics of the block-type fuels HTGR core obtained by the experiments and has developed the analytical methods and the computer programs simulating the experimental results. The results obtained by this study and aseismic design considerations are the following.

12.1 Block impact characteristics

The coefficient of restitution is about 0.6 and the contact duration is about 0.7 milli-seconds. Both values slightly decrease with impact velocity (Fig. 2.2, Fig. 2.3).

12.2 Stacked column characteristics

(1) Soft spring characteristics

The column resonant frequency decreases with excitation amplitude. The jump-up frequency of the column displacements are higher in sweep-up than in sweep-down. The column has a nonlinear resonance and exhibits a hysterisis response with jump points. These are the column softening characteristics due to column rocking, interface friction between blocks and loose dowel connections. The column displacements also increase with increasing excitation levels (Fig. 3.3).

(2) Vibration mode

The column bends at about two-thirds of the column length (Fig. 5.4).

(3) Subharmonic vibration

Subharmonic vibration takes place due to the friction contact of the upper and lower blocks and to the unsymmetrical support in upper column gaps and uneven gaps horizontally. The subharmonic vibration appears either with high excitation frequency at low acceleration levels or with low frequency at high acceleration levels (Fig. 5.7 and 5.8).

(4) Column whirling

The column whirling is more likely to occur in the corner-to-corner excitation direction than in the flat-to-flat direction (Fig. 5.5).

(5) Effect of gas pressure difference

The gas pressure difference between the upper and lower of the core has effects of raising the resonant frequency of the column and the column displacements decrease (Table 5.2).

(6) Column damping factor

The column damping factors are about 10~30% of the critical factors. It increases slightly with increasing displacement amplitude (Table 3.1).

(7) Hard spring characteristics

According to increasing the input accelerations, the resonant frequency shifts to the higher frequency, the impact forces to increase, and the frequency for rapid drop of the impact forces i. e. the jump -down frequency to increase. This nonlinear spring characteristics due to the column impact i. e. the hardening characteristics exist (Fig. 3.5 and 5.10).

(8) Effect of gap width

In increasing the gap width, both jump-up and jump-down frequencies of the impact forces shift to

lower frequencies. The range of impact frequency gets smaller with increasing gap width. The impact forces raise with increasing gap width (Fig. 3.6).

(9) Effect of gap width at column top

The top block gap has effects on column displacement mode. Increasing the top gap pushes the maximum displacement point of column upwards and makes motion more unstable (Chapter 5).

(10) Effect of excitation direction

The effect of excitation direction on the resonant frequency is almost negligible, but change in excitation direction results in a slight change of response displacements and impact forces. The column whirling of the corner-to-corner excitation is larger than the flat-to-flat excitation. Therefore impacts of the block occur by sliding along the neighbor block sides. The impact values are thus reduced by an amount of the momentum consumed in sliding friction (Chapter 3).

12.3 Characteristics of core dynamic behavior

(1) Resonant frequency

The resonance curve shows typical nonlinear hardening characteristics. The resonant frequency increases with an increase of input acceleration levels and are strongly amplitude dependent. The column displacement increase with an increases of input acceleration levels (Fig. 7.6 and 9.6).

(2) Lumping vibration

At low excitation frequency, all blocks in the core oscillates as a tightly lumped mass between the side fixed reflector boundaries. The lumping increases with increasing excitation frequency. At still higher frequency the lumping rapidly decreases (Fig. 8.5 and 10.14).

(3) Subharmonic vibration

At high frequency range subharmonic vibration of the column occurs and each column vibrates in random impacts with adjacent columns (Fig. 7.6).

(4) Hardening characteristics

The impact reaction forces increase with an increase of input acceleration levels. The resonant frequency is strongly excitation level dependent and shifts to high frequency with the increase of input acceleration levels. These characteristics are typical of the nonlinear hardening spring mass system (Fig. 7.10 and 9.8).

(5) Displacement characteristics in core

The displacements are larger in the core center than the core periphery (Fig. 7.4, 7.8, 9.10 and 11.10).

(6) Acceleration and force characteristics in core

The impact accelerations and forces are smaller in the core center than in the core periphery (Fig. 7.15, 9.10, 11.6 and 11.9).

(7) Effect of input acceleration

The core displacements, impact accelerations and impact reaction forces increase with input acceleration levels. The impact accelerations and impact reaction forces have the same tendency with varying excitation frequency (Fig. 7.14).

(8) Core damping factor

The core damping factors are 4~10% of critical. The damping factors increase with increasing column displacements. In the case of the core, the column displacements are small so the damping factors are small comparing with the damping factors of the single stacked column (Chapter 7).

(9) Effect of gap width between column top blocks

A small gap width between top blocks of the columns reduces the core displacements and the impact forces. The choice of a small gap width favorably affects the core design (Fig. 7.9 and 7.13).

(10) Effect of gas pressure difference between upper and lower of core

The gas pressure difference between the upper and lower of the core reduces the core displacements

and impact forces (Fig. 7.7 and 7.12).

12.4 Effect of side support stiffness

(1) Resonant frequency

With an increase of the side support stiffness, the resonant frequency shifts to higher frequency (Fig. 7.6, 7.11 and 9.6).

(2) Displacement characteristics

With an increase of the side support stiffness, the core displacements decrease (Fia. 7.6 and 9.7). The soft spring support results in large core displacements which affect the insertion of control rods. A core structural desigh with the soft spring support is therefore not favorable for control rod insertion during seismic disturbance.

(3) Impact characteristics

In the hard spring support, the impact reaction forces are larger than in the intermediate spring support. The intermediate spring support of the fixed side reflector block reduces the impact forces (Fig. 7.11 nd 9.9).

(4) Choice of core side support stiffness

The core side support stiffness significantly affects core displacements and impact forces. The core displacements decrease with increasing side support stiffness. On the other hand, the impact forces increase with increasing side support stiffness. The soft spring support results in larger core displacements. Maximum core displacements are expected over the total column gap. The hard spring support limits the core displacements to about the total column gap because of the high spring rate of the hard support. The support forces for the hard support are a little higher than for the soft spring support. Since a core design with soft spring support is not favourable for control rods insertion during seismic disturbance, the hard spring side support is better than the soft support.

The fuel block displacements are larger with preload than without preload in the case of the intermediate support condition. Preload from core periphery to core center could reduces displacements of fuel blocks (Fig. 9.7).

The impact reaction forces are smaller with preload than without preload in the case of the intermediate support condition. There is a favorable support condition in the HTGR core design. Furthermore, preload from core periphery to core center could reduces impact reaction forces (Fig. 9.9).

12.5 Effects of excitation direction and input wave on response

(1) Effect of excitation direction

The total gaps in the corner–to–corner excitation direction are larger than at in the flat–to–flat excitation direction so that the fuel blocks are easily displaced in the corner–to–corner excitation direction than in the flat–to–flat excitation direction. In aseismic design of the core, the maximum displacements will be the total gaps in the columns and the displacements which will be cause the maximum support reaction forces in the side fixed reflector blocks (Fig. 11.1).

The maximum reaction forces in the radial component are larger than that of the tangential. The maximum forces in the case of the flat–to–flat excitation direction are larger than that of the corner–to –corner excitation direction (Fig. 9.10, 9.11 and Fig. 11.10).

(2) Comparison between sinusoidal and seismic wave responses

The maximum displacements and impact forces for seismic waves are under 60% of that for simusoidal waves. The response values of seismic waves are estimated from those of the uni–axial sinusoidal flat–to–flat excitation direction (Fig. 7.18, 9.12 and 9.13).

12.6 Dowel force

(1) Effect of input acceleration level

With an increase in excitation levels, the dowel forces increase. With an increase of inpmt acceleration, the resonant frequency of the dowel force shifts to an higher value. These are caused by the hard spring characteristics of the dowel pin (Fig. 7.16).

(2) Effect of support stiffness

The dowel forces for the soft spring support are smaller than that for the intermediate support, since the columns are bent, with the soft support than with the hard support (Fig. 7.17).

(3) Relationship among impact acceleration, impact reaction force and dowel force

The impact accelerations, impact reaction forces and dowel forces have the same tendency with varying excitation frequency, acceleration and with the maximum occurrence point (Chapter 7).

12.7 Estimation of real core response from two-dimensional core response

From the results of seismic experiments with the scale model, it is verified that a real core response can be predicted by two following methods. These are the application of similarity laws to the experimental results and use of computer programs which are verified, on the basis of the model experiments. The response values of the real HTGR core could be estimated from the experimental and analytical results of the two-dimensional vertical and horizontal core models (Chapter 11).

12.8 Seismic response analysis method and computer program

(1) Seismic analysis method

The seismic analysis methods for the block type HTGR core have been developed for dynamic analysis of the two-dimensional vertical and horizontal cores (Chapter 8 and 10).

(2) Computer programs

The computer program SONATINA-2V for the two-dimensional vertical HTGR core and the computer program SONATINA-2H for the two-dimensional horizontal HTGR core have been developed. The analytical results were presented with the results of the experiments. Good agreement were obtaind between the analytical and the experimental results (Fig. 8.6~8.11 and Fig. 10.14~10.20).

(3) Simplified analytical methods

Successful application of a simplified model which uses one degree-of-freedom mass with nonlinear column stiffness and damping characteristics has been shown for the seismic response of a column. By the analysis and in comparing with the results of experiment and detailed analysis, good agreement was obtaind among them (Fig. 6.7 and 6.8).

Another simplified model is a reduced block number model, which is modeled to treat two or three blocks as a single block. Some calculations were made and results from the reduced model was compared with the experimental and the detailed model results and good agreement was obtained among them (Fig. 12.1).

The computer costs of time history analysis of the HTGR core by the simplified models are significantly lower than that of the detailed model.

(4) High speed computation

The seismic analysis computer programs SONATINA-2V and SONATINA-2H have been vectrized for high speed computation, so that about two to three times higher than the original programs (Table 12.1).

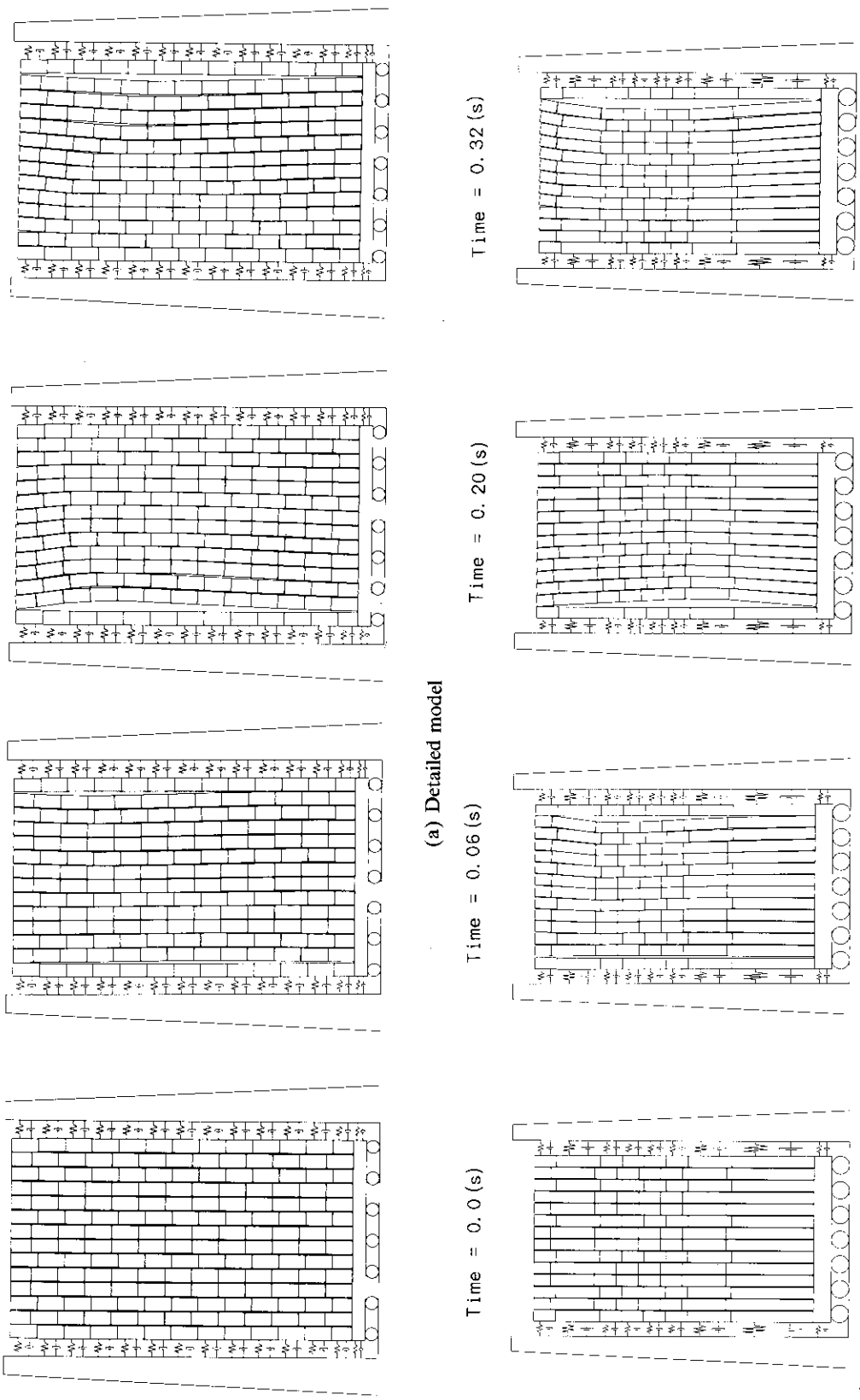

Fig. 12.1 Comparison of detailed model and reduced model on seismic behavior (Excitation 3.0 Hz, Max. acceleration 250 Gal)

Table 12.1 Comparison of computer CPU time between scalar and vector processors

Size of problem		Computer CPU time (s)	
Degrees-of-freedom	Number of seps	Scalar processor	Vector processor
320	15130	444.5 (1)	191.1 (1/2.33)
520	2000	137.6 (1)	49.7 (1/2.77)
520	18600	1201 (1)	444.9 (1/2.70)

ACKNOWLEDGMENTS

The author wishes to express his gratitude to Professors Hideomi Otsubo, Heki shibata, Ganki Yagawa, Shigeru Nakagiri, Masaharu Nakazawa and Takafumi Fujita of Tokyo University for their kind advices in preparing this thesis and continuous encouragement.

He also wishes to thank Drs. Masao Nozawa, Tetsuo Aochi, Michio Ichikawa, Shinzo Saito, Yoshitaka Naito and Toshiyuki Tanaka of Japan Atomic Energy Research Institute and Professor Hiroshi Takeda of Hosei University for their support and encouragement throughout this study.

The author is indebted to Drs. Kazuhiro Shiraki, Toshiaki Honma and their staffs of Mitsubishi Heavy Industries Co. Ltd. and Drs. Hiroshi Ishizuka, Akira Ide and their staffs of Fuji Electric Co. Ltd. for assistances of making vibration tests. He is also indebted to Dr. Toshio Nakazawa of Century Research Center Co. Ltd. for assistance of making computer programs.

REFERENCES

1) Neylan, A.J. and Gorholt, W., "Design Depelopment of HTGR Core and Its Support Structure Seismic Consideration", Nucl. Eng. Design, 29, pp. 231～242, (1974).
2) Olsen, B.E., Neylan, A.J. and Gorholt, W., "Seismic Test on a One-Fifth Scale HTGR Core Model", Nucl. Eng. Design, 36, pp. 355～365, (1976).
3) Shatoff, H.D., Wesley, D.A. and Olsen, B.E., "HTGR Core Seismic Verification Plan", GA-A 13934, (1976).
4) Olsen, B.E., et al., "Core Seismic Method Verification Report", GA-A 14812 (Vol. 1), (1979).
5) Olsen, B.E., et al., "Core Seismic Method Verification Report", GA-A 14812 (Vol. 2), (1979).
6) Rodkin, S.M. and Olsen, B.E., "HTGR Fuel Element Collision Dynamics Test Program", GA-A 14728, (1978).
7) Nau, P.V. and Olsen, B.E., "One-Fifth-Scale and Full-Scale Fuel Element Rocking Tests", GA-A 14086, (1978).
8) Fischer, J., Rakowski, J.E. and Olsen, B.E., "One-Fifth-Scale Fuel Element Column Shake Test, Final report", GA-A-14664, (1979).
9) Peterson, D. and Olsen, B.E., "One-Fifth-Scale Two-Dimensional Seismic Tests", GA-A 14087, (1978).
10) Waldman, L. and Olsen, B.E., "One-Fifth-Scale, Two-Dimensional Two-Axis Seismic Test", GA-A 14548, (1978).
11) Rakowski, J.E. and Olsen, B.E., "One-Fifth-Scale Full Array Test Report, Final report", GA-A 14546, (1978).
12) Rakowski, J.E. and Olsen, B.E., "Measuring the Seismic Response of an HTGR Core Model", Trans. 4th Int. Conf. SMiRT, K 7/7, (1977).
13) Rakowski, J.E., "One-Fifth-Scale Dowel Force Test Report", GA-A 14088, (1979).
14) Chiang, D.D., "Fatigue Tests of Dowel-Socket Systems", GA-A 13861, (1976).
15) Olsen, J.E., et al., "LHTGR Graphite Fuel Element Seismic Strength", GA-A 13920, (1980).
16) Tzung, F., "Study of Fuel Block Collision in HTGR Core", GA-A 14359, (1977).

ACKNOWLEDGMENTS

The author wishes to express his gratitude to Professors Hideomi Otsubo, Heki shibata, Ganki Yagawa, Shigeru Nakagiri, Masaharu Nakazawa and Takafumi Fujita of Tokyo University for their kind advices in preparing this thesis and continuous encouragement.

He also wishes to thank Drs. Masao Nozawa, Tetsuo Aochi, Michio Ichikawa, Shinzo Saito, Yoshitaka Naito and Toshiyuki Tanaka of Japan Atomic Energy Research Institute and Professor Hiroshi Takeda of Hosei University for their support and encouragement throughout this study.

The author is indebted to Drs. Kazuhiro Shiraki, Toshiaki Honma and their staffs of Mitsubishi Heavy Industries Co. Ltd. and Drs. Hiroshi Ishizuka, Akira Ide and their staffs of Fuji Electric Co. Ltd. for assistances of making vibration tests. He is also indebted to Dr. Toshio Nakazawa of Century Research Center Co. Ltd. for assistance of making computer programs.

REFERENCES

1) Neylan, A.J. and Gorholt, W., "Design Depelopment of HTGR Core and Its Support Structure Seismic Consideration", Nucl. Eng. Design, 29, pp. 231～242, (1974).
2) Olsen, B.E., Neylan, A.J. and Gorholt, W., "Seismic Test on a One-Fifth Scale HTGR Core Model", Nucl. Eng. Design, 36, pp. 355～365, (1976).
3) Shatoff, H.D., Wesley, D.A. and Olsen, B.E., "HTGR Core Seismic Verification Plan", GA-A 13934, (1976).
4) Olsen, B.E., et al., "Core Seismic Method Verification Report", GA-A 14812 (Vol. 1), (1979).
5) Olsen, B.E., et al., "Core Seismic Method Verification Report", GA-A 14812 (Vol. 2), (1979).
6) Rodkin, S.M. and Olsen, B.E., "HTGR Fuel Element Collision Dynamics Test Program", GA-A 14728, (1978).
7) Nau, P.V. and Olsen, B.E., "One-Fifth-Scale and Full-Scale Fuel Element Rocking Tests", GA-A 14086, (1978).
8) Fischer, J., Rakowski, J.E. and Olsen, B.E., "One-Fifth-Scale Fuel Element Column Shake Test, Final report", GA-A-14664, (1979).
9) Peterson, D. and Olsen, B.E., "One-Fifth-Scale Two-Dimensional Seismic Tests", GA-A 14087, (1978).
10) Waldman, L. and Olsen, B.E., "One-Fifth-Scale, Two-Dimensional Two-Axis Seismic Test", GA-A 14548, (1978).
11) Rakowski, J.E. and Olsen, B.E., "One-Fifth-Scale Full Array Test Report, Final report", GA-A 14546, (1978).
12) Rakowski, J.E. and Olsen, B.E., "Measuring the Seismic Response of an HTGR Core Model", Trans. 4th Int. Conf. SMiRT, K 7/7, (1977).
13) Rakowski, J.E., "One-Fifth-Scale Dowel Force Test Report", GA-A 14088, (1979).
14) Chiang, D.D., "Fatigue Tests of Dowel-Socket Systems", GA-A 13861, (1976).
15) Olsen, J.E., et al., "LHTGR Graphite Fuel Element Seismic Strength", GA-A 13920, (1980).
16) Tzung, F., "Study of Fuel Block Collision in HTGR Core", GA-A 14359, (1977).

17) Tzung, F.K. "Study of Fuel Block Collision HTGR Core", Trans. 4th Int. Conf. SMiRT, K 7/5, (1977).
18) Rickard, N.D., "CRUNCH-1D: A Computer Program for Seismic Analysis of the HTGR Core", GA-A 14120, (1977).
19) Lee, T.H., "Nonlinear Dynamic Analysis of a Stacked Fufl Column Subjected to Bondary Motion", Nucl. Eqg. Design, 32, pp. 337~350, (1975).
20) Lee, T.H. and Wesley, D.A., "Nonlinear Seismic Response of a Series of Interacting Fuel Columns Consisting of Stacked Elements", Trans. 3rd Int. Conf. SMiRT K 8/5, (1975).
21) Rickard, N.D., "COCO: A Computer Program for Seismic Analysis of a Single Column of the HTGR Core", GA-A 14600 (1978).
22) Thompson, R.W., "MCOCO: A Computer Program for Seismic Analysis of the HTGR Core", GA -A 14764, (1978).
23) Tow, D., "CRUNCH-2D: A Two-Dimensional Computer Program for Seismic Analysis of the HTGR Core", GA-A 14765, (1978).
24) Shatoff, H.D., Thompson, R.W. and Lee, T.H., "Nonlinear Dynamic Analysis of Prismatic Elements for High-Temperature Gas-Cooled Reactor Cores", GA-A 15370, (1979).
25) Lee, T.H. and Wesley, D.A., "Seismic Response of a Stacked HTGR Fuel Column Interacting with a Control Rod", GA-A 14351, (1977).
22) Lee, T.H. and Wesley, D.A., "Seismic Response of a Stacked HTGR Fuel Column Interacting with a Control Rod", Trans. 4th Int. Conf. SMiRT, K 7/6, (1977).
27) Muto, K., et al., "One-Dimensional Vibration Test and Simulation Analysis for HTGR Core", Trans. 3rd Int. Conf. SMiRT, K 8/8, (1975).
28) Muto, K., et al., "Two-Dimensional Vibration Test and Simulation Analysis for a Vertical Slice Model of HTGR Core", Trans. 4th Int. Conf. SMiRT, K 7/8, (1977).
29) Muto, K., et al., "Two-Dimensional Vibration Test and Its Simulation Analysis for Vertical Slice Model of HTGR Core", J. At. Energy Soc. Japan, 19 [12], pp. 853~861, (1977), (in Japanese).
30) Muto, K., et al., "Two-Dimensional Vibration Test and Its Simulation Analysis for a Horizontal Slice Model of HTGR Core", Trans. 5th Int. Conf. SMiRT, K 12/2, (1979).
31) Bezler, P., et al., "OSCIL: One-Dimensional Spring-Mass System Simulator for Seismic Analysis of High Temperature Gas Cooled Reactor Core", BNL-21023, (1976).
32) Reich, M. and Koplik, B., "Effect of Clearance and Distribution of Mass on the Dynamic Response of an HTGR Core", Trans. 4th Int. Conf. SMiRT, K 7/3, (1977).
33) Bezler, P. and Curreri, J.R., "Subharmonic Excitation in an HTGR Core", Trans. 4 th Int. Conf. SMiRT, K 7/4, (1977).
34) Reich, M., et al., "Dynamic Response of a Multielement HTGR Core", BNL-23197, (1977).
35) Reich, M. and Koplich, B., "Non-Linear Dynamic Response of a Multi-Mass System with Gaps", BNL-NUREG-21866, (1977).
36) Lasker, L. et al., "OSCIL and OSCVERT: Computer Codes to Evaluate the Nonlinear Seismic Response of an HTGR Core", Trans. 4th Int. Conf. SMiRT, K 7/2, (1977).
37) Curreri, J.R. and Bezler, P., "Effect of Damping on Response of a Nonlinear System with Multiple Sine Wave Excitation", Trans. 4th Int. Conf. SMiRT, K 8/9,(1977).
38) Curreri, J., et al., "A Three-Dimensional Test Program for the Nonlinear Dynamic Behavior of an HTGR Core", Trans. 5th Int. Conf. SMiRT, K 12/1, (1979).
39) Subudhi, M., et al., "A Three-Dimensional Computer Code for the Nonlinear Dynamic Response of an HTGR Core", Trans. 5th Int. Conf. SMiRT, K 12/7, (1979).
40) Subudhi, M. and Curreri, J.R., "Stability Analysis and Response Characteristics of Two-Degree of Freedom Nonlinear Systems", BNL-NUREG-25846, (1979).

41) Koplik, B., Subudhi, M. and Curreri, J., "Nonlinear Response of the Multiple Sine Weve Excitation of a Softening-Hardening System", BNL-NUREG-25902, (1979).
42) Dove, R.C., Bennett, J.G. and Merson, J.L., "Seismic Response of a Block-Type Nuclear Reactor Core", LA-NUREG-6377-MS, (1976).
43) Dove, R.C., "Scaling Laws for HTGR Core Block Seismic Response", LA-UR-77-2010, (1977).
44) Bennett, J.L. and Dove, R.C., "Proposal for Analysis of HTGR Core Response to Seismic Input", LA-5821-MS, (1975).
45) Merson, J.L. and Bennett, J.G., "A Computer Method for Analyzing HTGR Core Block Response to Seismic Excitation", LA-NUREG • 6473-MS, (1976).
46) Ishizuka, H., Ide, A. and Hayakawa, H., "Seismic Experiment of High Temperature Gas Cooled Core Structure (Part Ⅰ)", J. Fuji Giho 48 [8], pp. 447～453, (1975), (in Japanese).
47) Ishizuka, H., Ide, A. and Shingai, K., "Vibration Test of High Temperature Gas Cooled Reactor Core Structure", J. First Atomic Power Ind. Grop, 79 [11], pp. 9～15, (1975), (in Japanese).
48) Ishizuka, H., et al., "Basic Study on Seismic Response of HTR Core, Trans.", 4th Int. Conf. SMiRT, K 7/9, (1977).
49) Ide, A. and Hayakawa, H., "A Study on Vibration Response Analysis of HTR Core Vertical Section and the Use of Simplified Models", J. First Atomic Power Ind. Group, 91 [3], pp. 16～21, (1979), (in Japanese).
50) Buland, P., et al., "Seismic Study of HTGR Core", Trans. 3rd Int. Conf. SMiRT, K 8/9, (1975).
51) Buland, P., et al., "A Calculation Model for HTR Core Seismic Response Comparison with Experimental Results on the VESUVE Shaking Table", CEA CONF 3226, (1975).
52) Zako, M., et al., "Seismic Study on HTGR Graphite Fuel Block", Proceeding of JSME 780-14, pp. 29～31, (1978)(in Jananese).
53) Zako, M., et al., "Seismic Study on HTGR Graphite Fuel Block (Ⅱ)", proceeding of JSME 780-6, pp. 11～13, (1978),(in Japanese).
54) Zako, M., et al., "Seismic Study on HTGR Graphite Fuel Block (Ⅲ)", Proceeding of JSME 790-5, pp, 37～39, (1979), (in Japanese).
55) Zako, M., et al. "Seismic Study on HTGR Graphite Fuel Block (Ⅳ)", Proceeding of JSME 800-3, pp. 91～93, (1980), (in Japanese).
56) Zako, M. and Miyoshi, T., "Seismic Tests and Analyses on HTGR Graphite Fuel Block", Proceeding of JSME 800-12, pp. 95～102, (1980), (in Japanese).
57) Honma, T., et al., "Study on the Vibration Characteristics of High Temperature Gas Reactor Core Using One Region Model", Technical Report of Mitsubishi Heavy Industries, 16-[5], pp. 1～10, (1979), (in Japanese).

LIST OF PUBLICATIONS

The content in this thesis were published in the following journals.

1) Ikushima, T., et al., "Seismic Response of High Temperature Gas-cooled Reactor Core with Block-type Fuel (Ⅰ) Vibration Characteristics of Stacked Block Column", J. At. Energy Soc. Japan, 22 [1], pp. 55～67 (1980), (in Japanese).
2) Ikushima, T. and Nakazawa, T., "A Seismic Analysis Method for a Block Column Gas-cooled Reactor Core", Nucl. Eng. Design, 55, pp. 331～342 (1979).

41) Koplik, B., Subudhi, M. and Curreri, J., "Nonlinear Response of the Multiple Sine Weve Excitation of a Softening-Hardening System", BNL-NUREG-25902, (1979).
42) Dove, R.C., Bennett, J.G. and Merson, J.L., "Seismic Response of a Block-Type Nuclear Reactor Core", LA-NUREG-6377-MS, (1976).
43) Dove, R.C., "Scaling Laws for HTGR Core Block Seismic Response", LA-UR-77-2010, (1977).
44) Bennett, J.L. and Dove, R.C., "Proposal for Analysis of HTGR Core Response to Seismic Input", LA-5821-MS, (1975).
45) Merson, J.L. and Bennett, J.G., "A Computer Method for Analyzing HTGR Core Block Response to Seismic Excitation", LA-NUREG • 6473-MS, (1976).
46) Ishizuka, H., Ide, A. and Hayakawa, H., "Seismic Experiment of High Temperature Gas Cooled Core Structure (Part Ⅰ)", J. Fuji Giho 48 [8], pp. 447～453, (1975), (in Japanese).
47) Ishizuka, H., Ide, A. and Shingai, K., "Vibration Test of High Temperature Gas Cooled Reactor Core Structure", J. First Atomic Power Ind. Grop, 79 [11], pp. 9～15, (1975), (in Japanese).
48) Ishizuka, H., et al., "Basic Study on Seismic Response of HTR Core, Trans.", 4th Int. Conf. SMiRT, K 7/9, (1977).
49) Ide, A. and Hayakawa, H., "A Study on Vibration Response Analysis of HTR Core Vertical Section and the Use of Simplified Models", J. First Atomic Power Ind. Group, 91 [3], pp. 16～21, (1979), (in Japanese).
50) Buland, P., et al., "Seismic Study of HTGR Core", Trans. 3rd Int. Conf. SMiRT, K 8/9, (1975).
51) Buland, P., et al., "A Calculation Model for HTR Core Seismic Response Comparison with Experimental Results on the VESUVE Shaking Table", CEA CONF 3226, (1975).
52) Zako, M., et al., "Seismic Study on HTGR Graphite Fuel Block", Proceeding of JSME 780-14, pp. 29～31, (1978)(in Jananese).
53) Zako, M., et al., "Seismic Study on HTGR Graphite Fuel Block (Ⅱ)", proceeding of JSME 780-6, pp. 11～13, (1978),(in Japanese).
54) Zako, M., et al., "Seismic Study on HTGR Graphite Fuel Block (Ⅲ)", Proceeding of JSME 790-5, pp, 37～39, (1979), (in Japanese).
55) Zako, M., et al. "Seismic Study on HTGR Graphite Fuel Block (Ⅳ)", Proceeding of JSME 800-3, pp. 91～93, (1980), (in Japanese).
56) Zako, M. and Miyoshi, T., "Seismic Tests and Analyses on HTGR Graphite Fuel Block", Proceeding of JSME 800-12, pp. 95～102, (1980), (in Japanese).
57) Honma, T., et al., "Study on the Vibration Characteristics of High Temperature Gas Reactor Core Using One Region Model", Technical Report of Mitsubishi Heavy Industries, 16-[5], pp. 1～10, (1979), (in Japanese).

LIST OF PUBLICATIONS

The content in this thesis were published in the following journals.

1) Ikushima, T., et al., "Seismic Response of High Temperature Gas-cooled Reactor Core with Block-type Fuel (Ⅰ) Vibration Characteristics of Stacked Block Column", J. At. Energy Soc. Japan, 22 [1], pp. 55～67 (1980), (in Japanese).
2) Ikushima, T. and Nakazawa, T., "A Seismic Analysis Method for a Block Column Gas-cooled Reactor Core", Nucl. Eng. Design, 55, pp. 331～342 (1979).

3) Ikushima, T. and Honma, T., "Seismic response of High Temperature Gas-cooled Reactor Core with Block-type Fuel (Ⅱ) Three-dimensional Vibration Characteristics of Stacked Block Column", J. Nucl. Sci. Tech. 17 [9], pp. 655～667 (1980).
4) Ikushima, T. and Honma, T., "Aseismic Study of High Temperature Gas-cooled Reactor Core with Block-type Fuel (1st Report, Vibration Characteristics of Single Stacked Column", Trans. JSME, 47-415 (C), pp. 292～297 (1981), (in Japanese).
5) Ikushima, T. and Honma, T.. "Simplified Analytical Method for HTGR Core Seismic Response", J. Nucl. Sci. Tech. 16 [8], pp. 605～612 (1978).
6) Ikushima, T. and Honma, T., "Seismic Response of High Temperature Gas-cooled Reactor Core with Block-type Fuel (Ⅲ) Vibration Experiment of Two-Dimensional Vertical Slice Core Model", J. Nucl. Sci. Tech. 18 [7], pp. 514～524 (1981).
7) Ikushima, T., "Aseismic Study of High Temperature Gas-cooled Reactor Core with Block-type Fuel (2nd Report, An Analytical Method of Two-dimensional Vibration of Interacting Columns", Trans. JSME, 48-426(C), pp. 229～238 (1982) and Bulletin of the JSME 25-208, pp. 1610～1617 (1982).
8) Ikushima, T. and Honma, T., "Aseismic Study of High Temperature Gas-cooled Reactor Core with Block-type Fuel (3rd Report, Effect of Excitation Directions and Core Support Stiffness)", Trans. JSME, 51-464 (C) pp. 746～755 (1985) and Bulletin of JSME, 28-246, pp. 2986～2993 (1985).
9) Ikushima, T. and Honma, T., "Seismic Response of High Temperature Gas-cooled Reactor Core with Block-type Fuel (Ⅳ) Seismic Response of Actual Core Predicted from Experimental and Analytical Results of Two-Dimensional Core Models", J. At. Energy Soc. Japan, 27 [2], pp. 145～158 (1985), (in Japanese).
10) Ikushima, T., Honma, T. and Ishizuka, H., "Seismic Research on Block-type HTGR Core", Nucl. Eng. Design, 71, pp. 195～215 (1982).
11) Ikushima, T. and Honma, T., "Seismic Response of High Temperature Gas-cooled Reactor Core with Block-typed Fuel (V) An Analytical Method of Seismic Response for Two-dimensional Horizontal Slice Core Model", J. Nucl. Sci. Tech. 26 [10], pp. 913～930 (1989).

OTHER PUBLICATIONS (Seismic Research)

1) Ikushima, T., "PRELUDE-2: Seismic Response Analysis Code for Block-type Fuel Core", JAERI -M 5560, (1974).
2) Ikushima, T. and Kawakami, M., "Seismic Response Analysis for Block-type Fuel HTGR Core", Trans. 3rd Int. Conf. SMiRT, K 8/7, (1975).
3) Ikushima, T., "PRELUDE-2: Seismic Response Analysis Code for Block-type Fuel Core", LA-tr -75-9, (1975).
4) Ikushima, T. and Honma, T., "Seismic Verification Test Program on Experimental Very High-Temperature Gas-cooled Reactor Core", JAERI-memo 7719, (1978).
5) Ikushima, T., "Overview of Japanese Seismic Research Program for HTR", JAERI-M 7728, (1978).
6) Ikushima, T., et al., "One Stacked-Column Vibration Test and Analysis for VHTR Core", JAERI -M 7727, (1978).
7) Ikushima, T., "Seismic Response Analysis for Prismatic Fuel HTGR Core", JAERI-M 8273, (1979).

8) Ikushima, T., Nakamura, Y. and Onuma, Y., "GTOROTO: A Simulation System for HTGR Core Seismic Behavior", JAERI-M 8937, (1980).
9) Ikushima, T. and Ishizuka, H., "Seismic Test and Analysis of Single Stacked Block Column of HTGR Core", JAERI-M 9265, (1980).
10) Ikushima, T. and Honma, T., "Three-dimensional Vibration Characteristics of Stacked Block Column", JAERI-M 9199, (1980).
11) Ikushima, T., "SONATINA-1: A Computer Program for Seismic Analysis of a Single Column of the HTGR Core", JAERI-M 9165, (1980).
12) Ikushima, T., "SONATINA-2V: A Computer Program for Seismic Analysis of Two-dimensional Vertical Slice Core Model of the HTGR Core", JAERI 1279, (1982).
13) Ikushima, T. and Honma, T., "Two-Dimensional Vertical Model Seismic Test and Analysis for HTGR Core", JAERI 1282 (1983), (in Japanese).
14) Ikushima, T. and Honma, T., "Two-Dimensional Horizontal Model Seismic Test and Analysis for HTGR Core", JAERI-M 88-085 (1988), (in Japanese).
15) Ikushima, T. and Honma, T., "SONATINA-2H: A Computer Program for Seismic Analysis of Two -dimensional Horizontal Slice HTGR Core", JAERI M 90-003 (1990).